Lista portofoliului de lucrări

1. Dragoi, E.N., Blaga, A.C. (corresponding author), Cascaval, D., Galaction, A.I. - Experimental, modeling and optimisation of adipic acid reactive extraction using ionic liquids, Journal of Molecular Liquids, 2024, 410, 125564, https://doi.org/10.1016/j.molliq.2024.125564
2. Blaga, A.C., Dragoi, E.N., Tucaliuc, A., Kloetzer L., Puitel A.C., Cascaval, D., Galaction, A.I. - Reactive extraction of muconic acid by hydrophobic phosphonium ionic liquids - Experimental, modelling and optimisation with Artificial Neural Networks, Heliyon, 2024, 10(16), e36113, https://doi.org/10.1016/j.heliyon.2024.e36113
3. Blaga, A.C.; Dragoi, E.N.; Gal, D.G.; Puitel, A.C.; Tucaliuc, A.; Kloetzer, L.; Cascaval, D.; Galaction, A.I. - Selective separation of vitamin C by reactive extraction using ionic liquid: Experimental and modelling, Journal of Industrial and Engineering Chemistry, 2024, https://doi.org/10.1016/j.jiec.2023.11.057
4. Blaga, A.C.; Dragoi, E.N.; Tucaliuc, A.; Kloetzer, L.; Cascaval, D. Folic Acid Ionic-Liquids-Based Separation: Extraction and Modelling. Molecules 2023, 28, 3339. https://doi.org/10.3390/molecules28083339
5. Blaga, A.C.; Dragoi, E.N.; Munteanu, R.E.; Cascaval, D.; Galaction, A.I. Gallic Acid Reactive Extraction with and without 1-Octanol as Phase Modifier: Experimental and Modeling. Fermentation 2022, 8, 633. https://doi.org/10.3390/fermentation8110633
6. Lazar, RG; Blaga, AC (autor corespondent); Dragoi, EN; Galaction, AI; Cascaval, D - Mechanism, influencing factors exploration and modelling on the reactive extraction of 2-ketogluconic acid in presence of a phase modifier, Separation and Purification Technology, 255, 2021, 117740, https://doi.org/10.1016/j.seppur.2020.117740
7. Lazar, RG; Blaga, AC (autor corespondent); Dragoi, EN; Galaction, AI; Cascaval, D - Application of reactive extraction for the separation of pseudomonic acids: Influencing factors, interfacial mechanism, and process modelling, Canadian Journal Of Chemical Engineering, 2021, https://doi.org/10.1002/cjce.24124
8. Blaga, AC; Ciobanu, C; Cascaval, D; Galaction, AI - Enhancement of ergosterol production by *Saccharomyces cerevisiae* in batch and fed-batch fermentation processes using n-dodecane as oxygen-vector, Biochemical Engineering Journal, 131, 2018, 70-76, https://doi.org/10.1016/j.bej.2017.12.010
9. Blaga, AC; Cascaval, D; Galaction, AI - Improved Production of alpha-Amylase by *Aspergillus terreus* in Presence of Oxygen-Vector, Fermentation, 2022, 8 (6), 271, https://doi.org/10.3390/fermentation8060271

Separation and Purification Technology 255 (2021) 117740

Contents lists available at ScienceDirect

Separation and Purification Technology

journal homepage: www.elsevier.com/locate/seppur

Mechanism, influencing factors exploration and modelling on the reactive extraction of 2-ketogluconic acid in presence of a phase modifier

Lazar Roxana Georgiana [a], Blaga Alexandra Cristina [a,*], Dragoi Elena Niculina [a], Galaction Anca Irina [b], Cascaval Dan [a]

[a] "Gheorghe Asachi" Technical University of Iasi, Faculty of Chemical Engineering and Environmental Protection "Cristofor Simionescu", Iasi, Romania
[b] "Grigore T. Popa" University of Medicine and Pharmacy, Faculty of Medical Bioengineering, Iasi, Romania

ARTICLE INFO

Keywords:
2-Ketogluconic acid
Butyl acetate
Dichloromethane
Heptane
Octanol
Reactive extraction

ABSTRACT

Taking into account that limited research has been carried out on the reactive extraction of 2-ketogluconic acid, this study was focused on analyzing the pH dependent extraction performance and the molar ratios of acid and extractant (Amberlite LA-2) dissolved in three solvents with 1-octanol as phase modifier. Back extraction was successfully performed using NaOH solutions. The mechanism of the interfacial reaction in the presence of 1-octanol, pointed out that, indifferent of the pH value and solvent polarity, only one molecule of 2-ketogluconic acid and one of extractant react at the interface. The positive effect of 1-octanol on extraction efficiency was quantified by means of the amplification factor, its maximum values being 2.43 for dichloromethane, 3.67 for butyl acetate and 3.64 for n-heptane. In addition, the process was modelled using statistical regression and Artificial Neural Networks (ANNs) determined with chaos based Differential Evolution algorithm. The best ANN model had a mean squared error for the testing phase of 0.19 and modeled the process with an acceptable error.

1. Introduction

2-Keto-D-gluconic acid, 2-KGA, is a mild organic acid (p*K*a = 2.66) with multiple applications in food, cosmetic and pharmaceutic industries. Its chemical structure (Fig. 1) derives from a ketoaldonic acid that is D-gluconic acid in which the hydroxyl group at position 2 has been oxidized to a keto group. In food industry is an important intermediate in the D-isoascorbic acid (E315 – free acid and E316 – sodium salt) synthesis (vitamin C stereoisomer), used as GRAS (generally recognized as safe) antioxidant. This compound is produced over 40,000 tons/year due to its wide use as food antioxidant, its properties to maintain food color, flavors and aroma, and its ability to block the formation of ammonium nitrite (carcinogenic) during food processing [1,2].

Various bacterial strains are used for its production from glucose or starch hydrolysates (as carbon sources): *Gluconobacter, Preudomonas, Pseudogluconobacter, Artrobacter, Serratia, Erwinia* spp. [1–5]. At large scale the most widely used genus is *Pseudomonas* due to several advantages related to high selectivity, titer and conversion, but recently different strains of *Gluconobacter* (Table 1) have been investigated for selective production of 2-keto-D-gluconic acid. The main by-products resulting from the 2-KGA biosynthesis are gluconic acid and 5-ketogluconic acid, but the new engineered strains (*Gluconobacter oxydans, Pseudomonas plecoglossicida*) are capable to produce only 2-ketogluconic acid [3].

2-KGA is also a byproduct in the vitamin C production by biotechnological process (applied by all the manufacturers from China for industrial production) using two stages and mixed cultures of *Erwinia, Acetobacter, Gluconobacter* for the first stage (conversion of glucose to 2,5-diketogluconic acid and 2-ketogluconic acid) and *Brevibacterium* for the second step (conversion of 2,5-diketo-gluconic acid into 2-ketogulonic acid that transformed into ascorbic acid), less costly and more environment-friendly. The by-product, 2-keto-D-gluconic acid, obtained during the first step, is very difficult to separate from its optical isomer 2-keto-L-gulonic acid [6].

The development of a cost-effective and eco-friendly process for separating high purity 2- ketogluconic acid requires more studies, mainly due to involvement of multiple downstream steps that generates

Abbreviations: 2-KGA, 2-keto-D-gluconic acid; ANNs, Artificial Neural Networks; DE, Differential Evolution; E, extraction efficiency; R, stripping efficiency; D, Distribution ratio.

* Corresponding author at: Bulevardul Prof. Dimitrie Mangeron, nr. 73, Iasi 700050, Romania.
E-mail address: acblaga@tuiasi.ro (B. Alexandra Cristina).

https://doi.org/10.1016/j.seppur.2020.117740
Received 15 July 2020; Received in revised form 9 September 2020; Accepted 10 September 2020
Available online 15 September 2020

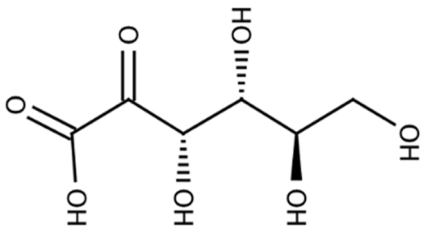

Fig. 1. 2- keto-D-gluconic acid structure.

Table 1
Strains used for 2-ketogluconic acid production.

No.	Strain	2-KGA production, g/L	Reference
1	*Pseudomonas fluorescens AR4*	178 (shaking flask); 444.96 (20 L fermenter, semi-continous process)	[2,4]
2	*Pseudomonas aeruginosa*	72 (immobilized cells)	[5]
3	*Pseudomonas plecoglossicida*	110/215 (two stage fermentation)	[2]
4	*Gluconobacter oxydans*	321 (overexpressed the ga2dh gene); 234.6 (using resting cells)	[3]
5	*Gluconobacter japonicus*	239.4	[1]

high costs. The downstream purification process for 2 KGA involves several steps (centrifugation, activated carbon adsorption, evaporation, crystallization, ion-exchange using a weakly basic anion exchange resin, followed by H_2SO_4-CH_3OH elution) being associated with high energy consumption, releasing high amount of wastewater and demanding relatively high manpower [7].

Reactive extraction (a clean, energy efficient and economical method) is a promising separation technique that combines simultaneously two operations: a selective solute distribution between two immiscible liquid phases (one aqueous and one organic) and a reaction between an extractant dissolved in the organic phase that has the ability to react with the target acid from the aqueous phase. This modified liquid extraction technique offers several advantages: it is a clean and economical method, energy efficient and can be used at industrial scale with existing equipment. It has been applied for different carboxylic acids: succinic acid, malic acid, fumaric acid, itaconic acid, propionic acid, formic acid, gallic acid, lactic acid etc. [8–13]. For the separation of succinic acid from fermentation broth, Alexandri (2019) analyzed different separation techniques: calcium precipitation, direct crystallization using acidification with sulfuric acid or cation-exchange resins, salting-out and reactive extraction, obtaining for the reactive extraction the higher purity for the crystals (97.2%) and a total yield for the downstream process of 73% [14].

The extractants, that are usually highly viscous, dissolved in an organic solvent in order to improve their physical properties like viscosity and surface tension, react with the solute from the aqueous phase to form complexes that are only soluble in the organic phase. From the large variety of extractants (high molecular weight aliphatic or aromatic amines, organophosphorus compounds, ionic liquids), for carboxylic acids, high molecular amines are the most effective extractants and offer advantages compared to phosphorus-bonded extractants such as: are less expensive and more effective in formation of a complex with carboxylic groups [15,16]. Due to the necessity of using green solvents for the extraction cumulated with these solvents poor solvation capabilities, several researchers increased the extraction efficiency by improving the solvent polarity through the addition of a phase modifier in the organic solvent for the reactive extraction of acetic, formic, fumaric, lactic, succinic acids [11,17–19].

Although reactive extraction is a mature separation and concentration technique in industrial extractive metallurgy, which was applied successfully in a variety of processes it is not yet applied for industrial separation of carboxylic acids. The main challenge in the use of reactive extraction for the recovery of organic acids is finding a selective, cheap and efficient extractant and diluent system, on the basis of maximum capacity and minimum toxicity, and to determine the optimal conditions for its implementation. Since limited research has been carried out on the reactive extraction of 2-KGA [20] for the intensification of its recovery from the fermentation broth, the present study is aimed on reactive extraction of 2-KGA from aqueous solution using Amberlite LA-2 dissolved in three solvents with different dielectric constants: n-heptane, butyl acetate and dichloromethane in the presence of 1-octanol, as phase modifier.

In order to extend the experimental knowledge, the process was modelled using two strategies: (i) classical statistical linear regression and (ii) Artificial Neural Networks (ANNs) determined by a version of Differential Evolution (DE) algorithm based on chaotic maps. The motivation behind using two different strategies relies in the fact that each approach uses differently the knowledge from the system (represented by experimental data) and can indicate different relations and interactions between the parameters. The ANNs are efficient tools that imitate the functioning of the mammalian brain. The manner in which the knowledge about a given problem is gathered in ANNs allows them to model highly non-linear relations, to work with continuous data and to be robust even in the presence of noise in the data [21]. As a result, ANNs were widely used to solve various complex problems. In the biochemical filed, some application examples include: modeling and optimization of cyanobacterial C-phycocyanin production [22], mixing efficiency modelling for *Yarrowia lipolytica* suspensions [23], estimation of fungal biomass [24], predicting sugar yields from lignocellulosic biomass [25], inactivation of *E. coli* by natural pyrite in presence of citrate and EDTA [26], optimization of L-Lysine production [27]. In order to use an ANN for a given problem, first, the ANN must be trained, and the quality of the training procedure determines the efficiency of the model. Therefore, various strategies for ANN training were developed. In this work, a neuro-evolutive technique is applied. It combines the ANN with DE, the training procedure being performed by DE. In this work, DE also performs a topological optimization (and determines the number of hidden layers and neurons in each hidden layer).

2. Materials and methods

2.1. Chemicals

All chemicals were purchased by Sigma Aldrich and used as received without further treatment, i.e. 2-ketogluconic acid (99%), dichloromethane (99%), butyl acetate (99%), 1-octanol (99%), heptane (99%), sulfuric acid (95.0–98.0%), sodium hydroxide (>97%), and lauryl trialkylmethylamine - Amberlite LA2 (99%).

2.2. Liquid – liquid extraction experiments

Liquid-liquid extraction experiments for 2-KGA separation were carried out in an extraction column with vibratory mixing that offers a high interfacial area. It consists of a glass column with 3.6 cm diameter and 25 cm height. For temperature control (all the reactive extraction experiments have been performed at 25 ± 0.02 °C and the stripping experiments at 50 ± 0.02 °C) during the experiments, a thermostatic jacket was used and for intense mixing of the two phases a vibratory mixer (perforated disk with 45 mm in diameter and a 20% free section), with 50 s^{-1} frequency and 5 mm amplitude was maintained at the initial interface between the two phases (aqueous and the organic in equal ratios – 20 mL). The extraction time was 1 min and the stripping time was 5 min, followed by phase separation in a centrifugal separator at 4000 rpm. 2-ketogluconic acid initial concentration in the aqueous phase was 1 g/L (5.15×10^{-3} M), and the concentrations of the amine extractant: Amberlite LA-2 in the organic phase varied between 0 and 120 g/L (0.321 M). The pH value of the aqueous phase varied between 1

and 6, for the reactive extraction, while for the stripping phase the pH of the aqueous solutions was 12. The pH was modified depending on the value of the prescribed pH, using the digital pH meter (CONSORT C 836) using a solution of 3% sulfuric acid or 3% sodium hydroxide.

2.3. Analytical procedures

The extraction process was analysed on the basis of the distribution coefficient and the extraction efficiency, calculated using the mass balance for the extraction system based on the 2-ketogluconic acid concentration in the initial aqueous solution and in the raffinate measured by high performance liquid chromatography technique (HPLC) as described in the literature [28]. For this purpose a HPLC system, UltiMate 3000 Dionex, was fitted with an Hamilton PRP-X300 column (150 mm × 4.1 mm, 5 μm), 4 mM sulfuric acid solution as mobile phase, detection being performed by UV absorbance at a wavelength of 210 nm, and the flow rate of 0.5 mL/min). The determinations were done at 25 °C.

2.4. Calculations

The parameter used to quantify the amount of 2-ketogluconic acid extracted into the organic phase is the extraction efficiency (E), while the amount transferred from the organic phase into the stripping phase is described by the stripping efficiency (R):

$$E = \left(\frac{C_0 - C}{C_0}\right) \cdot 100, \% \quad (1)$$

$$R = \left(\frac{C_s}{C_0 - C}\right) \cdot 100, \% \quad (2)$$

where C_0, C and C_s, (mol/L) are the concentrations of 2-ketogluconic acid in the aqueous initial solutions, raffinate (exhausted initial solution after extraction) and stripping solution, respectively.

Distribution ratio (D) of 2-ketogluconic acid between the organic and aqueous phases in equilibrium is defined in literature as follows:

$$D = \frac{C_{org}}{C} \quad (3)$$

where C_{org} (mol/L) is the concentration in the organic phase after extraction, calculated from the mass balance as a difference C_o-C, C is the concentration in the raffinate.

In order to quantify the phase modifier effect, the amplification factor has been used, calculated as the ratio between the extraction yield in the presence and in the absence of the phase modifier:

$$F = \frac{E_{oct}}{E} \quad (4)$$

To confirm the reaction mechanism the loading ratio was used, defined as the total concentration of acid in the organic phase divided by the total concentration of amine in organic phase:

$$Z = \frac{C_{org}}{C_{ALA2_{org}}} \quad (5)$$

2.5. Process modelling

In order to model the extraction efficiency, two strategies were considered. The first uses the standard regression technique (its role is to determine the modelling difficulty - if the process is well modelled by linear regression, then, the use of ANNs is not motivated). The second strategy is represented by ANNs combined with DE algorithm. The main motivation behind using a neuro-evolutive technique that combines ANNs with DE relies on: (i) the ANNs are easy to use but very difficult to determine in an optimal form; (ii) neuro-evolution is a process that can be overcome the drawback of standard training techniques of getting stuck in local optima; (iii) neuro-evolution can be applied at multiple levels and can simultaneously determine the topology (structure of the ANN) and its optimal internal parameters (training); (iv) from the multitude of optimizer algorithms that can be combined with ANNs in a neuro-evolutive technique, DE is efficient, fast and has the ability of providing good solution with an acceptable amount of resources consumed.

The motivation for chosen ANNs was based on their proven effectiveness on several reactive extraction systems [29–33]. The DE algorithm is based on the evolution principle developed by Darwin and if follows the classical idea of Evolutionary Algorithms: a population of potential solution (also known as the initial population) is evolved (through a series of steps that include mutation, crossover and selection) until a stop criterion is reached. The combination of DE with ANN will be further referred as cDE-ANN and its main working principle is shown in Fig. 2.

As it can be observed from Fig. 2, the process parameters are fed into the ANN. Then, the ANN parameters are fed into the DE algorithm that generates the optimized ANN values that are then used to make predictions regarding the extraction efficiency. In order to have an efficient optimizer, DE is improved with a series of techniques that include: (i) chaos theory (it uses the principles of chaos theory to generate the random numbers necessary in the majority of DE steps; for the current work, the logistic map is used); (ii) opposition based principle to improve the DE initial population (step 2 from Fig. 2); (iii) local improvement after step 5 (for each iteration, the best so far solution is improved by randomly choosing between BackPropagation- a classical ANN training algorithm- and Local Search algorithm).

For the parameter setting (step 1 from Fig. 2), for the current work, number of iterations that represent the stop criteria and the dimension of the population are considered, while for the other DE parameters, F (from step 3) and Cr (from step 4) a self-adaptive strategy is used. It implies the introduction of these parameters into the algorithm itself and changing their values using the same steps (mutation, selection and crossover) used for the ANN optimization.

The objective of the optimization procedure is to determine models with the highest performance (the lowest difference between the experimental data and predictions). Thus, the fitness function (Eq. (6)) used to determine the suitability of the individuals and their selection on next generation is based on the Mean Squared Error (MSE) in the training phase. This is due to the fact that, in the current case, DE evolves populations of encoded ANNs.

$$Fitness = \frac{1}{MSE_{train} + 10^{-10}} \quad (6)$$

The process parameters that are used for determining the efficiency of the extraction are represented by: the pH of the solution, the ALA-2 concentration, the dielectric constant of the solvent and the octanol concentration. In addition, as the process has two phases with different behaviour, an additional parameter is considered. It shows whether an extraction or a back-extraction process occurs (indicated by values 1 and 0).

3. Results and discussion

3.1. Influence of aqueous phase pH on the extraction efficiency

The pH-value of aqueous phase exhibits an important influence on reactive extraction efficiency, as it controls the form in which the acid exists in aqueous solutions: dissociated at pH value superior to p*K*a (2.66), and undissociated at pH value lower than p*K*a. Due to acids insolubility in all chosen solvents, the extraction is based on the formation of a complex between the extractant: Amberlite LA2 and the carboxylic group from the 2-ketogluconic acid structure (Fig. 3).

The complex can be obtained either through electrostatic interactions or hydrogen bond (at pH lower than pKa) or through ionic

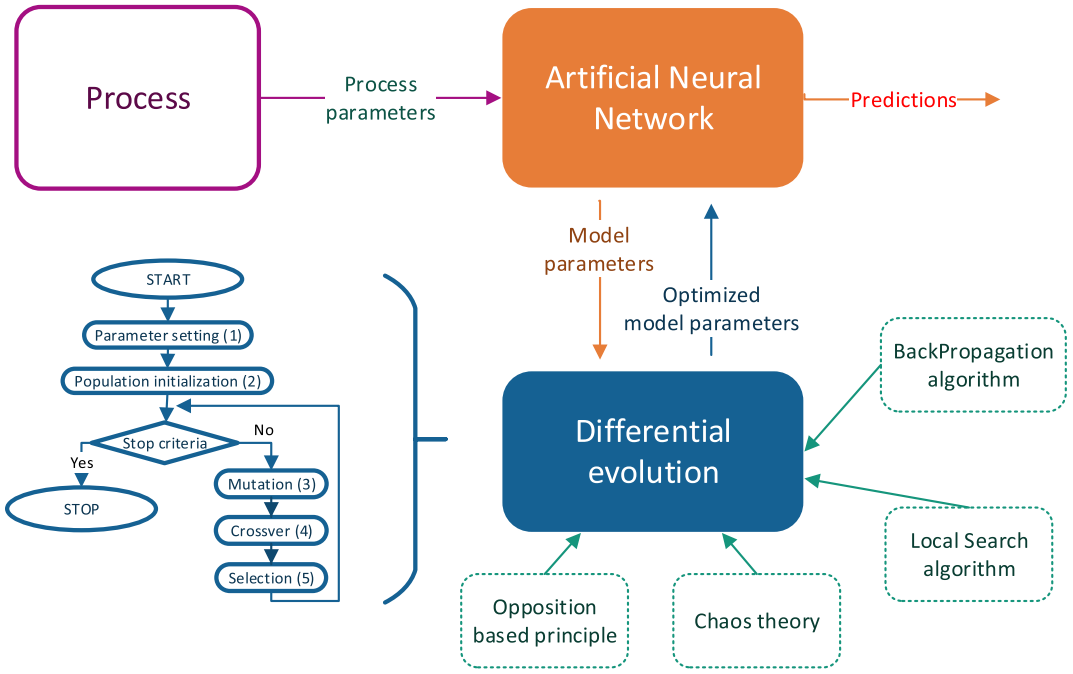

Fig. 2. General schema of the ANN based modelling.

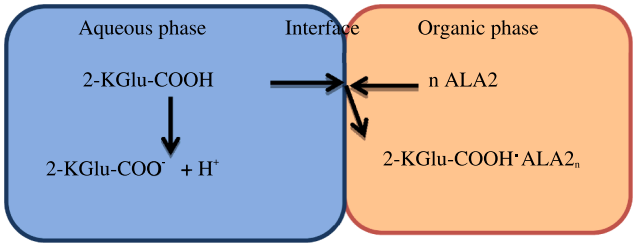

Fig. 3. Extraction mechanism of 2-ketogluconic acid.

type bond (at pH higher than p*Ka*) [11,20,34,35]. At the interface, three types of complexes can be formed: equimolecular (with only one molecule of each extraction system components), acidic adducts (with more than one molecule of acid bonded to the aminic extractant) or aminic adducts (with more than one molecule of amine extractant bonded to 2-ketogluconic acid). The formation of a certain complex is strongly influenced by the solvent polarity (low polarity solvents favors the formation of aminic adducts), solute and extractant structure and concentration (more complex and voluminous structures would sterically inhibit the formation of aminic or acidic adducts).

The pH influence on the reactive extraction system is depicted in Fig. 4 and indicates that the optimum pH for the extraction is 3, corresponding to the maximum extraction yield for all considered solvents, similar as the results obtained by Blaga et.al., in the absence of 1-octanol [20].

The maximum corresponding to pH 3 can be explained by the changes that appear in the solute structure with pH: at pH 1, 2-ketogluconic acid is able to form dimers in aqueous solutions [20,34,36] that would block the carboxylic group for the extraction, by further increase of pH the dimerization is less important – thus enabling the carboxylic group for the extraction and increasing the extraction yield, but the acid is dissociating according to its pKa (2.66) reducing the extraction efficiency at pH higher than 3. This variation suggests the combination between the proton from the 2-ketogluconic acid and the nitrogen atom from the amine's structure. The addition of 1-octanol in the three solvents increased significantly the extraction yield, without any effect on the curve variation, thus without influence on the extraction

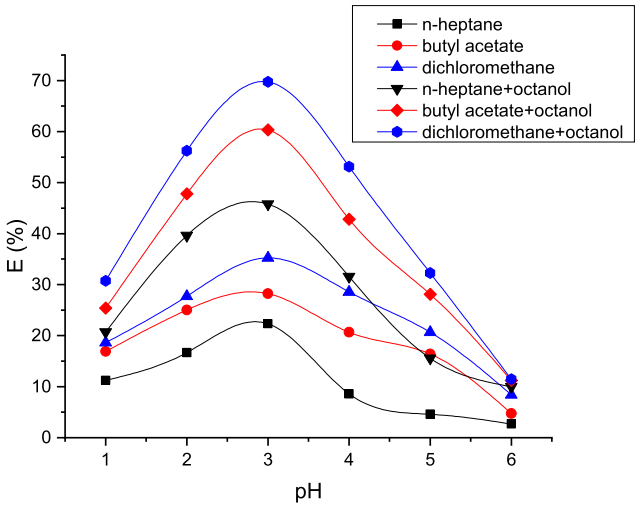

Fig. 4. pH influence on reactive extraction with and without 1-octanol addition (Amberlite LA-2 concentration 40 g/L, 2-KGA concentration 1 g/L).

mechanism.

To quantify the effect of 1-octanol addition on the extraction yield, the amplification factor (calculated as the ratio between the extraction yield in the presence and in the absence of the phase modifier) is presented in Fig. 5, with values larger than the unit for all pH domain analyzed. The addition of 1-octanol (dielectric constant 10.3 at 25 °C [31]) improved the extraction efficiency similar to other compounds (fumaric acid [11], acetic acid [17], acetic, formic and lactic acid [18], succinic acid [19]). This is attributed to an increase in the polarity of the organic phase with a stronger influence for n-heptane, the solvent with the lower dielectric constant (1.9 [37]) compared to butyl acetate (5.01 [37]), and dichloromethane (9.08 [37]), but also to the extraction capacity of its hydroxyl groups that can form hydrogen bonds with the solute (Fig. 6).

The presented results show that an increase in aqueous phase pH induces an increase of the amplification factor for all considered

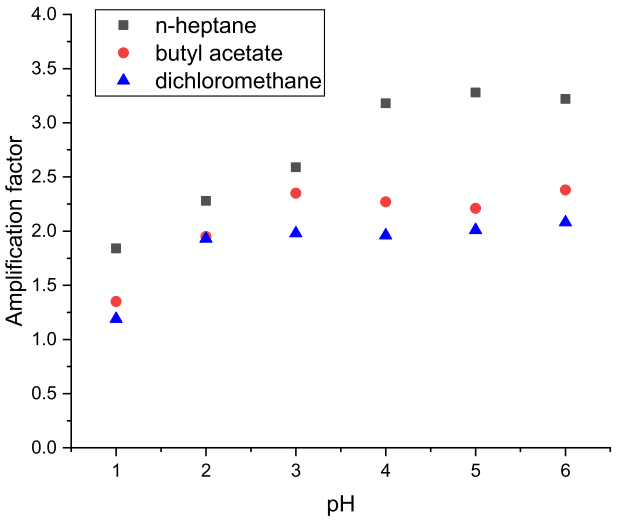

Fig. 5. The amplification factors values vs pH corresponding to 1-octanol addition.

solvents. Thus, its minimum level is reached at pH 1 (the increase in solvent polarity did not influence the dimerization process, hence the 2-ketogluconic acid extraction) and its maximum at pH = 6, variation that is a consequence of additional solubilization of ionized 2-ketogluconic acid molecules in the presence of 1-octanol at higher pH values. 1-Octanol addition in the organic solvent prevented the third phase formation and facilitated the separation between organic and aqueous phase, fact that is a major advantage for the industrial application of reactive extraction.

3.2. Influence of extractant concentration on the extraction efficiency

The reactive extraction of carboxylic acids, with an amine as extractant, occurs by means of an interfacial reaction with the formation of a strong hydrophobic compound. Solvation of this compound by the diluent is a critical factor in the extraction of most acids.

In Fig. 7 the influence of Amberlite LA2 concentration on the extraction efficiency is plotted, for pH = 3, as the maximum of the extraction degree was obtained for this value. It was observed that an increase in Amberlite LA2 concentration influences positively the extraction degree, due to the increase of the interfacial amount of one of the reactants. For all the solvents it can be observed that the increase in amines concentration in the organic phase [0 up to 0.321 M], over the stoichiometric ratio (2-ketogluconic acid concentration was $5.15x10^{-3}$ M), generates an improved extraction yield. This variation suggests an increase of interfacial compounds hydrophobicity and its improved solvation by extractant molecules.

The addition of 1-octanol (active diluent) in the inactive diluent n-heptane improved substantially the extraction degree for the same amine concentration, due to interactions of the acid–amine complex with the active diluent that increases its solubility and stabilized it (Fig. 7).

The amplification factor correlated with the extractant concentration is presented in Fig. 8, and values over the unit for the entire experimented domain of Amberlite LA-2 concentration were obtained. The higher value was recorded for 20 g/L Amberlite LA2 (0,053 M), and the lowest value for the maximum considered concentration of Amberlite LA2 (120 g/L – 0.321 M), fact that proves the reduction of extractant concentration influence in the presence of phase modifier –1-octanol - in the organic phase. For low Amberlite LA2 concentration in heptane, a third phase was observed in the extraction system, similar to other acidic compounds [38–40].

3.3. Synergic reactive extraction mechanism

The reactive extraction mechanism for 1-ketogluconic acid was analysed by Blaga et al, in the solvents considered without 1-octanol [20]. The results showed that the separation occurs by means of an interfacial reaction controlled by the solvent's polarity, and in the two solvents n-heptane or n-butyl acetate, the interfacial product is of aminic adduct type, its structure including two extractant molecules, while if as solvent is used dichloromethane with higher polarity, the reactive extraction involves one molecule of each reactant.

To analyse the mechanism in the presence of 1-octanol, the following

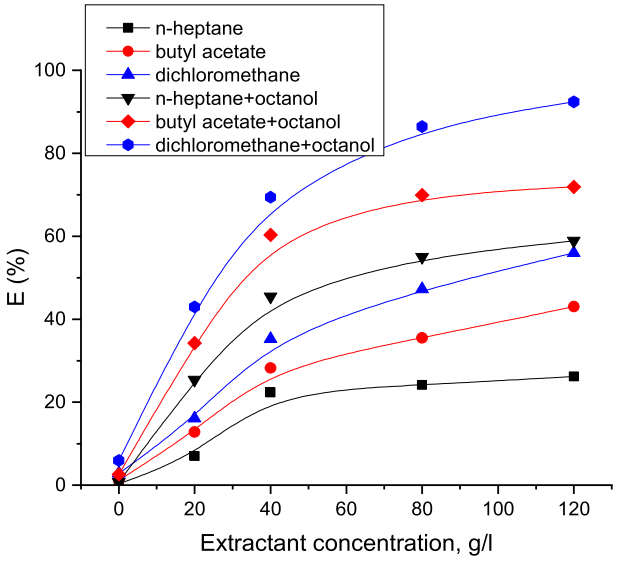

Fig. 7. Influence of Amberlite LA-2 concentration on reactive extraction with and without 1-octanol addition (pH = 3, 2-KGA concentration 1 g/L).

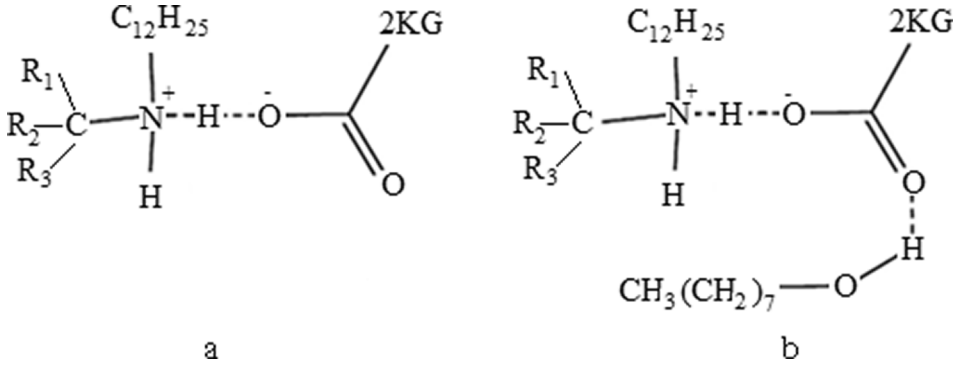

Fig. 6. Hydrophobic solute-extractant complex in the absence (a) and in the presence (b) of 1-octanol added in the organic phase.

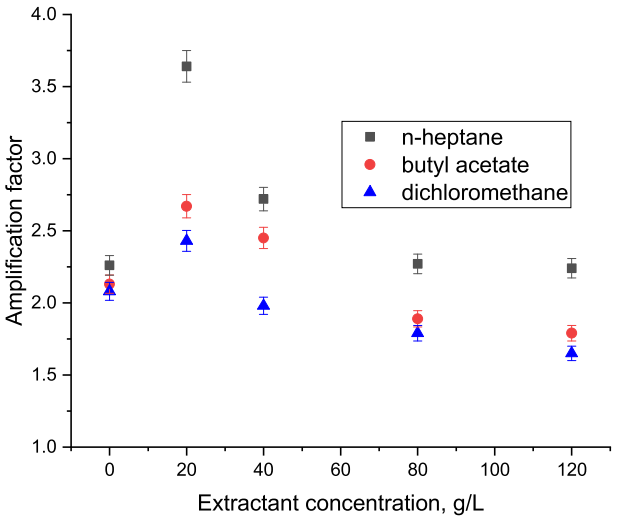

Fig. 8. The amplification factors values corresponding to 1-octanol addition.

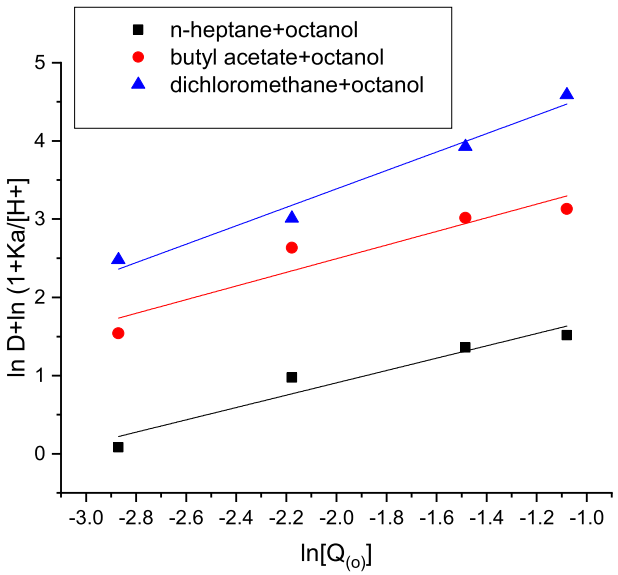

Fig. 9. The graphical representation of Equation (12).

equilibrium at the organic/aqueous interface (2-ketogluconic acid is insoluble in all organic solvents considered and Amberlite LA2 (Q) is insoluble in the aqueous phase) is considered:

$$2\text{KGlu}-\text{COOH}_{(aq)}+nQ_{(o)}\rightleftharpoons R-COOH\ Q_{n(o)} \tag{7}$$

For this system, the distribution coefficient, D can be calculated with the following expression: the ratio of total acid concentration in organic phase and total concentration in aqueous raffinate at the equilibrium state:

$$D=\frac{[2\text{KGlu}-\text{COOHQ}_{n(o)}]}{[2\text{KGlu}-\text{COOH}_{(aq)}]} \tag{8}$$

According to interfacial reaction, the equilibrium constant can be calculated using the following expression:

$$K_E=\frac{[2\text{KGlu}-\text{COOHQ}_{n(o)}]}{\left[\overline{2\text{KGlu}-\text{COOH}_{(aq)}}\right][Q_{(o)}]^n}\rightarrow[2\text{KGlu}-\text{COOHQ}_{n(o)}]$$
$$=K_E\cdot\left[\overline{2\text{KGlu}-\text{COOH}_{(aq)}}\right]\cdot[Q_{(o)}]^n \tag{9}$$

The concentration of undissociated 2-ketogluconic acid in the aqueous phase can be calculated by using its total concentration, $\overline{2\text{KGlu}-\text{COOH}_{aq}}$ and the dissociation constant, Ka:

$$[2\text{KGlu}-\text{COOH}_{(aq)}]=\frac{\overline{[2\text{KGlu}-\text{COOH}_{(aq)}]}}{1+\frac{K_a}{[H^+]}} \tag{10}$$

Using these three Eqs. (8)–(10) the distribution coefficient D can be calculated:

$$D=K_E\cdot\frac{[Q_{(o)}]^n}{1+\frac{K_a}{[H^+]}} \tag{11}$$

By applying the logarithm to relation (11) the equation of a straight line can be obtained:

$$\ln D+\ln\left(1+\frac{K_a}{[H^+]}\right)=\ln K_E+\ln[Q_{(o)}] \tag{12}$$

Graphical representation of this equation is presented in Fig. 9 for the extraction systems studied. From the slope of the straight line given by equation it is possible to determine the number of Amberlite LA-2 molecules, n, that participate in the formation of the interfacial adduct, and from its intercept the value of the extraction constant, K_E.

According to Fig. 9, independent on the polarity of the solvent, the number of amine molecules involved in the interfacial complex is 1 (Table 2), but the values of the extraction constant (Table 2) are dependent on the the polarity of the organic phase. The results obtained pointed out that, compared to the results recorded for the reactive extraction of 2-ketogluconic acid with Amberlite LA-2 without 1-octanol [20], the addition of the phase modifier changed the number of amine molecules included in the interfacial complex from 2 to 1 for n-heptane and butyl acetate, while for the dichloromethane the complex remained unchanged.

The phase modifier increases the polarity of the organic phase, thus preventing the formation of aminic aducts, effect that is less important in the case of dichloromethane with higher dielectric constant than the other two analyzed solvents.

To confirm these results the loading ratio, Z has been calculated and the results are presented in Table 3. The distribution coefficient increases with extractant concentration and also with the dielectric constant of the three solvents considered for the study.

The change in the loading ratio with Amberlite LA2 concentration occurs only when complexes having more acid molecules are formed at lower concentrations of the extractant and complexes having more extractant molecules are formed if the solvent phase is highly loaded usually at low extractant concentration and high acid concentrations. Since there is a decrease in the loading ratio by increasing extractant concentration, it can be confirmed that only complexes having one single amine molecule are formed [41].

3.4. Stripping analysis

In order to regenerate the acid from the loaded organic phase, the back-extraction of the bound 2-ketogluconic acid into water, is required. To this purpose, the 2-ketogluconic acid- Amberlite LA-2 complex needs to be split. The addition into the extract of an aqueous phase with a superior pH value (sodium hydroxide, pH 12) will generate the transformation of the carboxylic acid into its salt. The increase in temperature to 50 °C favored this reaction by reducing the complexation constant, thus increasing the recovery rate. The overall reactions can be written as

Table 2
Values of n and extraction constants for extraction systems with 1-octanol and Amberlite LA2.

Solvent	n	Ke, (L/mol)
n-heptane/octanol	0.788	11.94
Butyl acetate/octanol	0.86	65.95
Dichloromethane/ octanol	1.17	311.6

Table 3
Loading factor and distribution coefficient variation with Amberlite LA-2 concentration.

Solvent	$C_{ALA2,}$ mol/L	D	Z
n-heptane + octanol	0.053	0.41	0.034
	0.107	0.83	0.030
	0.214	1.22	0.018
	0.321	1.43	0.013
Butyl acetate + octanol	0.053	1.00	0.046
	0.107	1.57	0.041
	0.214	1.79	0.022
	0.321	2.52	0.016
Dichloromethane + octanol	0.053	1.33	0.078
	0.107	2.26	0.047
	0.214	3.67	0.028
	0.321	3.98	0.020

follows:

The results obtained for the back-extraction of 2-ketogluconic acid from the three analyzed solvents and 10% 1-octanol added at different aqueous phase initial pH values, are presented in Fig. 10 and for different concentrations of extractant (differently loaded organic phases) in Table 4 and can be discussed using the hydration theory and the salting in effect.

According to the hydration theory, by sodium hydroxide dissolution corresponding to an aqueous phase pH of 12, the dipoles of polar water molecules arrange themselves around the ions present in the solution (Na^+, OH^-) and form a layer of oriented dipoles surrounding them. During the striping intense mixing and intimate contact between the aqueous solution and the extract containing 2-ketogluconic acid, the ionization strength of the acid increases due to higher concentration of alkali Na^+ cations (electron acceptor) in the aqueous phase and therefore a higher amount of R-COO^- (carboxylate anions) becomes present in the aqueous phase, which results in a strong decrease of 2-ketogluconic acid solubility in all considered solvents (salting in effect).

The highest values of stripping efficiency were obtained for the solvent with the higher polarity: dichloromethane - octanol, in relations to highest extraction efficiency that will allow high concentration of 2-ketogluconic acid in the extract (Table 4).

3.5. Process modelling

The extraction efficiency was determined as a function of the type of process (extraction or back-extraction) –x1–, the dielectric constant of the solvent –x2–, the octanol concentration –x3-, pH of the solution –x4–, ALA-2 concentration –x5–. First, a linear regression approach was applied, resulting in the model represented in Eq (13). For this relation the coefficient of determination is 0.83 with residuals varying from −25.04 to 24.55 and an average relative error (ARE) of 29.21%. These high values indicated that the current process is not well approximated by a linear relation and that there are complex interactions between the process parameters that influence the extraction behavior.

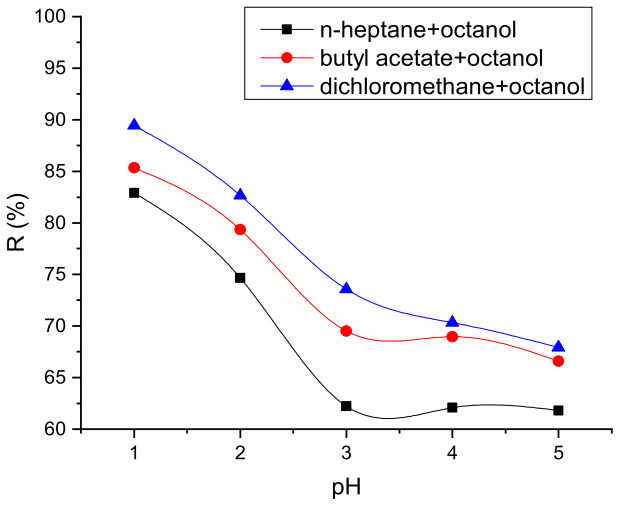

Fig. 10. Influence of initial phase pH on back extraction efficiency.

In case of ANN based modelling, part of the topology is fixed and determined by the number and type of process parameters. Therefore, there are 5 inputs and 1 output, corresponding to the same parameters considered for the linear regressing approach: type of process (extraction or back-extraction), the dielectric constant of the solvent, the octanol concentration, pH of the solution and ALA-2 concentration. The maximum number of hidden layers is set to two, with maximum number of neurons in the hidden layers 20 and respectively 10. Based on these limitations, the modified DE version performs the training (determination of the optimal values for weights, biases, activation functions and their parameters) and identifies the topology (number of hidden layers and neurons in each layer). The parameters of the DE are as follows: number of individuals in the population 80, number of iterations 1500. The F and Cr parameter for DE are included into a self-adaptive procedure that automatically modified them based on the search space characteristics (within the [0,1] interval).

Due to the random nature of DE (that dependents at different stages of evolution on random number generators), a set of 50 simulations were performed. Also, since for ANN determination, it is a standard approach to split the data into at least training and testing subsets, in this work the available dataset (93 exemplars) was split into 75% training and 25% testing (with data randomly assigned into one of the two groups). In addition, the data was normalized and transformed to the [0,1] interval using the Min-Max approach. In Table 5, the fitness indicates the suitability of the models to the environment (computed based on the Mean Squared Error -MSE- in the testing phase).

In Table 5, the best and worst models were selected based on their Fitness, the higher the value, the better the performance.

$$R(\%) = 35.60598926 - 28.47870249*x1 + 1.973979664*x2 + 2.054068788*x3 - 4.102307221*x4 + 0.357362289*x5 \quad (13)$$

$$\left.\begin{array}{l}(ALA2H^+, 2\text{-}KGluCOO^-)_{org} \leftrightarrow ALA2_{org} + 2\text{-}KGluCOOH_{aq} \\ 2\text{-}KGluCOOH_{aq} + HO^-_{aq} \leftrightarrow 2\text{-}KGluCOO^-_{aq} + H_2O\end{array}\right\}$$

$$(ALA2H^+, 2\text{-}KGluCOO^-)_{org} + HO^-_{aq} \leftrightarrow ALA2_{org} + 2\text{-}KGluCOO^-_{aq} + H_2O$$

Table 4
Extractant concentration influence on stripping ([2-KGA$_{(org)}$] − 2-KGA concentration in the organic phase before back-extraction).

Extractant concentration	[2-KGA$_{(org)}$], g/L	R, %	[2-KGA$_{(org)}$], g/L	R, %	[2-KGA$_{(org)}$], g/L	R, %
Solvent	n-heptane + octanol		butyl acetate + octanol		dicholoromethane + octanol	
20	0.25	55.42	0.34	64.65	0.42	69.34
40	0.45	62.24	0.60	69.51	0.69	73.56
80	0.54	69.67	0.69	77.09	0.86	82.51
120	0.58	73.85	0.71	78.36	0.93	87.23

Table 5
Statistics of the ANN models determined.

	Fitness	MSE train	MSE test	Correlation train	Correlation test	Topology
Best	467.6439	0.002138	0.19781	0.987675	0.9664	5:05:00:01
Worst	103.86	0.009628	0.216542	0.942022	0.9473	5:05:00:01
Average	136.6564	0.008067	0.21244	0.952303	0.951287	

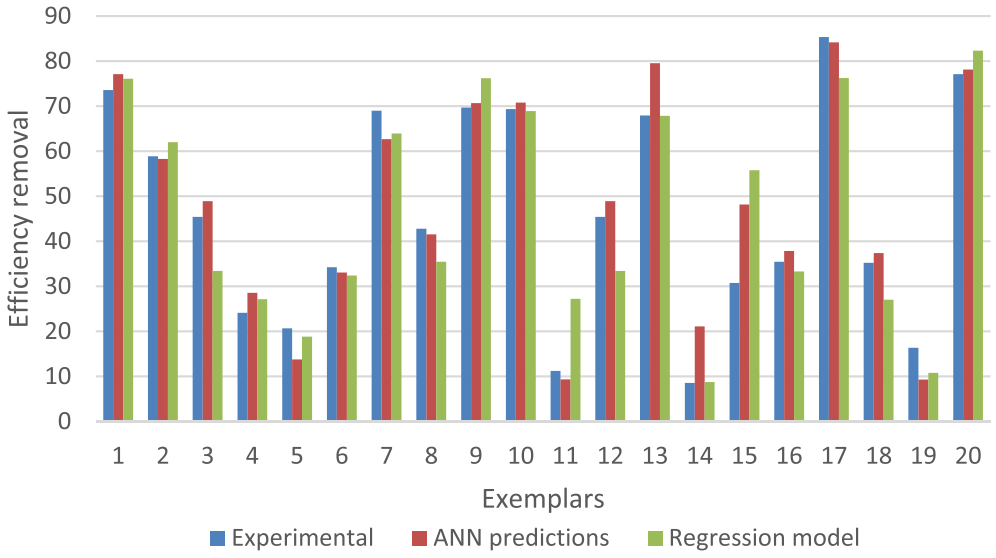

Fig. 11. Comparison between the ANN predictions and the regression model.

For both the best and the worst models the topology determined was similar. However, from the 50 models determined, the topology varied substantially. For the best model, the residuals varied within the [-17.4, 10.58] interval and the ARE is 19.41 for the testing phase and 19.42 for the training phase. A point by point comparison between the predictions generated for the testing data by the best ANN determined and the regression model is presented in Fig. 11.

The mathematical relations implemented in Python that describe the ANN model are represented by Eqs. (14)–(25), presented in Apendix. These relations can be further used to generate predictions for additional combinations of parameters. Although it is possible to test any combination of parameters, for the best predictions and lowest errors, it is indicated to use values within the limits indicated by the last differential term from Eqs. (14)–(18), presented in Appendix.

4. Conclusions

The downstream processing of dilute aqueous solutions from biotechnological processes is a key challenge in order to obtain a bio-based competitive economy that can be achieved by the use different synergies and classic methods improvement. The 2-ketogluconic acid production through biosynthesis is an extremely important process because of its multiple applications in food, cosmetic and pharmaceutical industries; reactive extraction could represent an advantageous alternative to current used downstream processes. Experimentally the highest extraction yield (69.4% for heptane, 86.4% for butyl acetate and 92.3% for dichloromethane) and distribution coefficient (1.43 for heptane, 2.52 for butyl acetate and 3.98 for dichloromethane) are achieved for pH of 3 and 120 g/L extractant, for all the studied solvents. The addition of 1-octanol as polar modifier strongly increased the extraction efficiency for all solvents, with bigger values for the inactive organic solvent with the lowest dielectric constant (n-heptane). The process was modeled using linear regression and ANNs modeled with DE. The errors from the linear regression were relatively high, indicating that, for the considered process, a linear model cannot efficiently provide the necessary generalization. The ANNs had lower errors compared with the regression, the average relative error being reduced to 19.41% in the testing phase.

CRediT authorship contribution statement

Lazar Roxana Georgiana: Investigation, Conceptualization, Formal analysis. **Blaga Alexandra Cristina:** Writing - original draft, Writing - review & editing. **Dragoi Elena Niculina:** . **Galaction Anca Irina:** Validation, Writing - review & editing. **Cascaval Dan:** Validation, Writing - review & editing, Supervision, Project administration.

Declaration of Competing Interest

The authors declare that they have no known competing financial interests or personal relationships that could have appeared to influence the work reported in this paper.

Appendix

$$INP_0 = -1E-20+0.001+(ProcessType-0)*(0.999-0.001)/(1-0) \tag{14}$$

$$INP_1 = -1E-20+0.001+(DielectricConstant-1.9)*(0.999-0.001)/(9.08-1.9) \tag{15}$$

$$INP_2 = -1E-20+0.001+(OctanolConcentration-0)*(0.999-0.001)/(10-0) \tag{16}$$

$$INP_3 = -1E-20+0.001+(pH-1)*(0.999-0.001)/(6-1) \tag{17}$$

$$INP_4 = -1E-20+0.001+(ALA2Concentration-20)*(0.999-0.001)/(120-20) \tag{18}$$

$$H1_0 = math.abs(+INP_0*0.510620482213915+INP_1*0.0311292282251747+INP_2*0.0597498867978941 +INP_3*0.940690751637173+INP_4*-0.742620724622526+-0.814809837991477) \tag{19}$$

$$H1_1 = math.sin(+INP_0*-0.539603386095338+INP_1*0.497221060183135+INP_2*0.251843642359137+INP_3* -0.555739731205647+INP_4*0.958461235459178+-0.367227552195319) \tag{20}$$

$$H1_2 = (2.0/(1.0+math.exp(-2*(+INP_0*0.138125162694939+INP_1*-0.2962553882786+INP_2*0.224173158392771 +INP_3*0.3500631583339+INP_4*0.654599716670967+0.300550217709745)))-1.0) \tag{21}$$

$$H1_3 = max(0,+INP_0*-0.963247176175909+INP_1*-0.0741058295528126+INP_2*-0.0628537692916737+INP_3* -0.965357950529181+INP_4*-0.0406610143816796+0.738616319779838) \tag{22}$$

$$H1_4 = (1.0/(1.0+math.exp(-0.749280472006278*(+INP_0*0.495726140070667+INP_1*-0.583084930431651+INP_2* -0.402381544618572+INP_3*0.245431860978348+INP_4*-0.435081543935651+0.39068309943157)))) \tag{23}$$

$$OUTPUT_1 = math.abs(+H1_0*-0.785000562668162+H1_1*0.585632535504261+H1_2*0.718711298955677 +H1_3*0.999224127083383+H1_4*-0.533548224447293+0.688466558620135) \tag{24}$$

$$Efficiency = (OUTPUT_1+1E-20-0.001)*(92.367-2.68)/(0.999-0.001)+2.68 \tag{25}$$

References

[1] W. Zeng, W. Cai, L. Liu, G. Du, J. Chen, J. Zhou, Efficient biosynthesis of 2-keto-D-gluconic acid by fed-batch culture of metabolically engineered *Gluconobacter japonicas*, Synth. Syst. Biotech. 4 (2019) 134–141.

[2] L. Sun, D.-M. Wang, W.-J. Sun, F.-J. Cui, J.-S. Gong, X.-M. Zhang, J.-S. Shi, Z.-H. Xu, Two-Stage Semi-Continuous 2-Keto-Gluconic Acid (2KGA) Production by *Pseudomonas plecoglossicida JUIM01* From Rice Starch Hydrolyzate, Front. Bioeng. Biotech. 8 (2020) 1–10.

[3] K. Li, X. Mao, L. Liu, J. Lin, M. Sun, D. Wei, S.i Yang, Overexpression of membrane-bound gluconate-2-dehydrogenase to enhance the production of 2-keto-d-gluconic acid by *Gluconobacter oxydans*, Microb. Cell. Fact. 15 (2016) 121–131.

[4] W.-J. Sun, Y.-Z. Zhou, Q. Zhou, F.-J. Cui, S.-L. Yu, L. Sun, Semi-continuous production of 2-keto-gluconic acid by *Pseudomonas fluorescens AR4* from rice starch hydrolysate, Bioresour. Technol. 110 (2012) 546–551.

[5] M. Chia, T.B. Van Nguyen, W.J. Choi, DO-stat fed-batch production of 2-keto-d-gluconic acid from cassava using immobilized *Pseudomonas aeruginosa*, Appl. Microbiol. Biotechnol. 78 (2008) 759–765.

[6] Y. Weichao, X. Hui, Industrial Biotechnology of Vitamins, Biopigments, and Antioxidants, First Edition. Edited by Erick J. Vandamme and José L. Revuelta. 2016 Wiley-VCH Verlag GmbH & Co. KGaA.

[7] CN102329226A - Method for separating and extracting 2-keto-D-gluconic acid – Patent.

[8] M. Benoit, M. Michel, P. Laurent, A. Frédéric, L.-L.-C. Damien, General design methodology for reactive liquid–liquid extraction: Application to dicarboxylic acid recovery in fermentation broth, Chem. Eng. Process. 113 (2017) 20–34.

[9] A. Emine, B. Nilay, C. Süheyla, Optimization of reactive extraction of propionic acid with ionic liquids using central composite design, Chem. Eng. Res. Des. 153 (2020) 666–676.

[10] P. Shitanshu, K. Sushil, Reactive extraction of gallic acid from aqueous solution with Tri-noctylamine in oleyl alcohol: Equilibrium, Thermodynamics and optimization using RSM-rCCD, Sep. Purif. Technol. 231 (2020), 115904.

[11] L. Kloetzer, R.-A. Ilica, D. Cascaval, A.-I. Galaction, Separation of fumaric acid by amine extraction without and with 1-octanol as phase modifier, Sep. Purif. Technol. 227 (2019), 115724.

[12] K. Prochaska, J. Antczak, M. Regel-Rosocka, M. Szczygiełda, Removal of succinic acid from fermentation broth by multistage process (membrane separation and reactive extraction), Sep. Purif. Technol. 192 (2018) 360–368.

[13] A. Krzyżkowska, M. Regel-Rosocka, The effect of fermentation broth composition on removal of carboxylic acids by reactive extraction with Cyanex 923, Sep. Purif. Technol. 236 (2020), 116289.

[14] M. Alexandri, A. Vlysidis, H. Papapostolou, O. Tverezovskaya, V. Tverezovskiy, I. K. Kookos, A. Koutinas, Downstream separation and purification of succinic acid from fermentation broths using spent sulphite liquor as feedstock, Sep. Purif. Technol. 209 (2019) 666–675.

[15] T. Brouwer, M. Blahusiak, K. Babic, B. Schuur, Reactive extraction and recovery of levulinic acid, formic acid and furfural from aqueous solutions containing sulphuric acid, Sep. Purif. Technol. 185 (2017) 186–195.

[16] M. Djas, M. Henczka, Reactive extraction of carboxylic acids using organic solvents and supercritical fluids: A review, Sep. Purif. Technol. 201 (2018) 106–119.

[17] D. Caşcaval, L. Kloetzer, A.-I. Galaction, Influence of Organic Phase Polarity on Interfacial Mechanism and Efficiency of Reactive Extraction of Acetic Acid with Tri-n-octylamine, J. Chem. Eng. Data 56 (2011) 2521–2526.

[18] N. Mungma, M. Kienberger, M. Siebenhofer, Reactive Extraction of Lactic Acid, Formic Acid and Acetic Acid from Aqueous Solutions with Tri-n-octylamine/1-Octanol/n-Undecane, Chem. Eng. 3 (2019) 43–56.

[19] Y.K. Hong, W.H. Hong, Extraction of succinic acid with 1-octanol/n-heptane solutions of mixed tertiary amine, Bioproc. Biosyst. Eng. 23 (5) (2000) 535–538.

[20] A.C. Blaga, A.-I. Galaction, D. Caşcaval, Reactive extraction of 2-keto-gluconic acid 1. Mechanism and influencing factors, Rom. Biotech. Lett. 15 (3) (2010) 5253–5259.

[21] A. Yardimci, Soft computing in medicine, Appl. Soft Comput. 9 (2009) 1029–1043.

[22] E.A. Del Rio-Chanona, E. Manirafasha, D. Zhang, Q. Yue, K. Jing, Dynamic modeling and optimization of cyanobacterial C-phycocyanin production process by artificial neural network, Algal Res. 13 (2016) 7–15.

[23] E.-N. Dragoi, S. Curteanu, D. Cascaval, A.-I. Galaction, Artificial Neural Network modeling of mixing efficiency in a split-cylinder gas-lift bioreactor for *Yarrowia lipolytica* suspensions, Chem. Eng. Commun. 203 (2016) 1600–1608.
[24] C. Murugan, P. Natarajan, Estimation of fungal biomass using multiphase artificial neural network based dynamic soft sensor, J. Microbiol. Methods 159 (2019) 5–11.
[25] P. Moodley, D.C. Rorke, E.B.G. Kana, Development of artificial neural network tools for predicting sugar yields from inorganic salt-based pretreatment of lignocellulosic biomass, Bioresour. Technol. 273 (2019) 682–686.
[26] R.R. Kalantary, M. Moradi, M. Pirsaheb, A. Esrafili, A.J. Jafari, M. Gholami, Y. Vasseghian, E. Antolini, E.-N. Dragoi, Enhanced photocatalytic inactivation of *E. coli* by natural pyrite in presence of citrate and EDTA as effective chelating agents: Experimental evaluation and kinetic and ANN models, J. Environ Chem. Eng. 7 (2019), 102906.
[27] V. Bhushanam, R. Malothu, Bioprocess optimization of L-Lysine production by using RSM and artificial neural networks from *Corynebacterium glutamicum* ATCC13032, Chem. Prod. Process. Model. 1 (2020).
[28] S. Sufang, L. Guorui, W. Yanhuan, Z. Yan, L. Cuifen, S. Yongmei, Simultaneous determination of 2-keto-L-Gulonic acid and 2-keto-D-Gluconic acid in fermentation broth by HPLC, Chem. J. Internet 9 (8) (2007) 35–41.
[29] N. Marchitan, C. Cojocaru, A. Mereuta, G.h. Duca, I. Cretescu, M. Gonta, Modeling and optimization of tartaric acid reactive extraction from aqueous solutions: A comparison between response surface methodology and artificial neural network, Sep. Purif. Technol. 75 (3) (2010) 273–285.
[30] A. Senol, Optimal extractive separation of chromium (VI) from acidic chloride and nitrate media by commercial amines: equilibrium modeling through linear solvation energy relation, Ind. Eng. Chem. Res. 52 (2013) 16321–16334.
[31] A. Senol, Liquid–liquid equilibria for ternary systems of (water + carboxylic acid + 1-octanol) at 293.15 K: modeling phase equilibria using a solvatochromic approach, Fluid Phase Equilib. 227 (2005) 87–96.
[32] H. Uslu, A. Gök, Ş.İ. Kırbaşlar, Phase equilibria of (water + levunilic acid + alcohol) ternary systems, Fluid Phase Equilib. 273 (2008) 21–26.
[33] H. Ghanadzadeh, A. Ghanadzadeh, S. Asgharzadeh, M. Moghadam, Measurement and correlation of phase equilibrium data of the mixtures consisting of butyric acid, water, cyclohexanone at different temperatures, J. Chem. Thermodyn. 47 (2012) 288–294.
[34] A.C. Blaga, T. Malutan, Selective Separation of Vitamin C by Reactive Extraction, J. Chem. Eng. Data 57 (2) (2012) 431–435.
[35] L. Kloetzer, A.S. Bompa, A.C. Blaga, A.I. Galaction, D. Cascaval, Study on rosmarinic acid separation by synergic extraction, Sep. Sci. Technol. 53 (2018) 645–654.
[36] V. Moses, M. Calvin, The path of carbon in photosynthesis. XXII. The identification of carboxyketopentitol diphosphates as products of photosynthesis, Proc. Natl. Acad. Sci., 1958, 260.
[37] R.C. Weast, Handbook of Chemistry and Physiscs, 54th ed., CRC Press, Cleveland, 1974.
[38] R. Canari, A.M. Eyal, Selectivity in Monocarboxylic Acids Extraction from Their Mixture Solutions Using an Amine-Based Extractant: Effect of pH, Ind. Eng. Chem. Res. 42 (2003) 1301–1307.
[39] L.M.J. Sprakel, B. Schuur, Solvent developments for liquid-liquid extraction of carboxylic acids in perspective, Sep. Purif. Technol. 211 (2019) 935–957.
[40] J.A. Tamada, A.S. Kertes, C.J. King, Extraction of carboxylic acids with amine extractants. 1. Equilibria and law of mass action modelling, Ind. Eng. Chem. Res. 29 (1990) 1319–1326.
[41] A. Eggert, T. Maßmann, D. Kreyenschulte, M. Becker, B. Heyman, J. Büchs, A. Jupke, Integrated in-situ product removal process concept for itaconic acid by reactive extraction, pH-shift back extraction and purification by pH-shift crystallization, Sep. Purif. Technol. 215 (2019) 463–472.

Journal of Molecular Liquids 410 (2024) 125564

Contents lists available at ScienceDirect

Journal of Molecular Liquids

journal homepage: www.elsevier.com/locate/molliq

Experimental, modeling and optimisation of adipic acid reactive extraction using ionic liquids

Elena Niculina Dragoi [a], Alexandra Cristina Blaga [a,*], Dan Cascaval [a], Anca Irina Galaction [b]

[a] "Gheorghe Asachi" Technical University of Iasi, "Cristofor Simionescu" Faculty of Chemical Engineering and Environmental Protection, Iasi, Romania
[b] "Grigore T. Popa" University of Medicine and Pharmacy, Faculty of Medical Bioengineering, Iasi, Romania

ARTICLE INFO

Keywords:
Reactive extraction
Mathematical modelling
Ionic liquid
Adipic acid
[$P_{666.\ 14}$][Phos]

ABSTRACT

Adipic acid (hexanedioic acid, AA) can be utilised as an essential monomer in the production of nylon-6,6 (75 %), but also for urethane foams, fibers, elastomers, tire reinforcements, and synthetic lubricants. Considerable work has been done to develop sustainable biosynthetic processes for its manufacture, especially for adipic acid efficient separation (one of the main challenges for industrialisation). As for scale-up, process optimisation, and thorough engineering mathematical models that describe the system efficiently are required, this study proposes mathematical models for a reactive extraction using ionic liquids as extractants for adipic acid separation to improve the biosynthetic route's sustainability, efficiency, and environmental performance. Heptane as the solvent and 117.8 g/L [$P_{6,6,6,14}$][Phos] as the extractant at 2.8 pH of the aqueous phase were the optimum mixture for reactive extraction, resulting in an extraction yield of 97.55 % for adipic acid. The process was modeled using an artificial neural network optimised with a differential evolution algorithm. The optimal model structure had one hidden layer with 20 neurons, and its performance in the testing phase was: explained variance score of 0.974, mean absolute error of 1.917, and coefficient of determination of 0.974.

1. Introduction

Within the ever-evolving domain of chemical process modeling and optimisation, Artificial Intelligence (AI) tools emerged as a powerful alternative that redefined and improved the notion of efficiency. AI can be used to find deeper insights into the complex areas of process parameter influence, nonlinear process dynamics, and intricate system interactions, which are being decoded with remarkable precision.

As an essential platform chemical, adipic acid (AA) is employed in many industrial sectors, such as food additives, lubricants, and nylons. Adipic acid's extensive range of uses in nylon-6,6-related activities, including being an essential component in its manufacture, drives its use in particular. Over 3 million tonnes of AA are produced globally yearly, and demand has risen at about 4 % per year [1–3]. The AA manufacturing market is expected to rise further, given that the world's production of nylon-6,6 was around 1.4 million tonnes in 2022. A consistent increase in the compound yearly growth rate of 5.09 % until 2035 is anticipated.

The main possibilities for producing AA are chemical, biological, and biochemical [4–7]. The most common industrial method is the chemical one, which involves the chemical oxidation of a mixture of cyclohexanone and cyclohexanol ("KA oil" – ketone and alcohol-oil). Petroleum, a non-renewable resource, can be used as a source of raw materials for this energy-intensive process that generates toxic products and uses harsh reaction conditions. The development of feasible, environmentally friendly, and sustainable alternative synthesis techniques for producing AA is in high demand. Several microorganisms have been genetically modified to produce AA through biosynthesis [7–15]. Using direct or indirect fermentation combined with chemical conversion, AA can be produced from biomass raw materials. For instance, the Verdezyne company uses a genetically modified yeast species to transform fatty acid into AA using a two-stage fed-batch method with 98 % selectivity.

Despite its advantages, separating adipic acid from fermentation broths is still a somewhat complex process. Although reliable, traditional separation techniques – crystallisation, membrane separation, and chromatography – stumble upon process bottlenecks due to high energy demands and scaling difficulties. Reactive extraction has emerged as a promising method for extracting important solutes due to the combination of chemical and physical processes that increase the extraction yield. By accelerating mass transfer and chemical reaction

* Corresponding author at: "Gheorghe Asachi" Technical University of Iasi, "Cristofor Simionescu" Faculty of Chemical Engineering and Environmental Protection, D. Mangeron Av., no 67, Iasi, Romania.
E-mail address: acblaga@tuiasi.ro (A.C. Blaga).

https://doi.org/10.1016/j.molliq.2024.125564
Received 29 March 2024; Received in revised form 12 July 2024; Accepted 17 July 2024
Available online 20 July 2024

rates, combining the two processes results in a larger solute distribution coefficient and increased extraction efficiency. Reactive extraction is also highly valued for its ease of use, technical accessibility, temperate conditions, and potential for using inexpensive, environmentally friendly, and effective chemicals. The present techniques for separating adipic acid have several shortcomings, such as low efficiency and higher final product costs, since the separation processes are highly complex and involve a lot of time and effort. Furthermore, volatile chemical solvents that pose a risk are frequently utilised. Owing to these disadvantages, creating more environmentally friendly extraction and purification techniques is imperative. One such technique that has generated interest is the application of ionic liquids (ILs) and deep eutectic solvents (DES), which have been suggested as promising extractants for carboxylic acids like lactic, butyric, and acetic due to their superior solvation ability.

The method of reactive extraction for separating organic acids from fermentation's aqueous stream has been the subject of numerous investigations [16–21]. Liu et al. (2023) analysed carboxylic acid extraction performance using a hydrophobic deep eutectic solvent composed of amides (N, N-di-n-butylacetamide and N, N-di-n-butylbutamide) and geraniol through molecular dynamics simulations and proved hydrogen bond-induced geraniol-carboxylic acid and amide-carboxylic acid multimolecular assembly for acetic, succinic and L-lactic acid [16]. In their review of the synthesis, physiochemical properties, and uses of TBP-based ILs, including the extraction of biomolecules, Akhlaq et al. (2024) showed that the ILs anions are tunable and the physiochemical properties of ILs may be tailored by selecting the right ones [17]. Zheng et al. (2024) examined the molecular mechanism underlying rutin's interaction with six imidazolium-based ILs ([bmim][TsO], [bmim][TfO], [bmim][Tf2N], [bmim][Br], [Bbmim][Br], [Bmbmim][Br]), demonstrating that electrostatic interactions between the anion and rutin, as well as van der Walls interactions between the cation and rutin, are the primary drivers of this interaction. While cations and anions may both form H-bonds with rutin, anions have a much stronger ability to do so than cations. On the other hand, cations' slight ability to increase the stability of the complexes system through cation-π stacking is what makes them distinctive. Consequently, increasing the stability of the complex system requires the anion and cation to work together in a synergistic manner [20]. In their assessment of the DES field of study, Prabhune and Dey (2023) concentrated on the several types of DESs, their potential for synthesis, and their commercial uses as sustainable and green solvents. Along with theoretical and computational models, their regeneration, scalability for industrial applications, and potential commercial uses have also been analysed. Gao *et al.* (2024) investigated metal separation and oil recovery from highly oily waste with a novel green hydrophobic DES synthesised from ethyl maltol and fatty acids, with an oil extraction efficiency of about 86.3 %, a dehydration rate surpassing 92 %, and a heavy metal removal rate ranging from 15 % to 75 %, at 60 °C [22,23].

Lang *et al.* (2021) analysed the latest advances in sustainable adipic acid production using biomass-based processes. They highlighted that the major challenge of its industrial production is adipic acid separation from aqueous solutions [24]. Based on an in-depth literature review, minimal research has been done for adipic acid separation from diluted aqueous solutions. Riveiro et al (2020) analysed trioctylphosphine oxide-based deep eutectic solvents: TOPO-Decanoic acid and TOPO-Dodecanoic acid for liquid–liquid separation of organic acids (adipic, levulinic and succinic acids) in aqueous solution and the performance of the DESs was compared with TOPO, the best extraction efficiencies obtained with TOPO [25]. However, studies that employ statistical techniques on the experimental design of adipic acid recovery from aqueous solution using an intensified process, such as a reactive liquid–liquid separation process, are missing in the literature.

Reactive extraction using a mixture of ionic liquids and heptane is an alternative for separating biosynthetic products (ascorbic acid, folic acid, muconic acid [26–29]) but requires numerous experiments with large raw material and time consumed. Innovative modeling and optimisation methods suited to the complexity posed by the adipic acid separation process are required to solve these problems. Integrating advanced computational approaches, particularly neuro-evolutionary techniques, holds the promise of solving this complex task. Neuro-evolution combines evolutionary algorithms with neural networks (ANNs) to tackle the complex problem of identifying the optimal ANN configuration in a multi-dimensional search space. It is based on the adaptive mechanics of evolutionary computation, which systematically mutates, recombines, and selects network parameters, resulting in neural architectures that increasingly fit the characteristics of the problem being solved [30,31]. The advantage of neuro-evolution relies on the iterative nature of the evolutionary process in combination with the use of performance metrics suited for multi-dimensional and non-linear landscapes.

In this context, in this work, ANNs were combined with differential evolution (DE). ANNs are well-recognised for their capability to identify complex and high-dimensional relationships within data sets, a characteristic especially useful for modeling the intricate variables seen in chemical processes [31]. Examples of applications where ANNs were effectively applied include: i) reactive extraction of itaconic acid [32], gallic acid [33], and malic acid [34]; ii) supercritical fluid extraction of phytochemicals [35]; iii) ultrasound extraction of phytocompounds [36,37]. In contrast, the DE algorithm is known for its performance in solving global optimisation problems, navigating through multiple local optima landscapes, and identifying robust, high-fidelity solutions [38]. This combination is motivated by the hypothesis that DE's adaptability and global search properties can be harnessed to optimise both the architecture and parameters of ANNs, potentially leading to models with superior predictive accuracy and generalisation capacity [38–40]. Examples of successful applications of DE (simple or in combination with other algorithms or methods include): i) pertraction of vitamin C [41]; ii) reactive extraction of pseudomonic acids [42], folic acid [26], and gallic acid [43].

The experimental analysis considering for the first time phosphonium-based ILs as extractants for adipic acid reactive extraction, combined with the modelling and optimisation procedure based on ANNs and DE, represent the current work's novelty. The selection of the appropriate extractant considered environmental impact, extraction capabilities, cost-effectiveness, and selectivity. Since this research will be the first to look into the separation of adipic acid by hydrophobic ionic liquids, it will provide crucial information for the future development of a plan for adipic acid recovery from the fermentation broth. The investigation carried out is based on the hypothesis that neuro-evolution applied to the separation of adipic acid can maximise efficiency through a series of parameter combinations that might be overlooked by traditional methodologies. This is based on the adaptability and learning capacity inherent to neuro-evolution, which can lead to optimised process parameters, hence minimising energy and chemical consumption while maximising yield.

2. Material and methods

2.1. Chemical and methods

All chemicals, including adipic acid (99.0 %), [$P_{6,6,6,14}$][Phos] – Trihexyltetradecylphosphonium bis(2,4,4-trimethylpentyl)phosphinate, [$P_{6,6,6,14}$][Dec] – Trihexyltetradecylphosphonium decanoate, [C_8mim][PF_6] – 1-octyl-3-methyl-imidazolium-hexafluorophosphate, [C_6mim][PF_6] – 1-hexyl-3-methyl-imidazolium-hexafluorophosphate, [C_4mim][PF_6] – 1-butyl-3-methyl-imidazolium-hexafluorophosphate, heptane (99 %), sodium hydroxide (>97 %), sulfuric acid (95.0–98.0 %), sodium phosphate (99.9 %) and acetonitrile (99.99 %), were purchased by Sigma Aldrich and used as received without further processing. The AA reactive extraction experiments were realised using equal amounts of aqueous and organic phases (2 mL, 1:1 v/v ratio), and were conducted using a

vibratory shaker operating at 1200 rpm. To ensure enough interfacial contact, the extraction tests were conducted for 5, 10, 20, and 30 min at 20 °C, 30 °C, 40 °C, and 50 °C. Phases were separated in a centrifugal separator operating at 4000 rpm following the extraction. For quantitative analysis, the raffinate aqueous phase was analysed through HPLC. Ionic liquid concentrations in the organic phase varied from 0 to 120 g/L, while the initial concentration of AA in the aqueous phase was 10 g/L (initial aqueous phase pH 4). During the extraction, the aqueous phase's pH value was adjusted to range from 2 to 6, being modified by using solutions of 4 % sulfuric acid or sodium hydroxide employing the indications of the digital pH meter (CONSORT C 836). The process was analysed based on extraction efficiency and distribution coefficient, calculated using the mass balance based on the AA concentration.

The distribution coefficient can be defined as the ratio between adipic acid concentration in the extract–organic phase, $[AA]_{org}$, and its concentration in the raffinate (exhausted aqueous phase), $[AA]_{aq}$ at equilibrium.

$$D = \frac{[AA]_{org}}{[AA]_{aq}} \quad (1)$$

Extraction efficiency can be defined as the ratio of AA concentration in the extract ($[AA]_{org}$) to the AA concentration in the initial aqueous phase $[AA]_{in}$:

$$E = \frac{[AA]_{org}}{[AA]_{in}} * 100, \ \% \quad (2)$$

AA concentration in the aqueous phases was measured by the high-performance liquid chromatography technique (HPLC). For this purpose, an UltiMate 3000 Dionex HPLC system was equipped with a Hypersil Gold column. The system operated with a mobile phase consisting of 35 % acetonitrile and 65 % sodium phosphate, with a flow rate of 0.75 ml/min. Detection at 210 nm was used.

2.2. Modelling and optimisation

A successful neuro-evolutionary approach is based on a foundation of high-quality experimental data. This data informs and shapes the predictive effectiveness of the resulting models, the entire modelling and simulation process starting with the acquisition of experimental data that includes variables and conditions observable in adipic acid separation processes. However, the need for extensive data for the ANN training in general and the neuro-evolutive approach, in particular, cannot always be met by experimental data due to the high limitations imposed by time and resources (experienced researchers, laboratory setup, chemicals consumed). As such, a data interpolation strategy is applied in this work. The objective is to extract information from a combination of two parameters while keeping the others fixed and applying an order three logistic regression approach. In this manner, from 32 experiments, a set of 298 points were extracted. After that, this data undergoes a series of preprocessing steps, pivotal for enhancing the signal-to-noise ratio and ensuring the relevance of the information that will be subsequently used. Normalisation standardizes the scale across different inputs while outlier detection and removal preserve the integrity of the dataset. These preprocessing techniques are essential to identifying an optimal neural network architecture that can effectively generalize unseen data. In this work, the normalization procedure applied in Min-Max [44] and a dataset analysis indicated no significant outliers.

Next, the data is partitioned into training and testing sets, a strategy indispensable for evaluating the generalization capabilities. The training set is used for the development of the ANNs and for generating the fitness function used by the DE algorithm to refine the structure and parameters iteratively. The validation set provides an unbiased assessment of the model's generalization capability. After initially generating a set of potential solutions (represented by encoded network parameters), DE is used to refine and optimize the architecture while the Adam optimizer performs the training procedure [45]. This phase is pivotal, as it aims to fine-tune the varied parameters – neural weights, biases, and network topology – to converge on an optimal solution that maximizes separation efficiency. With each iteration, DE explores the search space, adjusting and recalibrating the parameters in pursuit of the most advantageous configuration for the best model that fits the problem.

The genetics of the initial population set the stage by providing a varied base from which advantageous traits can emerge. The mutation step introduces necessary randomness, safeguarding the evolutionary trajectory from stagnation. There are various mutation strategies for the DE algorithm, among which DE/2/best was selected. This case uses two differential terms, and the current generation's best solution represents the base individual. The crossover step, synonymous with recombination in biological contexts, propagates favorable traits and introduces novel network topologies, thereby maintaining diversity within the population. The selection step influences the convergence rate and prevents maturation from local minima. A greedy procedure is applied based on the fitness function (represented by Mean Squared Error). The delicate interplay between these components governs the adaptive capacity of neuro-evolutionary systems, ultimately impacting the performance and generalizability of the models developed for intricate tasks such as the separation of adipic acid. Since the steps of the algorithm are controlled by parameters, in order to ensure that they are the best fit for the problem at hand, they are included in the algorithm. They are simultaneously evolved with the individuals (this is known as self-adaptation). In order to ensure tight integration of DE with ANNs, due to the particularities of each approach, an encoding procedure is required to translate the ANN parameters (phenotype) into structures that DE can evolve (genotype). This work applies a direct encoding, where there is a direct link between genotype and phenotype. Moreover, a limit on the maximum allowed topology (maximum of five hidden layers, each with a maximum of 20 neurons) is set to limit the search space to an acceptable area (in correlation with the available data). After the best ANN model for the considered process is determined, the next step consists of identifying the process conditions that lead to a maximization of extraction efficiency. This step is performed using the previously determined model and the DE algorithm. In the case of model optimization, the potential solutions were represented by encoded neural networks; for process optimization, the solutions are represented by the combination of process parameters. As such, the limitations for the solutions change to the characteristics of the process conditions, as obtained during the experimental phase. The other parameters of DE remain unchanged. Fig. 1 presents the general schema of the proposed approach. The code for the resulting model and the script for loading and using it are available at https://elenadragoi.ro/CV/Documents/adipic_acid_model.7z. The Python source code that implements the modelling and optimization strategy and that was used to determine the models detailed in this work is available at https://elenadragoi.ro/CV/Documents/ANNOptimizer.7z.

3. Results and discussions

3.1. Experimental

The solute's physical and chemical characteristics (hydrophobicity, acid-base properties), the extractant's properties (reactivity, ability to form hydrophobic compounds with the solute), and the conditions of the separation (pH, temperature, mixing intensity, concentration level, contact time, kinetics, phase ratio, etc.) all affect the effectiveness of the reactive extraction. These parameters must be balanced and optimized according to the particular system and desired results to reach an effective reactive extraction.

Reactive extraction relies heavily on the selection of extractants and solvents. To enable simple separation and the required extraction

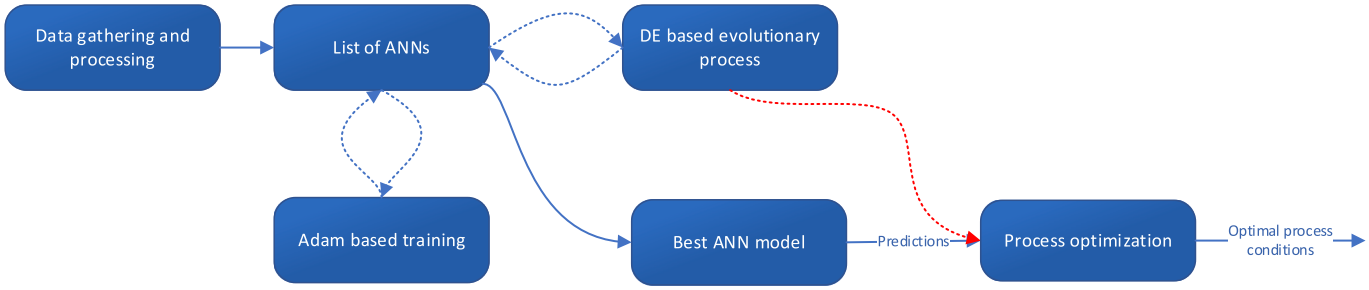

Fig. 1. Modelling strategy.

efficiency, they should have appropriate physical and chemical properties, be environmentally benign, and be immiscible with the aqueous phase. The solubility and partitioning behavior of AA are impacted by organic phase selection, which in turn impacts the extraction efficiency. Ionic liquids may be more environmentally friendly than traditional organic systems, but to ensure sustainable use, it is imperative to carefully analyze their features, application requirements, and environmental impact. In order to find an appropriate extractant for adipic acid separation five hydrophobic ionic liquids were considered: (trihexyl-tetradecyl-phosphonium bis(2,4,4-trimethylpentyl) phosphinate, [$P_{6,6,6,14}$][Phos]; trihexyl-tetradecyl-phosphonium decanoate, [$P_{6,6,6,14}$][Dec]; 1-octyl-3-methyl-imidazolium-hexafluorophosphate, [C_8mim][PF_6]; 1-hexyl-3-methyl-imidazolium-hexafluorophosphate, [C_6mim][PF_6]; 1-butyl-3-methyl-imidazolium-hexafluorophosphate, [C_4mim][PF_6]), based on their properties (water immiscibility and prior used in reactive extraction systems). The results, presented in Fig. 2, prove that only phosphonium ILs can efficiently extract adipic acid from diluted aqueous solutions, due to their superior basicity over imidazolium ILs. These ILs were chosen because of their hydrophobic nature, which renders them practically insoluble in aqueous solutions and facilitates their separation. The most effective ILs, phosphonium-based ILs, have previously been applied in industrial processes and are less costly and more stable than their imidazolium-based equivalents.

High viscosity ILs (319 cP for [$P_{6,6,6,14}$][Dec] and 805 cP for [$P_{6,6,6,14}$][Phos] [27]) can generate difficulties for equipment design and operation as well as for extraction performance.

In light of these results, the analysis of the two more effective hydrophobic ionic liquids ([$P_{6,6,6,14}$][Phos] and [$P_{6,6,6,14}$][Dec]) at different concentrations was conducted for AA extraction. The ILs chosen for AA extraction are hydrophobic. [$P_{6,6,6,14}$] ILs, in particular, are immiscible with water: The solubility at room temperature (20 ± 1 °C) for tri-hexyl-tetra-decyl-phosphonium decanoate [$P_{6,6,6,14}$][Dec], was determined to be 8.7 ± 0.2 mg/L and for tri-hexyl-tetra-decyl-phosphonium bis(2,4,4-trimethylpentyl) phosphinate, [$P_{6,6,6,14}$][Phos], 12.6 ± 0.3 mg/L [46]. The ILs were dissolved in heptane to decrease their high viscosity and to reduce the economic impact, as the price for ionic liquids is higher than that of heptane. The organic solvent (heptane) was chosen for its water insolubility, low toxicity, low density, slow evaporation rate, low boiling point, and relatively low price. The highest extraction efficiency (Fig. 3) was recorded in the case of [$P_{6,6,6,14}$][Phos] dissolved in heptane, 97.55 %, similar to other results obtained in literature for the reactive extraction of folic acid [16] and ascorbic acid [17]. As mentioned before, in order to extract adipic acid from aqueous solutions, Riveiro et al. (2020) investigated two hydrophobic TOPO-based deep eutectic solvents: TOPO-DecAc and TOPO-DodecAc (decanoic or dodecanoic acids). The experimental results revealed inferior extraction efficiency values for TOPO-DecAc and TOPO-Dodec at an initial concentration of 10 g/L: 84.58 % and 83.14 %, respectively, compared to 97.67 % for TOPO [25].

The main stage in the reactive extraction of adipic acid by an ILs extractant is the formation of an acid: ILs complex that is soluble only in the organic phase. In order to analyze the extraction mechanism for AA, the loading factor ($[AA]_{org}/[IL]_{org}$) was calculated (Table 1). The results show a substantial decrease in the loading factor with the increase in extractant concentration, correlated with a higher distribution coefficient. This variation and the values lower than 1, are consistent with no overloading in the formation of the complex, indicating the formation of an equimolecular complex involving only one molecule of both AA and ionic liquid.

The extraction mechanism for ILs containing hydrophobic anion

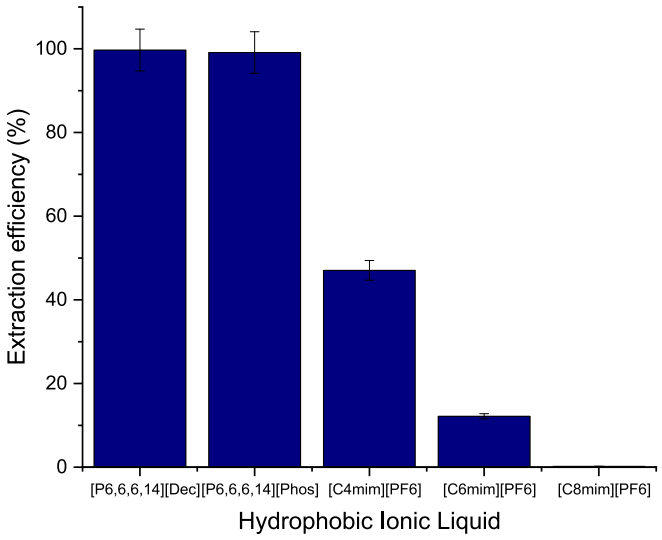

Fig. 2. Effect of ionic liquids on adipic acid extraction efficiency.

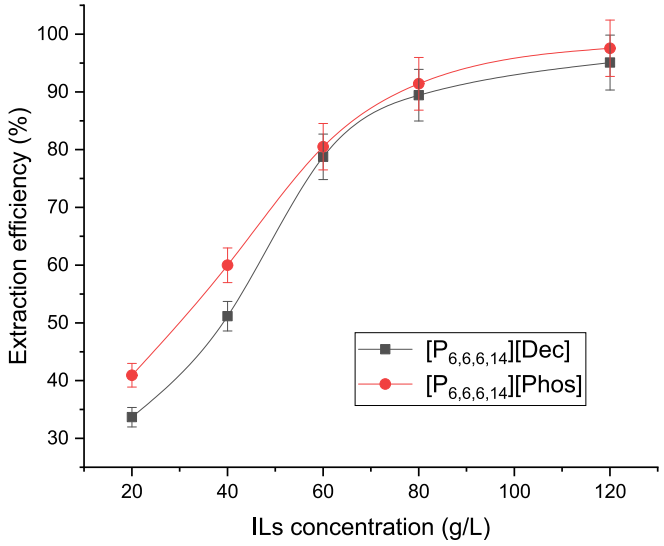

Fig. 3. ILs concentration influence on AA extraction efficiency.

Table 1
Loading factor and distribution coefficient values obtained for ILs in heptane.

	$[P_{6,6,6,14}]$ [Dec], M	D	Loading factor	$[P_{6,6,6,14}]$ [Phos], M	D	Loading factor
1	0.03	0.50	0.69	0.02	0.69	0.97
2	0.06	1.62	0.63	0.05	1.62	0.73
3	0.09	3.70	0.53	0.07	1.94	0.52
4	0.12	8.45	0.45	0.10	6.82	0.52
5	0.18	19.38	0.32	0.15	10.67	0.36

often involves the formation of H-bonds between the ionic liquid and the undissociated form of the organic acid (Fig. 4). The undissociated acid forms an H-bond to the binding sites in the anion of the IL (the oxygen from bis(2,4,4-trimethylpentyl) phosphinate – $[P_{6,6,6,14}]$[Phos] or from decanoate – $[P_{6,6,6,14}]$[Dec]).

The proposed extraction mechanism is supported by the dependence between the separation yield and the pH value of the initial aqueous solution of AA. According to Fig. 5, for both studied extractants, the reactive extraction efficiency increases continuously in the pH range 2–4, reaching its maximum value around pH=4, decreasing then. This variation of the extraction yield could be explained by the dissociation of the AA carboxylic groups, which promotes or avoids the formation of internal H-bonds, directly affecting the interfacial chemical reaction of acid with the extractants. The aqueous phase pH has a very important effect on extraction efficiency as it controls the acid dissociation:

$$\mathrm{HOOC\text{–}(CH_2)_4\text{-}COO\mathbf{H}_{(aq)} \leftrightarrow HOOC\text{–}(CH_2)_4\text{-}COO^-_{(aq)} + H^+},\ pKa_1 = 4.41$$

$$\mathrm{\mathbf{H}OOC\text{–}(CH_2)_4\text{-}COO^-_{(aq)} \leftrightarrow {}^-OOC\text{-}(CH_2)_4\text{-}COO^-_{(aq)} + H^+},\ pKa_2 = 5.41$$

In reactive extraction, AA can interact with the extractant in one of two ways: by hydrogen bonding when it is present as an undissociated molecule or by the formation of ion pairs when AA is present as a dissociated molecule (pH>pKa). Moreover, the pH of fermentation broth varies as acid is produced [18]. Thus, it becomes important to study the influence of the pH on extraction. From the cost perspective, it is beneficial if the separation is realized at a pH close to the one used in the fermentation process, preferably around the pKa of the acid, to avoid the formation of salts when a base is added to maintain the pH thereby reducing the cost of downstream processing. For adipic acid, the preferred process pH would then be lower than 4, since adipic acid has a pKa of 4.41 (first carboxylic group) and 5.41 (secondary carboxylic group).

For pH values below 4, both carboxylic groups of AA are undissociated, thus allowing the establishment of internal H-bonds with the formation of stable cyclic isomers [47]. This chemical configuration of AA does not allow it to react with the extractants. By increasing the pH, the dissociation of AA carboxylic groups is occurring. The anionic forms of

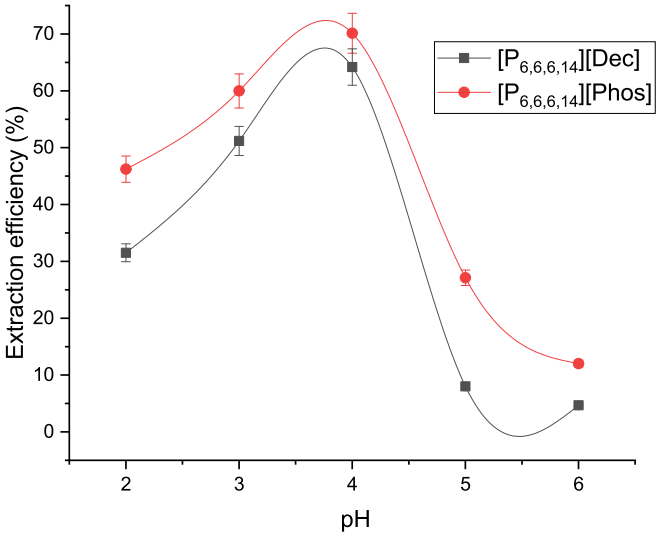

Fig. 5. Aqueous phase pH influence on AA extraction efficiency.

–COOH groups are also involved in forming internal H-bonds, but the cyclic structure is unstable, and the acid can easily react with ILs. Due to the important dissociation of the AA at a higher pH domain, the interfacial reaction is not possible, and the extraction yields become lower than 10 %.

In order to attain optimal extraction efficiency and provide the largest extraction yield while preserving the process's viability and cost-effectiveness, one crucial parameter that may be adjusted is the contact time. According to the experimental results (Fig. 6), increasing the contact time improves the efficiency of reactive extraction for AA within 5 min and then stays essentially unchanged. This rapid extraction is caused by an increase in interfacial area that results from intense mixing and reactants being available at the interface in vicinal aqueous and organic regions.

3.2. Modelling and optimization

Once the data was gathered and pre-processed, it was fed into the modelling and optimization procedure detailed in Section 2.2. The implementation was performed in Python and used the TensorFlow and Keras frameworks. The type of ANN considered was Sequential with Dense layers, with a kernel L1 regulation rate of 0.01 applied per each hidden layer. The types of neurons in the hidden layer were Relu and Linear for the output layer. The training procedure was performed using

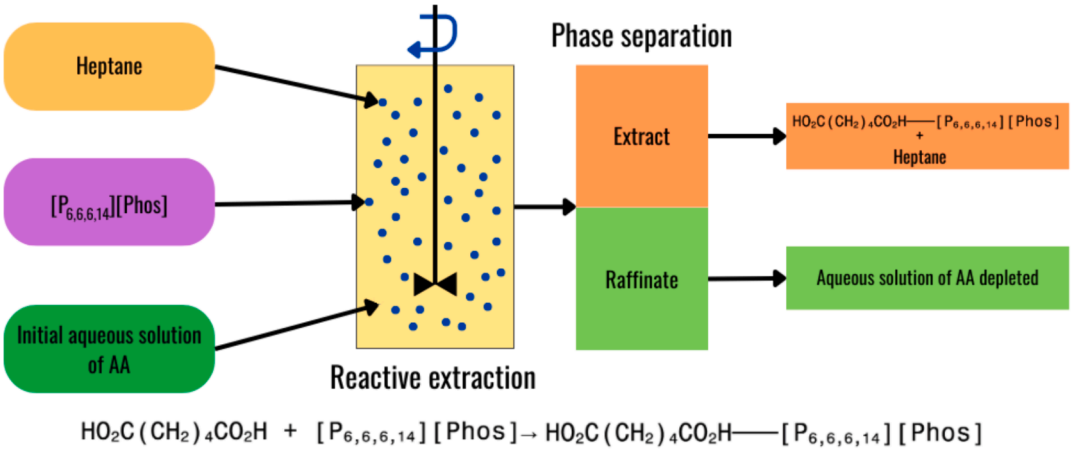

Fig. 4. Reactive extraction system for adipic acid using $[P_{6,6,6,14}]$[Phos] ionic liquid.

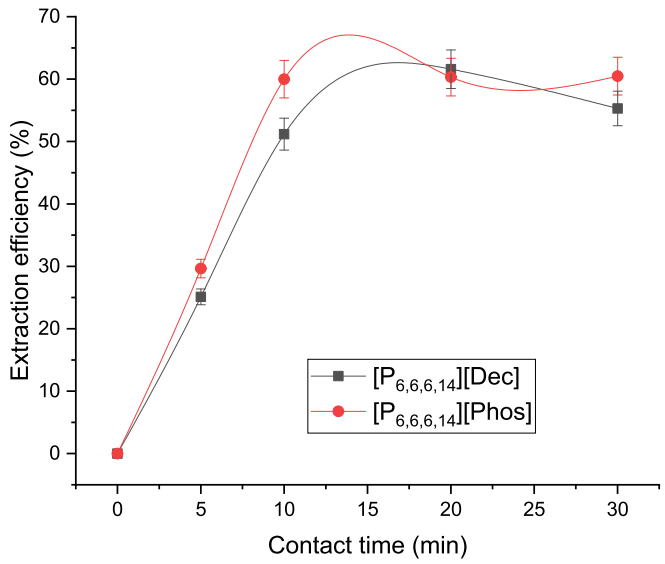

Fig. 6. Contact time influence on AA extraction efficiency.

the Adam optimizer, with a 0.05 learning rate. A validation split of 0.2 was applied in the training phase. The starting values for the DE parameters F and CR were 0.5. The total number of generations was set to 30.

After applying the optimization procedure, the best model obtained had one hidden layer with 20 neurons. The topologies were closely monitored during the evolutionary process, and the best solutions per iteration had hidden layers that varied between 1 and 3. This indicates that a simple network can capture its dynamic efficiently for the considered process. The statistical indicators that show the performance of the best model are for the training phase: explained variance score 0.98, mean absolute error 1.94, mean squared error 8.88, mean absolute percentage error 0.052, coefficient of determination 0.979 and for the testing phase: explained variance score 0.97, mean absolute error 1.91, mean squared error 7.49, mean absolute percentage error 0.082, coefficient of determination 0.974. In total, the number of trainable parameters was 161. A comparison between the initial testing values and the predicted ones is presented in Fig. 7.

As can be observed from Fig. 3, the differences between the experimental and predicted values are small for the majority of exemplars. This indicates that the model has a good generalization capacity and can, therefore, be used in the process optimization phase. Moreover, a sensitivity analysis based on the SHAP module was applied to determine the influence of inputs (process parameters) on the removal efficiency (Fig. 8).

In Fig. 8, the importance of the inputs is set from the highest to the lowest. IL indicates the concentration of the extractant ([$P_{6,6,6,14}$][Dec] and [$P_{6,6,6,14}$][Phos] indicates the type of the extractant). Since the extractant type is categorical, it was considered an input based on a one-hot encoding. As can be observed, the extractant concentration is the most influential parameter, with higher values positively influencing the extraction performance. pH is the second most influential parameter, and higher values tend to negatively influence extraction performance. Concerning the type of extractant, [$P_{6,6,6,14}$][Dec] tends to have a higher impact on the output than [$P_{6,6,6,14}$][Phos]. However, in terms of output, the presence of [$P_{6,6,6,14}$][Phos] tends to lead to a slightly higher extraction efficiency. The SHAP analysis indicates that lower temperatures increase extraction performance, while a significant trend was not observed for time.

The next step consisted of the identification of the best combination of process parameters that lead to a maximization of extraction efficiency. Table 2 presents a series of combinations obtained during this stage. Because the DE algorithm can find multiple solutions near the optimum, Table 3 contains only the ones with a significant difference.

As can be observed, most solutions consider [$P_{6,6,6,14}$][Phos]. For [$P_{6,6,6,14}$][Dec], the best solution revolves around 60 % efficiency at higher temperatures but lower IL concentrations compared with [$P_{6,6,6,14}$][Phos]. Forcing the optimization to focus only [$P_{6,6,6,14}$][Dec] also identifies reasonable solutions (Table 3). However, in this case, the prediction goes slightly over 100 %. This can be explained by the error induced by the model, and in all situations where the predicted efficiency is $>$ 100 %, it can be considered a maximum of 100 %.

The next step involved experimentally validating some of the obtained optimization conditions. The results are presented in Table 4, where No is correlated with the experimental conditions in Table 3. The validation data is slightly lower compared with the predictions over 100.

4. Conclusions

This work studied a novel extraction system with hydrophobic ILs as an effective extractant for separating adipic acid from aqueous solutions. The results showed that the extraction efficiency for AA was maximum when [$P_{6,6,6,14}$][Phos] was used as the extractant with the following

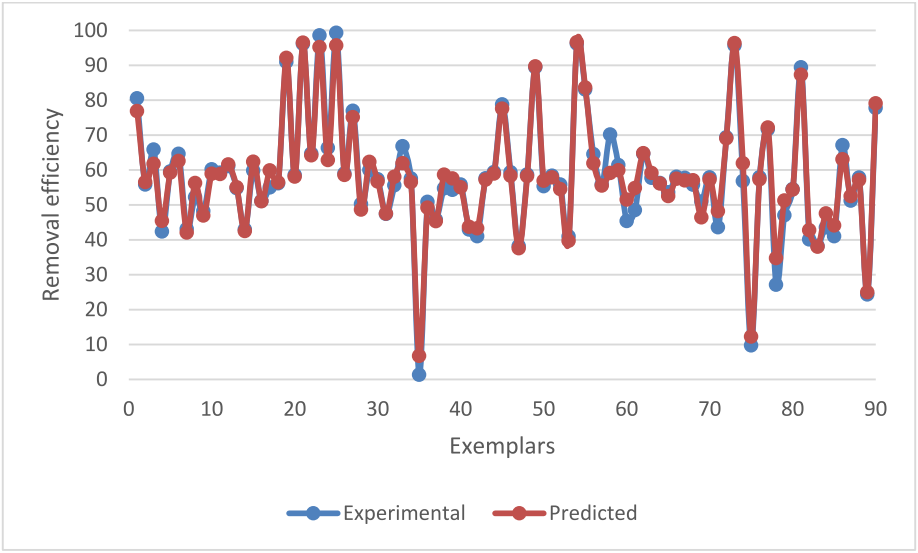

Fig. 7. Comparison between the experimental and predicted values in the testing phase.

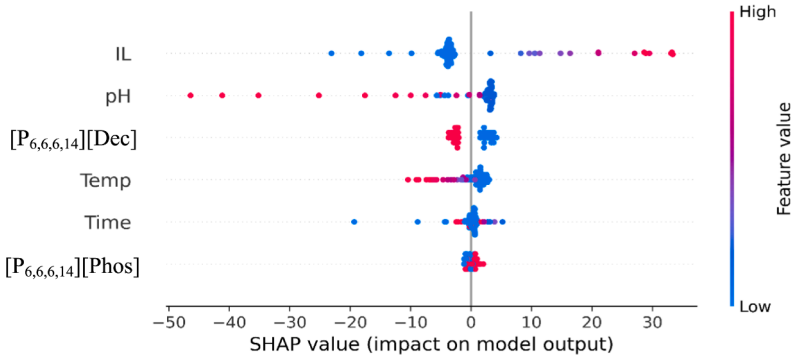

Fig. 8. Sensitivity analysis.

Table 2
Process optimization conditions.

pH	IL, g/L	Time, min	Temp, °C	[$P_{6,6,6,14}$][Dec]	[$P_{6,6,6,14}$][Phos]	Extraction efficiency, %
2.8	117.2	5	26	0	1	99.68
2.8	104.1	5	26	0	1	98.88
2.8	106.9	5.4	25	0	1	98.58
2.8	97.1	5	26	0	1	98.2
3	97.1	5	25	0	1	97.36
3.1	120	7	25	0	1	97.14
2.8	120	8.3	25	0	1	96.55
3	120	9.6	25	0	1	96.06
2.1	71.3	7.5	48	1	0	59.83

Table 3
Process optimization conditions for [$P_{6,6,6,14}$][Dec].

No.	pH	IL	Time	Temperature	Extraction efficiency
1	3.1	106.7	5	25	107.71
2	3.1	105.8	5.8	25	106.44
3	3.2	98.8	6.8	25	104.27
4	3.2	98.8	6.8	25	104.27
5	3.1	98.1	6.7	30	100.69
6	3.3	98.8	7.7	29	99.18
7	3	93.1	5.7	34	98.92
8	3.4	88.3	6.9	26	97.79

Table 4
Experimental validation.

No.	Extraction efficiency predicted	Extraction efficiency experimental
1	107.71	99.56
3	104.27	98.89
6	99.18	98.19

optimal extraction conditions: 5 min contact time, 30 °C temperature, and 120 g/L ionic liquid dissolved in heptane. The process was modelled and optimized using a neuro-evolutive approach combining ANNs and DE. A sensibility analysis on the best model obtained (with a coefficient of determination of 0.974 in the testing phase) indicated that IL and pH have the highest influence on the process output. In the optimization phase, the search is directed by the extractant type, and the best process conditions when no limits are imposed focus on [$P_{6,6,6,14}$][Phos]. Nevertheless, when a limit on the extractant type was set to [$P_{6,6,6,14}$][Dec], the DE algorithm could find good solutions, pointing out its capacity to efficiently explore the search space and identify near optimum solutions. The process can be efficiently simulated using the proposed approach and the obtained model, and predictions in different conditions can be used to extract meaningful information.

CRediT authorship contribution statement

Elena Niculina Dragoi: Writing – original draft, Software, Investigation, Formal analysis. **Alexandra Cristina Blaga:** Writing – review & editing, Writing – original draft, Visualization, Resources, Project administration, Funding acquisition, Conceptualization. **Dan Cascaval:** Writing – original draft, Visualization, Validation, Supervision. **Anca Irina Galaction:** Writing – review & editing, Validation, Supervision.

Declaration of competing interest

The authors declare that they have no known competing financial interests or personal relationships that could have appeared to influence the work reported in this paper.

Data availability

Data will be made available on request.

Acknowledgement

This work was supported by a grant of the Ministry of Research, Innovation and Digitization, CNCS - UEFISCDI, project number PN-III-P1-1.1-TE-2021-0153, within PNCDI III.

References

[1] S.M. Lee, J. Young Lee, J.-S. Hahn, Seung-Ho Baek. (2024) Engineering of Yarrowia lipolytica as a platform strain for producing adipic acid from renewable resource, Bioresource Technology, 391, Part A. 129920, DOI: 10.1016/j.biortech.2023.129920.
[2] D. Xu, C. Ma, Mengjia Wu, Yu Deng, Yu-Cai He, Improved production of adipic acid from a high loading of corn stover via an efficient and mild combination pretreatment, Bioresour. Technol. 382 (2023) 129196, https://doi.org/10.1016/j.biortech.2023.129196.
[3] M. Niakan, M. Masteri-Farahani, H. Haidary, Catalytic adipic acid production through the cyclohexene oxidation by a non-HNO3 route over SBA-16 supported Venturello catalyst, Colloids Surf A Physicochem Eng Asp 686 (2024) 133465, https://doi.org/10.1016/j.colsurfa.2024.133465.
[4] M. Wu, J. Di, L. Gong, Y.-C. He, C. Ma, Y. Deng, Enhanced adipic acid production from sugarcane bagasse by a rapid room temperature pretreatment, Chem. Eng. J. 452 (2) (2023) 139320, https://doi.org/10.1016/j.cej.2022.139320.
[5] Y. Zhou, M. Zhao, S. Zhou, Y. Zhao, G. Li, Y. Deng, Biosynthesis of adipic acid by a highly efficient induction-free system in Escherichia coli, J. Biotechnol. 314–315 (2020) 8–13, https://doi.org/10.1016/j.jbiotec.2020.03.011.
[6] X. Zhang, Y. Liu, J. Wang, et al., Biosynthesis of adipic acid in metabolically engineered *Saccharomyces cerevisiae*, J. Microbiol. 58 (2020) 1065–1075, https://doi.org/10.1007/s12275-020-0261-7.
[7] M.C. Morejón, A. Franz, R. Karande, F. Harnisch, Integrated electrosynthesis and biosynthesis for the production of adipic acid from lignin-derived phenols, Green Chem. 25 (2023) 4662–4666, https://doi.org/10.1039/D3GC01105D.
[8] W. Niu, H. Willett, J. Mueller, X. He, L. Kramer, B. Ma, J. Guo, Direct biosynthesis of adipic acid from lignin-derived aromatics using engineered *Pseudomonas putida* KT2440, Metab. Eng. 59 (2020) 151–161, https://doi.org/10.1016/j.ymben.2020.02.006.

[9] A.Y. Gulevicha, A.Y. Skorokhodovaa, V.G. Debabova, The effect of glyoxylate shunt inactivation on biosynthesis of adipic acid through inverted fatty acid β-oxidation by *escherichia coli* strains, Appl. Biochem. Microbiol. 59 (3) (2023) 267–274, https://doi.org/10.1134/S0003683823030080.
[10] M. Zhao, D. Huang, X. Zhang, M.A.G. Koffas, J. Zhou, Y. Deng, Metabolic engineering of *Escherichia coli* for producing adipic acid through the reverse adipate-degradation pathway, Metab. Eng. 47 (2018) 254–262, https://doi.org/10.1016/j.ymben.2018.04.002.
[11] X. Zhang, Y. Liu, J. Wang, Y. Zhao, Y. Deng, Biosynthesis of adipic acid in metabolically engineered *Saccharomyces cerevisiae*, J. Microbiol. 58 (12) (2020) 1065–1075, https://doi.org/10.1007/s12275-020-0261-7.
[12] J.H. Shin, A.J.C. Andersen, P. Achterberg, L. Olsson, Exploring functionality of the reverse β-oxidation pathway in corynebacterium glutamicum for production of adipic acid, Microb. Cell Fact. 20 (2021) 155, https://doi.org/10.1186/s12934-021-01647-7.
[13] J.H. Ju, B.-R. Oh, S.-Y. Heo, Y.-U. Lee, J.H. Shon, C.H. Kim, Y.M. Kim, J.W. Seo, W.-K. Hong, Production of adipic acid by short- and long-chain fatty acid acyl-CoA oxidase engineered in yeast *Candida tropicalis*, Bioprocess Biosyst. Eng. 43 (2020) 33–43, https://doi.org/10.1007/s00449-019-02202-w.
[14] M. Wu, J. Di, L. Gong, Y.C. He, C. Ma, Y. Deng, Enhanced adipic acid production from sugarcane bagasse by a rapid room temperature pretreatment, Chem. Eng. J. 452 (2023) 139320, https://doi.org/10.1016/j.cej.2022.139320.
[15] Y. Deng, Y. Mao, Production of adipic acid by the native-occurring pathway in *Thermobifida fusca* B6, J. Appl. Microbiol. 119 (2015) 1057–1063, https://doi.org/10.1111/jam.12905.
[16] L. Liu, H. Fang, Q. Wei, X. Ren, Extraction performance evaluation of amide-based deep eutectic solvents for carboxylic acid: molecular dynamics simulations and a mini-pilot study, Sep. Purif. Technol. 304 (2023) 122360, https://doi.org/10.1016/j.seppur.2022.122360.
[17] M. Akhlaq, M. Uroos, Applications of tetrabutylphosphonium-based ionic liquids: a state-of-the-art review, J. Mol. Liq. (2024) 125075, https://doi.org/10.1016/j.molliq.2024.125075.
[18] M.E. Marti, H. Zeidan, Using eco-friendly alternatives for the recovery of pyruvic acid by reactive extraction, Sep. Purif. Technol. 312 (2023) 123309, https://doi.org/10.1016/j.seppur.2023.123309.
[19] P. Demmelmayer, L. Steiner, H. Weber, M. Kienberger, Thymol-menthol-based deep eutectic solvent as a modifier in reactive liquid–liquid extraction of carboxylic acids from pretreated sweet sorghum silage press juice, Sep. Purif. Technol. 310 (2023) 123060, https://doi.org/10.1016/j.seppur.2022.123060.
[20] D. Zheng, S. Jiang, P. Zheng, D. Zhou, J. Qiu, L. Gao, Molecular mechanism for the interaction of natural products with ionic liquids: insights from MD and DFT study, J. Mol. Liq. 399 (2024) 124440, https://doi.org/10.1016/j.molliq.2024.124440.
[21] N. Vidal, M. Ventura, F. Martínez, J.A. Melero, Selective extraction of high-added value carboxylic acids from aqueous fermentative effluents with new hydrophobic eutectic solvents (HES), Sep. Purif. Technol. 346 (2024) 127540, https://doi.org/10.1016/j.seppur.2024.127540.
[22] A. Prabhune, R. Dey, Green and sustainable solvents of the future: deep eutectic solvents, J. Mol. Liq. 379 (2023) 121676, https://doi.org/10.1016/j.molliq.2023.121676.
[23] N. Gao, Y. Wang, H. Luo, Y. Xu, J. Liu, Y. Chen, pH-switchable hydrophobic deep eutectic solvents for sustainable recycling extraction of high oily waste, Chem. Eng. J. 495 (2024) 153339, https://doi.org/10.1016/j.cej.2024.153339.
[24] M. Lang, H. Li, Sustainable routes for the synthesis of renewable adipic acid from biomass derivatives, ChemSusChem 15 (2022) e202101531, https://doi.org/10.1002/cssc.202101531.
[25] E. Riveiro, B. González, Á. Domínguez, Extraction of adipic, levulinic and succinic acids from water using TOPO-based deep eutectic solvents, Sep. Purif. Technol. 241 (2020) 116692, https://doi.org/10.1016/j.seppur.2020.116692.
[26] A.C. Blaga, E.N. Dragoi, A. Tucaliuc, L. Kloetzer, D. Cascaval, Folic acid ionic-liquids-based separation: extraction and modelling, Molecules 28 (2023) 3339, https://doi.org/10.3390/molecules28083339.
[27] A.C. Blaga, E.N. Dragoi, D.G. Gal, A.C. Puitel, A. Tucaliuc, L. Kloetzer, D. Cascaval, A.I. Galaction, Selective separation of vitamin C by reactive extraction using ionic liquid: experimental and modelling, J. Ind. Eng. Chem. (2023), https://doi.org/10.1016/j.jiec.2023.11.057.
[28] S. Tönjes, E. Uitterhaegen, P. De Brabander, E. Verhoeven, T. Delmulle, K. De Winter, W. Soetaert, In situ product recovery as a powerful tool to improve the fermentative production of muconic acid in Saccharomyces cerevisiae, Biochem. Eng. J. 190 (2023) 108746, https://doi.org/10.1016/j.bej.2022.108746.
[29] D. Floreano, P. Durr, C. Mattiussi, Neuroevolution: from architectures to learning, Evol. Intel. 1 (1) (2008) 47–62, https://doi.org/10.1007/s12065-007-0002-4.
[30] K.O. Stanley, J. Clune, J. Lehman, R. Miikkulainen, Designing neural networks through neuroevolution, Nature Machine Intelligence 1 (1) (2019) 24–35, https://doi.org/10.1038/s42256-018-0006-z.
[31] T. H . Maul, A. Bargiela, C. S. Yew, A. S. (2014) Adamu Towards evolutionary deep neural networks. Proceedings - 28th European Conference on Modelling and Simulation, ECMS 2014, 2014, DOI: 10.7148/2014-0319.
[32] S. Chellapan, D. Datta, S. Kumar, H. Uslu, Statistical modeling and optimization of itaconic acid reactive extraction using response surface methodology (RSM) and artificial neural network (ANN), Chem. Data Collect. 37 (2022) 100806, https://doi.org/10.1016/j.cdc.2021.100806.
[33] S. Pandey, S. Kumar, Reactive extraction of gallic acid from aqueous solution with tri-n-octylamine in oleyl alcohol: equilibrium, thermodynamics and optimization using RSM-rCCD, Sep. Purif. Technol. 231 (2020) 115904, https://doi.org/10.1016/j.seppur.2019.115904.
[34] T. Evlik, Y.S. Aşçı, N. Baylan, H. Gamsızkan, S. Çehreli, Reactive separation of malic acid from aqueous solutions and modeling by artificial neural network (ANN) and response surface methodology (RSM), J. Dispers. Sci. Technol. 43 (2) (2022) 221–230, https://doi.org/10.1080/01932691.2020.1838920.
[35] A.K. Jha, N. Sit, Comparison of response surface methodology (RSM) and artificial neural network (ANN) modelling for supercritical fluid extraction of phytochemicals from Terminalia chebula pulp and optimization using RSM coupled with desirability function (DF) and genetic algorithm (GA) and ANN with GA, Ind. Crop. Prod. 170 (2021) 113769, https://doi.org/10.1016/j.indcrop.2021.113769.
[36] G.B. Raj, K.K. Dash, Ultrasound-assisted extraction of phytocompounds from dragon fruit peel: optimization, kinetics and thermodynamic studies, Ultrason. Sonochem. 68 (2020) 105180, https://doi.org/10.1016/j.ultsonch.2020.105180.
[37] C. Sabater, V. Sabater, A. Olano, A. Montilla, N. Corzo, Ultrasound-assisted extraction of pectin from artichoke by-products. An artificial neural network approach to pectin characterisation, Food Hydrocoll. 98 (2020) 105238, https://doi.org/10.1016/j.foodhyd.2019.105238.
[38] R. Storn, K. Price, Differential evolution - a simple and efficient heuristic for global optimization over continuous spaces, J. Glob. Optim. 11 (4) (1997) 341–359, https://doi.org/10.1023/A:1008202821328.
[39] M. Islam, X. Yao, Evolving Artificial Neural Network Ensembles. Computational Intelligence: A Compendium. J. Fulcher and L. Jain, Springer Berlin / Heidelberg. 115, 2008, 851-880, DOI: 10.1007/978-3-540-78293-3_20.
[40] P. Kordik, J. Koutnik, J. Drchal, O. Kovarik, M. Cepek, M. Snorek, Meta-learning approach to neural network optimization, Neural Netw. 23 (4) (2010) 568–582, https://doi.org/10.1016/j.neunet.2010.02.003.
[41] S. Curteanu, E.-N. Dragoi, A. C. Blaga, A. I. Galaction, D. Cascaval. (2021) Neuroevolutive Algorithms Applied for Modeling Some Biochemical Separation Processes. Artificial Neural Networks. H. Cartwright. New York, NY, Springer US. 115-138, DOI: 10.1007/978-1-0716-0826-5_5.
[42] R.G. Lazar, A.C. Blaga, E.N. Dragoi, A.I. Galaction, D. Cascaval, Application of reactive extraction for the separation of pseudomonic acids: influencing factors, interfacial mechanism, and process modelling, Can. J. Chem. Eng. 100 (S1) (2022) S246–S257, https://doi.org/10.1002/cjce.24124.
[43] A.C. Blaga, E.N. Dragoi, R.E. Munteanu, D. Cascaval, A.I. Galaction, Gallic acid reactive extraction with and without 1-octanol as phase modifier: experimental and modeling, Fermentation 8 (2022) 633, https://doi.org/10.3390/fermentation8110633.
[44] K. Priddy, P. Keller. (2005) Artificial Neural Networks: An introduction. Washington, SPIE Press.
[45] DP Kingma, J. Ba. Adam: A method for stochastic optimization. arXiv preprint arXiv:1412.6980, 2014, DOI: 10.48550/arXiv.1412.6980.
[46] E. Skoronski, M. Fernandes, F.J. Malaret, J.P. Hallett, Use of phosphonium ionic liquids for highly efficient extraction of phenolic compounds from water, Sep. Purif. Technol. 248 (2020) 117069, https://doi.org/10.1016/j.seppur.2020.117069.
[47] S.K. Min, M. Park, N.J. Singh, H.M. Lee, E.C. Lee, K.S. Kim, A. Lagutschenkov, G. Niedner-Schatteburg, Chiral transformation in protonated and deprotonated adipic acids through multistep internal proton transfer, Chem – A European J. 16 (2010) 10373–10379, https://doi.org/10.1002/chem.200903355.

Received: 15 January 2021 | Revised: 5 February 2021 | Accepted: 22 February 2021

DOI: 10.1002/cjce.24124

THE CANADIAN JOURNAL OF CHEMICAL ENGINEERING

Canadian Society for Chemical Engineering | *For Our Future*
Société canadienne de génie chimique | *Pour notre avenir*

ARTICLE

Application of reactive extraction for the separation of pseudomonic acids: Influencing factors, interfacial mechanism, and process modelling

Roxana Georgiana Lazar[1] | **Alexandra Cristina Blaga**[1] | **Elena Niculina Dragoi**[1] | **Anca Irina Galaction**[2] | **Dan Cascaval**[1]

[1]Faculty of Chemical Engineering and Environmental Protection "Cristofor Simionescu", "Gheorghe Asachi" Technical University of Iasi, Iasi, Romania

[2]Faculty of Medical Bioengineering, "Grigore T. Popa" University of Medicine and Pharmacy, Iasi, Romania

Correspondence
Alexandra Cristina Blaga, Faculty of Chemical Engineering and Environmental Protection "Cristofor Simionescu", "Gheorghe Asachi" Technical University of Iasi, Iasi, Romania.
Email: acblaga@tuiasi.ro

Funding information
This work was supported by the Ministry or Research and Innovation, CNCS – UEFISCDI, Grant/Award Numbers: PN III PCE 6/2017, code PN-III-P4-ID-PCE-2016-010

Abstract

Mupirocin (a mixture of A, B, C, and D pseudomonic acids—four complex, similar structures) is an antibiotic belonging to the monocarboxylic acid class, used to cure infections caused by bacteria (Gram-positive), especially methicillin-resistant *Staphylococcus aureus* (MRSA). Its biotechnological production and separation need constant attention, as improving antibiotics is important in the pharmaceutical industry. This is the first study regarding pseudomonic acids separation through reactive extraction; the experiments were focused on finding a proper combination of extractant and diluent for optimization of the separation yield. The pH influence (4–9) and extractant (TOA and Amberlite LA-2, 5–20 g/L) concentration dissolved in *n*-heptane (green solvent) have been analyzed, obtaining the maximum extraction yield (88.78%) at pH 4, 20 g/L extractant, and 10% octanol added to the organic solvent. The addition of the phase modifier, 1-octanol, improved the extraction yield by 2.6 times for Pseudomonic acid A due to interactions of formed complexes with the phase modifier that improves its solubility. The experimental results for determining the mechanism of the interfacial reaction showed that, regardless of the pH value and solvent polarity (modified by the addition of 1-octanol), only one molecule of Pseudomonic acid A and extractant react at the aqueous-organic interface. In addition, the system was modelled and optimized with a methodology combining artificial neural networks (ANN) and differential evolution.

KEYWORDS

mathematical modelling, mupirocin, octanol, separation, solvent extraction

1 | INTRODUCTION

Mupirocin is a topical antibiotic that acts by inhibiting protein synthesis in Gram-positive bacteria used to treat superficial infections of skin and soft tissue. It is produced as a mixture of four similar pseudomonic acids: A, B, C, and D (Figure 1), through biosynthesis, using *Pseudomonas fluorescens* NCIMB 10586 bacterium. The basic structure of pseudomonic acids, that implies a monic acid containing a pyran ring, connected through an ester linkage to 9-hydroxynonanoic acid, is different from other antibiotics.[1,2]

Mupirocin is produced by biosynthesis as a mixture of these four very similar compounds (Table 1) in different proportions: maximum 90% Pseudomonic acid A, 8% Pseudomonic acid B, 2% Pseudomonic acid C, and 2% Pseudomonic acid D; but for different growth conditions (including culture media) these proportions could vary (Pseudomonic acid B could reach up to 61%[1,3]). Pseudomonic acid A is responsible for most of the antimicrobial activity; the three minor metabolites share a similar spectrum, but their specific activity—especially that of Pseudomonic acid B—is considerably weaker.[4]

There are several reported methods for the recovery of mupirocin from fermentation broth that implies the removal of the biomass by centrifugation followed by the supernatant processing for mupirocin separation by liquid–liquid extraction or precipitation.[5–7] However, these separation methods imply multiple steps and high cost and energy consumption. This, correlated to the presence of various impurities and low concentration of mupirocin in the fermentation broths, necessitates the development of an effective, economic, and clean separation technique in order to obtain industrial feasible process.

In order to optimize the downstream part of several bioprocesses, an innovative approach, namely reactive extraction, was proposed by researchers as a selective route for the separation of bio-products in low concentration from a complex mixture.[8–14] The reactive extraction combines in one single unit operation the liquid–liquid extraction and a chemical reaction (which can lead to process intensification) and involves two immiscible phases: the aqueous phase that contains the product (mupirocin) and the organic phase that contains the extractant. The key stage of the process is the formation of a hydrophobic and reversible complex between the solute (mupirocin) and the extractant, the first being recovered from the complex by a stripping step with a dilute basic solution. The separation technology by reactive extraction is easily industrialized with relatively low energy consumption, but the selection of a good solvent is extremely important. An appropriate solvent needs to fulfil the following requirements[8,12–15]: suitable distribution ratios and immiscibility with the aqueous phase (viscosity and interfacial tension of two phases should be low), good recyclability, and environmental benignity to ensure economically feasible processes. There are several types of commercially available extractants (organophosphorus compounds or high molecular weight aliphatic or aromatic amines), but for antibiotics with a carboxylic group in their structure, higher extraction degrees are obtained for high molecular amines. Their efficiencies are supplemented with other advantages such as lower price and the improved ability to form complexes with carboxylic groups (higher affinity for carboxylic groups offer higher selectivity over other nonacidic components in the initial mixture).[14–16] These amines, often with high viscosity and low solvation ability, need to be used in order to improve the conditions and extraction efficiency in mixtures with an organic diluent; it is of great importance to find environmentally friendly ones. Ionic liquid extractants of improved safety, toxicological, and ecological characteristics (non-flammable, non-volatile, high thermal stability),[17] have been proposed as promising substituents in numerous processes, but their viscosity, ranging from 10–500 mPa s at room temperature (20–25°C), could be a drawback for their use as extractants.

Several carboxylic acids have been separated using ionic liquids obtaining higher extraction ability compared with the traditional solvents: nicotinic acid,[10] acetic acid,[18] and formic acid.[19] Caproic acid has been separated through reactive extraction using non-toxic green diluents (sunflower and soybean oils) with tributyl phosphate (TBP) as extractant, with better results (97.10% extraction efficiency) being obtained for sunflower oil at low temperature.[20] For the separation of itaconic acid, tri-n-butylphosphate and a quaternary amine (Aliquat 336) were used in sunflower oil, with superior values (76.62% compared to 36.17%) being reached for Aliquat 336.[21]

Based on the above discussion, in the present study, *n*-heptane (classified as a green solvent[22]) was used as

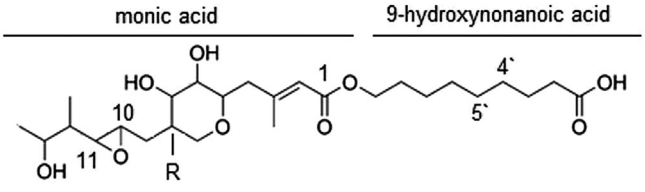

FIGURE 1 The pseudomonic acids chemical structure (R = H for Pseudomonic acid A; R = OH for Pseudomonic acid B; R = H, olefin C-10,11 for Pseudomonic acid; R = H, olefin C-4′, 5′ for Pseudomonic acid D)

Pseudomonic acid	Molecular formula	Molecular weight (g/mol)	pKa
A	$C_{26}H_{44}O_9$	500.629	4.83
B	$C_{26}H_{44}O_{10}$	516.62	4.83
C	$C_{26}H_{44}O_8$	484.63	4.76
D	$C_{26}H_{42}O_9$	498.613	4.83

TABLE 1 Properties of pseudomonic acids, Tucaliuc et al.[3]

diluent while lauryl tri-alkylmethylamine (Amberlite LA-2) and tri-octylamine (TOA) were used as extractants. In order to improve the extraction efficiency while using *n*-heptane, 1-octanol was added in the diluent as phase modifier, its main purpose being to increase the solvent polarity (by increasing the organic-phase polarity, 1-octanol facilitates the solubilization of polar molecules and therefore enhances the separation of pseudomonic acids) and to minimize the formation of the stable third phase (emulsion) that appears during reactive extraction. For liquid, physical, and reactive extraction, 1-octanol is one of the most used solvents (especially for carboxylic acids) and can be considered a suitable replacement for chlorinated solvents like 1,2-dichloroethane.[23,24] It is an environmentally friendly compound with applications as a flavouring agent in food and cosmetic products.[24,25] The results were discussed regarding separation yield and distribution coefficient, the extraction conditions were analyzed, and the extraction mechanism was discussed.

Furthermore, the mupirocin extraction process was modelled and optimized to determine the conditions that lead to the maximum extraction yield obtained for Pseudomonic acid A with the higher antimicrobial efficiency and the minimum extraction yield for the secondary pseudomonic acids. The methodology used to achieve this objective is represented by a modified differential evolution (DE) algorithm and artificial neural networks (ANNs). The strategy is called hSADE-NN[26] and was initially developed for modelling some gaseous streams' depollution process. Due to its flexibility, it can be adapted and efficiently used to model and/or optimize other types of processes, being successfully applied for modelling the polycyclic aromatic hydrocarbon formation in grilled meat products,[27] for modelling of aqueous mixtures of poly (ethylene glycol) transport and thermodynamic and thermophysical properties,[28] and for modelling and optimization of the UV/peroxydisulfate process used for acid blue 193 removal.[29] Also, similar strategies combining DE and ANNs were successfully applied for biotechnological processes,[30–32] indicating that the combination of these two algorithm is also suitable for these types of systems.

To the authors' knowledge, this is the first complete study (experimental, modelling, and optimization) on reactive extraction of pseudomonic acids from aqueous solution.

2 | MATERIALS AND METHODS

2.1 | Chemicals

All chemicals were purchased from Sigma Aldrich and used as received without further treatment, that is, mupirocin (99%) as solute, heptane (99%) as solvent, 1-octanol (99%) as phase modifier, sodium hydroxide (>97%) and sulphuric acid (95.0–98.0%) for pH modifications, and TOA (99.6%) and Amberlite LA-2 (99%) as extractants.

2.2 | Extraction experiments

Reactive extraction experiments for mupirocin separation were realized using an extraction column with vibratory mixing that can rapidly achieve steady state and provides a high interfacial area.[16] The glass extraction column has an inner diameter of 3.6 cm and 25 cm height, fitted with a thermostatic jacket for temperature control. For the mass transfer, the aqueous and organic phase (in equal volumes) were thoroughly mixed using a mixer consisting of a perforated 45 mm diameter disk with 20% free section (maintained at the initial interface between the two phases) that operated at 5 mm and amplitude 50 s^{-1} frequency. The time for each extraction experiment was 1 min and the phase's separation was done at 6000 rpm in a centrifugal separator. All the extractions were realized at 25 ± 0.02°C and were performed at least in duplicate.

The initial pseudomonic acids concentration in the aqueous phase was 0.0265 g/L ($5.3 \cdot 10^{-5}$ mol/L), with the following proportions: 90.2% Pseudomonic acid A, 5.82% Pseudomonic acid B, and 1.98% Pseudomonic acids C and D. The two aminic type extractants, Amberlite LA-2 and TOA, were dissolved individually in the organic solvent (*n*-heptane) with concentrations varied between 0–20 g/L (0.06 mol/L). The aqueous phase pH varied between 4–9, adjusted with a solution of 3% sodium hydroxide and 3% sulphuric acid, using the digital pH meter (CONSORT C 836).

2.3 | Analytical procedures

The extraction process was analyzed using the distribution coefficient and the extraction efficiency (the ratio between mupirocin concentration in the solvent and its concentration in the initial aqueous phase, %), calculated using the mass balance for the extraction system based on the pseudomonic acids concentration in the aqueous and in the exhausted solutions measured by a high performance liquid chromatography technique (HPLC), a method that allows for simultaneous quantification of Pseudomonic acids A, B, and C.[33] For this purpose, an UltiMate 3000 Dionex HPLC system was used with an Acclaim 120 C18 column (4.6 mm diameter, 150 mm long) and a UV detector set at 230 nm. The mobile phase with a flow rate of 0.8 ml/min was composed of 60%

0.05 mol/L ammonium acetate (modified with acetic acid to pH 5.0) and 40% acetonitrile. The determinations were done at 25°C.[33]

2.4 | Modelling and optimization

For modelling the mupirocin's extraction, in this study an algorithm hSADE-NN[26] was applied. It combines a modified version of DE[34]—a population-based, bio-inspired metaheuristic optimizer inspired by the Darwinian principle of evolution—with ANNs (mathematical representation of the functioning of the mammalian brain). In the hSADE-NN approach, DE represents the optimizer that determines the ANNs' parameters (by performing a simultaneous structural and internal parameter optimization), while the model of the process being analyzed is represented by the ANN. A simplified schematic of the hSADE-NN approach is presented in Figure 2.

As can be observed in Figure 2, DE is helped by three additional algorithms: opposition-based principle (which is applied at the initialization level) and local search and backpropagation (which have the role of improving the best-so-far found solution). In addition to these three modifications, another alteration to the base DE algorithm is represented by the introduction of the self-adaptation (where the parameters of the DE are included into the algorithm itself and adapted in accordance with the search space of the problem being solved). More details about the inner workings of the DE improvements made in hSADE-NN can be found in the results obtained by Curteanu et al.[26]

Depending on the problem being solved (process modelling or process optimization), the workflow of data from the process to the ANN and DE is different. In cases of process modelling, based on the process parameters, first the general topology of the ANN is determined in the form of inputs and outputs. Then, based on the user settings, all the remainder parameters representing the ANN (number of hidden layers and neurons in each layer, weights, biases, activation functions and their parameters) are encoded into a collection of real values and sent to DE.

Through a repetitive process, DE optimizes the ANN parameters so that the difference between the predictions generated by the ANN and the experimental data is at a minimum. Once optimized, the parameters are sent to the ANN and further process predictions can be generated. In cases of process optimization, DE uses the predictions generated by the model previously determined and uses the same repetitive process to optimize the process parameters in accordance with the specifics of the process (minimization, maximization, or a combination of minimum and maximum for specific outputs).

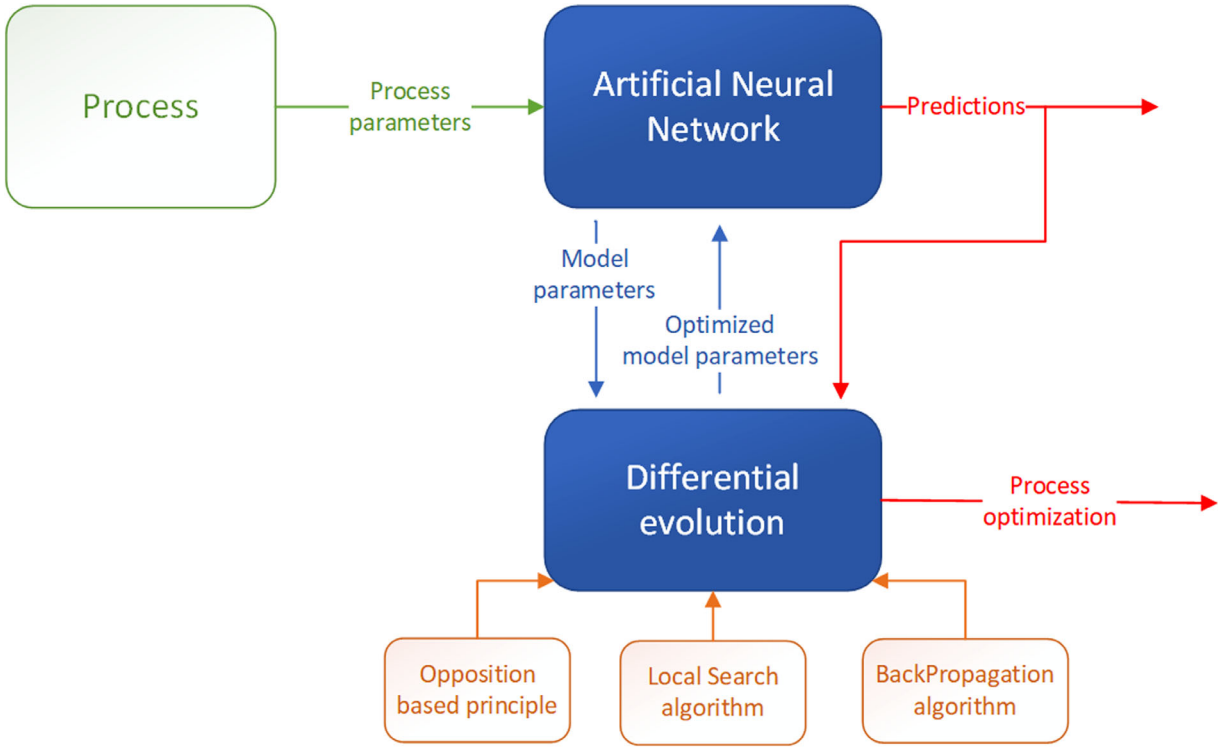

FIGURE 2 Simplified schema of the hSADE-NN algorithm

3 | RESULTS AND DISCUSSION

3.1 | Experimental analysis on reactive extraction

3.1.1 | The pH-value dependence

Pseudomonic acids have a complex structure (Figure 1, Table 1) with one carboxylic group and a theoretical pKa value between 4.76 (Pseudomonic acid C) and 4.83 (Pseudomonic acids A, B, and D).[3] Mupirocin is a mild acid, but the antibiotic activity in aqueous solutions is pH-dependent; the activity is maintained only between pH 4–9 (at pH 1, the antibiotic suffers molecular rearrangements in only 30 min, while at pH 13 only 30% of the compounds are degraded), so the extraction experiments were performed in this interval.

The following parameters strongly influence the reactive extraction efficiency: the amine basicity and the pKa of the pseudomonic acid, the extractant and acid initial concentration, steric hindrance, aqueous phase pH, and solvent type. The pH impact on the reactive extraction is presented in Figure 3; the results showed that pseudomonic acids are extracted with higher yields at acidic pH. This suggests that hydrogen bonding is the dominant interaction between pseudomonic acids and the aminic extractants, results that are in accordance with findings for the reactive extraction of other carboxylic acids, such as muconic acid, protocatechuic acid, and 2-ketogluconic acid.[11,35–37]

As can be noted from Figure 3, the variation of the extraction efficiency with the pH suggests that the extractant nature exhibits less influence on the separation performance compared to the solvent polarity.

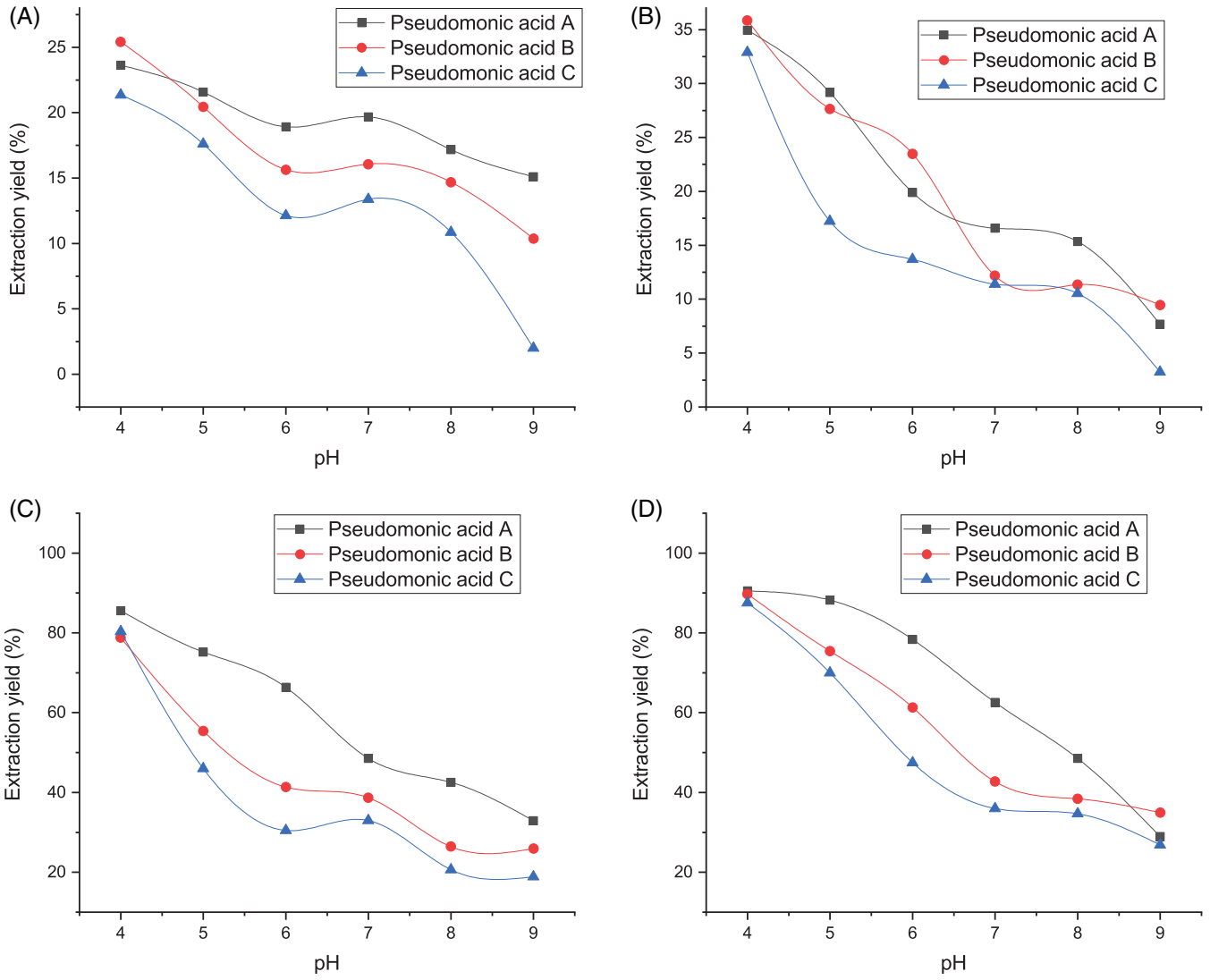

FIGURE 3 pH influence on the mupirocin extraction using Amberlite LA-2 and TOA (■—Pseudomonic acid A, ●—Pseudomonic acid B, ▲—Pseudomonic acid C)

In all systems, the reactive extraction efficiency decreases with the pH increase, suggesting hydrogen bond formation between pseudomonic acids and the amines, requiring that the first would be in un-dissociated form (the molecular form of pseudomonic acids is selectively extracted in the organic phase while the dissociated form remains in the aqueous phase). At pH value equal to acid's pKa, half of the pseudomonic acids quantity is dissociated, and the increase of the pH generates complete dissociation that will induce a more accentuated decrease of the extraction yield.

For the considered domain of pH values, the optimum pH for reactive extraction was found to be 4, for all systems analyzed, favourable both for the separation and for the stability and maintaining of antibacterial activity of the antibiotic. In *n*-heptane, pseudomonic acids are insoluble, so the reactive extraction with long chain amines occurs through a reaction that occurs at the organic/aqueous interface, followed by the resulting complex diffusion in the organic phase.

The 1-octanol (dielectric constant at 25°C: 10.3[38]) addition in heptane improved the extraction efficiency (by 2.5–3.3 times), by improving the solvation of the acid-amine complex, similar to other compounds (2-ketogluconic,[16] and fumaric,[24] acetic, formic, and lactic acid[39]), due both to enhancing the polarity of the organic phase, and to the extraction capacity of 1-octanol's hydroxyl groups being able to react with pseudomonic acid through hydrogen bonds:

n-heptane:

$$\text{Mup-COOH} + \text{HN-ALA2} \leftrightarrow \text{Mup-COO}^{-}\text{H---}^{+}\text{NH-ALA2}$$

n-heptane with 1-octanol:

$$\text{Mup-COOH} + \text{HN-ALA2} + \text{HO-(CH}_2\text{)}_7\text{-CH}_3 \leftrightarrow \text{Mup-C(=O}\cdots\text{H-O-(CH}_2\text{)}_7\text{-CH}_3\text{)-O}^{-}\text{H---}^{+}\text{NH-ALA2} \quad \text{(R1)}$$

$$\text{Mup-COOH} + \text{N-TOA} + \text{HO-(CH}_2\text{)}_7\text{-CH}_3 \leftrightarrow \text{Mup-C(=O}\cdots\text{H-O-(CH}_2\text{)}_7\text{-CH}_3\text{)-O}^{-}\text{H---}^{+}\text{N-TOA} \quad \text{(R2)}$$

Similar to the results published by Gorden et al.[11] and Canari and Eyal[8] for carboxylic compounds (muconic, succinic, lactic), the complex solute-extractant is formed based on hydrogen bonds between the hydrogen atom from the hydroxyl group of the pseudomonic acids and the central nitrogen atom of the amine (negative polarized). The H bond formation is easier for a higher negative polarization of the nitrogen atom, which is influenced both by the number and length of the carbon chains, the latter with higher influence. This could explain the better results obtained when Amberlite LA-2 (secondary amine) was used rather than TOA (tertiary amine), due to superior density of amine groups, the less steric hindrance around the reactive amine group, and secondary amines' higher basicity. Taking this into account, the extractant concentration influence was analyzed for Amberlite LA-2 only.

3.1.2 | Amine concentration dependence

The extractant concentration's influence on the separation efficiency is presented in Figure 4 and shows that there are significant improvements in extraction yield with the increase in Amberlite LA-2 concentration in the *n*-heptane (0–0.06 mol/L), over the stoichiometric ratio (the pseudomonic acids' concentration was 5.3×10^{-5} mol/L). This effect can be attributed both to the increase of the acid-amine complex hydrophobicity and its enhanced solvation by extractant molecules. The addition of the phase modifier, 1-octanol, for the same amine concentration substantially improved the extraction yield (from 33.45% to 88.78% for Pseudomonic acid A), due to interactions of the mupirocin-Amberlite LA-2 complexes with the phase modifier (1-octanol) that improves its solubility. It also facilitates phase separation and, by influencing the extractant basicity, modifies the stability of the complex formed.[37]

For low amines molecular concentration in heptane, the addition of 1-octanol inhibited the formation of the third phase (stable emulsion which is difficult to separate), similar to other acidic compounds.[11,36,37,40]

3.1.3 | Reactive extraction mechanism

The recovery of pseudomonic acids using amines extractant, Q, by the formation of a complex through hydrogen bonding in an interfacial reaction, can be represented as follows:

$$\text{MUP}-\text{COOH}_{(aq)} + \text{n Q}_{(o)} \leftrightarrow \text{MUP}-\text{COOHQ}_{\text{n (o)}} \quad \text{(R3)}$$

For mupirocin, the distribution coefficient, D, is calculated using Equation (1), the ratio between total concentrations of mupirocin in the organic phase and in the aqueous raffinate:

$$D = \frac{\left[\text{MUPCOOH Q}_{\text{n(o)}}\right]}{\left[\text{MUPCOOH}_{(aq)}\right]} \quad (1)$$

The equilibrium constant is calculated using Equation (2), taking into account the interfacial balance:

$$K_E = \frac{\left[\text{MUPCOOH Q}_{\text{n(o)}}\right]}{\left[\text{MUPC}\bar{\text{O}}\text{OH}_{(aq)}\right]\left[\text{Q}_{(o)}\right]^{\text{n}}} \rightarrow \left[\text{MUPCOOH Q}_{\text{n(o)}}\right] = K_E \cdot \left[\text{MUP C}\bar{\text{O}}\text{OH}_{(aq)}\right] \cdot \left[Q_{(o)}\right]^{n} \quad (2)$$

The concentration of un-dissociated acid from the aqueous phase can be calculated using Equation (3),

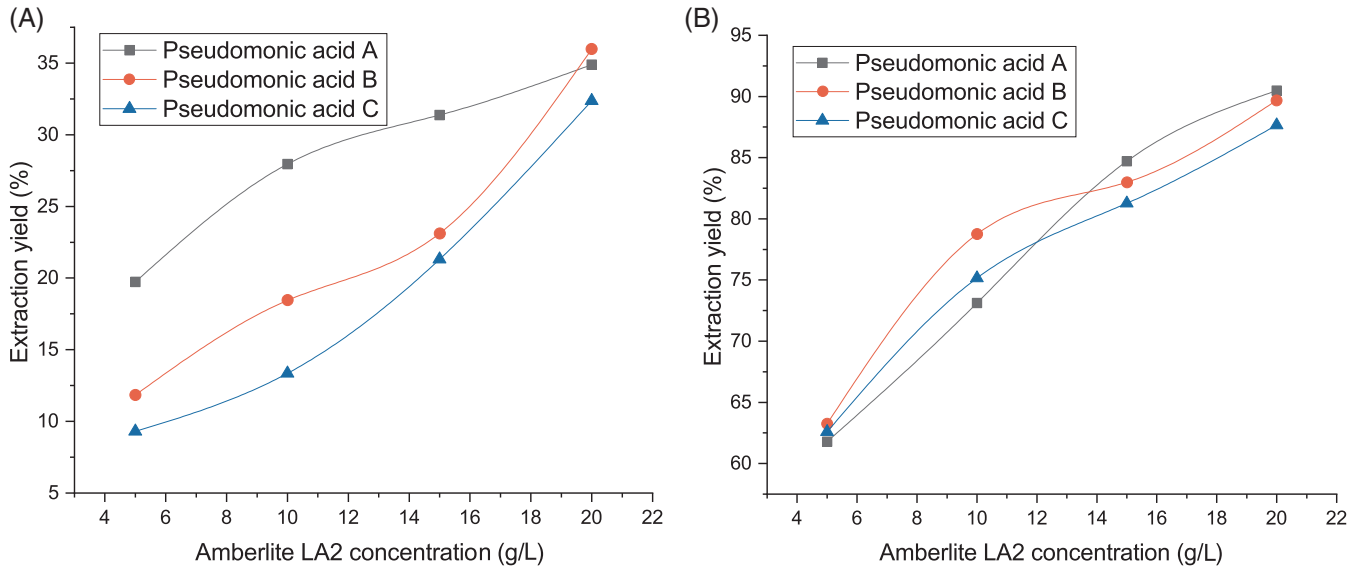

FIGURE 4 Extractant concentration influence on pseudomonic acids yield (■—Pseudomonic acid A, ●—Pseudomonic acid B, ▲—Pseudomonic acid C)

considering its total concentration in the aqueous phase and the dissociation constant, Ka:

$$\left[\mathrm{MUP-COOH}_{(aq)}\right]=\frac{\left[MUP-\bar{C}OOH_{(aq)}\right]}{1+\frac{K_a}{[H^+]}} \tag{3}$$

Using Equations (1)–(3), the distribution coefficient (D) equation takes the following form:

$$D=K_E\cdot\frac{\left[Q_{(o)}\right]^n}{1+\frac{K_a}{[H^+]}} \tag{4}$$

Using Equation (4) under logarithmic form, the equation of a straight line can be attained (Equation (5)), by whose graphic representation the number of extractant molecules (n) that are involved in the formation of the mupirocin-extractant complex (from the straight line slope) and the extraction constant, K_E (from the straight line intercept), can be determined:

$$\ln D-\ln\left(1+\frac{K_a}{[H^+]}\right)=\ln K_E+\ln\left[Q_{(o)}\right] \tag{5}$$

According to Figure 5 (graphical representation of Equation (5)), the number of aminic extractant molecules involved in the mupirocin-Amberlite LA-2 complex is 1 (Table 2), both in the presence and in the absence of 1-octanol, but the values of the extraction constant (Table 2) are influenced by the organic phase polarity (increased by 1-octanol addition in *n*-heptane).

These results indicate that, regardless of the pH value and the polarity of the solvent, one molecule from each component of the extraction system participates in the interfacial reaction. However, from Figure 4 it can be noted that in order to obtain high extraction yield, the amine concentration in the organic mixture need to be much higher than the stoichiometric need for the reaction with pseudomonic acids. At higher concentrations of Amberlite LA-2, the Pseudomonic acid A extraction was significantly improved (Figure 4), especially when octanol was added to the inactive diluent, *n*-heptane, and a higher strength of the complex solvation was noted for *n*-heptane/octanol mixture, as the K_E value was found to be much higher than in the case of using only *n*-heptane (Table 2).

This behaviour is caused by a slow interfacial reaction (by increasing the concentration of one reactant the reaction rate will increase and, respectively, the amount of pseudomonic acids extracted), cumulated with a reduced solubility of the non-reactive groups from the solute structure (Figure 1), that can be overcome by the formation of aminic associations that either include the complex solute-extractant in the organic phase or induce its solvation. Due to the large dimension of both molecules (extractant and solute), the formation of aminic adducts is inhibited by steric hindrance.

3.1.4 | Selective separation

The selectivity factor is presented in Figure 6, and was calculated as the ratio between the reactive extraction

yield of Pseudomonic acid A and the overall extraction yield of pseudomonic acids. In order to obtain a satisfactory selectivity for Pseudomonic A, a separation selectivity factor higher than 1 is required, but the obtained results indicated that the differences between the extraction degrees were not sufficient. This behaviour is caused by the structure similarity in the four pseudomonic acids; the acid-differentiating radical is not a chemically active one (acidic or basic) and the carboxylic active group of mupirocin is not affected by the type of substituent in the radical, as in the case of selective separation of gentamicin.[41]

The selectivity for Pseudomonic acid A increases with increasing Amberlite LA-2 concentration and the addition of 1-octanol; despite this, the experimental results show that Pseudomonic acid A cannot be selectively separated from Pseudomonic acids B and C. However, in terms of pseudomonic acids' selective separation from a fermentation broth, the results are interesting. *Pseudomonas fluorescens* NCIMB 10586 bacterium fermentation produces around 10% of the secondary acids, but Pseudomonic acid B can be produced up to 61% and has less antibiotic activity. Thus, Pseudomonic acid B could be maintained in the broth, while the other acids (A, C, and D) may be selectively separated through a multi-stage extraction by increasing the octanol content from the organic phase, influencing the selectivity.

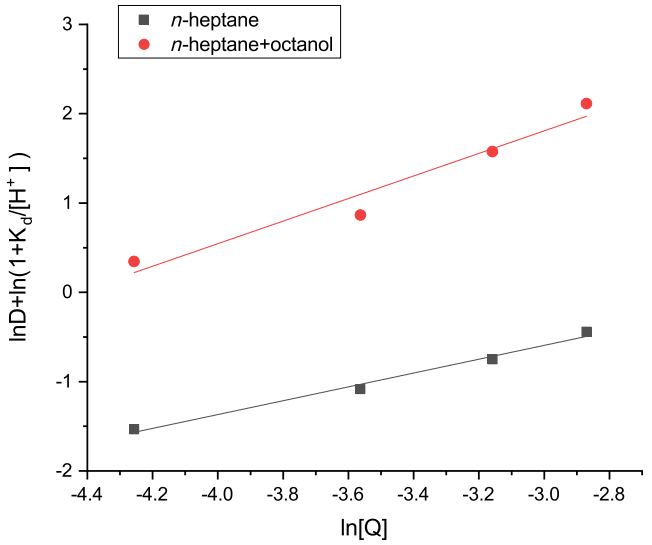

FIGURE 5 The graphical representation of Equation (5)

TABLE 2 Values of parameters from Equation (5) and Figure 5

Solvent	n	K_E (L/mol)
n-heptane	0.772 51	2.31
n-heptane/octanol	1.263 28	270

3.2 | Modelling and optimization

3.2.1 | Process modelling

After the experimental data was collected and analyzed (76 exemplars) and before using it for process modelling, it was pre-processed. This included a normalization procedure (the Min-Max approach), where all the data was reduced to the interval [0–1], a randomization step (the

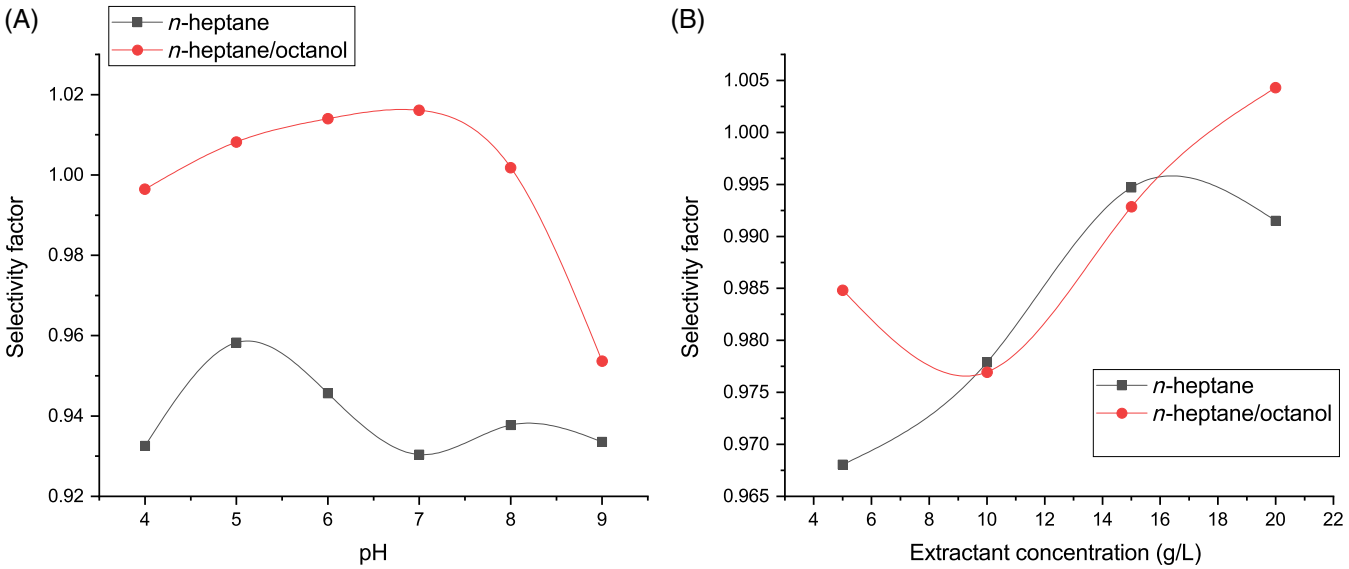

FIGURE 6 Influences of pH-value and extractant concentration on pseudomonic acid A selectivity factor (■—*n*-heptane, ●—*n*-heptane+octanol)

data was randomly re-arranged), and an assignment step (the first 75% from the randomized set was assigned for training and 25% for testing). The training dataset is used to train the ANN model (which in the case of hSADE-NN is performed simultaneously with the topology determination) and the testing set is used to determine the generalization capability of the trained ANN.

For the current process, the extraction yields of Pseudomonic acids A, B, and C were separately modelled as a function of concentration of octanol added, pH, and Amberlite LA-2 concentration.

Next, due to the random nature of the hSADE-NN, 50 simulations were performed for each case with the following settings: maximum number of hidden layers (1), maximum neurons in the hidden layer (20), population size (50), and generations (1000). The control parameters of the optimizer were limited in the interval [0,1] and they were automatically determined by the algorithm through the self-adaptive procedure. The statistics of all the models determined for the three types of pseudomonic acid are presented in Table 3; the architecture is presented in the form inputs: neurons_hidden_layer:outputs.

For comparison purposes, the three acids were also modelled using the standard linear regression approach (Equations (6–8)):

$$\text{Pseudomonic A} = 28.772\ 49 + 4.6698 \cdot \text{octanol} - 5.2249 \cdot \text{pH} + 1.4903 \cdot \text{ALA\_concentration} \quad (6)$$

$$\text{Pseudomonic B} = 47.7529 + 4.4606 \cdot \text{octanol} - 8.6796 \cdot \text{pH} + 1.2034 \cdot \text{ALA\_concentration} \quad (7)$$

$$\text{Pseudomonic C} = 73.8941 + 3.8909 \cdot \text{octanol} - 6.3539 \cdot \text{pH} - 1.0890 \cdot \text{ALA\_concentration} \quad (8)$$

The performance indicators of the regression models and of the best ANNs determined are presented in Table 4. As can be observed, although simple and easy to use, the regression models have high errors (especially for ARE) and cannot be further used in the optimization process. For Pseudomonic acid C, the highest errors obtained by the regression models are when the experimental values

TABLE 3 Statistic of all the determined models

Output	Perform. index	Fitness	MSE train	MSE test	R^2 train	Architecture of the combining model
Pseudomonic acid A	Average	563.2141	0.001 893	0.211 008	0.992 161	
	Best	789.6331	0.001 266	0.208 365	0.994 757	3:16:01
	Worst	310.3073	0.003 223	0.214 299	0.986 584	3:08:01
Pseudomonic acid B	Average	3136.145	0.000 368	0.225 612	0.998 162	
	Best	7912.976	0.000 126	0.224 647	0.999 409	3:14:01
	Worst	1507.154	0.000 664	0.230 393	0.996 647	3:11:01
Pseudomonic acid C	Average	141.087	0.007 157	0.185 946	0.961 567	
	Best	187.788	0.005 325	0.189 062	0.971 736	3:07:01
	Worst	123.7531	0.008 081	0.187 567	0.956 233	3:18:01

Abbreviations: MSE, mean squared error; perform., performance.

TABLE 4 Performance indexes of the best models determined

Output	Model	ARE train (%)	ARE test (%)	R^2 test
Pseudomonic acid A	Regression (Equation (6))	27.23	27.62	0.9591
	ANN(3:16:01)	7.51	10.94	0.9963
Pseudomonic acid B	Regression (Equation (7))	24.25	23.04	0.9749
	ANN(3:14:01)	3.209	2.802	0.9994
Pseudomonic acid C	Regression (Equation (8))	98.77	56.407	0.8655
	ANN(3:07:01)	16.49	13.58	0.9865

Abbreviations: ANN, artificial neural network; ARE, absolute average error; R^2, coefficient of determination.

are <15. This indicates that for an entire interval, the model is not able to efficiently capture the process dynamic. This is also true for the ANN model but, overall, its performance is much better (Figure 7).

3.2.2 | Process optimization

In the case of process optimization, the ANNs obtained in the modelling phase are used to generate predictions and to optimize the process. If in the case of model optimization, the objective of the optimizer is to determine the parameters of the ANN in order to minimize the error between prediction and experimental; in the case of process optimization, the objective is to determine the process independent parameters (concentration of octanol added, pH, and Amberlite LA-2 concentration) for which the maximum of Pseudomonic acid A and minimum of Pseudomonic acids B and C are obtained.

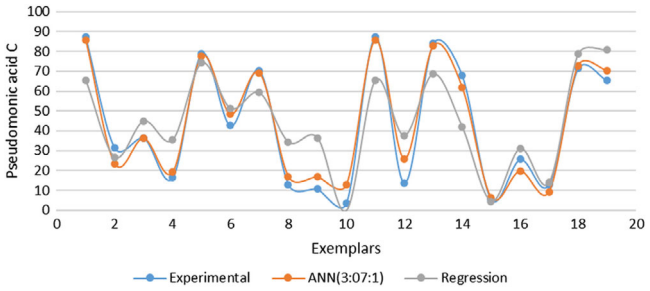

FIGURE 7 Comparison between experimental, regression, and artificial neural network (ANN) model for the testing data

In order to reach this objective, two cases were considered: where each type of acid is considered separately (CASE I) and where all acids were considered simultaneously (CASE II). In CASE I, the best models obtained are combined into a single model. Since the manner in which the process optimization is formulated is, in fact, a multi-objective problem, and since hSADE-NN was designed for single objective, the output of the combined model is represented in the following form (Equation (9)):

$$\text{Ouput} = \frac{\text{Pseudomonic}_{\text{Acid}_A}}{\text{Pseudomonic}_{\text{Acid}_B} + \text{Pseudomonic}_{\text{Acid}_C}} \quad (9)$$

The results obtained in CASE I are presented in Table 5, where the objective for Pseudomonic acid A is maximization and is minimization for Pseudomonic acids B and C. In addition to the objective followed in each case, the other two acids were determined using the process parameters and the models identified in the previous step. The results for CASE II are presented in Table 6.

As can be observed from Tables 5 and 6, when values higher than 100 were obtained (due to the fact that the models do not take into account the phenomenology of the process, the model automatically returns 100), the optimization procedure found various solutions that can be considered optimum in both CASE I and CASE II.

TABLE 5 Optimization results for CASE 1

Parameter optimized	Octanol conc.	pH	Amberlite LA-2 conc.	Pseudomonic acid A	Pseudomonic acid B	Pseudomonic acid C
Pseudomonic acid A-max	10	4	20	94.3822	89.8671	85.7203
	9.8	4	19.1	92.1635	87.0150	83.6610
	9	4	19.8	91.1329	81.7476	79.3242
	9.7	4.1	18.5	90.2485	83.7204	80.9335
	9.1	4.3	19.9	90.0162	77.7943	75.3277
Pseudomonic acid B-min	5.5	7.2	5.1	18.3738	8.5580	100.00
	8	8.6	5.2	31.9409	8.5236	100.00
	2.9	6	5.5	15.1388	8.5417	95.0854
	0.7	5	5.5	21.2908	8.5616	82.4264
	3.2	6.2	5.8	14.6856	8.5278	94.9627
Pseudomonic acid C-min	0.5	5.3	14.8	24.8823	17.4393	1.7831
	1	5.5	15.1	28.6087	18.0553	1.8206
	2	5.9	15.6	34.7107	19.2088	2.0915
	1.1	5.6	16	30.1410	19.1544	1.9051
	2.7	6.5	16.4	35.0788	18.9043	1.7923

Abbreviation: conc., concentration.

TABLE 6 Optimization results for CASE 2

No.	Octanol concentration	pH	Amberlite LA-2 concentration	Pseud. acid A	Pseud. acid B	Pseud. acid C
1	7.5	5.6	17.8	71.4421	43.5002	42.8172
2	6.2	5.1	18	71.1753	42.8928	42.9870
3	5.9	5	18.3	71.1577	43.0032	42.9676
4	7.4	5.8	19.3	71.4261	43.5939	40.1804
5	6.6	5.5	19.4	71.7829	43.1244	40.2581

Abbreviations: No., number; pseud., pseudomonic.

This indicates the capability of the optimization procedure to efficiently cover the search space represented by the process parameters and to provide combinations that could not be manually extracted from the experimental information. In this manner, new directions of development are provided.

4 | CONCLUSIONS

The processing of dilute aqueous solutions resulting from fermentation processes requires the use of different synergies to improve classical separation methods, a key challenge being to increase the economic competitiveness of biotechnological processes. The mupirocin production through biosynthesis leads to a mixture of four components in the fermentation broth that could be separated through a chemical extraction using a green solvent as *n*-heptane. Experimentally, the highest extraction yield and distribution coefficient are obtained for a pH of 4 and 20 g/L extractant. The reactive extraction is based on the H bond between the pseudomonic acids and the amines, with better results being obtained for Amberlite LA-2 compared to TOA. The addition of 1-octanol as polar modifier leads to the inhibition of the formation of a third phase and increases the extraction efficiency (influences the extraction equilibrium by increasing polarity and improves the acid-amine complex solubility in the organic phase). The mechanism of the interfacial reaction showed that only one molecule of Pseudomonic acid A and extractant react for the formation of the acid-extractant complex, indifferent of the pH value. The modelling and optimization of the process was performed by an algorithm combining DE and ANNs. First, the models for each type of acid were obtained in the form of stacked neural networks (formed from three independent ANNs and an additional network that combines the output of the independent models). In all cases, the best stacks obtained had an average absolute error in the testing phase of around 10% and therefore, they were further used in the optimization phase, where two cases were considered: (i) individual optimization (where for each acid, depending on its type, a maximization or minimization of output was performed) and (ii) simultaneous optimization (where the multi-objective problem of maximizing Pseudomonic acid A and minimizing Pseudomonic acids B and C was realized). In both optimization cases, multiple solutions were obtained, indicating that the optimizer is efficient in covering the entire search space formed by the process parameters.

ACKNOWLEDGEMENTS

This work was supported by the Ministry or Research and Innovation, CNCS –UEFISCDI, project PN III PCE 6/2017, code PN-III-P4-ID-PCE-2016-0100, within PNCDI III.

NOMENCLATURE

E	extraction efficiency (%)
D	distribution coefficient
K_E	extraction constant
Ka	dissociation constant
$[MupCOOH_{aq}]$	un-dissociated mupirocin's concentration in the aqueous phase
$\overline{[MUP-COOH_{(aq)}]}$	total mupirocin's concentration in the aqueous phase
$[Q_{org}]$	extractant concentration in the organic phase
n	number of amines molecules involved in the interfacial complex
S	selectivity factor
ANN	artificial neural networks
DE	differential evolution

ORCID

Alexandra Cristina Blaga https://orcid.org/0000-0001-8351-4258

REFERENCES

[1] S. Matthijs, C. V. Wauven, B. Cornu, L. Ye, P. Cornelis, C. M. Thomas, M. Ongena, *Res. Microbiol.* **2014**, *165*, 695.

[2] S. Khoshnood, M. Heidary, A. Asadi, S. Soleimani, M. Motahar, M. Savari, M. Saki, M. Abdi, *Biomed. Pharmacother.* **2019**, *109*, 1809.
[3] A. Tucaliuc, A. C. Blaga, A. I. Galaction, D. Cascaval, *Biotechnol. Lett.* **2019**, *41*, 495.
[4] K. Albrecht, G. Balogh, I. Barta, J. Erdei, E. Gulyas, I. Lang, J. M. N. Suto, M. Petroczki, I. M. Szabo, V. Szell, A. Tegdes, *European Patent, EP1151131A1*, 2003.
[5] I. Barta, A. Tegdes, V. Szell, C. Szabo, E. N. N. Arvai, W. Keri, D. Leonov, I. Lang, M. B. N. Igloy, G. Jerkovich, J. Salat, *US Patent 6,245,921 B1*, 2001.
[6] M. A. T. Bisschops, T. G. P. Reijns, A. Mathiesen, L. Aassveen, *US Patent, 7,619,102 B2*, 2009.
[7] A. D. Curzons, *US Patent 4639534*, 1987.
[8] R. Canari, A. M. Eyal, *Ind. Eng. Chem. Res.* **2003**, *42*, 1301.
[9] F. Chemarin, M. Moussab, F. Allais, I. C. Trelea, V. Athès, *Sep. Purif. Technol.* **2019**, *219*, 260.
[10] Y. Fan, D. Cai, L. Yang, X. Chen, L. Zhang, *Chem. Eng. Res. Des.* **2019**, *146*, 336.
[11] J. Gorden, T. Zeiner, G. Sadowski, C. Brandenbusch, *Sep. Purif. Technol.* **2016**, *169*, 1.
[12] S. Eda, A. Borra, R. Parthasarathy, S. Bankupalli, S. Bhargava, S. K. Thella, *Sep. Purif. Technol.* **2018**, *197*, 314.
[13] T. Brouwer, M. Blahusiak, K. Babic, B. Schuur, *Sep. Purif. Technol.* **2017**, *185*, 186.
[14] M. Djas, M. Henczka, *Sep. Purif. Technol.* **2018**, *201*, 106.
[15] B. Mizzi, M. Meyer, L. Prat, F. Augier, D. Leinekugel-Le-Cocq, *Chem. Eng. Process.* **2017**, *113*, 20.
[16] R. G. Lazar, A. C. Blaga, E. N. Dragoi, A. I. Galaction, D. Cascaval, *Sep. Purif. Technol.* **2021**, *255*, 117740.
[17] E. Ayan, N. Baylan, S. Çehreli, *Chem. Eng. Res. Des.* **2020**, *153*, 666.
[18] N. Baylan, S. Çehreli, *Sep. Purif. Technol.* **2019**, *224*, 51.
[19] N. Baylan, S. Çehreli, *Chem. Eng. Commun.* **2020**, *207*, 1426.
[20] S. Mukherjee, B. Munshi, *Chem. Eng. Process.* **2020**, *153*, 107936.
[21] K. L. Wasewar, D. Shende, A. Keshav, *J. Chem. Technol. Biot.* **2011**, *86*, 319.
[22] P. G. Jessop, *Green Chem.* **2011**, *13*, 1391.
[23] T. G. Susanti, E. Meinds, B. Pinxterhuis, B. Schuur, J. G. de Vries, B. L. Feringa, J. G. M. Winkelman, J. Yue, H. J. Heeres, *Green Chem.* **2017**, *19*, 4334.
[24] L. Kloetzer, R. A. Ilica, D. Cascaval, A. I. Galaction, *Sep. Purif. Technol.* **2019**, *227*, 115724.
[25] H. A. E. Benson, M. S. Roberts, V. R. Leite-silva, K. Walters, *Cosmetic Formulation: Principles and Practice*, CRC Press, Boca Raton, FL **2019**.
[26] S. Curteanu, G. D. Suditu, A. M. Buburuzan, E. N. Dragoi, *Environ. Sci. Pollut. R.* **2014**, *21*, 12856.
[27] M. Pirsaheb, E. N. Dragoi, Y. Vasseghian, *Polycycl. Aromat. Comp.* 2020, https://doi.org/10.1080/10406638.2020.1720750.
[28] M. Pirdashti, M. Ketabi, P. Mobalegholeslam, S. Curteanu, E. N. Dragoi, A. Barani, *Int. J. Thermophys.* **2019**, *40*, 84.
[29] Y. Vasseghian, E. N. Dragoi, *J. Environ. Eng.* **2018**, *144*, 06018003.
[30] E. N. Dragoi, S. Curteanu, D. Fissore, *Chem. Eng. Sci.* **2012**, *72*, 195.
[31] E. N. Dragoi, S. Curteanu, D. Cascaval, A. I. Galaction, *Environ. Eng. Manag. J.* **2015**, *14*, 533.
[32] E. N. Dragoi, S. Curteanu, D. Cascaval, A. I. Galaction, *Chem. Eng. Commun.* **2016**, *203*, 1600.
[33] J. B. Rubenick, A. M. Rubim, F. Bellé, D. R. Nogueira-Librelotto, C. M. B. Rolim, *Braz. J. Pharm. Sci.* **2017**, *53*, e16101.
[34] R. Storn, K. Price, *Differential Evolution - A Simple and Efficient Adaptive Scheme for Global Optimization over Continuous Spaces*, Berkeley, Berkeley, CA **1995**.
[35] F. M. Antony, K. L. Wasewar, *Sep. Purif. Technol.* **2018**, *207*, 99.
[36] A. G. Demesa, A. Laari, E. Tirronen, I. Turunen, *Chem. Eng. Res. Des.* **2015**, *93*, 531.
[37] L. M. J. Sprakel, B. Schuur, *Sep. Purif. Technol.* **2019**, *211*, 935.
[38] S. H. Yalkowsky, J. P. Yan He, *Handbook of Aqueous Solubility Data*, 2nd ed., CRC Press, Boca Raton, FL **2010**.
[39] N. Mungma, M. Kienberger, M. Siebenhofer, *ChemEngineering* **2019**, *3*, 43.
[40] D. Caşcaval, L. Kloetzer, A.-I. Galaction, *J. Chem. Eng. Data* **2011**, *56*, 2521.
[41] D. Caşcaval, A. I. Galaction, N. Nicuţă, A. C. Blaga, *Sep. Purif. Technol.* **2007**, *57*, 264.

How to cite this article: Lazar RG, Blaga AC, Dragoi EN, Galaction AI, Cascaval D. Application of reactive extraction for the separation of pseudomonic acids: Influencing factors, interfacial mechanism, and process modelling. *Can J Chem Eng*. 2021;1–12. https://doi.org/10.1002/cjce.24124

Journal of Industrial and Engineering Chemistry 133 (2024) 183–194

Contents lists available at ScienceDirect

Journal of Industrial and Engineering Chemistry

journal homepage: www.elsevier.com/locate/jiec

Selective separation of vitamin C by reactive extraction using ionic liquid: Experimental and modelling

Alexandra Cristina Blaga [a,*], Elena Niculina Dragoi [a], Diana Georgiana Gal [a], Adrian Catalin Puitel [a], Alexandra Tucaliuc [a], Lenuta Kloetzer [a], Dan Cascaval [a,*], Anca Irina Galaction [b]

[a] "Gheorghe Asachi" Technical University of Iasi, "Cristofor Simionescu" Faculty of Chemical Engineering and Environmental Protection, Iasi, Romania
[b] "Grigore T. Popa" University of Medicine and Pharmacy, Faculty of Medical Bioengineering, Iasi, Romania

ARTICLE INFO

Keywords:
Reactive extraction
Ionic liquid
Ascorbic acid
[P6 6 6 14][Phos]
Extraction mechanism

ABSTRACT

Vitamin C (ascorbic acid), is an important nutrient widely used as a dietary supplement in the food, beverage, cosmetic and feed industries or as a drug in the pharmaceutical industry. It can be produced by a traditional two-step fermentation or a novel one-step process, but its separation from the fermentation broth still needs improvement. This study investigated a reactive extraction method to selectively separate vitamin C from 2-keto-gluconic acid using an ionic liquid as the extracting agent and heptane as diluent. The separation efficiency and selectivity factor, as well as the analysis of extraction conditions (type and ionic liquid concentration, pH of the aqueous phase, contact time, temperature) influence and extraction mechanism were discussed. Heptane as the solvent and 100 g/L $[P_{6,6,6,14}][Phos]$ as the extractant were the optimum mixture for reactive extraction, resulting in an extraction yield of 99.98 % for vitamin C. A maximum selectivity factor of 3.5 was obtained for ascorbic acid for 160 g/L $[P_{6,6,6,14}][Phos]$ and pH 3 of the aqueous phase. The process was modeled and optimized using an Artificial Neural Networks (ANNs) and Differential Evolution (DE) algorithm. Based on the performance parameters evaluated and extraction yields obtained, ionic liquids have great potential for vitamin C separation.

Introduction

The metabolism of all living organisms depends on vitamins, which are defined as organic substances capable of sustaining life and enhancing growth, essential nutrients for the human body that are used and recycled in various processes. Although they do not have a high energy value and do not contribute to increased body mass, all living organisms require vitamins for growth, development and reproduction [1]. Their deficiency in the diet can lead to slowed or even blocked metabolic processes. Numerous coenzymes, enzymes or enzyme systems are synthesized from or with the help of vitamins, which maintain all human physiological functions [2].

Vitamin C (ascorbic acid, AA) is a vital water-soluble antioxidant and a nutrient used in many food additives, supporting a critical number of biological processes [3–6]. It is an essential vitamin involved in dental, bone, skin and blood vessel health, repairing tissues and preventing heart disease by acting as an antioxidant [3]. AA is usually helpful in relieving allergy symptoms and preventing or reducing viral and bacterial infections [1]. AA is obtained by extraction from various plant materials, through chemical synthesis, biosynthesis, or combined processes (chemical synthesis and biosynthesis). At the industrial level, two processes are used: biosynthesis combined with chemical conversion (the Reichstein process in seven steps) and fermentation in two steps using a single or mixed microbial culture [7]. The estimated 95,000 tonnes of AA recorded globally in 2021 were primarily produced in China (81 %). Data Bridge Market Research estimates that the global AA market will grow exponentially between 2022 and 2030, from USD 1,143.00 million in 2022 to USD 2,131.00 million in 2030. The most significant amount of AA is consumed in the pharmaceutical sector, which accounts for one-third of total production.

The Reichstein technique was essential for producing commercial AA for over 60 years [5]. This process converts L-sorbose into 2-keto-L-

* Corresponding authors at: at: "Gheorghe Asachi" Technical University of Iasi, "Cristofor Simionescu" Faculty of Chemical Engineering and Environmental Protection, Bdul D. Mangeron, no 67, Iasi, Romania.
E-mail addresses: acblaga@tuiasi.ro (A.C. Blaga), dancasca@tuiasi.ro (D. Cascaval).

https://doi.org/10.1016/j.jiec.2023.11.057
Received 15 September 2023; Received in revised form 1 November 2023; Accepted 28 November 2023
Available online 29 November 2023

gulonic acid (2-KLG), obtained using D-glucose as a substrate via five chemical reactions and a single biological reaction. This method has been the primary method of producing AA, although it has some disadvantages. These consist of long production time, complicated steps, high pressure and temperature requirements, continuous operation problems, and the need to use harmful chemicals. In addition, sorbitol in high initial concentrations prevents the development of bacteria and slows down oxidation. Because of these disadvantages, the two-step fermentation process was developed and is currently used on an industrial scale [4]. In this approach, *G. oxydans* converts D-sorbitol to L-sorbose in the first step with an efficiency of 98 %, which is then converted to 2-KLG in the second step by a mixed microbial culture (*Ketogulonigenium vulgare* - Gram negative and *Bacillus megaterium* - Gram positive) with a yield of 97 %. The two-stage fermentation is less complicated than the Reichstein method because there are fewer processes, lower pressure and temperature requirements, lower capital and operating costs (2/3 of Reichstein costs). The one-step fermentation process using glucose or sorbitol as substrate has been analyzed for direct production of AA in a system with a single culture of either bacteria (*Erwinia herbicola*) or yeast (*Saccharomyces cerevisiae*) or a mixed bacterial culture: *K. vulgare* and *G. oxydans* [7]. In the fermentation broth, glucose conversion leads to the formation of AA and 2-ketogluconic acid (2-KGA) [8].

Vitamin C separation from the fermentation broth is difficult due to its low stability in aqueous solutions [9]. The downstream process involves two steps: pre-purification, which removes the by-products by ion exchange, followed by vacuum concentration of the obtained solution and crystallization at low temperatures and in an acidic environment. Different techniques have been analyzed for the extraction of ascorbic acid: liquid-phase, solid-phase, ultrasonic and microwave-assisted extraction [10]. A reactive extraction procedure was analyzed for separating vitamin C using dichloromethane and Amberlite LA-2. An extraction efficiency of 96 % was obtained at a pH of 2 in the aqueous phase and a concentration of 160 g/L of extractant [11]. Jahromi et al. (2017) used $[Aliquat^{+}]_2[MnCl_4^{2-}]$ in a single-drop microextraction technique for ascorbic acid determination in effervescent tablets and orange juice [12]. Considering the request to develop eco-friendly processes, this work identified a more environmentally friendly and efficient extraction approach to reduce pollution from conventional volatile solvents (as dichloromethane).

Liquid-liquid extraction is a separation technique used to extract a specific component (solute) in a system of two immiscible liquids (aqueous and organic), commonly used in chemical laboratories for purification, separation, and concentration of compounds. It is also employed in industries such as pharmaceuticals, food processing, environmental analysis, and nuclear reprocessing, where selective separation of specific components is required. The technique relies on the differences in solubility or partitioning behavior of the desired compound between the two liquid phases. Reactive extraction is a specialized form of liquid–liquid extraction that involves chemical reactions occurring simultaneously with the extraction process. It combines the principles of extraction and reaction in a single step, allowing for the simultaneous removal and transformation of a target compound from a mixture. The reactive extraction process offers several advantages over conventional extraction methods: selectivity, enhanced efficiency, minimization of byproducts, reduced process duration, and the possibility of being realized in continuous systems [13–16].

There has been much research done on reactive liquid–liquid extraction as a technique for separating valuable compounds [11–21], such as natural products, pharmaceutical intermediates, and bioactive molecules from fermentation broths, using different solvents (dichloromethane, octanol, chloroform, etc.). Reactive extraction systems usually contain a solvent (diluent) and an extractant that interacts with the dissolved target substance (solute) and forms complexes. A practical alternative to classical extractants (long chain amines, ammonium salts, organophosphorus acid type extractants) is ionic liquids (greener choice), which contain a large, asymmetric organic cation and a small, often inorganic anion in their structure. Due to some essential properties, such as low vapor pressure and high thermal stability, ionic liquids have attracted much interest due to the increasing environmental awareness and the vast demand for efficient and environmentally friendly solvents. As extractants in reactive extraction, ionic liquids have been used for the separation of carboxylic acids: butyric, lactic, succinic, glycolic, valeric, propionic, adipic, nicotinic [19]. The separation of fat-soluble vitamins (vitamin D3 and E) was investigated with good results using a pyrrolidinium-based ionic liquid ([BMPr][NTf_2]), and a methylimidazolium-based ionic liquid [C_4C_1im]Cl respectively [15].

Because both efficiency and environmental impact must be considered in the extraction of bioproducts, this study analyzed five hydrophobic ionic liquids (trihexyl-tetradecyl-phosphonium bis(2,4,4-trimethylpentyl) phosphinate, [$P_{6,6,6,14}$][Phos]; trihexyl-tetradecyl-phosphonium decanoate, [$P_{6,6,6,14}$][Dec]; 1-butyl-3-methyl-imidazolium-hexafluorophosphate, [C_4mim][PF_6]; 1-hexyl-3-methyl-imidazolium-hexafluorophosphate, [C_6mim][PF_6]; 1-octyl-3-methyl-imidazolium-hexafluorophosphate, [C_8mim][PF_6]) for the selective separation of AA from 2-KGA from aqueous solutions such as fermentation broth. Considering both the unfavorable physical properties of the pure extractants – very high viscosity, and their relatively high cost, they were also investigated in diluted form with an inactive diluent (heptane). The influence of the main factors on the separation, namely pH of the aqueous phase, contact time, temperature, type and concentration of ILs were analyzed in terms of extraction efficiency, selectivity and loading factor. This is the first article to report on separating vitamin C with ionic liquids from aqueous solutions. Furthermore, the stripping process was analyzed to investigate the ILs reusability and the process was modeled and optimized using ANNs.

Experimental

Materials

All chemicals, including ascorbic acid (99.0 %), 2-ketogluconic acid (99 %), [$P_{6,6,6,14}$][Phos], [$P_{6,6,6,14}$][Dec], [C_4mim][PF_6], [C_6mim][PF_6], [C_8mim][PF_6] (99 %), 1-octanol (99 %), heptane (99 %), sodium hydroxide (>97 %), sulfuric acid (95.0–98.0 %), and acetonitrile (99.99 %), were purchased by Sigma Aldrich and used as received without further processing.

Reactive extraction experiments

Reactive extraction experiments for AA and 2-KGA separation were carried out using equal volumes of aqueous and organic phases (2 mL, 1:1 v/v ratio forming a two-phase system) using a vibratory shaker with 1200 rpm. The extraction experiments were performed at 20 °C, 30 °C, 40 °C and 50 °C with a duration of 5, 10, 20 and 30 min to assure good interfacial contact. After the extraction, phases were separated in a centrifugal separator at 4000 rpm. The separated organic phase was employed in stripping experiments and the aqueous phase was used for quantitative analysis (HPLC). AA initial concentration in the aqueous phase was 5 g/L (2.83×10^{-2} M), 2-KGA concentration was 1g/L (5.15×10^{-3} M), the concentrations of the ionic liquids in the organic phase varying between 0 and 160 g/L. The pH value of the aqueous phase varied between 1 and 5 for the extraction, being modified by using solutions of 3 % sulfuric acid or 3 % sodium hydroxide by means of the indications of the digital pH meter (CONSORT C 836).

Stripping experiments

Stripping experiments for AA and 2-KGA separation were carried out using diluted sodium hydroxide solution (pH 10, modified by means of the indications of the digital pH meter (CONSORT C 836) in equal

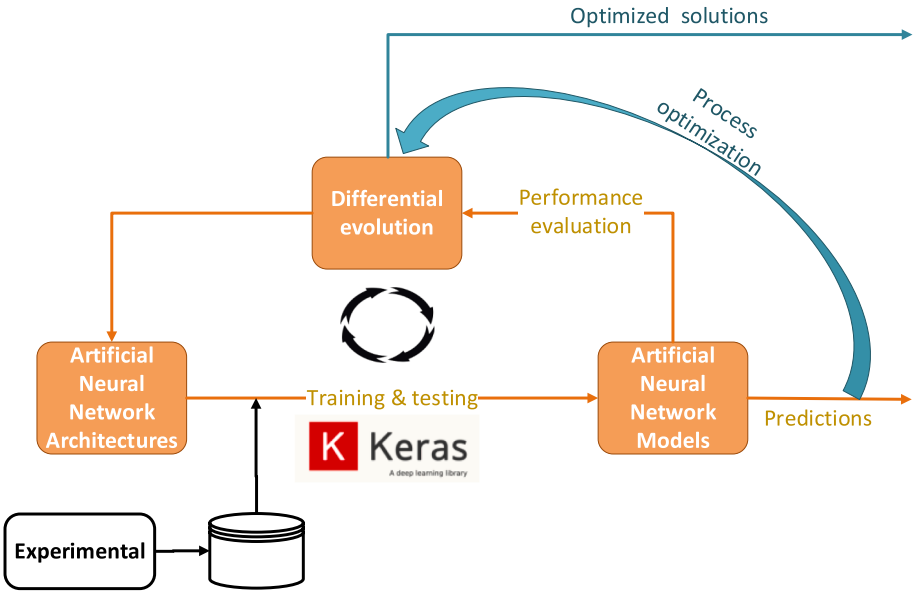

Fig. 1. The main steps for process modeling and optimization.

volumes with loaded organic phases organic phase (2 mL) using a vibratory shaker with 1200 rpm. The stripping experiments were performed at 50 °C with a duration of 20 min to assure good interfacial contact. The pH value of the aqueous phase varied between 1 and 5 for the extraction and 10 for the stripping experiments, being modified by using solutions of 3 % sulfuric acid or 3 % sodium hydroxide.

HPLC analysis

The processes were analyzed based on extraction efficiency, calculated using the mass balance based on the AA and 2-KGA concentration in the aqueous phases measured by high-performance liquid chromatography technique (HPLC) [16]. For this purpose, an HPLC system, UltiMate 3000 Dionex, provided with a Hamilton PRP-X300 column (150 mm × 4.1 mm, 5 µm), 4 mM sulfuric acid solution used as mobile phase, with detection by UV absorbance at 210 nm wavelength, and the flow rate of 0.5 mL/min was used.

FTIR analysis

FTIR spectra of organic phase (fresh and loaded) were recorded using an Agilent Cary 630 FTIR instrument (32 scans per sample at 4 cm^{-1} spectral resolution and 4000–400 cm^{-1} range).

Calculations

The percentages of extraction efficiency (AA and 2KGA amount extracted into the organic phase), stripping/re-extraction efficiency (AA and 2-KGA amount transferred from the loaded organic phase into the stripping phase) were defined by Eqs. (1), (2), where C_0, C and C_s, (mol/L) are AA and 2-KGA concentrations in the aqueous initial solutions, raffinate (exhausted initial solution after extraction) and stripping solution, respectively:

$$E = \left(\frac{C_0 - C}{C_0}\right) \bullet 100, \% \quad (1)$$

$$R = \left(\frac{C_s}{C_0 - C}\right) \bullet 100, \% \quad (2)$$

The selectivity factor, S, is calculated as the ratio between the extraction degree of AA and that of 2-KGA:

$$S = \frac{E_{AA}}{E_{2KGA}} \quad (3)$$

To confirm the reaction mechanism the loading ratio was used, defined as the total AA and 2-KGA concentration in the organic phase (calculated from the mass balance as a difference C_o-C) divided by the total concentration of ionic liquid in organic phase:

$$Z = \frac{C_{org}}{C_{IL_{org}}} \quad (4)$$

Modelling and optimization

Artificial Neural Networks (ANNs) are complex mathematical models that determine non-linear interactions between a system's inputs and outputs. As such, simple or combined with other Artificial Intelligence techniques, they were efficiently applied to various types of processes and systems, examples focusing on reactive extractions of compounds such as 2-keto gluconic acid [14], malic acid [17], gallic acid [18,19], itaconic acid [20], tartaric acid [21]. Although simple to use, the optimal ANN setup is a problem that must be carefully solved to ensure good results. The two main aspects that influence performance are: i) network topology (the structure of the network, such as the number of hidden layers and neurons in each hidden layer) and ii) the network training (internal parameters such as weights, biases). Network topology is usually set through a trial-and-error approach, where different combinations are manually tested. Training is usually performed by a series of training algorithms (mainly gradient-based), the most known being BackPropagation. Compared with the classical approaches, this work applies the neuro-evolution principle to automatically determine the ANN's topology automatically. The general schema of the modeling and optimization procedure is presented in Fig. 1.

In other words, a bio-inspired metaheuristic (Differential Evolution – DE) is applied to identify the optimal arrangement of neurons and hidden layers for the ANN represented by the Keras Sequential Model. The training phase is performed using Adam [22]. The implementation was performed in Python and was previously applied to efficiently model the transition of five-ring bent-core molecules [23]. After the best model was determined, the impact of the inputs on the model outputs was determined using the SHapley Additive exPlanations (SHAP) strategy [24]. Next, the DE algorithm was applied to optimize the process and identify the conditions leading to a maximum efficiency extraction of

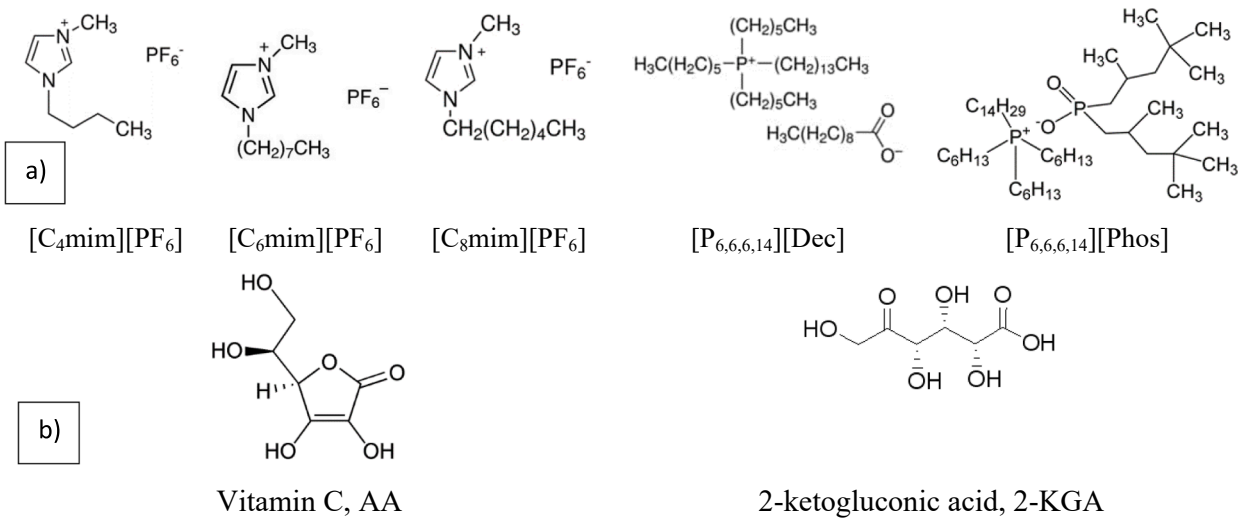

Fig. 2. Chemical structure of ionic liquids (a) and solutes (b) analyzed in this study.

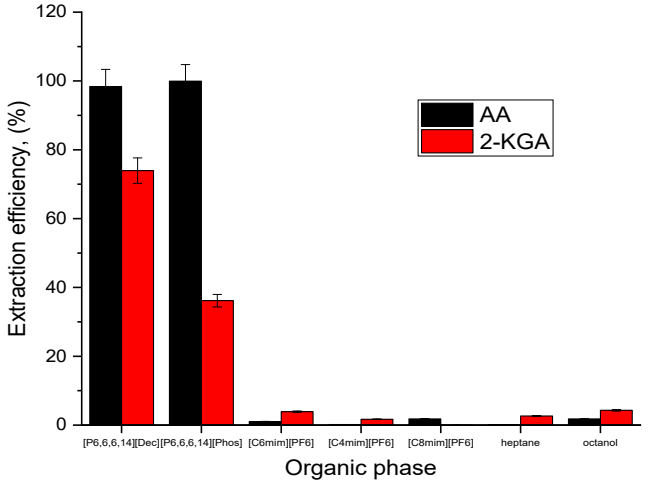

Fig. 3. Effect of organic phase on vitamin C and 2-ketogluconic acid extraction efficiency.

AA.

Results and discussions

Reactive extraction

The efficiency of the reactive extraction depends on the physical and chemical characteristics of the solute (hydrophobicity, acid-base properties), properties of the extractant (reactivity, ability to form hydrophobic compounds with the solute) and separation conditions (pH, temperature, mixing intensity, presence of impurities, concentration level, contact time, reaction kinetics, phase ratio etc.). It is essential to optimize and balance these factors based on the specific system and desired outcomes to achieve efficient and selective reactive extraction. Experimental design, process control, and characterization techniques can be employed to identify and optimize the key factors affecting the efficiency of the reactive extraction process.

The choice of solvents and extractants used in reactive extraction plays a crucial role. They should be eco-friendly, immiscible with the aqueous phase, and with suitable physical and chemical properties to facilitate easy separation and the desired extraction efficiency. Organic phase selection affects the solubility and partitioning behavior of AA and 2-KGA, thereby influencing the extraction efficiency. Ionic liquids have the potential to be greener alternatives to classical organic systems. However, carefully considering their properties, application requirements, and environmental impact is necessary to ensure sustainable use. Considering this, five hydrophobic ionic liquids (Fig. 2a) and two organic solvents (with different polarities – heptane and octanol) were analyzed for AA and 2-KGA (Fig. 2b) extraction, with the results presented in Fig. 2. The intention at this stage was not to perform an exhaustive screening but to find the most promising system for further optimization.

The structural differences between AA and 2-KGA are due to the lactonic structure (Fig. 2b), so their physical–chemical characteristics are quite similar. AA and 2-KGA solubility is influenced by the four hydrophilic hydroxyl groups and, in the case of 2-ketogluconic acid, by the specific carboxylic acid group [16]. Both compounds have shown similar properties in terms of solubility: they are almost insoluble in both organic solvents analyzed: heptane, an aprotic solvent (dielectric constant 1.9), and octanol, protic solvent (dielectric constant 10.3).

The highest extraction efficiency was recorded for both compounds (Fig. 3) in the case of trihexyl-tetradecyl-phosphonium ([$P_{6,6,6,14}$]) ionic liquids, corelated to their superior basicity compared cu imidazolium ionic liquids (basicity reduces in the following sequence phosphonium > ammonium > pyrrolidinium > pyridinium > imidazolium) [25]. [$P_{6,6,6,14}$][Dec] (98.39 % for AA and 73.95 % for 2-KGA) allowed the highest extraction for 2-ketogluconic acid, while for vitamin C, the best results were obtained for [$P_{6,6,6,14}$][Phos] (99.94 % for AA and 36.16 % for 2-KGA). This is due to the formation of stronger hydrogen bonds (due to the presence of oxygen atoms with non-bonding pairs of electrons). These results were confirmed in literature in the case of other vitamins: vitamin B9 [26] or carboxylic acids: lactic, malic, succinic [27]. [$P_{6,6,6,14}$] ILs offer several attractive properties for their use in developmental and industrial applications: they are liquid at room temperature, are immiscible with water (9.1 g/m^3 water solubility for [$P_{6,6,6,14}$][Phos] [26], but a three-phase system forms in excess water [28]), have high thermal stability, are miscible with organic solvents, are stable under basic conditions (important for stripping) and have a lower cost compared to other ionic liquids.

Viscosity plays an essential role in influencing the efficiency of reactive extraction because it affects mass transfer, the efficiency of mixing of the two phases and their separation. As far as the organic phase is concerned, the use of ionic liquids with high viscosity (319 cP for [$P_{6,6,6,14}$][Dec] and 805 cP for [$P_{6,6,6,14}$][Phos] [27]) can pose a challenge to extraction performance, affecting the mass transfer of IL-based extraction systems [29], but also for equipment design and

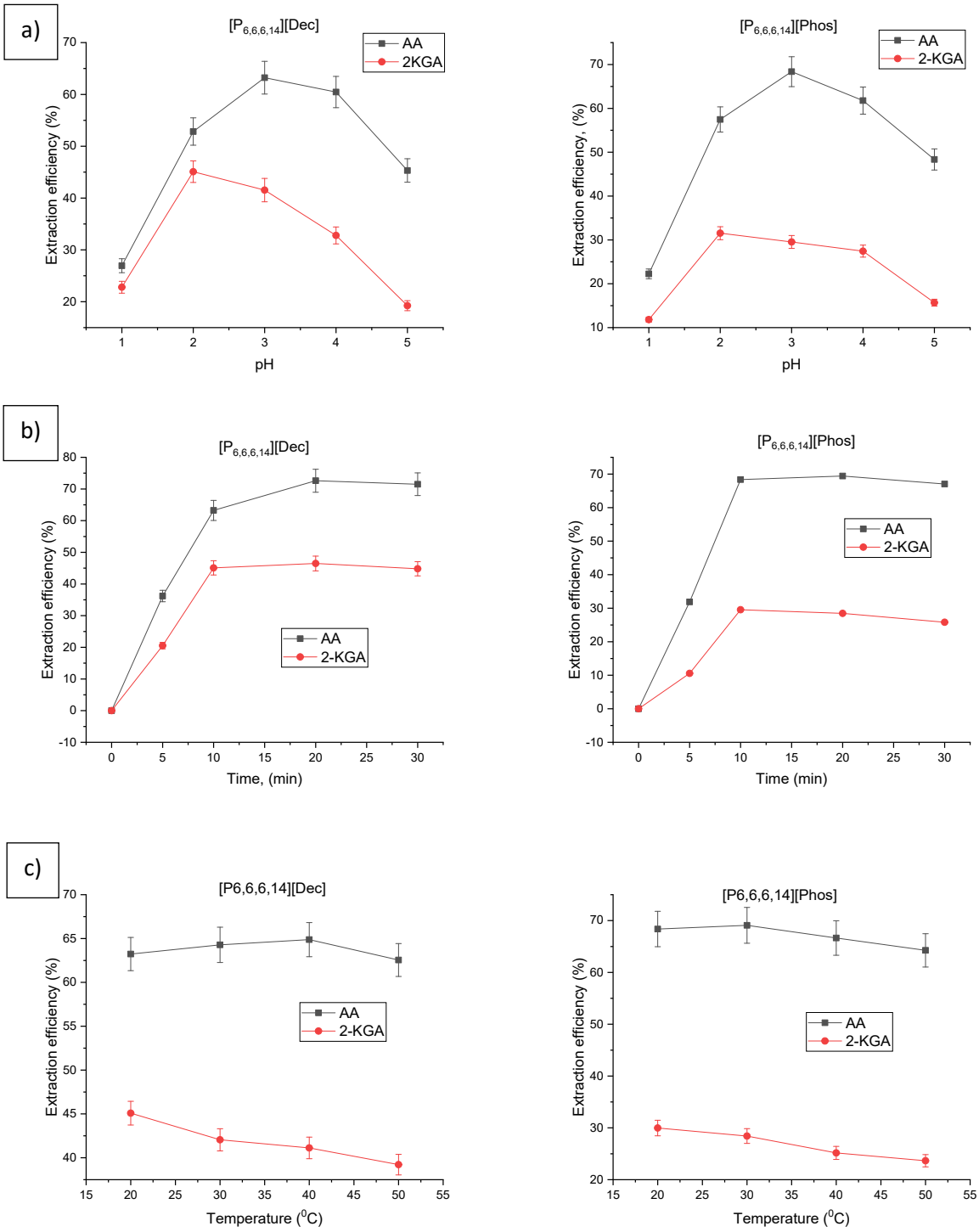

Fig. 4. Parameter's influence on extraction efficiency a) - pH, b) - time, c) - temperature (ILs concentration 40 g/L).

operation (e.g., higher viscosity of the organic phase may require modifications of the equipment and operating parameters to account for the increased flow resistance). Considering this, heptane, a non-polar solvent, was investigated as a possible diluent for both [$P_{6,6,6,14}$] ILs to reduce the viscosity and surface tension.

Parameter influence on the extraction efficiency

The impact of aqueous phase pH, contact time and temperature on the extraction efficiency was studied. The pH of the aqueous phase plays a crucial role in the reactive extraction of acidic compounds, which can be undissociated (pH < pKa), but also dissociated/ionized (pH > pKa), the degree of ionization affecting the solubility and partitioning behavior of the acidic compounds between the aqueous and organic phases. The results obtained for pH influence in the case of 2-KGA and AA separation from their mixture are presented in Fig. 4a for both [$P_{6,6,6,14}$] ILs. AA is a monobasic acid (pKa = 4.1 at 25 °C), the acidity being conferred by the HO– enolic group in position 3, the HO– enolic group in position 2 having a pronounced basic character (pKb = 11.6 at 25 °C) [11]. 2-KGA is one of the strongest monobasic carboxylic acids (pKa = 2.66 at 25 °C) [13]. For 40 g/L ionic liquids in heptane, the maximum extraction degree was obtained for AA at pH 3 (68.37 % using [$P_{6,6,6,14}$][Phos]; 63.23 % using [$P_{6,6,6,14}$][Dec]) and at pH 2 for 2-KGA

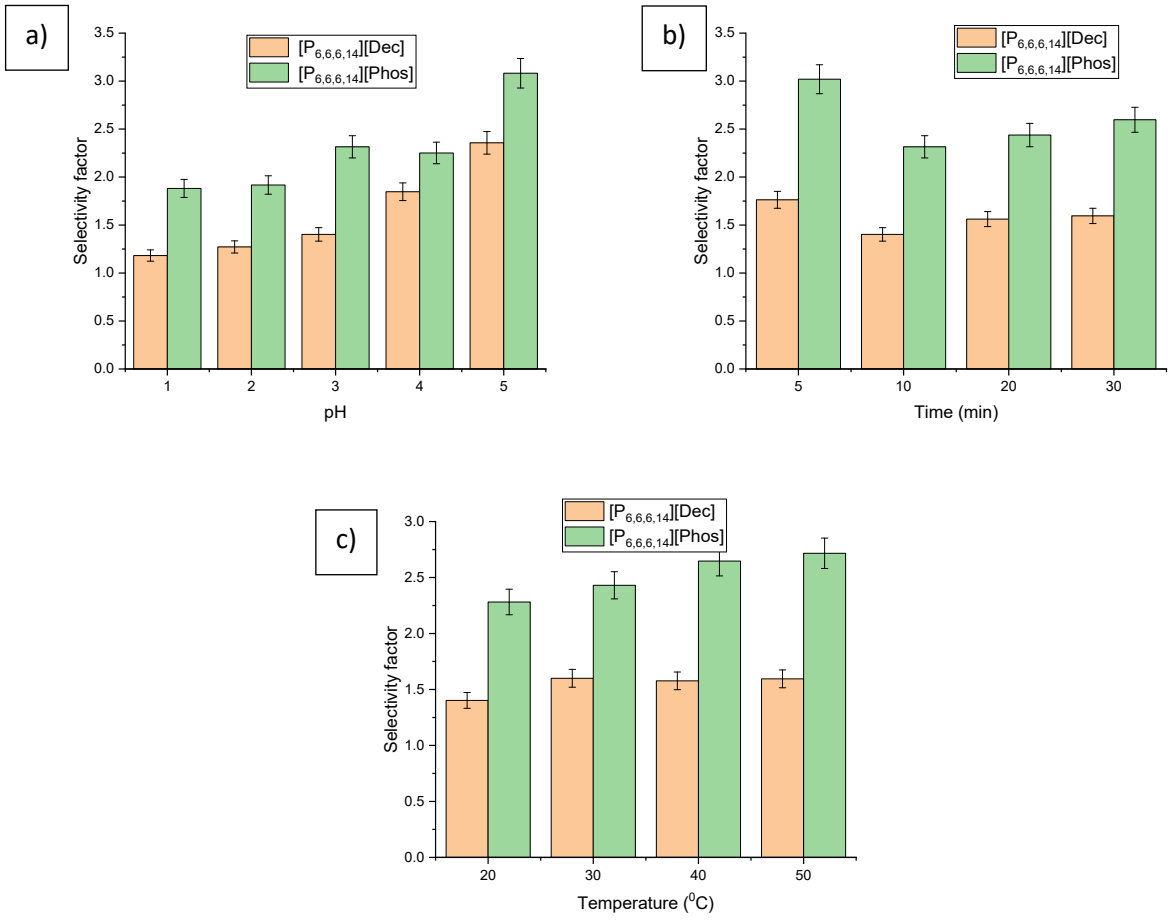

Fig. 5. Parameter's influence on AA selectivity a) - pH, b) - time, c) - temperature (ILs concentration 40 g/L).

(45.08 % using [$P_{6,6,6,14}$][Dec] and 29.53 % using [$P_{6,6,6,14}$][Phos]).

The experimental results showed a maximum extraction efficiency at a pH lower than pKa; as the pH increases, the acid equilibrium shifts to dissociation, and the extraction efficiency decreases. This variation can be explained by considering the properties of solutes and ILs. For hydrophobic anion-containing ILs, the extraction mechanism usually implies H-bonds between the ionic liquid and the organic acid undissociated form. Thus, to achieve maximum extraction efficiency, the pH of the aqueous phase should be significantly below the pKa of the acid.

The extraction mechanism assumes the attachment of the protonated acid via an H-bond to the binding sites in the anion of the IL (for example, the oxygen of bis(2,4,4-trimethylpentyl) phosphinate, in the case of [$P_{6,6,6,14}$][Phos] or from decanoate - carboxylate for [$P_{6,6,6,14}$][Dec]). The addition of sulfuric acid for the pH control (at pH 1) influences the extraction efficiency, reducing the IL's extractant capacity for both ascorbic acid and 2-ketogluconic acid. Sulfuric acid determines the extractant protonation (induced by the protons of the strong mineral acid), that generates counter-anions extraction to preserve the neutrality, similar to the results obtained for lactic and butyric acid [26,27,30]. In addition, 2-KGA forms dimers at low pH in the aqueous phase [14], reducing the number of carboxyl groups available for H-bond formation with [$P_{6,6,6,14}$] ILs. The 2-KGA higher acidity (pKa: 2.6 compared to 4.1 for AA) supports the higher extraction efficiencies obtained in the case of [$P_{6,6,6,14}$][Dec], similar to other carboxylic acids: lactic, folic and butyric acids [26,30] and the difference between the optimal pH-value for the extraction of 2-KGA (pH = 2) and for AA (pH = 3). For the pH correction at pH 4 and 5, the addition of NaOH (strong mineral base) generates the preferential neutralization of the stronger acid in the system (2-KGA), leading to a sharp decrease of its extraction efficiency.

The contact time is an important parameter that can be optimized to achieve the desired extraction efficiency since the optimal process duration can be determined by varying the contact time. That will provide the highest extraction yield while maintaining the feasibility and cost efficiency of the process [31]. If the contact time is too short, incomplete extraction may result in low separation efficiency. However, if the contact time is too long, the degradation of the solute may also appear [32]. The experimental results (Fig. 4b) show that increasing the contact time increases reactive extraction efficiency in 10 min and remains almost unchanged after that for 2-KGA, while for vitamin C the extraction efficiency reaches its' maximum value after 20 min of contact time (determined by its lower acidity) and only then remains at approximately the same value, extraction efficiency between 10 and 20 min of contact time increases for about 10 %. The rapid extraction is due to the increased interfacial area resulting from the intense mixing and availability of the reactants to the interface in vicinal aqueous and organic regions. Similar results were obtained for reactive extraction of lactic acid [32] or acetic acid [33].

The temperature significantly affects reactive extraction and influences the efficiency of the process, affecting carboxylic acid's solvation and interactions in aqueous phases [13]. It affects the rate of the chemical reaction that occurs during reactive extraction. An increase in temperature leads to an acceleration of the reaction kinetics (higher temperatures provide more energy to the reacting species, which increases the collision frequency and reaction rate), allowing faster and more complete reactions between the solute and the extractant. In addition, solubility increases with temperature, resulting in a higher solute concentration in the organic phase and improving extraction efficiency (more solute molecules can be dissolved and extracted from the

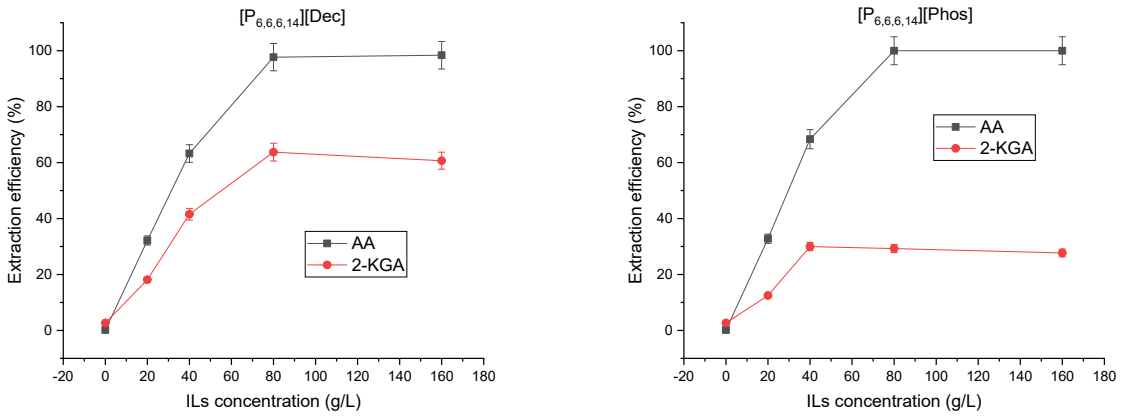

Fig. 6. IL's concentration influence on extraction efficiency (aqueous phase pH = 3, contact time 10 min, temperature 20 °C).

Table 1
Z values for AA and 2-KGA.

$[P_{6,6,6,14}][Dec]$, M	Z (AA)	Z (2-KGA)	$[P_{6,6,6,14}][Phos]$, M	Z (AA)	Z (2-KGA)
0.03	0.317	0.022	0.02	0.365	0.018
0.06	0.307	0.034	0.05	0.324	0.043
0.12	0.234	0.020	0.10	0.278	0.010
0.24	0.117	0.009	0.20	0.139	0.003

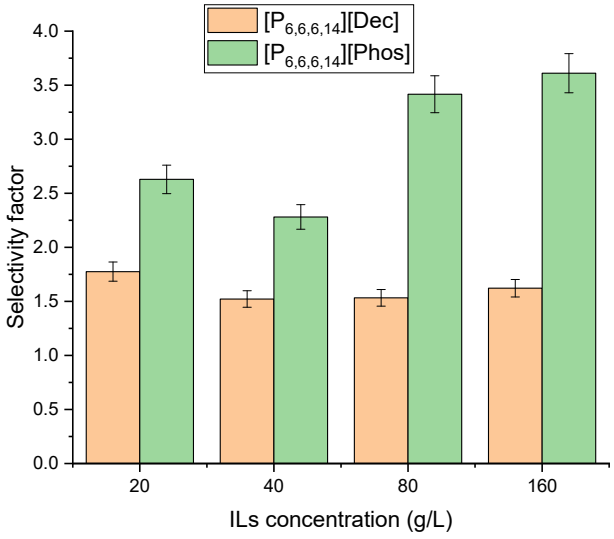

Fig. 7. IL's concentration influence on the selectivity factor (aqueous phase pH = 3, contact time 10 min, temperature 20 °C).

aqueous phase). Temperature affects the mass transfer rate between the aqueous and solvent phases: higher temperatures improve the diffusion coefficient and reduce the solvent's viscosity, intensifying the mass transfer. This can lead to higher extraction efficiency, as the solute molecules can diffuse more easily from the aqueous to the organic phase. The influence of this parameter was studied under similar batch conditions for the temperature range 20 – 50 °C at an aqueous phase pH of 3, 10 min contact time and an IL concentration of 40 g/L. The experimental results show that temperature has the lowest effect on reactive extraction efficiency, a small decrease can be recorded with increasing temperature, presented in Fig. 4c. This phenomenon could be related to the apparition of the back extraction phenomenon with increasing temperature, which decreases the overall efficiency of the process. The system's decreased entropy leads to complexes forming in the organic phase, which increases the reaction order. Based on the obtained results, it can be concluded that the temperature of 20 °C is the desired temperature to achieve higher extraction efficiency. These results are similar to other published data for caproic acid [34] and protocatechuic acid [35].

The selectivity factor, S, is calculated as the ratio between the extraction degree of AA and that of 2-KGA, and the experimental results show that the values of S for $[P_{6,6,6,14}][Phos]$ are higher regardless of pH, temperature, and time, which is attributed to the superior efficiency of this IL for the reactive extraction of AA. From Fig. 5, it can be seen that S varies as a function of pH and is closely related to the extraction efficiency for the two compounds, with the highest selectivity obtained at pH = 5 for both ionic liquids, due to a very low extraction efficiency of 2-KGA at this pH. The minimum value for pH = 1 are in agreement with the very close extraction efficiencies for both compounds obtained at this pH. The highest selectivity factor was obtained at a contact time of 5 min, when the extraction of vitamin C with $[P_{6,6,6,14}][Phos]$ is faster than the reaction of 2-ketogluconic acid with IL. The temperature of 40 °C provides the highest selectivity factor due to the more efficient extraction of vitamin C.

Reactive extraction mechanism

The analysis of the effects of pH on the degree of extraction indicated that the reactive extraction process is based on H-bonding between the undissociated form of the acids and the ionic liquids. Due to the insolubility of the two compounds (AA and 2-KGA) in heptane and of the extractant in the aqueous phase, the reactive extraction with $[P_{6,6,6,14}]$ ILs proceeds via an interfacial reaction followed by diffusion of the reaction product into the organic phase. To investigate the mechanism of reactive extraction, the effect of extractant concentration on reactive extraction was studied for the optimum conditions: aqueous phase pH 3, temperature 20 °C and 10 min contact time. The results presented in Fig. 6 show an important increase in extraction efficiency with increasing concentration of the extractant in heptane up to 100 g/L, further increase (160 g/L ILs) only slightly improved both L- AA and 2-KGA extraction.

The loading ratio (Z) indicates the number of molecules of solute and extractant involved in forming the hydrophobic complex and is used to estimate the reaction stoichiometry. Z is influenced by the equilibrium concentration of the solute, but also by the nature of the diluent of the organic phase (heptane) and the extractant ($[P_{6,6,6,14}]$ IL) properties. Table 1 shows the values obtained for $[P_{6,6,6,14}]$ IL extraction in both AA and 2-KGA cases. All values obtained are less than 1, so no overloading of the ionic liquid can be assumed.

The decrease of the loading ratio with the increase of the extractant concentration indicates that only equimolecular (1:1) acid-extractant complexes are formed for both studied compounds, independent of IL. This is supported by the obtained values of Z lower than 0.5 associated with low solute concentrations in the organic phase [36]. For the

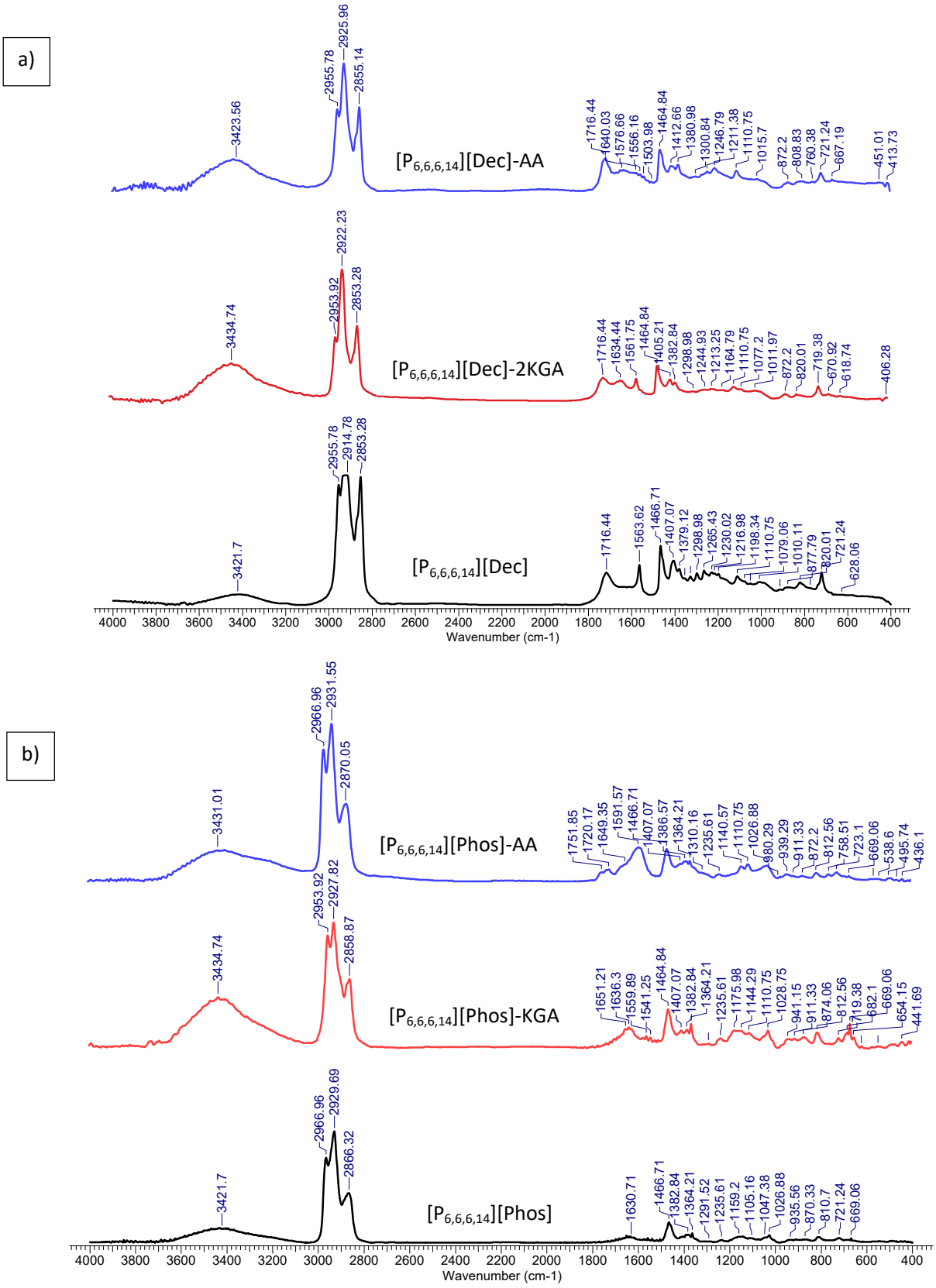

Fig. 8. FTIR spectra for ionic liquids (a-[$P_{6,6,6,14}$][Dec]; b-[$P_{6,6,6,14}$][Phos]) in heptane and extracts (loaded), 40 g/L ionic liquid concentration in heptane.

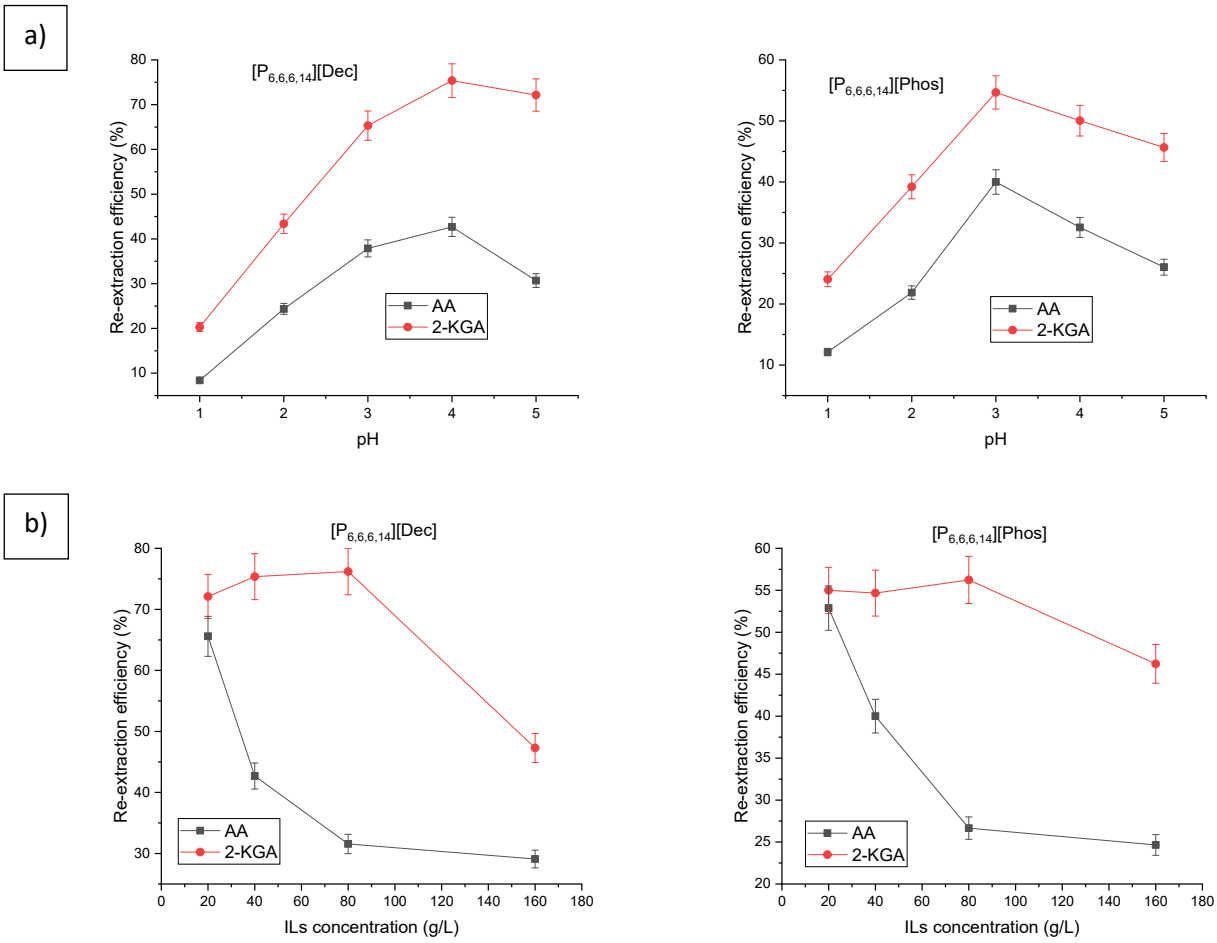

Fig. 9. Influence of pH (a) and extractant concentration (b) on back extraction efficiency.

Table 2
Statistic indicators of the best ANN models obtained.

Model	Dataset	EVS	MAE	MSE	MAPE	R^2
AA	Training	0.984	1.380	3.782	0.024	0.983
	Testing	0.982	2.044	7.322	0.037	0.981
2-KGA	Training	0.899	3.237	21.589	0.099	0.898
	Testing	0.797	3.271	22.149	0.1077	0.793

duration of the extraction process, no change in the viscosity and density of the organic phase (heptane with $[P_{6,6,6,14}]$ IL) was observed at equilibrium, so no co-extraction with water was considered. This is the effect of short extraction time, but also to weak water co-extraction associated to monocarboxylic acids (e.g. 2-KGA, at low acid concentrations) [37].

The selectivity factor (Fig. 7) increases by increasing extractant concentration from the value of 1.94, corresponding to a concentration of 40 g/L, to 3.55, for 160 g/L $[P_{6,6,6,14}]$[Phos]. For $[P_{6,6,6,14}]$[Dec], the highest value (1.83) was obtained at 20 g/L extractant concentration, due to its higher efficiency towards 2-KGA extraction.

In order to confirm the extraction mechanism, IR spectra (Fig. 8) of the two ionic liquids in heptane and obtained extracts were analyzed.

The FTIR spectra of the organic phase (ionic liquid in heptane and extracts) are not very different, but a significant change was recorded in the 3400–3500 cm^{-1} domain. As observed, the major peaks in the 2800–3000 cm^{-1} range (H-C–H stretch: asymmetric and symmetric) correspond to the solvent–heptane, the ionic liquid peaks are mainly visible in the 1700–600 cm^{-1} domain. At 3400–3500 cm^{-1} domain, the OH (hydrogen-bonded) stretch valence oscillation can be recognized, and an increasingly large peak can be observed in both extracts spectrum, proving the formation of hydrogen bonds of both AA and 2-KGA with the extractant, similar to other extraction systems (citric acid and TOA [38]). In the FTIR spectra recorded for ionic liquids in heptane, peaks at 1466 cm^{-1} are due to P-C stretching, at 1382 cm^{-1} are due to C - H in-plane bending, and the characteristic vibrations reflecting the presence of IL anions (e.g. POO^- at ca. 1026 cm^{-1}, P-CH_2 at ca. 1467 cm^{-1} and COO^- at ca. 1563 cm^{-1} and ca. 1406 cm^{-1} [39], stretching vibration of C = O (decanoate) at ca. 1716 cm^{-1} [40]) were also detected. FTIR spectroscopy revealed new bands at ca. 1634–1636 cm^{-1} (C = O stretching mode vibration), ca. 1559–1561 cm^{-1} (carboxylate peak [40]) for the spectrum of KGA extract and at 1591 cm^{-1} (C = C) and 1720 cm^{-1} (C = O stretch [41]) for the spectrum of AA extract.

Study of stripping process

In this study, the stripping step was performed by pH variation (NaOH solutions with pH 12 were used for solute recovery) and temperature variation (re-extraction was performed at 50 °C).

The results from Fig. 9 showed a more efficient stripping of 2-KGA compared to AA, regardless of the pH of the starting phase or the concentration of the extractant. This is due to the higher acidity of KGA, which favors its reaction with NaOH. For AA, the highest efficiency was obtained at an extract concentration of 20 g/L, while for 2-KGA the best results were obtained at 80 g/L. The carboxylic acid is transformed into its salt when an aqueous sodium hydroxide solution is added to the extract. Lowering the complexation constant and increasing the recovery rate, raising the temperature to 50 °C promoted this reaction. The re-extraction process is more efficient at low concentrations of extractant in the organic phase when the extraction efficiency is reduced. Thus, a smaller solute quantity is available in the organic phase forming

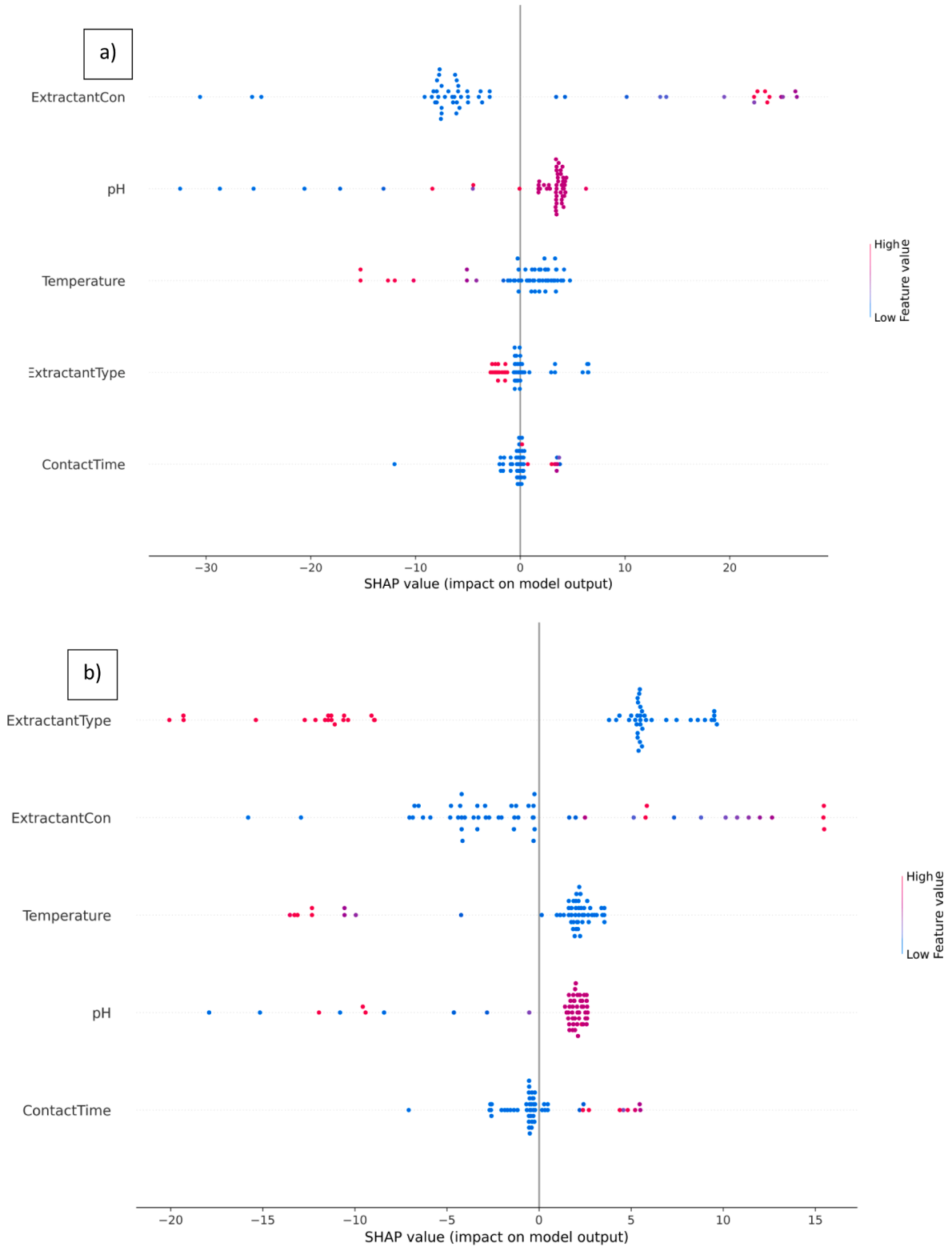

Fig. 10. The SHAP values for a) AA model; b) 2-KGA model.

hydrophobic complexes with the ionic liquid.

Modelling and optimization

The modeling procedure used a Keras sequential model with an Adam optimizer with a 0.05 learning rate. The maximum allowed topology consisted of 5 hidden layers with a maximum of 20 neurons in each hidden layer. The topology identification step used a self-adaptive DE algorithm with a population size of 15 individuals and 10 generations. Since the experimental dataset contained relatively few points, an interpolation procedure was applied to extend the dataset and ensure sufficient exemplars for the ANN to efficiently capture the process's dynamic. The interpolation procedure consisted of identifying the trendlines that best fit the experimental points grouped by specific

Table 3
Optimization results.

Objective	No.	pH	Extractant Conc, g/L	Extractant Type	Contact Time	Temperature, °C	AA predicted	2-KGA predicted	Selectivity factor
AA max	1	3.1	95.3	1	5	20	109.65	31.99	3.43
	2	3.7	97.5	1	8.15	20.3	109.46	48.88	2.24
	3	2.9	105	2	6.23	20	106.67	2.04	52.29
	4	2.8	116.2	2	6.52	20	105.02	3.48	30.18
2-KA min	5	2	96.2	2	27.49	40.7	18.11	0.73	24.81
	6	4.6	53.6	1	20.88	41.7	39.39	9.4	4.19
	7	1.4	83.3	2	16.92	37.3	24.01	1.73	13.88
	8	2	34.4	1	16.12	50	42.29	12.15	3.48
Selectivity factor max	9	2.9	105	2	6.23	20	106.67	2.04	52.29
	10	1.3	68.9	1	8.05	37.1	47.28	1.94	24.39
	11	3	36.5	2	21.11	49.3	14.47	0.71	20.49
	12	3.4	99	2	9.96	43.6	37.32	2.31	16.14
	13	2.3	48.9	2	19.28	39.6	17.88	1.28	14.01
	14	3.3	83.6	1	5	40.7	79.26	6.57	12.07
	15	1	99.9	2	25.44	29.8	38.79	3.58	10.84
	16	3.3	104.1	2	9.37	36.3	55.71	5.39	10.34
	17	1.2	103.1	2	22.6	34.1	34.62	3.49	9.92
	18	3.1	101.1	2	9.24	33.1	64.72	6.96	9.30

Table 4
Experimental validation.

No.	AA predicted	AA experimental	2-KGA predicted	2-KGA experimental	Selectivity factor predicted	Selectivity factor experimental
1	109.65	98.98	31.99	27.33	3.43	3.62
8	42.29	37.56	12.15	15.42	3.48	2.43
9	106.67	98.31	2.04	4.99	52.29	19.70
14	79.26	74.82	6.57	10.31	12.07	7.25

characteristics (for example, the data presented in Fig. 6). The final dataset contained 180 points and 5 process parameters: pH, extractant concentration, extractant type (encoded 1 for $[P_{6,6,6,14}][Dec]$and 2 for $[P_{6,6,6,14}][Phos]$), contact time and temperature. Next, the data were normalized using a Min-Max approach and randomly assigned to the training or the testing dataset. 20 % of the training data is assigned to the validation set. Due to the stochastic nature of the DE algorithm, 10 runs were performed. The statistics of the best models obtained from AA and 2-KGA are presented in Table 2, where EVS indicates the explained variance score, MAE is the mean absolute error, MSE is the mean squared error, MAPE is the mean absolute percentage error, and R^2 is the coefficient of determination. The 2-KA model had a topology with one hidden layer and 11 neurons, while the AA model had a topology with three hidden layers with 16, 4 and 8 neurons, respectively.

As can be observed, all statistical metrics show that the AA model performs better than 2-KGA. This indicates that the propped approach better captured the process's dynamic concerning the AA extraction efficiency. For 2-KGA, the separation process involves a more complex dynamic due to the formation of dimers in the aqueous phase.

In the next step, the Shapley values were determined to identify each input's influence on the output. Fig. 10 a and b present the beeswarm plot for the AA and 2-KGA model, respectively. The process parameters are organized from the highest importance to the lowest. If for the AA, the extractant concentration has the highest influence on the output, for the 2-KGA, the extractant type is the most influential. Nevertheless, the contact time is the least influential parameter in both cases. As Fig. 10a shows, lower values of the extractant concentration and pH are correlated with lower values of the AA extraction efficiency. An opposite effect is observed for temperature, where lower temperature values correlate to higher AA extraction efficiency predictions. The same tendencies can also be observed for 2-KGA, indicating that the process parameters influence the two outputs similarly. All these aspects can also be observed from the experimental data (Fig. 4).

After the ANNs were determined and analyzed, the same DE procedure applied to determine the topology was combined with the best models to optimize the process. The objective was to identify the process parameters that will lead to a maximization of AA and a minimization of 2-KGA. These objectives were set separately and not simultaneously, and a series of results for each case are presented in Table 3, where No. indicates the number of the solution. As can be observed from Table 3, different combinations of parameters that lead to a similar output were identified. In the case of AA maximization, the predicted efficiency is higher than 100 % due to the model's error and the tendency of the predictions to be slightly higher than the experimental values.

The next step consisted of experimentally validating some of the obtained optimization conditions. The results are presented in Table 4, where No is correlated with the experimental conditions in Table 3. For the AA model, it can be observed that the validation data is slightly lower compared with the predictions over 100. As identified by the statistical indicators, the validation of the 2-KGA model shows that the experimental-predicted differences are higher than the AA model. Since the selectivity factor depends on both AA and 2-KGA, the errors in the predictions of these outputs are propagated. Following only the selectivity factor, from an optimization perspective, is not an indicated approach.

Conclusions

This work studied a novel extraction system with hydrophobic ILs as an effective extractant for separating ascorbic acid from 2-ketogluconic acid in aqueous solutions. The results showed that the extraction efficiency for AA was maximum when $[P_{6,6,6,14}][Phos]$ was used as the extractant with the following optimal extraction conditions: pH = 3.0, 10 min contact time, 30 °C temperature, and 160 g/L ionic liquid dissolved in heptane. For 2-KGA, the best results were obtained with 160 g/L $[P_{6,6,6,14}][Dec]$, pH = 2, 10 min contact time, 20 °C temperature, but the efficiency of the process was lower than for AA extraction. Moreover, the mechanism of the extraction system was analyzed, demonstrating an equimolecular hydrophobic complex for both compounds analyzed. The process was also modeled and optimized using ANNs and DE algorithms. The influence of the considered parameters on the model's output correlate well with the experimental data analysis, and the optimization

procedure provided different conditions for obtaining high extraction efficiency for AA.

Declaration of Competing Interest

The authors declare that they have no known competing financial interests or personal relationships that could have appeared to influence the work reported in this paper.

Acknowledgment

This work was supported by a grant of the Ministry of Research, Innovation and Digitization, CNCS - UEFISCDI, project number PN-III-P1-1.1-TE-2021-0153, within PNCDI III.

References

[1] A. Gironés-Vilaplana, D. Villaño, J. Marhuenda, D.A. Moreno, C. García-Viguera, Vitamins, in Charis M. Galanakis(Eds.), Nutraceutical and Functional Food Components, Academic Press, 2017, pp. 159-201. https://doi.org/10.1016/B978-0-12-805257-0.00006-5.

[2] Y.S. Tian, Y.D. Deng, W.H. Zhang, et al., Metabolic engineering of *Escherichia coli* for direct production of vitamin C from D-glucose, Biotechnol. Biofuels 15 (2022) Article 86. https://doi.org/10.1186/s13068-022-02184-0.

[3] S.A. Mason, L. Parker, P. van der Pligt, G.D. Wadley, Vitamin C supplementation for diabetes management: A comprehensive narrative review, Free Radic Biol Med. 194 (2023) 255–283, https://doi.org/10.1016/j.freeradbiomed.2022.12.003.

[4] C. Ye, W. Zou, N. Xu, L. Liu, Metabolic model reconstruction and analysis of an artificial microbial ecosystem for vitamin C production, J Biotechnol. 182–183 (2014) 61–67, https://doi.org/10.1016/j.jbiotec.2014.04.027.

[5] S.M. Lim, M.S.L. Lau, E.I.J. Tiong, et al., Process design and economic studies of two-step fermentation for production of ascorbic acid. SN Appl. Sci. 2 (2020) Article 816. https://doi.org/10.1007/s42452-020-2604-8.

[6] C. Bremus, U. Herrmann, S. Bringer-Meyer, H. Sahm, The use of microorganisms in L-ascorbic acid production, J Biotechnol. 124 (2006) 196–205, https://doi.org/10.1016/j.jbiotec.2006.01.010.

[7] A. Tucaliuc, A. Cîşlaru, L. Kloetzer, A.C. Blaga, Strain development, substrate utilization, and downstream purification of Vitamin C. Processes 10 (2022) Article 1595. https://doi.org/10.3390/pr10081595.

[8] S. Sufang, L. Guorui, W. Yanhuan, Z. Yan, L. Cuifen, S. Yongmei, Simultaneous determination of 2-keto-L-Gulonic Acid and 2-keto-D-Gluconic acid in fermentation broth by HPLC, Chemistry Mag. 9 (2007). Article 8.

[9] A.M. Bode, L. Cunningham, R.C. Rose, Spontaneous decay of oxidized ascorbic-acid (dehydro-L-ascorbic acid) evaluated by high-pressure liquid-chromatography, Clinical Chem. 36 (10) (1990) 1807–1809.

[10] R.D. Fernandes, M. Dinç, I.M. Raimundo, B. Mizaikoff, Synthesis and characterization of porous surface molecularly imprinted silica microsphere for selective extraction of ascorbic acid, Microporous Mesoporous Mater. 264 (2018) 28–34, https://doi.org/10.1016/J.MICROMESO.2017.07.019.

[11] A.C. Blaga, A.I. Galaction, E. Folescu, D. Caşcaval, Separation of vitamin C by reactive extraction 1, Mechanism and Influencing Factors, Rom Biotech Lett 9 (6) (2004) 1917–1924.

[12] Z. Jahromi, A. Mostafavi, T. Shamspur, M. Mohamadim, Magnetic ionic liquid assisted single-drop microextraction of ascorbic acid before its voltammetric determination, J. Sep. Sci. 40 (2017) 4041–4049, https://doi.org/10.1002/jssc.201700664.

[13] M.E. Marti, H. Zeidan, Using eco-friendly alternatives for the recovery of pyruvic acid by reactive extraction, Sep. Purif. Technol. 312 (2023), 123309, https://doi.org/10.1016/j.seppur.2023.123309.

[14] R.G. Lazar, A.C. Blaga, E.N. Dragoi, A.I. Galaction, D. Cascaval, Mechanism, influencing factors exploration and modelling on the reactive extraction of 2-ketogluconic acid in presence of a phase modifier, Sep. Purif. Technol. 255 (2021), 117740, https://doi.org/10.1016/j.seppur.2020.117740.

[15] S.P.M. Ventura, F.A. de Silva, M.V. Quental, D. Mondal, M.G. Freire, J.A. P. Coutinho, Ionic-Liquid-Mediated Extraction and Separation Processes for Bioactive Compounds: Past, Present, and Future Trends, Chem. Rev. (2017) 6984–7052, https://doi.org/10.1021/acs.chemrev.6b00550.

[16] A.C. Blaga, T. Malutan, Selective Separation of Vitamin C by Reactive Extraction, J. Chem. Eng. Data 57 (2) (2012) 431–435, https://doi.org/10.1021/je2010193.

[17] T. Evlik, Y.S. Aşçı, N. Baylan, H. Gamsızkan, S. Çehreli, Reactive separation of malic acid from aqueous solutions and modeling by artificial neural network (ANN) and response surface methodology (RSM), J Dispers Sci Technol 43 (2) (2022) 221–230.

[18] K. Rewatkar, D. Shende, K. Wasewar, Reactive separation of gallic acid: experimentation and optimization using response surface methodology and artificial neural network, Chem Biochem Eng Q 31 (1) (2017) 33–46.

[19] A.C. Blaga, A. Tucaliuc, L. Kloetzer, Applications of ionic liquids in carboxylic acids separation. Membranes 12 (2022) Article 771. https://doi.org/10.3390/membranes12080771.

[20] S. Chellapan, D. Datta, S. Kumar, H. Uslu, Statistical modeling and optimization of itaconic acid reactive extraction using response surface methodology (RSM) and artificial neural network (ANN), Chem. Data Collect 37 (2022), 100806, https://doi.org/10.1016/j.cdc.2021.100806.

[21] N. Marchitan, C. Cojocaru, A. Mereuta, G. Duca, I. Cretescu, M. Gonta, Modeling and optimization of tartaric acid reactive extraction from aqueous solutions: A comparison between response surface methodology and artificial neural network, Sep. Purif. Technol. 75 (3) (2010) 273–285, https://doi.org/10.1016/j.seppur.2010.08.016.

[22] D.P. Kingma, J. Ba, (2014). Adam: A method for stochastic optimization. arXiv preprint arXiv:1412.6980.

[23] E.N. Drăgoi, I. Cârlescu, R. Puf, T. Vasiliu, E.-L. Epure, Neuro-evolutive modeling of transition temperatures for five-ring bent-core molecules derived from resorcinol, Crystals 13(4) (2023) Article 583. https://doi.org/10.3390/cryst1304058.

[24] S.M. Lundberg, S.-I. Lee, (2017), A unified approach to interpreting model predictions. Advances in neural information processing systems 30. https://doi.org/10.48550/arXiv.1705.07874.

[25] N. Nasirpour, M. Mohammadpourfard, S.Z. Heris, Ionic liquids: Promising compounds for sustainable chemical processes and applications, Chem. Eng. Res. Des. 160 (2020) 264–300.

[26] A.C. Blaga, E.N. Dragoi, A. Tucaliuc, L. Kloetzer, D. Cascaval, Folic acid ionic-liquids-based separation: extraction and modelling. Molecules 28 (2023), Article 3339. https://doi.org/10.3390/molecules28083339.

[27] Š. Schlosser, J. Marták, M. Blahušiak, Specific phenomena in carboxylic acids extraction by selected types of hydrophobic ionic liquids, Chem. Pap. 72 (2018) 567–584, https://doi.org/10.1007/s11696-017-0365-7.

[28] T. Liptaj, J. Marták, Š. Schlosser, NMR study of structural changes of alkyl-phosphonium decanoate ionic liquid induced by water and butyric acid extraction, J. Mol. Liq 302 (2020), 112573, https://doi.org/10.1016/j.molliq.2020.112573.

[29] N.D. Oktaviyanti, K. Kartini, M.A. Hadiyat, E. Rachmawati, A.C. Wijaya, H. Hayun, A. Mun'im, A green extraction design for enhancing flavonoid compounds from *Ixora javanica* flowers using a deep eutectic solvent, R Soc Open Sci. 7 (10) (2020), 201116, https://doi.org/10.1098/rsos.201116.

[30] K. Tonova, Ionic liquid-assisted biphasic systems for downstream processing of fermentative enzymes and organic acids, Phys. Sci. Rev 6 (3) (2021) 1–33, https://doi.org/10.1515/psr-2018-0068.

[31] M.E. Marti, Recovery Of Formic Acid By Reactive Extraction Using An Environmentally-Friendly Solvent, SUJEST 5 (1) (2017) 26–37. https://doi.org/10.15317/Scitech.2017.67.

[32] P. Demmelmayer, M. Kienberger, Reactive extraction of lactic acid from sweet sorghum silage press juice, Sep. Purif. Technol. 282 (2022), 120090, https://doi.org/10.1016/j.seppur.2021.120090.

[33] A.F. Morales, J. Albet, G. Kyuchoukov, G. Malmary, J. Molinier, Influence of extractant (TBP and TOA), diluent, and modifier on extraction equilibrium of monocarboxylic acids, J. Chem. Eng. Data 48 (4) (2003) 874–886, https://doi.org/10.1021/je020179o.

[34] S. Gadekar-Shinde, R.B. Kumar, S. Gaikwad, Reactive extraction of caproic acid using tri n-octylamine + 2 octanol system, Materials Today: Proceedings 72 (2023) 260–267, https://doi.org/10.1016/j.matpr.2022.07.265.

[35] F.M. Antony, K. Wasewar, Effect of temperature on equilibria for physical and reactive extraction of protocatechuic acid, Heliyon 6 (5) (2020) e03664.

[36] S. Eda, A. Borra, R. Parthasarathy, S. Bankupalli, S. Bhargava, P.K. Thella, Recovery of levulinic acid by reactive extraction using tri-n-octylamine in methyl isobutyl ketone: Equilibrium and thermodynamic studies and optimization using Taguchi multivariate approach, Sep. Purif. Technol. 197 (2018) 314–324, https://doi.org/10.1016/j.seppur.2018.01.014.

[37] L.M.J. Sprakel, B. Schuur, Solvent developments for liquid-liquid extraction of carboxylic acids in perspective, Sep. Purif. Technol. 211 (2019) 935–957, https://doi.org/10.1016/j.seppur.2018.10.023.

[38] N. Thakre, A.K. Prajapati, S.P. Mahapatra, A. Kumar, A. Khapre, D. Pal, Modeling and optimization of reactive extraction of citric acid, J. Chem. Eng. Data 61 (2016) 2614–2623, https://doi.org/10.1021/acs.jced.6b00274.

[39] H. Beneš, J. Kredatusová, J. Peter, S. Livi, S. Bujok, E. Pavlova, J. Hodan, S. Abbrent, M. Konefał, P. Ecorchard, Ionic Liquids as Delaminating Agents of Layered Double Hydroxide during In-Situ Synthesis of Poly (Butylene Adipate-co-Terephthalate) Nanocomposites. Nanomaterials (Basel) 9(4) (2019) Article 618. https://doi.org/10.3390/nano9040618.

[40] L. Nolte, M. Nowaczyk, C. Brandenbusch, Monitoring and investigating reactive extraction of (di)carboxylic acids using online FTIR – Part I: Characterization of the complex formed between itaconic acid and tri-n-octylamine, J. Mol. Liq. 352 (2022), 118721, https://doi.org/10.1016/j.molliq.2022.118721.

[41] V.R. Dhongde, B.S. De, K.L. Wasewar, Experimental study on reactive extraction of malonic acid with validation by Fourier Transform Infrared Spectroscopy, J. Chem. Eng. Data. 64 (3) (2019) 1072–1084, https://doi.org/10.1021/acs.jced.8b00972.

molecules

MDPI

Article

Folic Acid Ionic-Liquids-Based Separation: Extraction and Modelling

Alexandra Cristina Blaga *, Elena Niculina Dragoi, Alexandra Tucaliuc, Lenuta Kloetzer and Dan Cascaval

"Cristofor Simionescu" Faculty of Chemical Engineering and Environmental Protection, "Gheorghe Asachi" Technical University of Iasi, D. Mangeron 73, 700050 Iasi, Romania; elena.dragoi@tuiasi.ro (E.N.D.); alexandra.tucaliuc@academic.tuiasi.ro (A.T.); lenuta.kloetzer@academic.tuiasi.ro (L.K.); dan.cascaval@academic.tuiasi.ro (D.C.)

* Correspondence: acblaga@tuiasi.ro

Abstract: Folic acid (vitamin B9) is an essential micronutrient for human health. It can be obtained using different biological pathways as a competitive option for chemical synthesis, but the price of its separation is the key obstacle preventing the implementation of biological methods on a broad scale. Published studies have confirmed that ionic liquids can be used to separate organic compounds. In this article, we investigated folic acid separation by analyzing 5 ionic liquids (CYPHOS IL103, CYPHOS IL104, [HMIM][PF_6], [BMIM][PF_6], [OMIM][PF_6]) and 3 organic solvents (heptane, chloroform, and octanol) as the extraction medium. The best obtained results indicated that ionic liquids are potentially valuable for the recovery of vitamin B9 from diluted aqueous solutions as fermentation broths; the efficiency of the process reached 99.56% for 120 g/L CYPHOS IL103 dissolved in heptane and pH 4 of the aqueous folic acid solution. Artificial Neural Networks (ANNs) were combined with Grey Wolf Optimizer (GWO) for modelling the process, considering its characteristics.

Keywords: CYPHOS IL103; vitamin B9; ionic liquid; extraction; modelling

Citation: Blaga, A.C.; Dragoi, E.N.; Tucaliuc, A.; Kloetzer, L.; Cascaval, D. Folic Acid Ionic-Liquids-Based Separation: Extraction and Modelling. *Molecules* **2023**, *28*, 3339. https://doi.org/10.3390/molecules28083339

Academic Editor: Mara G. Freire

Received: 2 March 2023
Revised: 17 March 2023
Accepted: 8 April 2023
Published: 10 April 2023

1. Introduction

Vitamins are chemical substances whose derivatives are engaged in the vital metabolic pathways of all living organisms [1]. Since only bacteria, yeast and plants have endogenous routes for vitamin production, humans must obtain most of these crucial nutrients from food [2]. A form of B vitamin called folic acid (folate in its natural form [3])—Figure 1 aids in the maintenance and production of new cells in the body and prevents nucleic acid alterations [2]. Several physiological processes in humans, including the biosynthesis of nucleotides, cell division, and gene expression, as well as the prevention of vascular diseases, megaloblastic anemia, and neural tube defects in developing children, depend on a proper supply of folic acid (FA) or folates.

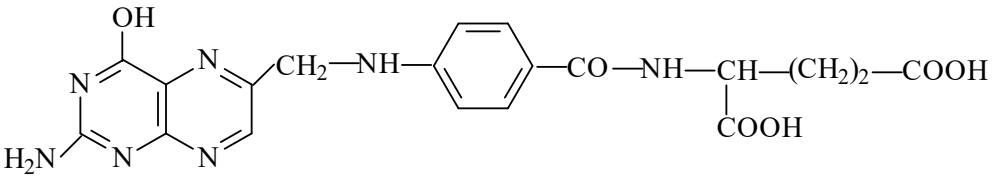

Figure 1. Folic acid (FA) chemical structure.

FA has numerous applications in the pharmaceutical, nutraceutical, food and beverages industries [4], but its stability decreases when exposed to light, moisture, strong acidic or alkaline media, oxygen and high temperatures. It can be found in foods, including oranges, whole-wheat products, dry beans, peas, lentils, oranges, liver, asparagus, beets, broccoli, brussels sprouts and spinach [5].

The estimated value of the global FA market in 2022 was USD 166.8 million. By 2028, it is anticipated to grow to USD 220.9 million, the leading producers being BASF, DSM, Nantong Changhai Food Additive Co., Ltd., Niutang, Zhejiang Shengda, Parchem Fine & Specialty Chemicals, Xinjiang Wujiaqu Xingnong Cycle Chemical Co., Ltd., Xinfa Pharmaceutical Co., Medicamen Biotech Ltd., Jiangxi Tianxin Pharmaceutical Co., Ltd., and Zydus Pharmaceuticals Ltd. [6].

FA is used as a dietary supplement and is currently produced through chemical synthesis, but this process requires the reduction of ecologically harmful effects. Significant research has been employed to develop microbial strains (*Ashbya gossypii* ATCC 10895, *Lactococcus lactis* NZ9000, *Bacillus subtilis* 168) in order to manufacture FA [7–10]. The highest production value to date has been recorded for *A. gossypii*, which can synthesize 6.59 mg/L of folic acid after metabolic engineering (from its natural ability to produce 0.04 mg/L) [11]. For this process to be successfully employed, efficient separation methods must be developed. More research is required to create a method that is both economical and environmentally benign for producing high-purity FA, because its industrial separation involves many expensive downstream steps and requires mild conditions due to acid's instability.

Various technologies can be used to separate carboxylic acids (ion exchange, electrodialysis, ultrafiltration, solvent extraction, and membrane processes) [12]. However, reactive extraction using particular extractants has been proven to be an excellent alternative to classical methods, due to its many advantages [13]. Reactive extraction is based on a reaction between an extractant (dissolved in the organic solvent) and the target solute (e.g., carboxylic acids dissolved in the aqueous phase). Several carboxylic acids (gallic acid [14,15], keto-gluconic acid [16], pseudo-monic acid [17], lactic acid [18]), and vitamins (vitamin C [19], vitamin B5 [20]) have been successfully separated through this method at laboratory scale. For sustainability of this process, finding a selective, affordable, and effective extractant and diluent system based on maximal efficiency and minimal toxicity and determining the ideal implementation circumstances are the key challenges in using reactive extraction for the recovery of organic acids. Several characteristics must be considered for the choice of the organic phase, such as selectivity, solubility, cost and operational safety, hydrophobicity, density, polarity, viscosity, recoverability and environmental effects (the use of volatile organic solvents harms the environment). Thus, based on their superior characteristics, ionic liquids (tunable organic salts obtained as a combination of an organic cation and either an organic or a polyatomic inorganic anion in a liquid state below 100 °C) are effective alternatives to classical solvents. The use of most ionic liquids has several advantages over organic solvents, and they play crucial roles in the extraction processes; high thermal stability, negligible vapor pressure, and biocompatibility make them environmentally friendly substances with excellent solvation ability. Based on their properties, most ionic liquids can be employed in green chemistry concepts [21,22]. Lactic acid, citric acid, mevalonic acid [23], and butyric acid [24] have all been successfully extracted using ionic liquids. For the micro-solid phase extraction (for preconcentration and analysis) of pyridoxine and folic acid from biological samples, Zare et al. (2015) investigated a sorbent obtained through the synthesis of gold nanoparticles (Au NPs) and their subsequent transfer to aqueous solution by the application of the ionic liquid: 1-hexyl-3-methylimidazolium bis(trifluoro-methyl-sulfonyl)imide [25].

For the scale-up application of reactive extraction, rigorous modelling and optimization of laboratory-scale studies are essential and different models can be applied [15–17]. ANNs are inspired by the biological brain, and GWO is inspired by the grey wolf's social hierarchy and hunting mechanism [26]. In this work, ANN represents the process model, while GWO is used for model optimization. This combination was considered based on the difficulties in identifying the optimal characteristics of an ANN for a given problem. From the multitude of ANN types, the fully connected feed-forward multilayer perceptron was selected because it is well suited to the complexity and characteristics of the studied process. Moreover, this type of network was successfully applied to solve

different problems, including modeling of phytocompounds extraction from dragon fruit peel [27], pectinase extraction from cashew apple juice [28], and separation of pseudo-monic acids [16]. As a bio-inspired metaheuristic, GWO was efficiently applied to optimize the extraction of essential oil from Cleome Coluteiodes Boiss [29], or biodiesel production from waste oils [30,31].

To the authors' knowledge, this is the first study regarding folic acid's separation using ionic liquids (IL) and a liquid–liquid approach. For this research, five ionic liquids (Trihexyl-tetradecyl-phosphonium decanoate, Trihexyl-tetradecyl-phosphonium bis(2,4,4-trimethylpentyl)phosphinate, 1-Butyl-3-methylimidazolium hexafluorophosphate, 1-Octyl-3-methylimidazolium hexafluorophosphate, 1-Hexyl-3-methylimidazolium hexafluorophosphate—Figure 2) were analyzed for FA extraction in order to find an optimal system for the separation process.

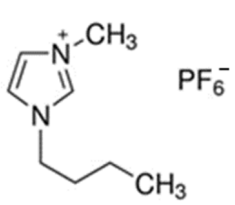

1-Butyl-3-methyl-imidazolium-hexafluorophosphate, [BMIM][PF_6]

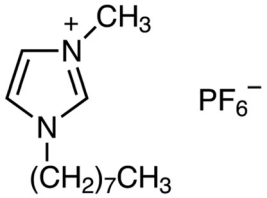

1-Octyl-3-methyl -imidazolium-hexafluorophosphate, [OMIM][PF_6]

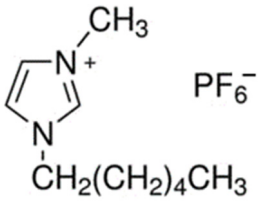

1-Hexyl-3-methyl-imidazolium-hexafluorophosphate, [HMIM][PF_6]

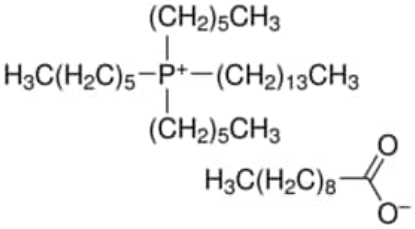

Tri-hexyl-tetradecyl-phosphonium decanoate, CYPHOS IL 103

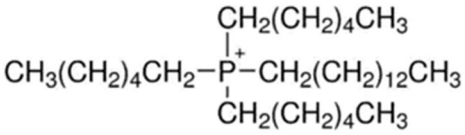

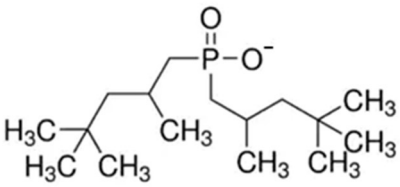

Tri-hexyl-tetradecyl-phosphonium bis(2,4,4-trimethylpentyl) phosphinate, CYPHOS IL 104

Figure 2. Ionic Liquids (IL) chemical structure.

Considering the physical characteristics of the ionic liquid (such as high density, viscosity and surface tension) and their high price, three solvents were analyzed as diluents (heptane, chloroform and octanol). The results were discussed from the viewpoint of the extraction mechanism, separation yield and distribution coefficient for different extraction conditions (aqueous phase pH and ionic liquids concentration in the organic phase). Supplementary Artificial Neural Networks (ANNs) were combined with Grey Wolf Optimizer (GWO) to model the considered process.

2. Results and Discussions

2.1. Extraction Process

Liquid–liquid extraction is a low-energy separation process with simple technical requirements and gentle operating conditions. Its effectiveness is influenced by several variables, including the type of solute and solvent, the utilized diluent and its physicochemical properties, and the solution pH. For FA extraction 5 ionic liquids with different chemical structures (Figure 2) and properties (Table 1) and 3 organic solvents with different dielectric constants (heptane—1.92, chloroform—4.81 and octanol—10.3 [32]) were investigated. The extraction system was chosen based on its low environmental impact. The ionic liquids chosen are highly hydrophobic [33] and were successfully used for the separation of other carboxylic acids (e.g., lactic acid) [34]. Phosphonium ILs offer, in specific cases and applications, several advantages over other types of ILs, including higher thermal stability, lower viscosity and higher stability in strongly basic or strongly reducing conditions [35].

Table 1. Main ionic liquids' physical properties used in biosynthetic compounds extraction [21,36,37].

Ionic Liquid	Molecular Formula	mol. wt., g/mol	Viscosity, cP, 25 °C	log P	Toxicity
[BMIM][PF_6]	$C_8H_{15}F_6N_2P$	284.18	274	4.49	log EC_{50} * = 3.32 µM
[OMIM][PF_6]	$C_{12}H_{23}F_6N_2P$	340.29	682	6.05	log EC_{50} * = 2.24 µM
[HMIM][PF_6]	$C_{10}H_{19}F_6N_2P$	312.24	585	5.27	log EC_{50} * = 1.25 µM
CYPHOS IL 103	$C_{42}H_{87}O_2P$	665.11	319	14.32	Inhib. ** = 1.5 cm
CYPHOS IL 104	$C_{48}H_{102}O_2P_2$	773.27	805.8	18.28	Inhib. ** = 2.6 cm

* Determined against *A. fischeri.* ** Determined against *Shewanella* sp. (inhibition zone, ±0.2).

The results obtained are presented in Figure 3. It can be observed that, without regarding the used organic solvent, the separation yield is very low, proving that physical extraction in classical organic solvents (based only on diffusion and solubilization) is practically impossible for FA. Simultaneously, the ionic liquids can effectively remove FA from the aqueous phase. In general, various variables, including the hydrophobic effect, hydrogen bonding, steric hindrance, and π-π interaction, affect how well ILs can extract carboxylic acids.

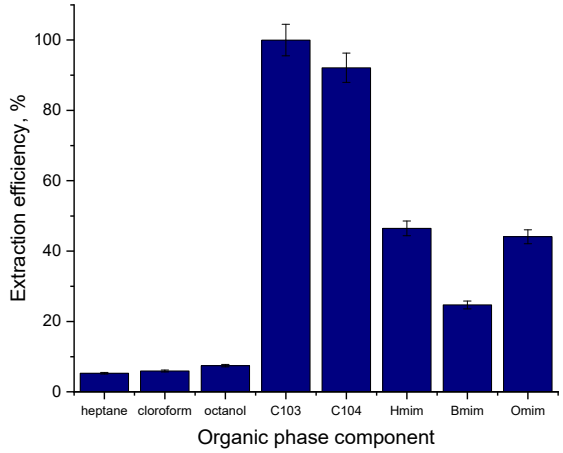

Figure 3. The organic phase composition influence on FA extraction (pH = 4, pure substances).

The highest efficiency was obtained for quaternary phosphonium salts: CYPHOS IL103 (99.98%) and CYPHOS IL104 (92.85%), the anions decanoate and bis(2,4,4-trimethylpentyl) phosphinate providing significantly superior yields than the hexafluorophosphate $\left[PF_6^-\right]$ anion, due to stronger hydrogen bonds established between the anion and FA, and to the hydrophobic behavior of the trihexyl(tetradecyl)phosphonium cation (phosphonium IL possesses the highest hydrophobicity among ILs [34]), present in both CYPHOS IL103 and CYPHOS IL104 structure). The superior efficiency that was obtained using CHYPHOS IL103 can be explained by the effect of both the interference of sterically hindrance in CYPHOS IL104 case during the chemical reaction (CYPHOS IL104 has a larger structure compared to CYPHOS IL103 due to the presence of bis(2,4,4-trimethylpentyl)phosphinate ion compared to decanoate anion) and the superior viscosity of CYPHOS IL104 (Table 1)—according to the Wilke-Chang equation, diffusivity varies inversely with viscosity [34]. Similar results (superior values for CYPHOS IL103 compared with other ionic liquids) were obtained by Schlosser et al., 2018, for lactic and butyric acids [38]. These results proved that FA could be successfully separated using ionic liquids; however, their high viscosity and high price are vital points that require more research on this matter.

Due to mass transfer at the liquid–liquid interface, which influences the time required to set the equilibration stage between the aqueous and IL phases, viscosity is a crucial element that affects the kinetics of IL-based extraction systems. Conventional extraction systems using organic solvents may typically reach equilibrium in a short contact time (minutes), whereas IL-based systems require a longer contact time (minutes to hours) due

to the high viscosity value, which is in this case (Table 1), between 274 and 805 cP (viscosity of water is 0.89 cP at 25 °C). Because of the influence on the Coulombic interaction between ions, adding an inert solvent could reduce IL viscosity [39]. In this context, the use of heptane, a non-polar solvent, as a diluent to decrease the viscosity and surface tension of the very viscous ionic liquids used, was analyzed as an alternative solution to pure ionic liquids for both CYPHOS IL. For [HMIM][PF_6], the solvent considered was chloroform, since this ionic liquid and heptane are not miscible. The FA from the aqueous phase can react with the strong hydrophobic ionic liquid dissolved in heptane to generate complexes that are only soluble in the organic phase:

$$R(COOH)COOH(aq) + [C_{14}C_6C_6C_6P][BTMPP] \rightarrow [C_{14}C_6C_6C_6P][R(COOH)COO] + BTMPPH$$

$$R(COOH)COOH(aq) + [C_{14}C_6C_6C_6P][CH_3(CH_2)_8COO] \rightarrow [C_{14}C_6C_6C_6P][R(COOH)COO] + CH_3(CH_2)_8COOH$$

The extraction mechanism could be characterized in terms of displacement reaction since ionic liquids are organic salts and contain tri-hexyl(tetradecyl) phosphonium ([$C_{14}C_6C_6C_6P$]) as a cation and bis(2,4,4-trimethylpentyl) phosphinate ([BTMPP]—CYPHOS IL104 and decanoate -CYPHOS IL103) as an anion. The anionic component of the acid ($C_{13}H_{11}N_6O$-CH(CH_2-CH_2-COOH)-COO) can displace the anionic species of IL in this reaction (pKa of decanoic acid is 5.7 while folic acid pKa are 4.69; 6.80). The extraction mechanism can also imply hydrogen bonding, the values for hydrogen-bonding interaction energy in the equimolar cation-anion mixture (E_{HB}/(kJ/mol) are −38.64 for decanoate $[C_9H_{20}CO_2]^-$ and −38.45 for Bis(2,4,4-trimethylpentyl)phosphinate, $[C_{16}H_{34}O_2P]^-$ [39].

FA is a weak acid in aqueous solutions, stable between pH 2–10, without heating [40], but its maximum stability is in the pH range of 4–10. The aqueous phase pH has a significant effect on extraction efficiency as it controls acid dissociation:

$$R(COOH)COOH_{(aq)} \leftrightarrow R(COOH)COO^-_{(aq)} + H^+, pKa_1 = 4.69$$
$$R(COOH)COO^-_{(aq)} \leftrightarrow R(COO^-)COO^-_{(aq)} + H^+, pKa_2 = 6.8$$

The extraction efficiency using the purposed extraction system (ionic liquids mixed with an organic diluent) decreases with the increase of aqueous phase pH, as highlighted by the experimental results depicted in Figure 4. Better results were obtained for CYPHOS (dissolved in heptane) compared to [HMIM][PF_6] (dissolved in chloroform), similar to the results obtained for protocatechuic acid or adipic acid [21]. Due to this fact (extraction efficiency much lower for [HMIM][PF_6]), the ionic liquid concentration influence was only analyzed for CYPHOS IL103 and CYPHOS IL104.

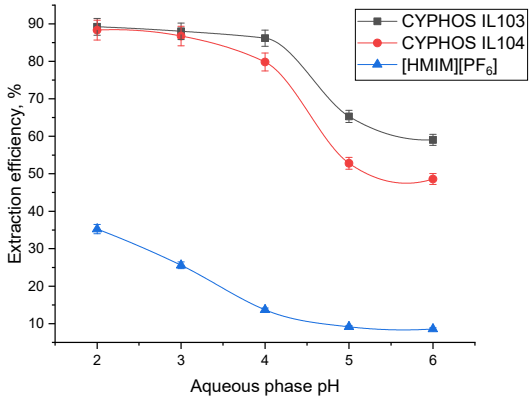

Figure 4. Aqueous phase pH influence on extraction efficiency (ionic liquid concentration 40 g/L).

The experimental results proved that FA could only be extracted by CYPHOS IL103 and CYPHOS IL104 in its undissociated state through H-bond coordination. FA is present in the aqueous solution in an undissociated form at pH lower than 4.5, as determined by

the pKa values of 4.69 for the first carboxylic group and 6.80 for the second carboxylic group. This supports the idea that FA will be reactively extracted utilizing a coordination mechanism similar to lactic acid extraction, using CYPHOS IL104 [41]. Furthermore, the results prove that satisfactory separation efficiency can be achieved even at pH equal to 4, at which FA stability is considered maximum.

The extraction efficiency of FA increases with IL (CYPHOS IL103 and CYPHOS IL104) concentrations in heptane, as seen in Figure 5, proving that this parameter has a critical impact on extraction efficiency. This variation is due to the increase of one reactant concentration at the reaction interface; a higher concentration of IL is more likely to extract a higher concentration of the targeted folic acid from the aqueous phase. No third phase formation was observed in the experiments.

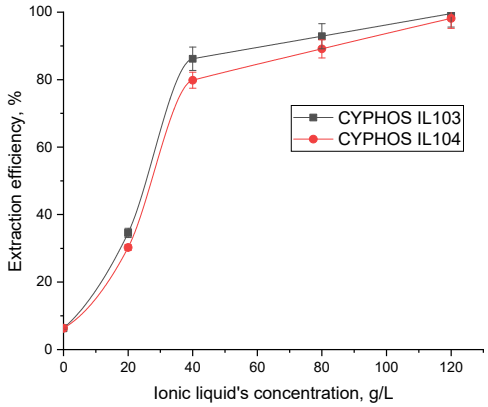

Figure 5. Ionic liquid concentration influence on extraction efficiency (initial phase pH = 4).

The influence of ionic liquids concentration on extraction efficiency was analyzed at pH 4 to avoid denaturation [40]. In order to establish how many molecules of acid and ionic liquid are involved in the formation of the interfacial complex, the loading factor, Z, defined as the ratio between the concentrations of FA and ionic liquid in the organic phase: [FA]org/[IL]org, was calculated (Table 2).

Table 2. Loading factor and distribution coefficient values obtained for C103 and C104 in heptane.

	CYPHOS IL103 conc., M	D	Loading Factor	CYPHOS IL104 conc., M	D	Loading Factor
1	0.03	0.52	0.43	0.02	0.43	0.43
2	0.06	6.24	0.53	0.05	3.95	0.57
3	0.12	12.99	0.28	0.10	8.19	0.32
4	0.18	231.18	0.20	0.15	53.51	0.23

Two cases can be considered when the variation of the Z parameters is assessed [42]. The first implies that, as the concentration of the ionic liquid increases, so do the loading factor values. This phenomenon, known as overloading (loading larger than unity), shows the formation of complexes with more than one acid per ionic liquid molecule. The maximum value obtained for the loading factor was 0.53 and 0.57 for both ionic liquids, so no overloading was noted in the system. The second case implies that complexes include more than one ionic liquid molecule if the loading factor values decrease as the IL concentration rises. The obtained results, presented in Table 2, showed that for ionic concentrations below the value equal to 40 g/L (0.05 M and 0.06 M for CYPHOS IL104 and CYPHOS IL103, respectively), the loading ratio slowly increases (from 0.43 to 0.53/0.57) between the concentrations 0.03 M and 0.06 M (20–40 g/L), followed by a significant decrease of Z with the increase in ionic liquid concentration. Thus, two types of complexes are formed in direct connection with the ionic liquid concentration:

- For concentrations lower than 40 g/L, echi-molecular complexes (involving only one molecule of both FA and ionic liquid) for both cases: [FA][CYPHOS IL103] and [FA][CYPHOS IL104] are formed, while
- For concentrations higher than 40 g/L, the decrease of Z with increasing ionic liquid concentration in the organic phase indicates the formation of complexes involving two molecules of ionic liquid per folic acid molecule: [FA][CYPHOS IL103]$_2$ and [FA][CYPHOS IL104]$_2$. This suggests that it may be more cost-effective to enhance the extractant concentration when the process efficiency is below the optimum level than to raise the process efficiency while maintaining the extractant concentration [42].

Schlosser [37] described two methods for water coextraction in the organic phase using Cyphos IL-104 dissolved in dodecane: the production of reverse micelles, and the incorporation of water into hydrated complexes including lactic acid and IL, complexes that include two molecules of water. In this study, no modifications of the two phases volume were recorded after the extraction using heptane as an organic solvent. This could be due to the short extraction time—10 min, or to the large structure of folic acid and its lower concentrations than the ionic liquid.

2.2. Modeling

The proposed ANN-GWO approach was applied to model the process. To reach this objective, the extraction yield for FA was determined as a function of the type of solvent used, aqueous phase pH, type of extractant and its concentration. Since the type of solvent and type of extractant are categorical values, they were coded with numerical integer values. This strategy allowed the development of a single model for all possible combinations regarding the considered parameters. This represents one significant advantage over the classical regression methods usually used to determine a process model.

Since the experimental work aimed to perform a reduced number of experiments and since ANNs work better with large datasets, in this work the experimental data were supplemented with a series of additional points by performing an interpolation procedure for simple, individual cases of combinations of parameters. For these cases, based on 2D plot representation, the trendlines that best fit the experimental points were determined using the R^2 metric, and the identified equation was then used to generate additional data. In this manner, the available dataset was extended from 27 experimental points to 103, thus allowing the ANN model to better capture the dynamic and influence of all process parameters on the extraction yield. Next, following the standard procedures regarding the application of ANNs, the data was normalized and randomly split into two groups (training and testing). The normalization procedure scales all the parameters to the $[-1,1]$ interval and reduces the impact of inputs with higher orders of magnitude. The type of normalization considered in this work is the Min-Max approach [43]. Afterward, the entire available dataset was randomly attributed: 75% to training and 25% to testing. The statistical indicators for these two subsets are presented in Table 3.

In the next step, the limits for the maximum ANN topology and the settings for GWO were set. Regarding topology, to reduce the number of ANN parameters that need to be identified based on the available data, the maximum number of hidden layers was set to 1, with 20 neurons in the hidden layer. This limitation was based on a set of preliminary runs that indicated that, for the current process, an ANN with a single hidden layer could efficiently capture the system's dynamic. Concerning the GWO parameters, the population size was set to 50 individuals, and the number of runs was set to 500. Next, 50 simulations were performed to determine the best ANN model for the process. The statistics of these runs are presented in Table 4, where Fitness measures model efficiency and is determined based on the Mean Squared Error (MSE) obtained in the training phase. The ANN with the highest fitness, referred to as ANN (4:05:01), indicates the best model for the process. In Table 4, topology is represented using an Input:HiddenLayer:Output notation, where Input represents the number of inputs corresponding to the process parameters (type of solvent used, aqueous phase pH, type of extractant and its concentration), HiddenLayer indicates

the number of neurons in the hidden layer and Output indicates the number of process outputs (which for the current problem is FA).

Table 3. Statistics descriptors for the subsets used for ANN training and testing.

Subset	Indicator	Type of Solvent	Type of Extractant	Aqueous Phase pH	Extractant Concentration	FA
Training	Mean	1.155844	1.727273	4.084416	48.7013	63.0724
	Median	1	2	4	40	79.8336
	Standard Deviation	0.365086	0.718851	0.874164	28.2191	32.09486
	Sample Variance	0.133288	0.516746	0.764162	796.3175	1030.08
	Kurtosis	1.792505	−0.94144	0.632868	0.556316	−1.11127
	Skewness	1.935617	0.461642	−0.01714	0.909524	−0.65705
	Minimum	1	1	2	0	6.229
	Maximum	2	3	6	120	98.33493
	Count	77	77	77	77	77
Testing	Mean	1.269231	1.923077	3.75	51.15385	62.5145
	Median	1	2	4	40	81.54103
	Standard Deviation	0.452344	0.796145	0.806226	26.08861	32.47939
	Sample Variance	0.204615	0.633846	0.65	680.6154	1054.911
	Kurtosis	−0.84995	−1.37721	1.646948	0.895838	−1.59354
	Skewness	1.105353	0.143288	−0.10853	1.188646	−0.49504
	Minimum	1	1	2	15	8.340475
	Maximum	2	3	5.75	120	99.5693
	Count	26	26	26	26	26

Table 4. Statistic indicators for 50 runs for the ANN-GWO approach.

	Fitness	MSE Training	MSE Testing	Topology
Best	647.7774	0.001544	0.000624	4:05:01
Worst	137.7863	0.007258	0.006111	4:08:01
Confidence interval	318.34 ± 41.06	0.004 ± 0.0005	0.003 ± 0.0004	0.985 ± 0.0018

The average absolute error computed in the training phase for ANN (4:05:01) presented in Figure 6 was 6.8%, and in the testing phase was 3.8%. In Figure 6, the hidden layer contains in total 5 neurons, numbered Neuron1 through Neuron5.

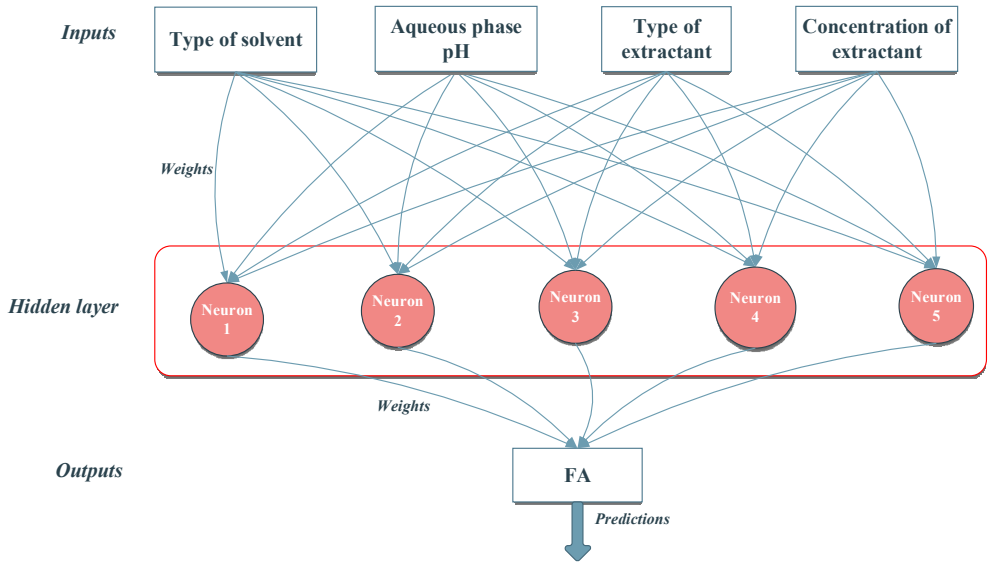

Figure 6. Topology of the best ANN model obtained.

These results and the low values for MSE (Table 4) indicate the selected model's performance. One explanation for the MSE in the training phase being higher than in the testing phase is related to the fact that it contains the only two examples in the entire dataset with a 0 value for the extractant concentration. Only for these two cases is the absolute error high (~50%), with an experimental value of 6.2 and predicted values of ~9.2.

An analysis of the data obtained in laboratory settings showed that the identified ANN captures well the system's behavior in different combinations of solvent-extractant (Figure 7a–c). The relations describing the model are presented in the Supplementary Material.

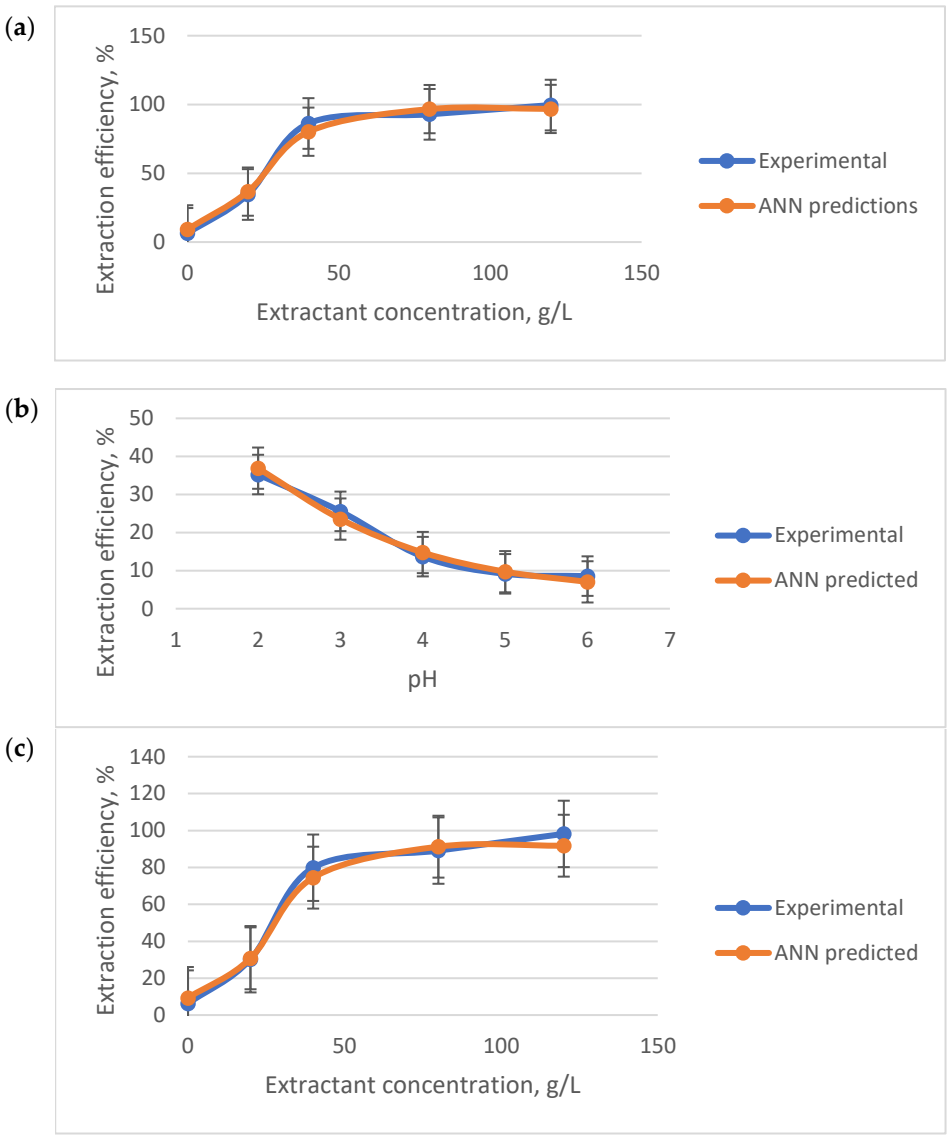

Figure 7. Comparison between the experimental data and the ANN predictions for (**a**) Heptane and CYPHOS IL103 when pH = 4; (**b**) chloroform and [HMIM][PF_6] when extractant concentration is 40; (**c**) Heptane and CYPHOS IL104 when pH = 4.

3. Materials and Methods

3.1. Extraction Process

The experiments performed for FA extraction were carried out using a vibration shaker (WIZARD IR Infrared Vortex Mixer, VELP Scientifica Srl, Usmate (MB), Italy) that ensured a stirring speed of 1200 rpm (extraction time—10 min and temperature 22 °C), using equal volumes (2 mL) of FA solution, and the organic phase using a glass cell. FA

was extracted from aqueous solutions whose initial concentration was 0.04 g/L (due to limited solubility in water). The extraction was carried out either using only pure ionic liquids (preliminary studies): [BMIM][PF_6]: 1-Butyl-3-methylimidazolium hexafluorophosphate, [HMIM][PF_6]: 1-Hexyl-3-methylimidazolium hexafluorophosphate, [OMIM][PF_6]: 1-Octyl-3-methylimidazolium hexafluorophosphate, CYPHOS IL103—Trihexyl-tetra-decyl-phosphonium decanoate, and CYPHOS IL104—Tri-hexyl-tetra-decyl-phosphonium bis(2,4,4-trimethylpentyl)phosphinate, or organic solvents with different dielectric constants (heptane, chloroform and octanol) and a mixture of ionic liquid and organic solvent (CYPHOS IL103 and heptane, CYPHOS IL104 and heptane and [HMIM][PF_6] and chloroform). All reagents were procured from Sigma-Aldrich [Merck KGaA, Darmstadt, Germany]. The ionic liquid concentration in the organic phase varied between 0 and 120 g/L. The pH of the initial aqueous phase was corrected to the predetermined value, using 4% sulfuric acid and sodium hydroxide solutions, based on the indications of a Hanna Instruments pH 213 digital pH meter (Woonsocket, Rhode Island). After extraction, the samples were separated by centrifugation at 4000 rpm for 5 min, using a DLAB centrifuge (Beijing, China).

The analysis of the acid extraction process was carried out using the separation yield. It was calculated by determining the FA concentration from the initial solution and the raffinate solution, using a Dionex Ultimate HPLC system (Thermo Fisher Scientific Inc., Waltham, MA, USA) equipped with an Acclaim PA2 column, the mobile phase being a mixture of acetonitrile and 30 mM KH_2PO_4 solution with a flow rate of 0.5 mL/min, detection at 270 nm. All experiments were performed in triplicate (n = 3, error between 1.5 and 4.5%).

3.2. Modeling

Combining mathematical modeling with experimental research can offer a tool for anticipating extraction performance. In order to extend experimental knowledge, the FA separation process was modelled. The methodology applied in this work combined ANNs with the GWO algorithm to model the considered process. The role of GWO is to optimize the ANN characteristics. This combination of bio-inspired metaheuristic-ANN belongs to the neuro-evolutive procedures. Neuro-evolution can be applied at different levels: (a) topology; (b) connection weights; (c) learning rule; (d) node behavior [44]. In this work, GWO was applied simultaneously for topology (the number of hidden layers and neurons in each hidden layer), connections' weights (parameters usually set in the training procedure with algorithms such as Backpropagation) and node behavior (the selection of transfer function and its associated properties) and, to incorporate all these parameters into the structure of real numbers used by GWO, a direct encoding procedure is used. Once this structure is established, the GWO optimizes a population of randomly generated networks until a stop criterion is reached. The stop function is represented by the number of iterations set at the start of the run.

Distinctively from other bio-inspired metaheuristics such as Genetic Algorithms or Differential Evolution, in GWO the population is divided into four groups that simulate the hierarchical structure of wolfs: alpha (the leaders), beta (that supports the alpha), delta (that executes the commands of alpha and beta), omega (that are managed by the delta and are at the bottom of the hierarchy) [45]. The hunting mechanisms that GWO mathematically simulates include: (a) encircling (where the entire pack works together to chase and direct the prey in a strategy to increase the chance of catching it); (b) hunting (movement of wolfs around the prey guided by the alpha); and (c) attacking (attacking the prey when it stopped moving). These principles were implemented in Visual Studio C#, following the mathematical relations described in the work of Mirjalili et al., 2014 [26].

4. Conclusions

This study presents the extraction of FA from aqueous solutions using reactive extraction with hydrophobic IL diluted with heptane (a greener alternative to classical solvents [46]) as an efficient technological alternative for this vitamin's separation. Almost

100% (99.56%) extraction yield was obtained for 120 g/L CYPHOS IL103 and aqueous phase pH equal to 4, the reactive extraction mechanism being based on hydrogen bonding between FA and IL. The analysis of the loading factor indicated no overloading in the extraction systems in optimum conditions. The process was modelled using a combined ANNs with the GWO algorithm; the data obtained showed good accordance between predicted and experimental results. According to the findings of this study, it is possible to use efficiently phosphonium-based ionic liquids for folic acid extraction or reactive extraction. Moreover, the separation procedures were straightforward and free of volatile organic solvents.

Supplementary Materials: The following supporting information can be downloaded at: https://www.mdpi.com/article/10.3390/molecules28083339/s1, Figure S1: FTIR spectra for folic acid, Cyphos IL103 ionic liquid in heptane and extract; Figure S2: UV-VIS spectra for Cyphos IL103 ionic liquid in heptane and Chyphos Il103 loaded with FA.

Author Contributions: Conceptualization, A.C.B.; methodology, A.C.B., A.T. and L.K.; software and modelling, E.N.D.; validation, D.C.; investigation, A.C.B.; resources, A.C.B.; writing—original draft preparation, A.C.B.; writing—review and editing, D.C.; visualization, A.T. and L.K.; project administration, A.C.B.; funding acquisition, A.C.B. All authors have read and agreed to the published version of the manuscript.

Funding: This work was supported by a grant of the Ministry of Research, Innovation and Digitization, CNCS—UEFISCDI, project number PN-III-P1-1.1-TE-2021-0153, within PNCDI III.

Institutional Review Board Statement: Not acceptable.

Informed Consent Statement: Not acceptable.

Data Availability Statement: Data is contained in the article and Supplementary Material.

Conflicts of Interest: The authors declare no conflict of interest.

References

1. Yang, H.; Zhang, X.; Liu, Y.; Liu, L.; Li, J.; Du, G.; Chen, J. Synthetic Biology-Driven Microbial Production of Folates: Advances and Perspectives. *Bioresour. Technol.* **2021**, *324*, 124624. [CrossRef]
2. Menezo, Y.; Elder, K.; Clement, A.; Clement, P. Folic Acid, Folinic Acid, 5 Methyl TetraHydroFolate Supplementation for Mutations That Affect Epigenesis through the Folate and One-Carbon Cycles. *Biomolecules* **2022**, *12*, 197. [CrossRef] [PubMed]
3. Park, S.Y.; Do, J.R.; Kim, Y.J.; Kim, K.S.; Lim, S.D. Physiological Characteristics and Production of Folic Acid of Lactobacillus plantarum JA71 Isolated from Jeotgal, a Traditional Korean Fermented Seafood. *Korean J. Food Sci. Anim. Resour.* **2014**, *34*, 106–114. [CrossRef] [PubMed]
4. San, H.H.M.; Alcantara, K.P.; Bulatao, B.P.I.; Sorasitthiyanukarn, F.N.; Nalinratana, N.; Suksamrarn, A.; Vajragupta, O.; Rojsitthisak, P.; Rojsitthisak, P. Folic Acid-Grafted Chitosan-Alginate Nanocapsules as Effective Targeted Nanocarriers for Delivery of Turmeric Oil for Breast Cancer Therapy. *Pharmaceutics* **2023**, *15*, 110. [CrossRef] [PubMed]
5. Crider, K.S.; Bailey, L.B.; Berry, R.J. Folic Acid Food Fortification—Its History, Effect, Concerns, and Future Directions. *Nutrients* **2011**, *3*, 370–384. [CrossRef]
6. Quadintel. *Global Folic Acid Market Size study, by Application (Dietary Supplements, Cosmetics, Pharmaceuticals, and Other Applications), and Regional Forecasts 2022–2028*; Report ID: QI037; Bizwit Research & Consulting: Indore, India, 2022.
7. Hamzehlou, P.; Akhavan Sepahy, A.; Mehrabian, S.; Hosseini, F. Production of Vitamins B3, B6 and B9 by Lactobacillus isolated from Traditional Yogurt Samples from 3 Cities in Iran, Winter 2016. *Appl. Food Biotechnol.* **2018**, *5*, 107–120.
8. Laiño, J.E.; Levit, R.; de LeBlanc, A.d.M.; Savoy de Giori, G.; LeBlanc, J.G. Characterization of folate production and probiotic potential of *Streptococcus gallolyticus* subsp. macedonicus CRL415. *Food Microbiol.* **2019**, *79*, 20–26. [CrossRef]
9. Hugenschmidt, S.; Miescher Schwenninger, S.; Lacroix, C. Concurrent high production of natural folate and vitamin B12 using a co-culture process with *Lactobacillus plantarum* SM39 and *Propionibacterium freudenreichii* DF13. *Process Biochem.* **2011**, *46*, 1063–1070. [CrossRef]
10. Serrano-Amatriain, C.; Ledesma-Amaro, R.; Lopez-Nicolas, R.; Ros, G.; Jimenez, A.; Revuelta, J.L. Folic acid production by engineered *Ashbya gossypii*. *Metab. Eng.* **2016**, *38*, 473–482. [CrossRef]
11. Wang, Y.; Liu, L.; Jin, Z.; Zhang, D. Microbial Cell Factories for Green Production of Vitamins. *Front. Bioeng. Biotechnol.* **2021**, *9*, 661562. [CrossRef]
12. Roy, S.; Olokede, O.; Wu, H.; Holtzapple, M. In-situ carboxylic acid separation from mixed-acid fermentation of cellulosic substrates in batch culture. *Biomass Bioenergy* **2021**, *151*, 106165. [CrossRef]

13. Galaction, A.I.; Blaga, A.C.; Cascaval, D. The influence of pH and solvent polarity on the mechanism and efficiency of folic acid extraction with Amberlite LA2. *Chem. Ind. Chem. Eng. Q.* **2005**, *11*, 63–68. [CrossRef]
14. Aras, S.; Demir, Ö.; Gök, A. Reactive extraction of gallic acid by trioctylphosphine oxide in different kinds of solvents: Equilibrium modeling and thermodynamic study. *Braz. J. Chem. Eng.* **2022**. [CrossRef]
15. Blaga, A.C.; Dragoi, E.N.; Munteanu, R.E.; Cascaval, D.; Galaction, A.I. Gallic Acid Reactive Extraction with and without 1-Octanol as Phase Modifier: Experimental and Modeling. *Fermentation* **2022**, *8*, 633. [CrossRef]
16. Lazar, R.G.; Blaga, A.C.; Dragoi, E.N.; Galaction, A.I.; Cascaval, D. Application of reactive extraction for the separation of pseudomonic acids: Influencing factors, interfacial mechanism, and process modelling. *Can. J. Chem. Eng.* **2021**, *100*, S246–S257. [CrossRef]
17. Georgiana, L.R.; Cristina, B.A.; Niculina, D.E.; Irina, G.A.; Dan, C. Mechanism, influencing factors exploration and modelling on the reactive extraction of 2-ketogluconic acid in presence of a phase modifier. *Sep. Purif. Technol.* **2020**, *255*, 117740. [CrossRef]
18. Demmelmayer, P.; Kienberger, M. Reactive extraction of lactic acid from sweet sorghum silage press juice. *Sep. Purif. Technol.* **2022**, *282*, 120090. [CrossRef]
19. Blaga, A.C.; Malutan, T. Selective Separation of Vitamin C by Reactive Extraction. *J. Chem. Eng. Data* **2012**, *57*, 431–435. [CrossRef]
20. Poştaru, M.; Bompa, A.S.; Galaction, A.I.; Blaga, A.C.; Caşcaval, D. Comparative Study on Pantothenic Acid Separation by Reactive Extraction with Tri-n-octylamine and Di-(2-ethylhexyl) Phosphoric Acid. *Chem. Biochem. Eng. Q.* **2016**, *30*, 81–92. [CrossRef]
21. Blaga, A.C.; Tucaliuc, A.; Kloetzer, L. Applications of Ionic Liquids in Carboxylic Acids Separation. *Membranes* **2022**, *12*, 771. [CrossRef]
22. de Jesus, S.S.; Filho, R.M. Are ionic liquids eco-friendly? *Renew. Sustain. Energy Rev.* **2022**, *157*, 112039–112061. [CrossRef]
23. Li, Q.; Jiang, X.; Zou, H.; Cao, Z.; Zhang, H.; Xian, M. Extraction of short-chain organic acids using imidazolium-based ionic liquids from aqueous media. *J. Chem. Pharm. Res.* **2014**, *6*, 374–381.
24. Blahusiak, M.; Schlosser, S.; Martak, J. Extraction of butyric acid with a solvent containing ammonium ionic liquid. *Sep. Purif. Technol.* **2013**, *119*, 102–111. [CrossRef]
25. Zare, F.; Ghaedi, M.; Daneshfar, A. Application of an ionic-liquid combined with ultrasonic-assisted dispersion ofgold nanoparticles for micro-solid phase extraction of unmetabolized pyridoxine and folic acid in biological fluids prior to high-performance liquid chromatography. *RSC Adv.* **2015**, *5*, 70064–70072. [CrossRef]
26. Mirjalili, S.; Mirjalili, S.M.; Lewis, A. Grey Wolf Optimizer. *Adv. Eng. Softw.* **2014**, *69*, 46–61. [CrossRef]
27. Raj, G.B.; Dash, K.K. Ultrasound-assisted extraction of phytocompounds from dragon fruit peel: Optimization, kinetics and thermodynamic studies. *Ultrason. Sonochem.* **2020**, *68*, 105180.
28. Abdullah, S.; Pradhan, R.C.; Pradhan, D.; Mishra, S. Modeling and optimization of pectinase-assisted low-temperature extraction of cashew apple juice using artificial neural network coupled with genetic algorithm. *Food Chem.* **2021**, *339*, 127862. [CrossRef]
29. Sodeifian, G.; Ardestani, N.S.; Sajadian, S.A.; Ghorbandoost, S. Application of supercritical carbon dioxide to extract essential oil from Cleome coluteoides Boiss: Experimental, response surface and grey wolf optimization methodology. *J. Supercrit. Fluids* **2016**, *114*, 55–63. [CrossRef]
30. Sukpancharoen, S.; Srinophakun, T.R.; Aungkulanon, P. Grey wolf optimizer (GWO) with multi-objective optimization for biodiesel production from waste cooking oil using central composite design (CCD). *Int. J. Mech. Eng.* **2020**, *9*, 1219–1225. [CrossRef]
31. Samuel, O.D.; Okwu, M.O.; Oyejide, O.J.; Taghinezhad, E.; Afzal, A.; Kaveh, M. Optimizing biodiesel production from abundant waste oils through empirical method and grey wolf optimizer. *Fuel* **2020**, *281*, 118701. [CrossRef]
32. Weast, R.C. *Handbook of Chemistry and Physics*, 54th ed.; CRC Press: Cleveland, OH, USA, 1974.
33. Nosrati, S.; Jayakumar, N.; Hashim, M. Performance evaluation of supported ionic liquid membrane for removal of phenol. *J. Hazard. Mater.* **2011**, *192*, 1283–1290. [CrossRef] [PubMed]
34. Matsumoto, M.; Panigrahi, A.; Murakami, Y.; Kondo, K. Effect of Ammonium- and Phosphonium-Based Ionic Liquids on the Separation of Lactic Acid by Supported Ionic Liquid Membranes (SILMs). *Membranes* **2011**, *1*, 98–108. [CrossRef]
35. Fraser, K.J.; MacFarlane, D.R. Phosphonium-Based Ionic Liquids: An Overview. *Aust. J. Chem.* **2009**, *62*, 309–321. [CrossRef]
36. Gonçalves, A.R.P.; Paredes, X.; Cristino, A.F.; Santos, F.J.V.; Queirós, C.S.G.P. Ionic Liquids—A Review of Their Toxicity to Living Organisms. *Int. J. Mol. Sci.* **2021**, *22*, 5612. [CrossRef] [PubMed]
37. Kebaili, H.; Pérez de los Ríos, A.; José Salar-García, M.; Ortiz-Martínez, V.M.; Kameche, M.; Hernández-Fernández, J.; Hernández-Fernández, F.J. Evaluating the Toxicity of Ionic Liquids on *Shewanella* sp. for Designing Sustainable Bioprocesses. *Front. Mater.* **2020**, *7*, 578411. [CrossRef]
38. Schlosser, Š.; Marták, J.; Blahušiak, M. Specific phenomena in carboxylic acids extraction by selected types of hydrophobic ionic liquids. *Chem. Pap.* **2018**, *72*, 567–584. [CrossRef]
39. Kurnia, K.A.; Lima, F.; Cláudio, A.F.; Coutinho, J.A.; Freire, M.G. Hydrogen-bond acidity of ionic liquids: An extended scale. *Phys. Chem. Chem. Phys.* **2015**, *17*, 18980–18990. [CrossRef]
40. Gazzali, A.M.; Lobry, M.; Colombeau, L.; Acherar, S.; Azaïs, H.; Mordon, S.; Arnoux, P.; Baros, F.; Vanderesse, R.; Frochot, C. Stability of folic acid under several parameters. *Eur. J. Pharm. Sci.* **2016**, *10*, 419–430. [CrossRef]
41. Marták, J.; Schlosser, S. Extraction of lactic acid by phosphonium ionic liquids. *Sep. Purif. Technol.* **2007**, *57*, 483–494. [CrossRef]

42. DeSimone, D.; Counce, R.; Watson, J. Predicting the loading ratio and optimum extractant concentration for solvent extraction. *Chem. Eng. Res. Des.* **2020**, *161*, 271–278. [CrossRef]
43. Priddy, K.; Keller, P. *Artificial Neural Networks: An introduction*; SPIE Press: Washington, DC, USA, 2005.
44. Islam, M.; Yao, X. Evolving Artificial Neural Network Ensembles. In *Computational Intelligence: A Compendium*; Fulcher, J., Jain, L., Eds.; Springer: Berlin/Heidelberg, Germany, 2008.
45. Torabi, S.; Safi-Esfahani, F. Improved Raven Roosting Optimization algorithm (IRRO). *Swarm Evol. Comput.* **2018**, *40*, 144–154. [CrossRef]
46. Jessop, P.G. Searching for green solvents. *Green Chem.* **2011**, *13*, 1391–1398. [CrossRef]

fermentation

Article

Gallic Acid Reactive Extraction with and without 1-Octanol as Phase Modifier: Experimental and Modeling

Alexandra Cristina Blaga [1], Elena Niculina Dragoi [1], Raluca Elena Munteanu [1], Dan Cascaval [1,*] and Anca Irina Galaction [2]

[1] "Cristofor Simionescu" Faculty of Chemical Engineering and Environmental Protection, "Gheorghe Asachi" Technical University of Iasi, 700454 Iasi, Romania
[2] Faculty of Medical Bioengineering, "Grigore T. Popa" University of Medicine and Pharmacy, 700454 Iasi, Romania
* Correspondence: dan.cascaval@academic.tuiasi.ro

Abstract: Gallic acid (GA) is a naturally occurring phenolic acid that can be found in the leaves, roots, flowers, or stems of a wide variety of plant species. It has a broad range of uses in the food and pharmaceutical industries. The objective of this research is to investigate the GA reactive extraction process employing dichloromethane and n-heptane as solvents, 1-octanol as a phase-modifier, and Amberlite LA-2 as an amine extractant dissolved in the organic phase. The separation yield and distribution coefficient data were discussed, along with the analysis of the extraction conditions and the extraction mechanism. Dichloromethane employed as the solvent, 80 g/L Amberlite LA2 used as the extractant, and 10% phase modifier were determined to be the ideal conditions for the reactive extraction onto a biphasic organic-aqueous system. Statistical regression and artificial neural networks (ANNs) established with the differential evolution (DE) algorithm were also used to model and optimize the process.

Keywords: reactive extraction; phase modifier; gallic acid; Amberlite LA2; extraction mechanism

check for updates

Citation: Blaga, A.C.; Dragoi, E.N.; Munteanu, R.E.; Cascaval, D.; Galaction, A.I. Gallic Acid Reactive Extraction with and without 1-Octanol as Phase Modifier: Experimental and Modeling. *Fermentation* **2022**, *8*, 633. https://doi.org/10.3390/fermentation8110633

Academic Editor: Diomi Mamma

Received: 17 October 2022
Accepted: 9 November 2022
Published: 12 November 2022

1. Introduction

Gallic acid (3,4,5-trihydroxybenzoic acid, Figure 1) (GA) is a phenolic acid of natural origin, found in the leaves, roots, flowers, or stem of a large number of plant species (*Bergia suffruticosa*, *Ceratonia siliqua*, *Tectonagrandis*, and *Casuarina equisetifolia*) with numerous applications in the food and pharmaceutical industries [1].

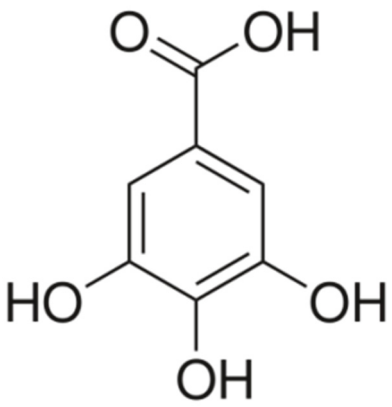

Figure 1. Chemical structure of gallic acid.

GA is a white or pale-yellow crystalline compound, with the structural formula presented in Figure 1 and the main physicochemical properties in Table 1.

Table 1. Main characteristics of gallic acid [2].

Characteristic	Value
Molar mass	170.12 g/mol (anhydrous)
Density	1.694 g/cm^3
Solubility in water	1.19 g/100 mL (anhydrous, 20 °C)
Melting point	260 °C
Acidity constant	3.94 (COOH) 8.45, 11.4, and 13 (phenolics OH)

From the pharmacological point of view, GA has antimicrobial, anti-inflammatory and antioxidant action [1,3]. In addition, GA inhibits the adhesion and development of microorganisms from the species *Pseudomonas aeruginosa*, *Staphylococcus aureus*, *Streptococcus mutans*, *Chromobacterium violaceum*, *Listeria monocytogenes*, and *Shigella flexneri* [4–9]. Moreover, it is able to exhibit degradative action on the cell wall of some Gram-negative microorganisms and an inhibitory effect on the activity of some enzymes (HIV-1 integrase, HIV-1 transcriptase, HCV serine protease, etc.) [10–12]. Additionally, a few studies present models for the use of GA and its derivatives in various diseases, including cancer [13]. The cytotoxic and antitumoral effect of GA results from modulating pro- and anti-oxidant activities [3].

Conventionally, GA can be obtained by acid hydrolysis of tannic acid. However, it implies high cost, low yield, low purity, and generation of toxic effluents. A more efficient process involves microbial hydrolysis of tannic acid (Table 2) using tannase (tannin-acyl-hydrolase, EC 3.1. 1.20, an enzyme that catalyzes the breakdown of ester bonds in gallotannins) produced by fungal and bacterial strains.

Table 2. Production of gallic acid using tannase-producing microorganisms [14–18].

Microorganism	Process	Culture Media	GA Produced
B. subtilis AM1	Anaerobic batch fermentation, 30 °C, 48 h	$FeSO_4 \times 7H_2O$, 0.01; $NaNO_3$, 3; K_2HPO_4, 1; $MgSO_4 \times 7H_2O$, 0.5; KCl, 0.5; and tannic acid 1%.	24.16 g/L
L. plantarum CIR1	Anaerobic batch fermentation, 30 °C, 48 h	$FeSO_4 \times 7H_2O$, 0.01; $NaNO_3$, 3; K_2HPO_4, 1; $MgSO_4 \times 7H_2O$, 0.5; KCl, 0.5; and tannic acid 1%.	23.73 g/L
Sporidiobolus ruineniae A45.2	Aerobic batch fermentation, 1L stirred tank fermenter, 250 rpm, aeration rate of 0.2 vvm 30 °C for 48 h	3 g/L yeast extract, 3 g/L malt extract, 5 g/L peptone, 10 g/L glucose, 5 g/L tannic acid	11.2 g/L
Bacillus sphaericus	Batch fermentation, pH 6.0, 37 °C, 100 rpm, 48 h	2.0% tannic acid, 2.5% galactose, 0.25% ammonium chloride, and 0.1% $MgSO_4$	90.8%
Rhizopus oryzae NRRL 21498, *Aspergillus foetidus* MTCC 3557	Modified solid-state fermentation, 30 °C and 80% relative humidity, pH 5	Powdered fruits of *Terminalia chebula* and powdered pod cover of *Caesalpinia digyna*	94.8%
Aspergillus fischeri MTCC 150	Batch fermentation 35 °C, pH: 4.0 to 3.5, agitation: 250 rpm	NH_4NO_3, 1.65 g/L, KNO_3, 1.9 g/L, $MgSO_4 \times 7H_2O$, 0.371.65 g/L, $CaCl_2 \times 2H_2O$, 0.44 g/L, KH_2PO_4, 0.17 g/L, H_3BO_3, 6.2 mg/mL, $MnSO_4 \times H_2O$, 16.9 mg/mL, $ZnSO_4 \times 7H_2O$, 8.6 mg/mL, $Na_2MoO_4 \times 2H_2O$, 0.25 mg/mL, $CuSO_4 \times 5H_2O$, 0.025 mg/mL, $CoCl_2 \times 6H_2O$, 0.025 mg/mL, $FeSO_4 \times 7H_2O$, 5.6 mg/mL, and Na_2EDTA, 7.6 mg/mL, tannic acid 5.0 g/L	7.35 g GA/g biomass; 23% conversion obtained at 50 g/L tannic acid
Penicillium rolfsii (CCMB 714)	Submerged fermentation, 30 °C	10% tannic acid	21.51 g/L

Several studies have analyzed reactive extraction for the GA separation [19–22], showing its potential. Rewatkar et al. [19] obtained-under optimum conditions of 2.34 g/L GA, 65.65% *v*/*v* tri-n-butyl phosphate in hexanol, 19 °C, and pH 1.8-an extraction efficiency of 99.43% for gallic acid from an aqueous stream. Joshi et al. [20] obtained the following distributions coefficient of GA 1.94–27.57 for 2-octanone: 1.12–8.83 for lauryl alcohol, and 0.20–22.07 for n-heptane, increased values being obtained by adding 0.3652 mol/L TBP (tri-butyl phosphate) as an extractant. Pandey et al. [21,22] obtained the maximum GA extraction of 90.1%, at an initial acid concentration of 0.0588 mol/L, initial TOA concentration

of 0.2762 mol/L, pH 2, and temperature of 25.0 °C. However, none of these studies have analyzed GA back extraction from organic solvents.

This study aims to provide a complete analysis (extraction, stripping, and optimization) of the GA reactive extraction process using Amberlite LA2 dissolved into two solvents with different dielectric constants: dichloromethane and n-heptane and a phase modifier (1-octanol). For reactive extraction of carboxylic acids during the intense mixture necessary for a good mass transfer, a third phase is formed—a stable emulsion very difficult to separate. The addition of a phase modifier, 1-octanol, prevents its formation, facilitating the organic and aqueous phase separation, and, it also increases the solvent polarity increasing the reactive extraction efficiency [23–25]. The results were discussed from the viewpoint of the extraction mechanism, separation yield and distribution coefficient, for different extraction conditions. Back extraction was successfully performed using NaOH solutions. In addition, the process was modeled and optimized using statistical regression and Artificial Neural Networks (ANNs) determined with the Differential Evolution (DE) algorithm. The objective is to rapidly identify the extraction efficiency without additional experiments and determine the optimal conditions that lead to maximum efficiency.

2. Materials and Methods

2.1. Chemicals

All chemicals, including gallic acid (98.0%), dichloromethane (99%), 1-octanol (99%), heptane (99%), sulfuric acid (95.0–98.0%), sodium hydroxide (>97%), lauryl tri-alkylmethyl-amine—Amberlite LA2 (99%), and acetonitrile (99.99%), were purchased by Sigma Aldrich (Burlington, VT, USA) and used as received without further processing.

2.2. Reactive Extraction Experiments

Reactive extraction and stripping experiments for GA separation were carried out using equal volumes of aqueous and organic phases (20 mL) in an extraction column with vibratory mixing (50 s^{-1} frequency and 5 mm amplitude, the stirrer being maintained at the initial interface between the two phases), consisting in a glass column with a diameter of 36 mm and 250 mm height, provided with a thermostatic jacket that allowed temperature control: 25 ± 0.02 °C for all the reactive extraction experiments and 50 ± 0.02 °C for the back extraction. The reactive extraction experiments were performed using two solvents with different polarities: dichloromethane (dielectric constant 9.08 [26]) and n-heptane (dielectric constant 1.9 [26]). The first solvent, suitable for polar compounds, was chosen based on efficient reactive extraction obtained for other carboxylic acids (2-ketogluconic acid, formic acid, pseudomonic acid, acetic acid, etc. [23–25,27]), while the second one was chosen due to its green classification [28]. As a phase modifier, 1-octanol (dielectric constant 10.3 at 25 °C [26]) was added to the organic solution to increase the polarity of the solvent and to facilitate the phases separations (1-octanol prevents the formation of a third phase—a stable emulsion between the two phases). Solvent selection is an essential parameter since it influences the extraction efficiency and the design of a continuous extraction process and solvent regeneration cycle.

After the extraction and the stripping (each process having a duration of 1 min), phases were separated in a centrifugal separator at 4000 rpm. GA initial concentration in the aqueous phase was 5 g/L (2.29×10^{-2} M), and the concentrations of the amine extractant, Amberlite LA-2, in the organic phase varied between 0 and 80 g/L (0.215 M). The pH value of the aqueous phase was between 2 and 5 for the extraction and 8 for the stripping experiments, modified using solutions of 3% sulfuric acid or 3% sodium hydroxide, by means of the indications of the digital pH meter (CONSORT C 836) (Turnhout, Belgium).

2.3. Analytical Procedures

The processes were analyzed on the basis of distribution coefficients and extraction efficiency, calculated using the mass balance based on the GA concentration in the aqueous phases measured by the high-performance liquid chromatography technique (HPLC) as

described in the literature [19]. For this purpose, an HPLC system, UltiMate 3000 Dionex (Sunnyvale, CA, USA), provided with an Acclaim C18 (150 mm × 4.1 mm, 5 µm) column (Sunnyvale, CA, USA), 90% water, and 10% acetonitrile solution were used as mobile phase, with detection by UV absorbance at 264 nm wavelength, and the flow rate of 0.8 mL/min.

2.4. Modelling and Optimization

In order to model and optimize the considered process, two strategies were considered. One is based on the classical approaches that use statistical methods, and the other uses artificial intelligence techniques: ANNs and bio-inspired metaheuristics.

2.4.1. Statistic Approaches

The statistical analysis of the process was performed using Minitab (Coventry, UK), with a regression model with interactions through order 2 and terms through order 2, with a 95% confidence level for all intervals, and a forward selection strategy for parameter optimization. For process optimization, the Response Optimizer option was used.

2.4.2. Artificial Neural Networks and Differential Evolution

In this case, the process modeling was performed using ANNs. Although ANNs are relatively easy to use, their optimal configuration and hyper-parameters are a problem in themselves. Thus, a Keras sequential model was considered in this work, with an Adam optimizer and ReLU activation function for the hidden layers and a linear activation function for the output layer. Consequently, the training of the ANN is performed using the Keras framework. However, before training, an optimal architecture must be selected. This step is performed by DE, a population-based bio-inspired metaheuristic that showed a good capability to solve various problems from different areas. For example, in simple or different combinations, it was applied for: the prediction of polycyclic aromatic hydrocarbons formation in grilled meats [29] prediction of reactive extraction of pseudomonic acids [23], modeling the biogas production from anaerobic wastewater treatment plant [30], and optimization of biogas power plant feedstock [31].

Except for the determination of the ANN model architecture, in this work, DE is also applied to optimize the process. Since this step cannot be performed without a model, in this work, the ANN model was used in combination with DE.

Since DE is a population-based algorithm that uses vectors of real numbers, each of the two optimization problems is individually solved. In each case, a direct encoding transforms the problem into a structure that DE can work with. In the case of ANN optimization, the parameters considered are strictly related to the architecture: the number of hidden layers and neurons in each hidden layer. In the case of process optimization, the parameters considered are related to the process parameters: solvent, octanol addition, pH, and ALA-2 concentration.

Compared with the standard DE algorithm [32], the variant used in this work uses a self-adaptive procedure for the control parameters. This strategy is applied to eliminate the need for manually tuning the F and CR parameters that influence the algorithm's performance. The F parameter controls the mutation rate of the individuals in the population. CR is the crossover rate that influences how the trial individuals are generated from the current and mutated population. Overall, the DE algorithm has fewer steps: initialization, mutation, crossover, and selection. In the initialization phase, the population is randomly generated using the limits of the considered problem. The limits are previously set for the ANN problem depending on how large a model is allowed. For process optimization, the limits are the ones used in the experimental phase. The mutation and the crossover phases are the ones responsible for generating new individuals. The mutation introduces changes in the individuals, and the crossover combines the characteristics of two parents to create children. Finally, in the selection phase, the best individuals are selected to participate in the next generation. The steps mutation, crossover, and selection are repeated until a stop criterion is reached (maximum number of generations).

The general schema of the workflow of the steps performed in this work is presented in Figure 2.

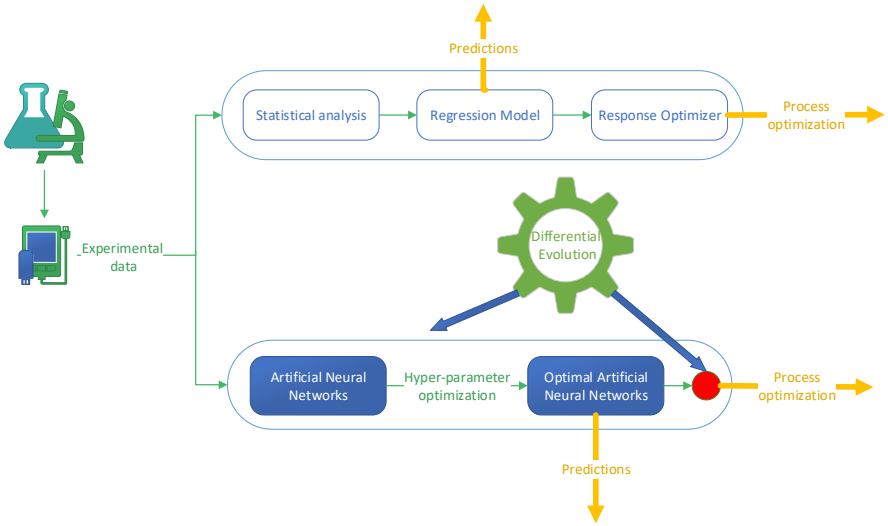

Figure 2. The workflow of the methods applied for process modeling and optimization.

3. Results

3.1. Reactive Extraction

Reactive extraction is a separating technique that implies a chemical reaction between one or more components from a liquid mixture and a selective extractant dissolved in an organic solvent. The efficiency of the reactive extraction depends on the physical and chemical characteristics of the solute (hydrophobicity, acid-base properties), on properties of the extractant (reactivity, ability to form hydrophobic compounds with the solute) and on separation conditions (pH, mixing intensity, concentration level, etc.). Due to these conditions, the mechanism of interaction between solute and extractant, the optimal extraction conditions in correlation with the separation factors, and the extraction mechanism constitute the main study directions in reactive extraction.

3.1.1. Influence of Aqueous Phase pH on the Extraction Efficiency

The pH-value of aqueous solutions is an important parameter that influences the reactive extraction process, as it controls the form in which the acid is found in aqueous solutions: undissociated at pH value lower than pKa (3.94 for the carboxylic group), and dissociated at pH value superior to pKa. GA contains in his molecule a carboxylic group and three hydroxyl groups and the dissociation of these functional groups is represented in Figure 3:

However, due to polarizable hydroxyl from phenolic groups, GA can form hydrogen bonds, generating dimers [33].

Due to GA insolubility in both chosen solvents, the extraction is based on forming a complex between the extractant (Amberlite LA2) and the carboxylic group from the acid structure. The pH influence on the extraction efficiency (E, %—the ratio of GA concentration in the extracted phase and its initial concentration), depicted in Figure 4, suggest hydrogen bond formation between the un-dissociated acid and the extractant (for pH < pKa1, the acid dissociation in the aqueous phase can be considered negligible).

Adding 1-octanol increased the extraction efficiency for both solvents (Table 3), with a more significative influence at pH over 4. The organic phase consists either of two (diluent and extractant) or three components (diluent, extractant, and modifier). The extractant reacts with gallic acid, forming an amine–acid complex that is soluble only in the diluent (used primarily for decreasing extractant viscosity), solubility being improved by the modifier addition. The most important influence of 1-octanol is observed in the case of

n-heptane, by improving its low transfer capabilities of the acid–amine complex in the organic phase.

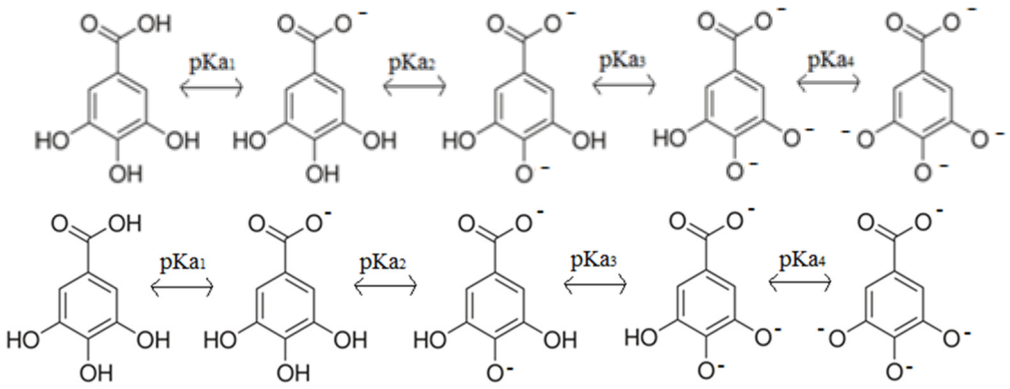

Figure 3. Gallic acid dissociation in aqueous solutions.

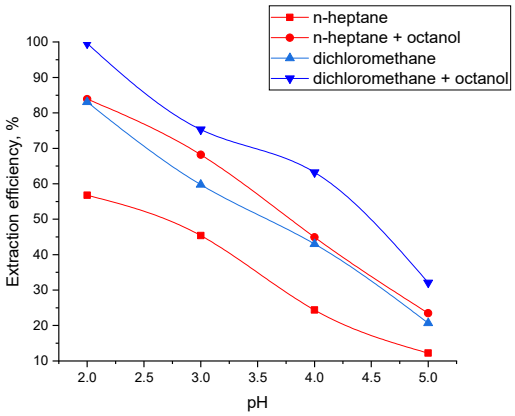

Figure 4. pH influence on extraction efficiency (C_{ALA2} = 40 g/L).

Table 3. The amplification factor values corresponding to 1-octanol addition (C_{ALA2} = 40 g/L).

Solvent/pH	2	3	4	5
n-Heptane	1.47	1.50	1.84	1.92
Dichloromethane	1.19	1.26	1.47	1.55

The most important increase in the values of amplification factors has been reached for pH over 4, in the domain corresponding to the higher extent of carboxyl group dissociation.

3.1.2. Influence of Amine Concentration on the Extraction Efficiency

The reactive extraction of carboxylic acids, which are usually present in low concentrations in the fermentation broth, with an aminic extractant occurs, at equilibrium, at the organic-aqueous interface, with the formation of a strong hydrophobic compound. Solvation of this compound by the diluent is a critical factor in the extraction of most acids.

The experimental results regarding the influence of Amberlite LA2 concentration on the extraction efficiency are illustrated in Figure 5, for pH = 2 (pH value corresponding to the maximum extraction efficiency).

Physical extraction was found to be very poor in both used solvents. An increase in ALA2 concentration in the organic phase from 0 to 0.226 M, over the stoichiometric ratio (GA concentration was 2.935×10^{-2} M), induces the continuous increase of the extraction degrees. These high extraction yield values suggest improved solvation by extractant molecules by increasing interfacial compounds hydrophobicity. Similar trends can be observed for other acid-extraction systems [23–25,27].

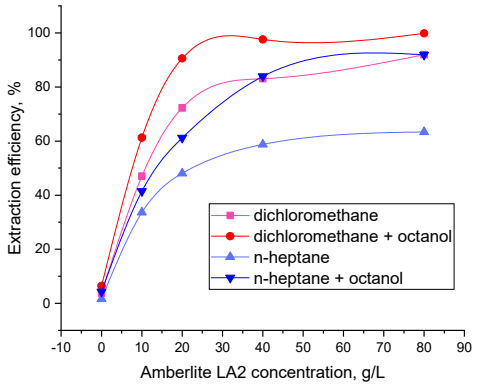

Figure 5. Amberlite LA2 concentration influence on extraction efficiency (pH = 2).

Adding 1-octanol improves the solvation power of the acid–amine complex, as shown by the amplification factors values presented in Table 4. In the case of the solvent with the lower polarity, the 1-octanol addition generates the lowest influence at low amine concentration in the organic phase. This proves that the modifier presence is more important for increased extractant quantities in the solvent, probably due to the formation of gallic acid dimers through intermolecular hydrogen bonds, resulting in carboxylic groups blocked and requiring higher amounts of extractant to make the interfacial reaction possible. The octanol provides a good solvation media for the interfacial product (acid–amine complex), but it can also form hydrogen bonds with gallic acid, due to the alcohol functional group. In the dichloromethane case, the highest influence can be observed at low amine concentrations, but the values are comparable with those obtained for n-heptane. At higher extractant concentrations in dichloromethane, the phase modifier influence is diminished, the extraction degree being high even in the absence of 1-octanol, due to increased solvent polarity.

Table 4. The amplification factors values corresponding to 1-octanol addition (pH = 2).

Solvent/A LA2 Concentration	10	20	40	80
n-Heptane	1.23	1.27	1.47	1.45
Dichloromethane	1.30	1.25	1.19	1.08

3.1.3. Study of the Reactive Extraction Mechanism

To analyze the reactive extraction mechanism with and without 1-octanol as the phase modifier, the following interfacial equilibrium is considered (gallic acid is insoluble in n-heptane and in dichloromethane and Amberlite LA2 is insoluble in the aqueous phase). The purpose is to determine the extraction equilibrium constant (K_E) and the number of extractant molecules (n), using the law of mass action. As concluded from the pH influence, Amberlite LA2 extracts the non-dissociated form of GA when the pH < pK_a:

$$\mathrm{Gal-COOH_{(aq)}} + n\mathrm{Q_{(o)}} \leftrightarrow \mathrm{Gal-COOHQn_{(o)}} \quad (1)$$

For this system, the distribution coefficient, D, is determined using Equation (2), the ratio of gallic acid concentration in the solvent phase and in the aqueous phase at equilibrium:

$$D = \frac{\left[\mathrm{Gal-COOH\,Q_{n(o)}}\right]}{\left[\mathrm{Gal-COOH_{(aq)}}\right]} \quad (2)$$

According to the interfacial reaction proposed, the equilibrium constant can be determined with Equation (3):

$$K_E = \frac{\left[\text{Gal} - \text{COOH}\,\text{Q}_{\text{n(o)}}\right]}{\left[\overline{\text{Gal} - \text{COOH}_{\text{(aq)}}}\right]\left[\text{Q}_{\text{(o)}}\right]^n} \rightarrow \left[\text{Gal} - \text{COOH}\,\text{Q}_{\text{n(o)}}\right] = K_E \cdot \left[\overline{\text{Gal} - \text{COOH}_{\text{(aq)}}}\right] \cdot \left[\text{Q}_{\text{(o)}}\right]^n \quad (3)$$

The concentration of un-dissociated gallic acid in the aqueous solution is calculated through Equation (4), by using its total concentration, $\overline{\text{Gal} - \text{COOH}_{\text{aq}}}$ and *Ka*, the dissociation constant:

$$\left[\text{Gal} - \text{COOH}_{\text{(aq)}}\right] = \frac{\left[\overline{\text{Gal} - \text{COOH}_{\text{(aq)}}}\right]}{1 + \frac{K_a}{[H^+]}} \quad (4)$$

Using these three Equations (2)–(4) the equation for distribution coefficient *D* becomes:

$$D = K_E \cdot \frac{\left[\text{Q}_{\text{(o)}}\right]^n}{1 + \frac{K_a}{[H^+]}} \quad (5)$$

By applying the logarithm to relation Equation (5), the following equation (straight line) can be obtained:

$$\ln D + \ln\left(1 + \frac{K_a}{[H^+]}\right) = \ln K_E + n \ln\left[\text{Q}_{\text{(o)}}\right] \quad (6)$$

Using the graphical representation of Equation (6), in Figure 6, it is possible to determine the number of Amberlite LA-2 molecules, *n*, which participate in the formation of the interfacial adduct (from the slope), and the value of the extraction constant, $K_{E,}$ (from its intercept).

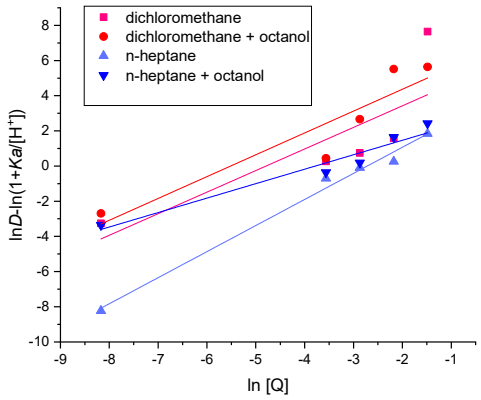

Figure 6. Equation (6) graphical representation.

The results presented in Table 5, demonstrate that in the absence of the phase modifier, the reactive extraction occurs through the formation of an aminic adduct that contains two molecules of extractant for n-heptane, while for dichloromethane it occurs by forming an equimolecular complex between Amberlite LA2 and GA. The addition of 1-octanol changes the mechanism for the inert solvent n-heptane, for both solvents the interfacial complex containing one molecule of each reactant.

As can be observed from Table 5, the increase of organic phase polarity leads to the increase of the extraction constant K_E, thus suggesting the moving of the interfacial equilibrium towards the formation of extraction compounds. In order to confirm these results, the loading factor, Z, [Gal-COOH$_{\text{(o)}}$]/[Q$_{\text{(o)}}$] was calculated, the values being presented in Figure 7.

Table 5. Values of n and K_E for extraction systems with 1-octanol and Amberlite LA2.

Solvent	n	K_E,
n-Heptane	1.86	56.56, L^2/ mol^2
Dichloromethane	1.18	358.31, L/mol
n-Heptane + octanol	1.08	82.43, L/mol
Dichloromethane + octanol	1.16	947.97, L/mol

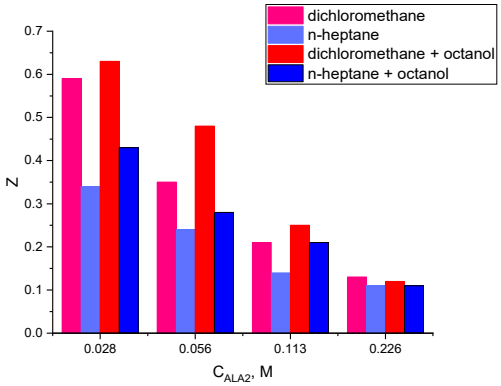

Figure 7. Loading factor variation with extractant concentration (initial phase pH = 2).

The decrease in the loading ratio, with Amberlite LA2 increasing concentration cumulated with values smaller than 0.5, confirms that only acid—extractant 1:1 (for dichloromethane with or without 1-octanol and n-heptane with 1-octanol) or 1:2 (for n-heptane)—complex is formed in the organic phase. The values of Z superiors to 0.5, obtained for dichloromethane at low Amberlite LA-2 concentrations (with or without the phase modifier) assume the formation of an acid: extractant complexes of 2:1 and 3:1 [22].

3.1.4. Study of Stripping Efficiency

Stripping is a necessary step for the recovery of GA from the interfacial complex, which can be attained by the reaction with NaOH that will convert the acid into its salt, regenerating the extractant in the same time. The results obtained for GA are presented in Figure 8.

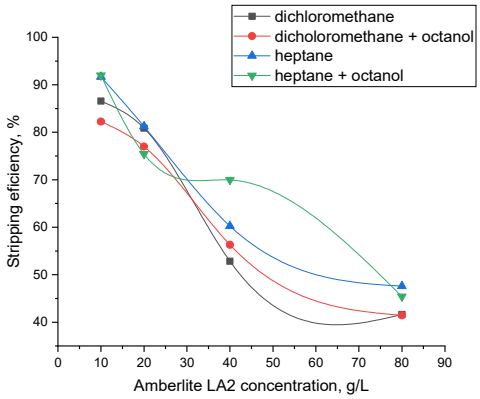

Figure 8. Influence of extractant concentration on back extraction efficiency.

The study was performed at an initial phase pH equal to 2, corresponding to the maximum efficiency of the reactive extraction process and different extractant concentrations. The maximum recovery yield was obtained at low amine concentrations in the organic phase corresponding to smaller equilibrium concentration of gallic acid in organic phase. The increase in temperature for the re-extraction at 50 °C facilitates the back extraction as the formation of the complex between gallic acid and Amberlite LA2 through hydrogen

bonds is exothermic and decreases the system entropy. Increasing the system temperature diminishes the amount of gallic acid extracted, thus increasing the stripping efficiency.

3.2. Modelling and Optimization

3.2.1. Statistical Approaches

The regression model was determined based on the process parameters: solvent types (described by the dielectric constant), the octanol addition (0 if no octanol is added and 1 if octanol is added), pH, and ALA-2 concentration. The software used was MINITAB 17.1.0, and a forward selection was applied for parameter selection. The resulting model had an R^2 of 91.63% and an adjusted R^2 of 89.15%. The analysis of variance for the resulting model is presented in Table 6, where DF indicates the degrees of freedom, Adj_SS is the adjusted sum of squares, Adj_MS is the measure of the adjusted mean of squares, and F-value indicates if the term is associated with the response. Finally, *p*-value is the probability that indicates the evidence against the null hypothesis.

Table 6. ANOVA analysis.

Source	DF	Adj_SS	Adj_MS	F-Value	*p*-Value
Regression	8	25,395.6	3174.45	36.94	0
pH	1	133.2	133.2	1.55	0.224
ALA_2	1	9175	9175.02	106.78	0
Solvent	1	1537.4	1537.36	17.89	0
Octanol	1	140.3	140.26	1.63	0.212
pH × pH	1	0.2	0.17	0	0.964
ALA_2 × ALA_2	1	6947.4	6947.38	80.86	0
pH × Octanol	1	209.7	209.69	2.44	0.13
ALA_2 × Octanol	1	828.8	828.79	9.65	0.004

The resulting models are indicated by Equations (7)–(10). The main explanation for the fact that there are four equations for the process is related to the fact that in the model, there are two categorical predictors: the solvent type and the octanol addition. Equation (7) corresponds to the case where the solvent used is n-heptane, and no octanol is added. Equation (8) corresponds to the case where n-heptane with octanol is used. Equation (9) corresponds to the case where the solvent used is dichloromethane, and Equation (10) describes the dichloromethane and octanol case.

$$Eff = 42.6 - 18.2 \times pH + 2.558 \times ALA\_2 + 0.1 \times pH^2 - 0.02516 \times ALA\_2^2 \quad (7)$$

$$Eff = 54.4 - 22.8 \times pH + 3.007 \times ALA\_2 + 0.1 \times pH^2 - 0.02516 \times ALA\_2^2 \quad (8)$$

$$Eff = 55.7 - 18.2 \times pH + 2.558 \times ALA\_2 + 0.1 \times pH^2 - 0.02516 \times ALA\_2^2 \quad (9)$$

$$Eff = 67.4 - 22.8 \times pH + 3.007 \times ALA\_2 + 0.1 \times pH^2 - 0.02516 \times ALA\_2^2 \quad (10)$$

The next step was determining the optimal conditions that lead to a maximization of efficiency. In MINITAB, this was performed using the Response Optimizer option. The solutions that resulted are presented in Table 7, where Fit indicates the efficiency of the process, and Desirability is a measure that indicates the effectiveness of the response to the desired conditions.

Table 7. Optimization solutions obtained in MINITAB.

Solution	Solvent	Octanol	pH	ALA-2	Fit	Desirability
1	9.08	1	2.07477	80	100	1
2	1.9	1	2	59.7469	96.929	0.98891
3	9.08	0	2	50.8301	84.727	0.84183
4	9.08	1	3.5	59.7273	78.556	0.77792

3.2.2. Artificial Intelligence

In order to determine the optimal ANN model for the considered process, the DE algorithm in combination with the classical BackPropagation training technique optimized with Adam (a combination implemented in Python and using the Tensorflow library) was applied. As previously mentioned, two DE control parameters were included in a self-adaptive approach to eliminate the need for manual tuning. However, DE does not have only two parameters. It is also controlled by the number of individuals in the population and the number of generations. However, following the classical DE idea, these parameters are fixed through the run and, thus, can be easier to set up manually. Thus, based on a preliminary test series, the generations were set to 50 and the number of individuals to 25. These settings were used in all the optimization cases.

Regarding the ANN optimization problem, due to the direct encoding of the parameters, a set of limits were set to the ANN topology not to complicate the model too much. Thus, the maximum number of hidden layers was set to 5, with 50, 50, 30, 30, and 15 maximum number of neurons, respectively. After all the parameters were set, the experimental data were pre-processed (randomized, split into training and testing, and normalized) and fed to the DE procedure. Since the DE is a high stochastic algorithm, 10 runs were performed, and the best ANN was chosen from the pool of generated solutions based on the mean squared error (MSE) computed in the training phase. Due to the relatively low number of experimental points and the high number of hyperparameters that need to be determined during the architecture determination and training, the best ANN determined—although it had a better performance than the regression models in a few cases—had an unacceptable low performance. This indicated that the ANN did not efficiently capture the process's dynamic in all cases due to the low number of experimental data.

To solve this problem, the number of points was enlarged using a procedure that generates synthetic data based on actual data. First, the process's dynamic was graphically determined for each type of solvent (with or without octanol), and intermediary points were obtained using the Digitizer tool from Origin. After that, the new extended dataset underwent the same procedure to determine the process model as in the original experimental data. The best model obtained had a single hidden layer with 50 neurons. Table 8 presents the main statistic indicators for this ANN model, which will be further referred as ANN (4:50:1).

Table 8. Statistical indicators for the best ANN obtained.

	Training	**Testing**
Explained variance score	0.996	0.996
Mean absolute error	1.141	1.212
Mean squared error	2.552	2.794
Mean absolute percentage error	0.0401	0.032
Coefficient of determination	0.995	0.994

A comparison between the experimental data, the statistical regression model's predictions, and the ANN (4:50:1) model for a concentration of ALA-2 of 40 is presented in Figure 9. As observed, the regression model does not efficiently capture the efficiency dynamic and tends to be linear. On the other hand, the ANN predictions are closer to the experimental data. Moreover, there is a single ANN that models all the cases, and there is no need to change the relation based on the initial conditions. However, in terms of predicted values, especially at low pH, for n-heptane, the predicted values for the regression are far from the experimental data.

After that, the ANN model was applied for process optimization using the DE optimizer. The best results obtained are presented in Table 9.

As it can be observed, the DE algorithm provided various solutions for each combination of solvents with or without octanol.

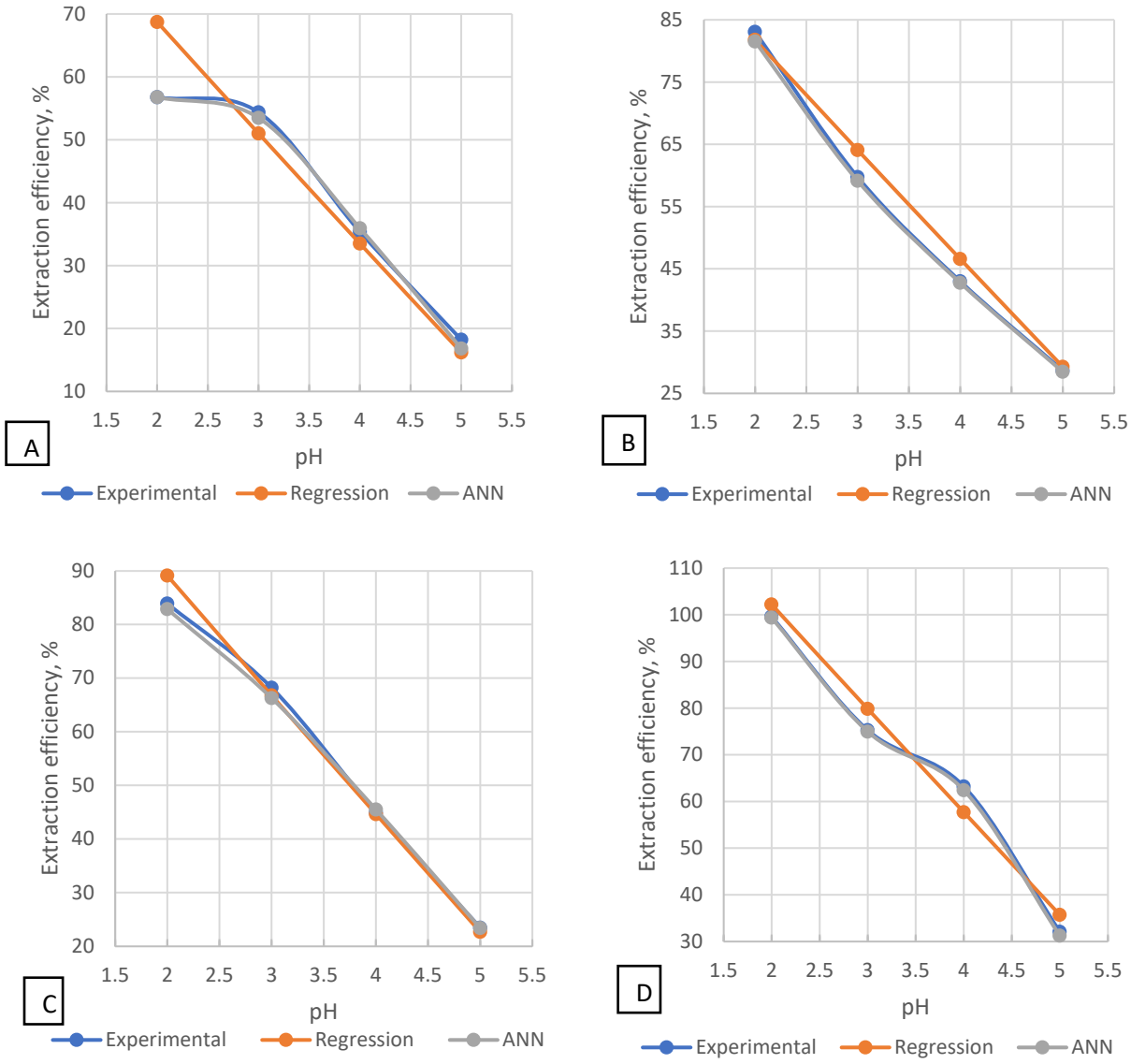

Figure 9. Comparison between experimental, regression, and ANN model predictions for (**A**) n-heptane without octanol addition; (**B**) n-heptane with octanol; (**C**) dichloromethane without octanol addition; and (**D**) dichloromethane with octanol.

Table 9. Process optimization using DE with ANN (4:50:1).

Solvent	Octanol	pH	ALA-2	Fit
9.8	1	2.018	46.518	100.000
9.8	1	2.005	25.699	99.621
9.8	1	2.145	56.867	97.834
9.8	1	2.310	42.744	93.193
9.8	1	2.310	28.929	92.596
9.8	1	2.409	56.697	90.889
1.9	1	2.047	67.956	89.606
9.8	1	2.477	56.784	89.105
9.8	1	2.477	44.331	88.840
9.8	1	2.537	32.539	86.787
9.8	1	2.560	37.518	86.524
9.8	1	2.560	35.597	86.397

Table 9. *Cont.*

Solvent	Octanol	pH	ALA-2	Fit
9.8	0	2.060	39.118	83.427
1.9	1	2.253	47.333	82.726
9.8	0	2.129	35.986	80.973
1.9	1	2.643	78.369	78.558
1.9	1	2.495	52.322	78.328
9.8	0	2.060	31.291	77.855
1.9	1	2.344	37.328	75.971
9.8	1	3.285	68.010	74.854
9.8	0	2.129	52.254	74.464
9.8	1	3.467	53.442	73.858
9.8	0	2.060	24.065	70.132
1.9	0	2.000	80.000	63.486
1.9	0	2.000	76.601	63.481
1.9	0	2.040	77.793	63.003
1.9	0	2.000	66.550	61.763

4. Conclusions

This article reports a comprehensive study on gallic acid separation including: reactive extraction, stripping, and modeling. The optimum conditions for the reactive extraction onto a biphasic organic-aqueous system were: pH of aqueous phase 2, dichloromethane used as solvent, 80 g/L Amberlite LA2 used as extractant, and 10% phase modifier (1-octanol). The extraction mechanism analysis confirmed the formation of complexes involving hydrogen bonds between 1 molecule of GA and 1 of extractant, for dichloromethane (with or without 1-octanol) and n-heptane with 10% 1-octanol, and 1:2 (acid:extractant) complexes for n-heptane. The organic phase is regenerated at a high temperature (323 K) with sodium hydroxide, allowing its simultaneous regeneration. Moreover, the process was modeled and optimized with statistical approaches and artificial intelligence tools (ANNs and DE). The results indicated that an effective model process could be further used to generate predictions and eliminate the need for additional experimental work.

Author Contributions: Conceptualization, A.C.B. and D.C.; methodology, R.E.M.; software, E.N.D.; validation, D.C., A.I.G. and A.C.B.; investigation, R.E.M.; writing—original draft preparation, A.C.B.; writing—review and editing, D.C. and A.I.G.; visualization, D.C. All authors have read and agreed to the published version of the manuscript.

Funding: This research received no external funding.

Data Availability Statement: Data are contained in the article.

Conflicts of Interest: The authors declare no conflict of interest.

References

1. Nayeem, N.; Asdaq, S.M.B.; Heba, S.; El-Alfqy, A.H. Gallic Acid: A Promising Lead Molecule for Drug Development. *J. Appl. Pharm. Sci.* **2016**, *8*, 8–11. [CrossRef]
2. Fernandes, F.H.A.; Salgado, H.R.N. Gallic Acid: Review of the Methods of Determination and Quantification. *Crit. Rev. Anal. Chem.* **2015**, *46*, 257–265. [CrossRef] [PubMed]
3. Kahkeshani, N.; Farzaei, F.; Fotouhi, M.; Alavi, S.S.; Bahramsoltani, R.; Naseri, R.; Momtaz, S.; Abbasabadi, Z.; Rahimi, R.; Farzaei, M.H.; et al. Pharmacological effects of gallic acid in health and disease: A mechanistic review. *Iran. J. Basic Med. Sci.* **2019**, *22*, 225–237. [CrossRef] [PubMed]
4. Shao, D.; Li, J.; Tang, R.; Liu, L.; Shi, J.; Huang, Q.; Yang, H. Inhibition of Gallic Acid on the Growth and Biofilm Formation of *Escherichia coli* and *Streptococcus mutans*. *J. Food Sci.* **2015**, *80*, M1299–M1305. [CrossRef] [PubMed]
5. Borges, A.; Maria, J.; Simoes, M. The activity of ferulic and gallic acids in biofilm prevention and control of pathogenic bacteria. *Biofouling* **2012**, *28*, 755–767. [CrossRef]
6. Kang, J.; Liu, L.; Liu, M.; Wu, X.; Li, J. Antibacterial activity of gallic acid against *Shigella flexneri* and its effect on biofilm formation by repressing mdoH gene expression. *Food Control* **2018**, *94*, 147–154. [CrossRef]

7. Kang, M.-S.; Oh, J.-S.; Kang, I.-C.; Hong, S.-J.; Choi, C.-H. Inhibitory effect of methyl gallate and gallic acid on oral bacteria. *J. Microbiol.* **2008**, *46*, 744–750. [CrossRef]
8. Lee, J.; Choi, K.-H.; Min, J.; Kim, H.-J.; Jee, J.-P.; Park, B.J. Functionalized ZnO Nanoparticles with Gallic Acid for Antioxidant and Antibacterial Activity against Methicillin-Resistant *S. aureus*. *Nanomaterials* **2017**, *7*, 365. [CrossRef]
9. Liu, M.; Wu, X.; Li, J.; Liu, L.; Zhang, R.; Shao, D.; Du, X. The specific anti-biofilm effect of gallic acid on *Staphylococcus aureus* by regulating the expression of the ica operon. *Food Control* **2017**, *73*, 613–618. [CrossRef]
10. Nutan; Modi, M.; Goel, T.; Das, T.; Malik, S.; Suri, S.; Rawat, A.K.S.; Srivastava, S.K.; Tuli, R.; Malhotra, S.; et al. Ellagic acid & gallic acid from Lagerstroemia speciosa L. inhibit HIV-1 infection through inhibition of HIV-1 protease & reverse transcriptase activity. *Indian J. Med. Res.* **2013**, *137*, 540–548.
11. Singh, A.; Pal, T.K. Docking analysis of gallic acid derivatives as HIV-1 protease inhibitors. *Int. J. Bioinform. Res. Appl.* **2015**, *11*, 540–546. [CrossRef] [PubMed]
12. Govea-Salas, M.; Rivas-Estilla, A.M.; Rodríguez-Herrera, R.; Lozano-Sepúlveda, S.A.; Aguilar-Gonzalez, C.N.; Zugasti-Cruz, A.; Salas-Villalobos, T.B.; Morlett-Chávez, J.A. Gallic acid decreases hepatitis C virus expression through its antioxidant capacity. *Exp. Ther. Med.* **2015**, *11*, 619–624. [CrossRef] [PubMed]
13. Liao, C.-L.; Lai, K.-C.; Huang, A.-C.; Yang, J.-S.; Lin, J.-J.; Wu, S.-H.; Wood, W.G.; Lin, J.-G.; Chung, J.-G. Gallic acid inhibits migration and invasion in human osteosarcoma U-2 OS cells through suppressing the matrix metalloproteinase-2/-9, protein kinase B (PKB) and PKC signaling pathways. *Food Chem. Toxicol.* **2012**, *50*, 1734–1740. [CrossRef] [PubMed]
14. Aguilar-Zárate, P.; Cruz, M.A.; Montañez, J.; Rodríguez-Herrera, R.; Wong-Paz, J.E.; Belmares, R.E.; Aguilar, C.N. Gallic acid production under anaerobic submerged fermentation by two bacilli strains. *Microb. Cell Fact.* **2015**, *14*, 1–7. [CrossRef]
15. Kanpiengjai, A.; Khanongnuch, C.; Lumyong, S.; Haltrich, D.; Nguyen, T.-H.; Kittibunchakul, S. Co-production of gallic acid and a novel cell-associated tannase by a pigment-producing yeast, *Sporidiobolus ruineniae* A45.2. *Microb. Cell Factories* **2020**, *19*, 95. [CrossRef]
16. Raghuwanshi, S.; Dutt, K.; Gupta, P.; Misra, S.; Saxena, R.K. *Bacillus sphaericus*: The highest bacterial tannase producer with potential for gallic acid synthesis. *J. Biosci. Bioeng.* **2011**, *111*, 635–640. [CrossRef]
17. Banerjee, R.; Mukherjee, G.; Patra, K.C. Microbial transformation of tannin-rich substrate to gallic acid through co-culture method. *Bioresour. Technol.* **2005**, *96*, 949–953. [CrossRef]
18. Bajpai, B.; Patil, S. A new approach to microbial production of gallic acid. *Braz. J. Microbiol.* **2008**, *39*, 708–711. [CrossRef]
19. Rewatkar, K.; Shende, D.Z.; Wasewar, K.L. Reactive Separation of Gallic Acid: Experimentation and Optimization Using Response Surface Methodology and Artificial Neural Network. *Chem. Biochem. Eng. Q.* **2017**, *31*, 33–46. [CrossRef]
20. Joshi, N.; Keshav, A.; Poonia, A. Modeling and optimization of reactive extraction equilibria and kinetic study of gallic acid using tributyl phosphate in isoamyl alcohol. *Sep. Sci. Technol.* **2020**, *56*, 1035–1046. [CrossRef]
21. Pandey, S.; Kumar, S. Reactive extraction of gallic acid from aqueous solution with Tri-n-octylamine in oleyl alcohol: Equilibrium, Thermodynamics and optimization using RSM-rCCD. *Sep. Purif. Technol.* **2019**, *231*, 115904. [CrossRef]
22. Pandey, S.; Pal, D.; Kumar, S. Reactive extraction of gallic acid using tri-n-octylamine in a biocompatible mixture of diluents. *Chem. Data Collect.* **2022**, *41*, 100908. [CrossRef]
23. Weast, R.C. *Handbook of Chemistry and Physiscs*, 54th ed.; CRC Press: Cleveland, OH, USA, 1974.
24. Lazar, R.G.; Blaga, A.C.; Dragoi, E.N.; Galaction, A.I.; Cascaval, D. Application of reactive extraction for the separation of pseudomonic acids: Influencing factors, interfacial mechanism, and process modelling. *Can. J. Chem. Eng.* **2021**, *100*, S246–S257. [CrossRef]
25. Georgiana, L.R.; Cristina, B.A.; Niculina, D.E.; Irina, G.A.; Dan, C. Mechanism, influencing factors exploration and modelling on the reactive extraction of 2-ketogluconic acid in presence of a phase modifier. *Sep. Purif. Technol.* **2020**, *255*, 117740. [CrossRef]
26. Kloetzer, L.; Ilica, R.-A.; Cascaval, D.; Galaction, A.-I. Separation of fumaric acid by amine extraction without and with 1-octanol as phase modifier. *Sep. Purif. Technol.* **2019**, *227*, 115724. [CrossRef]
27. Caşcaval, D.; Kloetzer, L.; Galaction, A.I. Influence of Organic Phase Polarity on Interfacial Mechanism and Efficiency of Reactive Extraction of Acetic Acid with Tri-n-octylamine. *J. Chem. Eng. Data* **2011**, *56*, 2521–2526. [CrossRef]
28. Jessop, P.G. Searching for green solvents. *Green Chem.* **2011**, *13*, 1391–1398. [CrossRef]
29. Pirsaheb, M.; Dragoi, E.-N.; Vasseghian, Y. Polycyclic Aromatic Hydrocarbons (PAHs) Formation in Grilled Meat products—Analysis and Modeling with Artificial Neural Networks. *Polycycl. Aromat. Compd.* **2020**, *42*, 156–172. [CrossRef]
30. Karamichailidou, D.; Alexandridis, A.; Anagnostopoulos, G.; Syriopoulos, G.; Sekkas, O. Modeling biogas production from anaerobic wastewater treatment plants using radial basis function networks and differential evolution. *Comput. Chem. Eng.* **2021**, *157*, 107629. [CrossRef]
31. Topić, D.; Barukčić, M.; Mandžukić, D.; Mezei, C. Optimization model for biogas power plant feedstock mixture considering feedstock and transportation costs using a differential evolution algorithm. *Energies* **2020**, *13*, 1610. [CrossRef]
32. Storn, R.; Price, K. Differential evolution—A simple and efficient adaptive scheme for global optimization over continuous spaces. *J. Glob. Optim.* **1995**, *11*, 341–359. [CrossRef]
33. Carvalho, J.C.T.; Gosmann, G.; Schenkel, E.P.; Simões, C.M.O.; Schenkel, E.P.; Gosmann, G.; Mello, J.C.P.; Mentz, L.A.; Petrovick, P.R. (Eds.) *Farmacognosia Da Planta Ao Medicamento*, 5th ed.; EDUFRGS/UFRGS/EDUFSC.; Editora da UFSC: Florianópolis, Brasil, 2004; pp. 519–535.

Biochemical Engineering Journal 131 (2018) 70–76

Contents lists available at ScienceDirect

Biochemical Engineering Journal

journal homepage: www.elsevier.com/locate/bej

Enhancement of ergosterol production by *Saccharomyces cerevisiae* in batch and fed-batch fermentation processes using *n*-dodecane as oxygen-vector

Alexandra Cristina Blaga [a], Corina Ciobanu [a], Dan Caşcaval [a,*], Anca-Irina Galaction [b]

[a] "Gheorghe Asachi" Technical University of Iasi, Dept. of Biochemical Engineering, D. Mangeron 73, 700050, Iasi, Romania
[b] "Gr.T. Popa" University of Medicine and Pharmacy of Iasi, Dept. of Biomedical Science, M. Kogalniceanu 9-13, 700454, Iasi, Romania

ARTICLE INFO

Article history:
Received 5 September 2017
Received in revised form 7 December 2017
Accepted 12 December 2017
Available online 13 December 2017

Keywords:
Ergosterol
S. cerevisiae
Oxygen-vector
n-Dodecane
Ethanol
Fermentation

ABSTRACT

The effect of *n*-dodecane used as oxygen-vector in batch and fed-batch fermentations of *S. cerevisiae* for producing ergosterol has been comparatively investigated. Regardless of *n*-dodecane concentration, the results indicated the increase for about three times of ergosterol content inside the yeasts cells in fed-batch process. In both fermentation systems, by adding the oxygen-vector, the ergosterol concentration increased with over 50%. The oxygen-vector concentration corresponding to the maximum level of ergosterol depended mainly on biomass concentration, being 5% vol. for batch fermentation, and 10% vol. for fed-batch one. The increase of biomass concentration in the fed-batch process partially affected the positive influence of oxygen-vector, effect that became less significant only for hydrocarbon concentration over 10% vol. The inhibitory phenomenon induced at higher concentration of hydrocarbon also limits the positive influence of oxygen-vector, but this effect was partially counteracted in the fed-batch process due to the higher amount of yeasts biomass produced.

1. Introduction

Ergosterol (ergosta-5,7,22-trien-3β-ol, Fig. 1) was firstly isolated from fungal species *Claviceps*, but it was also found in yeasts and few herbs [1–4]. Similarly to the cholesterol in mammalian cells, this sterol plays the main role in ensuring the cellular membrane integrity and controlling its normal functions as fluidity or permeability and transport, as well as the plasma-membrane proteins activity and cellular cycle [1–3].

In the yeasts cells, ergosterol is encountered in membranes, being stored in its free form in the plasma-membrane, and as fatty acids esters in lipids [5,6]. The mechanism of ergosterol production in yeasts is complex and was the subject of multiples studies which led to a rather complete view on this sterol biosynthesis pathway. Specific enzymes are involved in the ergosterol biosynthesis by catalyzing the conversion of squalene to lanosterol, zymosterol, episterol, and finally to ergosterol [7–10].

Ergosterol is the precursor of ergocalciferol, also known as vitamin D2, being converted into it *via* viosterol by exposing to UV light [11]. For this reason, ergosterol is known as provitamin D2.

Nomenclature

d	Impeller diameter (mm)
d'	Impeller diameter (mm)
D	Bioreactor diameter
h	Distance from the stirrer to the bioreactor bottom (mm)
H	Bioreactor height (mm)
l	Impeller blade length (mm)
l'	Oxygen electrode immersed length (mm)
R	Ratio between the ergosterol concentrations in fed-batch and batch fermentations
s	Baffle width (mm)
Y	Product yield factor related to glucose (g ergosterol/g glucose)
w	Impeller blade height (mm)

Recently, other medical applications, as antitumor agent or specific target for antifungal compounds, have been developed [12–15].

Due to the presence of an asymmetric center in ergosterol molecule, its chemical synthesis is complicated and requires many steps with high materials and energy consumptions, while the

* Corresponding author.
E-mail addresses: dancasca@yahoo.com, dancasca@tuiasi.ro (D. Caşcaval).

https://doi.org/10.1016/j.bej.2017.12.010
1369-703X/

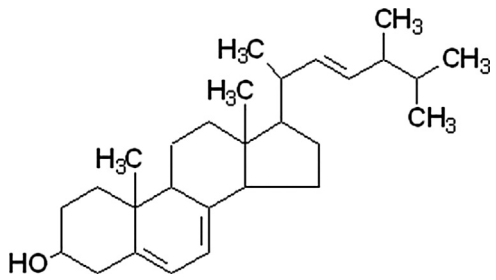

Fig. 1. Chemical structure of ergosterol.

yield is low [16]. Consequently, the aerobic fermentation processes became the most attractive methods for ergosterol production. Among various potential producers of ergosterol, different strains of *S. cerevisiae* have been preferred, especially due to their easier manipulation and the better knowledge on this sterol biosynthesis pathway [10]. The literature indicated that this sterol was produced by batch or fed-batch fermentations, on glucose or corn hydrolysis substrates, using different programs for substrate or oxygen feeding [6,16–18]. From these studies it was concluded that one of the main parameters which control the ergosterol yield is the level of dissolved oxygen in the broths or the oxygen uptake rate.

Therefore, the oxygen supply into the yeasts broths constitutes one of the decisive factors of ergosterol biosynthesis at a satisfactory level. Generally, the bioreactor capacity to generate high rate of oxygen diffusion from air to the broths, or of dissolved oxygen transfer through the liquid phase to the microorganisms, depends on its design and operational characteristics. However, as it was observed for the biosynthesis of single-cell protein on various water insoluble hydrocarbon substrates, the addition of a nonaqueous organic phase could induce the significant increase of oxygen transfer rate from air to microorganisms, without needing a supplementary intensification of mixing [19–21]. The oxygen solubility in these compounds, called oxygen-vectors, is from several to over thirty times higher than in water. The main classes of oxygen-vectors tested in fermentations were hydrocarbons, perfluorocarbons, and oils [19–24]. Besides their high ability to dissolve oxygen, oxygen-vectors have to exhibit no toxicity against the cultivated microorganisms, and could be consumed as supplementary substrates (sources of carbon and energy).

Our previous studies on oxygen transfer inside *S. cerevisiae* broths indicated that the addition of *n*-dodecane led to the increase of oxygen mass transfer coefficient for up to 5 times [20]. The magnitude of this effect depends on the hydrocarbon concentration and specific power input.

On the basis of these results concerning the positive influence of *n*-dodecane addition on oxygen transfer rate and of the relation between the oxygen transfer efficiency and the amount of produced ergosterol, these experiments are aimed to investigate the possible positive effect of this oxygen-vector on ergosterol biosynthesized by *S. cerevisiae*. In this purpose, the influence of *n*-dodecane will be analyzed comparatively for batch and fed-batch fermentation systems related to the glucose feeding.

2. Materials and method

2.1. Bioreactor and operating parameters

The experiments were carried out in 2 l laboratory stirred bioreactor (Fermac, Electrolab), provided with computer-controlled and recorded parameters. The bioreactor mixing system consists of one turbine impeller and three baffles. The bioreactor and impeller characteristics are given in Table 1.

The sparging system consists of a perforated tube with 7 mm diameter, placed at 15 mm from the vessel bottom, having 4 holes with 1 mm diameter. The air volumetric flow rate was 5 l h^{-1}. The rotation speed was maintained at 300 rpm. The dissolved oxygen concentration has been calculated as percent from the saturation level, according to the oxygen probe calibration.

The fermentation was carried out comparatively in batch and fed-batch systems. In both fermentation systems, the temperature was 30 °C. The pH-value was maintained at 5.4, being automatically adjusted by addition of 25% ammonia solution.

2.2. Strain and medium

In the experiments *S. cerevisiae* has been used. In order to obtain the inoculum, a plate culture (plate media: 20 g l^{-1} peptone, 20 g l^{-1} glucose, 10 g l^{-1} yeast extract, 12 g l^{-1} agar [25]) of yeast cells has been grown at 30 ± 1 °C for 20 h. Then, the yeast cells were transferred into a 250 ml flask containing 50 ml of sterile culture medium and incubated for 20 h at 30 ± 1 °C and 180 rpm.

The stirred bioreactor contained 1 l working volume of an optimized medium consisting of 60 g l^{-1} glucose, 31.2 g l^{-1} yeast extract, 7.8 g l^{-1} ammonium sulfate, 3.7 g l^{-1} potassium dihydrogen phosphate, 3.1 g l^{-1} magnesium sulfate, 1.25 g l^{-1} calcium chloride, 0.4 g silicon oil in tap water. After sterilization at 121° C for 20 min, the medium was inoculated with 5% vol. inoculum. For the feed-batch fermentation, 60 ml of 600 g l^{-1} glucose solution was added into the bioreactor every 30 min, in the purpose to maintain the glucose level at minimum 10 g l^{-1}.

n-Dodecane (SIGMA Chemie GmbH) was used as oxygen-vector (density 750 g l^{-1} at 20 °C, oxygen solubility $54.9 \cdot 10^{-3}$ g l^{-1} at 35 °C and atmospheric air pressure [26]). The sterilized hydrocarbon has been added into the bioreactor at the beginning of fermentation, its volumetric concentration into the broth varied between 0 and 15%.

2.3. Measurement and analysis methods

The values of oxygen transfer rate, quantified by means of k_La, have been calculated using the static method previously described [20].

For ergosterol extraction from biomass, 0.2 g dry cells have been treated with 10 ml alcoholic solution of potassium hydroxide obtained by dissolving 8 g potassium hydroxide into 32 ml 60% vol. alcoholic solution [18]. The extraction occurred 3 h at 80 °C. After cooling at the room temperature, 10 ml of petroleum ether were added, the mixture being stirred for 2 min with a vortex. The phases were separated and 2 ml extract was subjected to evaporation. The extracted ergosterol was quantified by HPLC method (Dionex Ultimate 3000 system using a Lichrospher Si 100 column 250 × 4.6 mm, 5 μm), the mobile phase consisting of a mixture of *n*-hexane and tetrahydrofuran with volumetric ratio 85:15 and flow rate 1.0 ml min^{-1} [18]. The HPLC system was provided with PDA detector at 280 nm. The ergosterol content has been considered as percent from the biomass amount.

Besides ergosterol percent accumulated at the fermentation end, the variations of glucose, biomass, ethanol, and dissolved oxygen concentrations during the fermentation have been analyzed for the batch and fed-batch operating conditions. The analysis of glucose and alcohol was performed also through HPLC method, using the same system equipped with refractive index detector and a HyperRez carbohydrate column (300 × 7.7 mm, 8 μm), with water as mobile phase at 0.6 ml min^{-1}. The column temperature was 80 °C.

The biomass variation was analyzed spectrophotometrically by measuring the turbidity at 660 nm [18].

Table 1
Characteristics of bioreactor and impeller.

d	d/D	H/D	w/d	l/d	h/d	No. blades	No. baffles	s/d	d'/d	l'/d
55	0.46	1.46	0.27	0.31	0.64	6	3	0.20	0.018	1.82

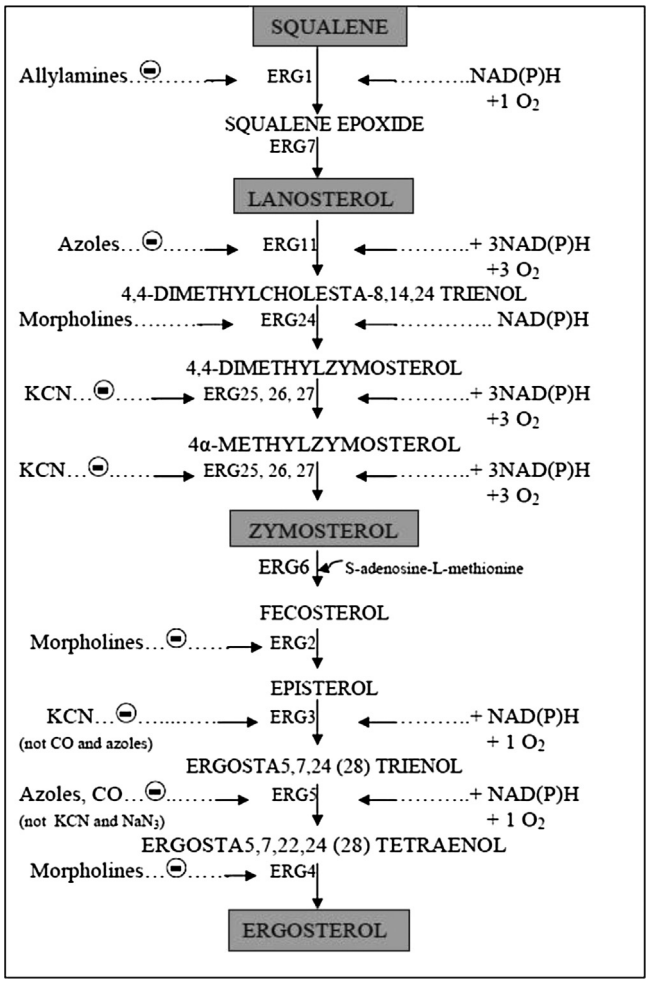

Fig. 2. Metabolic pathway for ergosterol production by *S. cerevisiae* (ERG1 – squalene epoxidase; ERG2 – sterol C-8 isomerase; ERG3 – sterol C-5 desaturase; ERG4 – sterol C-24 reductase; ERG5 – sterol C-22 desaturase; ERG6 – sterol C-24 methyltransferase; ERG7 – lanosterol synthase; ERG11 (CYP51) – lanosterol C-14 demethylase; ERG24 – sterol C-14 reductase; ERG25 – sterol C-4 methyloxydase; ERG26 – sterol C-3 dehydrogenase (C4-decarboxylase); ERG27 – sterol C-3 ketoreductase).

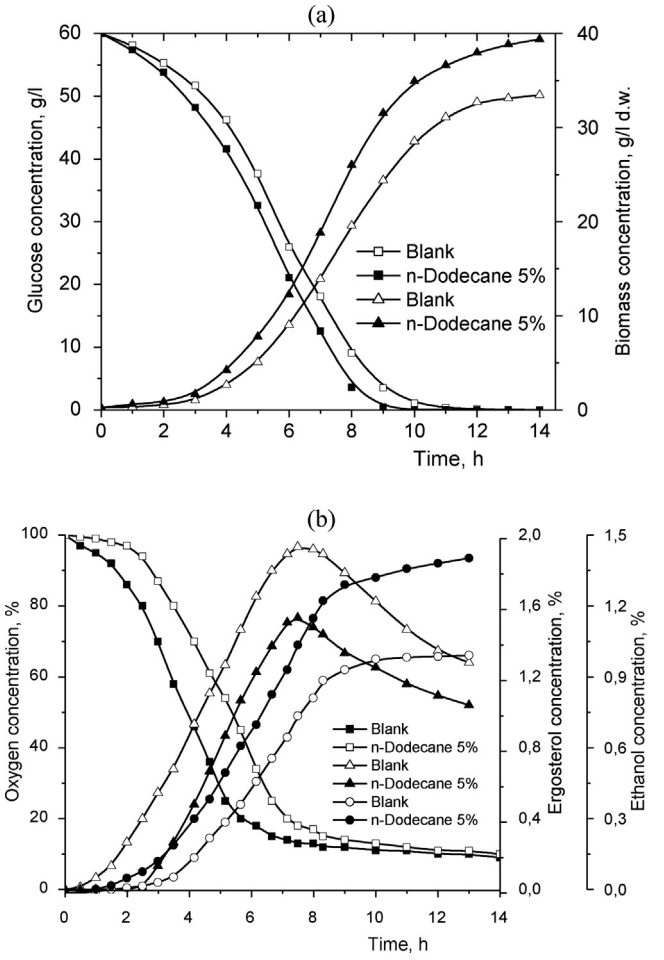

Fig. 3. Variation of glucose and biomass concentrations (a), as well as of oxygen, ethanol, and ergosterol concentrations (b) during batch fermentation process ((a): □, ■ – glucose concentration; Δ,▲- biomass concentration (b): □, ■ – oxygen concentration; Δ,▲- ethanol concentration; ○,● – ergosterol concentration).

Each experiment has been carried out for at least three times, considering identical conditions, the average value of measured parameters being used. The maximum experimental error varied between of 4.22 and 5.08%.

3. Results and discussion

3.1. Batch fermentation system

According to the mechanism proposed by Rosenfeld and Beauvoir [27], twelve molecules of oxygen are non-respiratory used to convert squalene in the ergosterol biosynthesis pathway from *S. cerevisiae* cells (Fig. 2) [27]. Therefore, the level of oxygen concentration into the broths not only limits the yeasts growth, but also represents the factor controlling the ergosterol accumulation inside the cells.

For both fermentations, without and with *n*-dodecane, Fig. 3a indicates the significant decrease of glucose concentration during the first 9 h, this substrate being entirely consumed over 12 h. The *n*-dodecane addition leads to a superior rate of glucose consumption, due to an increased rate of yeasts growth under higher dissolved oxygen concentration. Obviously, the amount of *S. cerevisiae* biomass increases exponentially during the period which corresponds to the highest rate of glucose consumption. Over 9 h, the low level of glucose concentration induced the attenuation of the biomass growth.

Although this variation of biomass concentration is similar for both fermentation processes, from Fig. 3a it can be observed that the accumulation rate of *S. cerevisiae* cells is higher in presence of oxygen-vector. As it was before mentioned, this difference is induced by the increased concentration of dissolved oxygen in the broths containing *n*-dodecane. Moreover, the addition of *n*-dodecane allows the yeast biomass to grow after the moment corresponding to the entire consumption of glucose (in absence of the hydrocarbon, the biomass concentration reached a constant level at fermentation duration over 12 h). This difference can be

attributed to the ability of yeasts to use *n*-dodecane as supplementary source of carbon and energy, thus counteracting the absence of other substrates [20].

The level of oxygen concentration controls not only the yeast cells growth, but also the metabolic equilibrium between the utilization of glucose for CO_2, H_2O and energy production, as well as for alcohol production. From this point of view, the yeasts can be divided into "Crabtree-negative" yeasts, which are able to convert glucose to alcohol under anaerobic conditions only (e.g. *Candida spp.*, *Debaryomyces spp.*, *Kluyveromyces spp.*, *Pichia spp.*), and "Crabtree-positive" ones, which can combine the respiratory process with alcoholic fermentation even in presence of oxygen, at high glucose concentration (e.g. *Saccharomyces spp.*, *Brettanomyces spp.*, *Schizosaccharomyces spp.*) [27,28].

According to Fig. 3a and b, the oxygen concentration into the broths varies contrarily to that of biomass one, both for fermentations without and with *n*-dodecane. In can be observed that in the first 9 h of fermentation, the values of dissolved oxygen concentration are significantly higher in presence of hydrocarbon, due to its positive effect on oxygen transfer from air bubble to liquid phase. This effect of oxygen-vector is diminished towards the end of fermentation, the level of oxygen concentration for the system with *n*-dodecane becoming similar to that in absence of this hydrocarbon. The reduction of the hydrocarbon influence on oxygen transfer could be the consequence of the three phenomena occurring at higher *S. cerevisiae* cells amount. The first one is the increase of the broth apparent viscosity, thus affecting the oxygen solubility and mass transfer rate, effect that is more important at larger amount of biomass accumulated in presence of *n*-dodecane [20]. Another phenomenon represents the consumption of *n*-dodecane as alternative source of carbon and energy, especially at higher yeast cells and low glucose concentrations. Moreover, as it was previously reported [20], the yeasts exhibit a specific affinity for the hydrocarbon, the cells being adsorbed to droplets surface and block the interface needed for oxygen transfer between the organic and aqueous phases. The cells-droplets associations could be furthermore attached to the air bubbles, thus generating an additional resistance by reducing the bubble surface available for oxygen diffusion.

Acting as "Crabtree-positive" yeast, *S. cerevisiae* is able to convert glucose into ethanol in aerobic conditions. For this reason, from Fig. 3b it can be observed that ethanol is produced in both cases, its concentration increasing during the first 8–9 h of fermentation, decreasing then. The maximum amount of alcohol corresponds to the almost entire consumption of glucose (85% without *n*-dodecane, 94% with *n*-dodecane) and, implicitly, to the end of the exponential growth of yeast cells. Obviously, the highest amount of alcohol was recorded for the fermentation without *n*-dodecane, due to the lower oxygen concentration dissolved into the broth. The following decrease of alcohol concentration is the result of its utilization as supplementary substrate, the relative magnitude of this process being more important in absence of *n*-dodecane (which can compensate partially the low amount of glucose).

The variation of ergosterol concentration inside the *S. cerevisiae* cells can be related to the variations of glucose and oxygen concentrations into the broths, as well as to the amount of biosynthesized ethanol (Fig. 3b). Therefore, for both fermentation processes, the ergosterol amount strongly increases simultaneously with the significant growth of the yeast cells, period limited between 2 – 3 and 8 – 9 h from the fermentation start and correlated with the rapid consumption of glucose and oxygen. However, the low level of glucose and dissolved oxygen concentrations is not the main reason for the low rate of ergosterol accumulation over 9 h of fermentation. As it was reported in literature, hypoxia and ethanol formation exhibit negative influence on ergosterol biosynthesis and accumulation inside the yeasts cells [29]. This effect is more important for the fermentation without *n*-dodecane, owing to the higher concentration of alcohol. Consequently, over 9 h of fermentation, from Fig. 3b it can be seen that the concentration of ergosterol remains at a constant level in absence of *n*-dodecane, but increases slowly in presence of this hydrocarbon. Moreover, at the fermentation end, the content of ergosterol in *S. cerevisiae* cells reached almost 2% for the system with *n*-dodecane, compared to 1.3% in absence of oxygen-vector. In term of product yield factors related to glucose, Y, it can be observed that Y = 0.045 in presence of 5% *n*-dodecane, while in absence of this hydrocarbon the yield factor reached only 0.026.

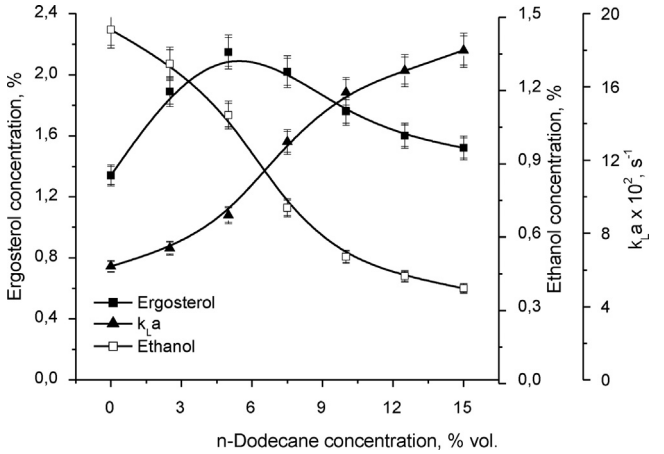

Fig. 4. Influence of *n*-dodecane concentration on ergosterol concentration, oxygen transfer rate, and ethanol concentration for batch fermentation process.

As it was above discussed, the hydrocarbon concentration exhibits a significant influence on ergosterol production mainly by accelerating the oxygen transfer rate. Therefore, for the fermentation moment corresponding to the maximum ergosterol content (9 h), Fig. 4 indicated that the oxygen mass transfer coefficient, k_La, is amplified for about 3 times by increasing the volumetric concentration of *n*-dodecane from 0 to 15%. Moreover, the increase of dissolved oxygen concentration by adding *n*-dodecane leads to the diminution for 3.5 times of the produced alcohol amount.

However, the maximum content of ergosterol inside the yeast cells is reached for 5% *n*-dodecane, not for the highest experimented concentration of hydrocarbon. This variation could be the consequence of the inhibition effect induced on *S. cerevisiae* growth at higher concentration of *n*-alkanes with over 8 carbon atoms chain, in this case *n*-dodecane [30]. This conclusion is supported also by the more important decrease of ethanol production for hydrocarbon concentration over 5%, due to *n*-dodecane inhibitory effect on the "Crabtree-positive" metabolism of yeast cells.

3.2. Fed-batch fermentation system

The supplementary amount of glucose was added into the broth when its concentration became slightly lower than 10 g l^{-1}. Due to the difference of the glucose rates consumption between the fermentation without and with *n*-dodecane, the substrate addition was necessary over the first 8 h for the fermentation process without oxygen-vector, and over 6.5 h in presence of hydrocarbon.

Regardless of *n*-dodecane content into the fermentation broth, by using the fed-batch system, the biomass concentration was significantly increased compared to the batch system, as the result of the extension of biomass exponential growth period. Therefore, according to Fig. 5a, it can be observed that in absence of oxygen-vector, the *S. cerevisiae* cells concentration reached 46 g l^{-1} d.w. over 14 h of fermentation (compared to 34 g l^{-1} d.w. for batch system), this value being increased to almost 60 g l^{-1} d.w. at 20 h from the process start.

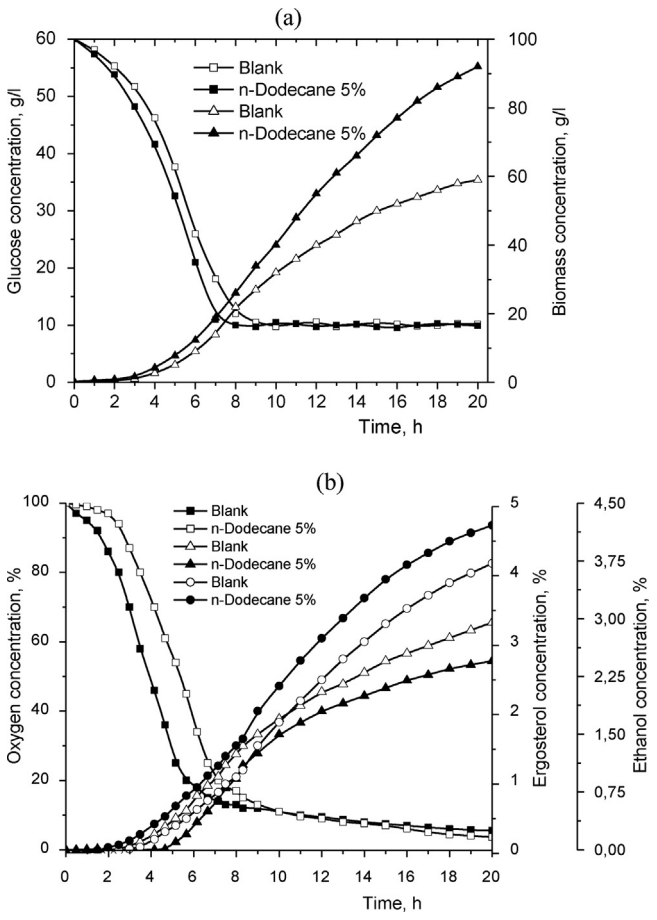

Fig. 5. Variation of glucose and biomass concentrations (a), as well as of oxygen, ethanol, and ergosterol concentrations (b) during fed-batch fermentation process ((a): □, ■ – glucose concentration; Δ,▲- biomass concentration (b): □, ■ – oxygen concentration; Δ,▲- ethanol concentration; ○,● – ergosterol concentration).

The acceleration of yeasts growth rate is more important in presence of *n*-dodecane, the biomass concentration reaching 61g l^{-1} d.w. over 14 h of fermentation (compared to 40 g l^{-1} d.w. for batch system), and 92 g l^{-1} d.w. over 20 h. Compared to the limitation of cells growth by the substrate, in the case of fed-batch fermentation the positive effect of oxygen-vector is amplified by the constant level of glucose, which avoids the hydrocarbon consumption as alternative source of carbon and energy.

The variation of oxygen concentration into the broths is similar to that recorded for batch fermentation, the level of oxygen being generally higher for the broths containing hydrocarbon (Fig. 5b). However, after the moment considered for substrate feeding, the dissolved oxygen amount in the system with *n*-dodecane becomes initially equal and then lower than that for the classical fermentation system, this suggesting the significant diminution of the positive effect of oxygen-vector. In this case, the magnitude of some phenomena above discussed which contribute to the attenuation of the positive influence of hydrocarbon on oxygen transfer is amplified. The *S. cerevisiae* biomass amount in presence of hydrocarbon is for 1.5 times greater than in absence of the oxygen-vector (Fig. 5b). Although by respecting a constant level of glucose the alternative consumption of hydrocarbon is avoided in the fed-batch fermentation, the higher yeasts concentration induces stronger limitation on oxygen diffusion from air bubbles to yeast cells in presence of *n*-dodecane, as the result of corresponding higher apparent viscosity of broth and more extended interfacial area between air bubbles and broth blocked by the adsorbed associations between hydrocarbon droplets and yeast cells.

Compared to the batch process, the ethanol concentration increases during the entire considered duration of both fed-batch fermentations, over 20 h becoming double compared to the maximum alcohol level corresponding to the previous case (Fig. 5b). The accumulation of ethanol is supported by maintaining the glucose amount level into the broth, this operating system providing constantly the required substrate and, implicitly, avoiding the alcohol consumption in absence of glucose. Moreover, as the consequence of the diminution of the influence of oxygen-vector presence at higher yeasts biomass concentration, the value of ethanol concentration biosynthesized in presence of *n*-dodecane is closer to that produced without adding this hydrocarbon into the fermentation medium. Therefore, over 20 h of fermentation, the ethanol concentration obtained in absence of *n*-dodecane is with about 20% higher than that reached in presence of hydrocarbon (in the batch fermentation, at the maximum level of ethanol concentration accumulated into the broth, the related difference between the processes without and with oxygen-vector is of 40%, Fig. 3b).

Also for the fed-batch fermentation, the level of ergosterol biosynthesized inside the yeasts cells depends directly on substrate, oxygen, and ethanol concentrations into the broths (Fig. 5b). However, in this case, regardless of the addition of *n*-dodecane, the ergosterol content increases continuously during the first 20 h of fermentation. Because over 9 h of fed-batch fermentation the dissolved oxygen concentration in broth containing hydrocarbon become close or slightly smaller to that in the broth without oxygen-vector, the ergosterol concentration reached over 20 h in the process without *n*-dodecane tends to equalize its value obtained in the presence of this hydrocarbon (the ergosterol concentration in *S. cerevisiae* cells grown in presence of 5% vol. *n*-dodecane was for 1.1 times higher than that obtained in the absence of oxygen-vector in fed-batch fermentation, compared to over 1.5 times corresponding to the batch fermentation). However, the ergosterol yield factor related to glucose in presence of *n*-dodecane is 0.186, for about 1.7 times greater than that recorded for the fermentation system without oxygen-vector (Y = 0.110). Both values are significantly higher that those corresponded to the batch fermentation systems without and with hydrocarbon.

Analyzing the magnitude of the influences of substrate, oxygen, and ethanol amounts on ergosterol biosynthesis in fed-batch system, it can be concluded that the negative role of ethanol accumulation inside the broth is diminished by maintaining the constant concentration of glucose, probably due to the higher concentration of yeasts biomass. This factor could be responsible also for the superior level of ergosterol obtained in fermentation with *n*-dodecane even in the case of lower oxygen concentration inside the broth.

In fed-batch fermentation process, the positive influence of hydrocarbon on oxygen transfer rate is amplified mainly at its higher concentration level, as the result of the increased yeasts cells amount (Fig. 6). Thus, at 20 h from the fermentation start, by varying *n*-dodecane concentration from 0 to 15% vol., the k_La value increase becomes more important than for the batch fermentation, being of 4 times. In fact, this effect could be considered important for *n*-dodecane concentration over 5% vol.

Although the produced ethanol concentration is for about 2 times greater compared to the batch fermentation, the inhibition effect on its biosynthesis induced by presence of oxygen-vector is more significant, the amount of alcohol being reduced for 4.5 times from the broth without *n*-dodecane to that containing 15% vol. *n*-dodecane (Fig. 6). Similar to the variation of k_La, influence of *n*-dodecane concentration on hindering the ethanol production is more relevant for hydrocarbon concentration over 5% vol.

As it was above discussed, the value of oxygen-vector concentration of 5% vol., which represents the limit between its low influences on oxygen transfer rate and alcohol production and the

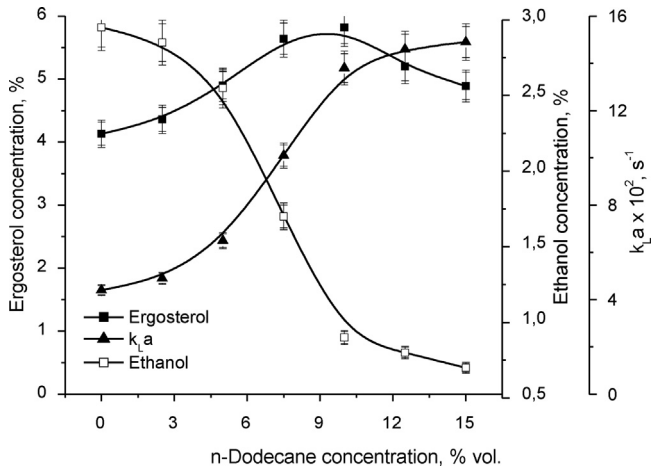

Fig. 6. Influence of *n*-dodecane concentration on ergosterol concentration, oxygen transfer rate, and ethanol concentration for fed-batch fermentation process.

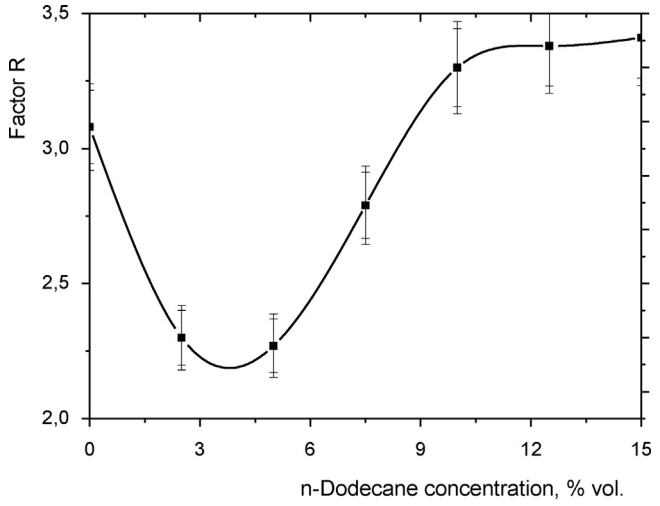

Fig. 7. Influence of oxygen-vector concentration on factor R.

strong ones, is the result of the high biomass amount accumulated in the fed-batch process. The high concentration *S. cerevisiae* biomass diminishes the positive role of *n*-dodecane on aeration efficiency by increasing the broth apparent viscosity and intensifying the interactions of adsorption type between the hydrocarbon droplets – yeast cells associations and air bubbles. For this reason, in the batch fermentation, the maximum level of ergosterol corresponded to 5% vol. *n*-dodecane, while in the fed-batch system it is related to double concentration of hydrocarbon, namely 10% vol. (Fig. 6). According to Fig. 6, by operating the fermentation using the fed-batch program, the maximum ergosterol content inside the *S. cerevisiae* cells becomes 5.8 – 6%, being reached for 10% vol. *n*-dodecane. For higher oxygen-vector concentration, the inhibitory influence of hydrocarbon on *S. cerevisiae* growth and "Crabtree-positive" metabolism leads to the reduction of ergosterol biosynthesis rate.

The relative effect of oxygen-vector on ergosterol productivity on the batch and fed-batch fermentation processes is suggested by Fig. 7. The comparison was made by means of the factor R, which represents the ratio between the ergosterol concentrations in fed-batch and batch fermentations, respectively.

Fig. 7 underlines the superior efficiency of fed-batch system related to ergosterol production and, obviously, yeasts biomass accumulation, the factor R being over 2 or 3 for the entire considered domain of oxygen-vector concentrations. However, the factor R decreases initially by increasing the *n*-dodecane concentration up to 5% vol., this variation confirming that the relative magnitude of the positive effect of hydrocarbon is more important for the batch fermentation at lower levels of hydrocarbon amount. Between 5 and 10% vol. oxygen-vector concentration, the factor R increases strongly, remaining at a rather constant level for higher concentrations of hydrocarbon. The significant increase of factor R can be attributed to the more important influence of hydrocarbon in broth containing high amount of *S. cerevisiae* biomass when its concentration exceeds 5% vol.

According to the previous discussions, the inhibitory effect of hydrocarbon is amplified at *n*-dodecane concentration over 10% vol. and limits the production of ergosterol for both fermentation systems. Consequently, the factor R reaches a rather constant level of 3.3 in this domain of hydrocarbon concentration. This value of factor R suggests that the inhibitory effect of the *n*-dodecane concentration over 10% vol. is partially counteracted by the higher amount of yeasts biomass produced in the fed-batch process.

4. Conclusions

The production of ergosterol by *S. cerevisiae* cells has been studied in batch and fed-batch fermentation systems. Because this compound biosynthesis is strongly dependent on the dissolved oxygen concentration, in both cases the experiments have been carried out comparatively in absence and presence of *n*-dodecane as oxygen-vector.

Regardless of *n*-dodecane addition, by maintaining the glucose concentration at a constant level in the fed-batch process, the amount of ergosterol accumulated into the yeasts cells has been almost tripled, while the product yield factor related to glucose increased for over 4 times. In presence of hydrocarbon, the ergosterol concentration increased with over 50%, and the ergosterol yield factor with almost 70%. The value of oxygen-vector concentration corresponding to the maximum level of ergosterol depends mainly on biomass concentration, due to its negative influences on broth viscosity and interfacial phenomena of air bubbles blockage through the adsorption of hydrocarbon droplets – yeast cells associations. Therefore, for the batch process, the maximum ergosterol amount was reached for 5% vol. *n*-dodecane, while for the fed-batch process for 10% vol. hydrocarbon.

The increase of biomass concentration in the fed-batch process partially counteracted the positive influence of oxygen-vector, the highest amplitude of this effect being recorded for hydrocarbon concentration below 5% vol.

References

[1] K.E. Bloch, Sterol structure and membrane function, CRC Crit. Rev. Biochem. 14 (1983) 47–92.
[2] M. Bard, N.D. Lees, T. Turi, D. Craft, L. Cofrin, R. Barbuch, C. Koegel, J.C. Loper, Sterol synthesis and viability of erg11 (cytochrome P450 lanosterol demethylase) mutations in Saccharomyces cerevisiae and Candida albicans, Lipids 28 (1993) 963–967.
[3] L.W. Parks, W.M. Casey, Physiological implications of sterol biosynthesis in yeast, Ann. Rev. Microbiol. 49 (1995) 95–116.
[4] L. Huang, Y. Cao, H. Xu, G. Chen, Separation and purification of ergosterol and stigmasterol in Anoectochilus roxburghii (wall) Lindl by high-speed counter-current chromatography, J. Sep. Sci. 34 (2011) 385–392.
[5] M. Veen, U. Stahl, C. Lang, Combined overexpression of genes of the ergosterol biosynthetic pathway leads to accumulation of sterols in Saccharomyces cerevisiae, FEMS Yeast Res. 4 (2003) 87–95.
[6] M. Shobayashi, S. Mitsueda, M. Ago, T. Fujii, K. Iwashita, H. Iefuji, Effects of culture conditions on ergosterol biosynthesis by Saccharomyces cerevisiae, Biosci. Biotechnol. Biochem 69 (2005) 2381–2388.
[7] G. Daum, N.D. Lees, M. Bard, R. Dickson, Biochemistry, cell biology and molecular biology of lipids of Saccharomyces cerevisiae, Yeast 14 (1998) 1471–1510.
[8] N.D. Lees, M. Bard, D.R. Kirsch, Biochemistry and molecular biology of sterol synthesis in Saccharomyces cerevisiae, Crit. Rev. Biochem. Mol. Biol. 34 (1999) 33–47.

[9] L.W. Parks, J.H. Crowley, F.W. Leak, S.J. Smith, M.E. Tomeo, Use of sterol mutants as probes for sterol functions in the yeast Saccharomyces cerevisiae, Crit. Rev. Biochem. Mol. Biol. 34 (1999) 399–404.
[10] C.M. Souza, T.M. Schwabe, H. Pichler, B. Ploier, E. Leitner, X.L. Guan, M.R. Wenk, I. Riezman, H. Riezman, A stable yeast strain efficiently producing cholesterol instead of ergosterol is functional for tryptophan uptake, but not weak organic acid resistance, Metab. Eng. 13 (2011) 555–569.
[11] K. Rajakumar, S.L. Greenspan, S.B. Thomas, M.F. Holick, Solar ultraviolet radiation and vitamin D: a historical perspective, Am. J. Public Health 97 (2007) 1746–1754.
[12] C.W. Roberts, R. McLeod, D.W. Rice, M. Ginger, M.L. Chance, L.J. Goad, Fatty acid and sterol metabolism: potential antimicrobial targets in apicomplexan and trypanosomatid parasitic protozoa, Mol. Biochem. Parasitol. 126 (2003) 129–142.
[13] D. Ellis, Amphotericin B: spectrum and resistance, J. Antimicrob. Chemother. 49 (2002) 7–10.
[14] Y. Yazawa, M. Yokota, K. Sugiyama, Antitumor promoting effect of an active component of Polyporus, ergosterol and related compounds on rat urinary bladder carcinogenesis in a short-term test with concanavalin A, Biol. Pharm. Bull. 11 (2000) 1298–1302.
[15] T. Takaku, Y. Kimura, H. Okuda, Isolation of an antitumor compound from Agaricus blazei Murill and its mechanism of action, J. Nutr. 131 (2001) 1409–1413.
[16] H. Wu, Y. Li, G. Song, D. Xue, Producing ergosterol from corn straw hydrolysates using Saccharomyces cerevisiae, African J. Biotechnol 11 (2012) 11160–11167.
[17] T. Tan, M. Zhang, H. Cao, Ergosterol production by fed-batch fermentation of Saccharomyces cerevisiae, Enz. Microb. Technol. 33 (2003) 366–370.
[18] F. Shang, S. Wen, X. Wang, T. Tan, High-cell-density fermentation for ergosterol production by Saccharomyces cerevisiae, J. Biosci. Bioeng. 101 (2006) 38–41.
[19] E. Dumont, Y. Andres, P. Le Cloirec, Effect of organic solvents on oxygen mass transfer in multiphase systems: application to bioreactors in environmental protection, Biochem. Eng. J. 30 (2006) 245–252.
[20] D. Caşcaval, A.I. Galaction, E. Folescu, M. Turnea, Comparative study on the effects of n-dodecane addition on oxygen transfer in stirred bioreactors for simulated, bacterial and yeasts broths, Biochem. Eng. J. 31 (2006) 56–66.
[21] K.G. Clarke, P.C. Williams, M.S. Smit, S.T.L. Harrison, Enhancement and repression of the volumetric oxygen transfer coefficient through hydrocarbon addition and its influence on oxygen transfer rate in stirred tank bioreactors, Biochem. Eng. J. 28 (2006) 237–242.
[22] F. Xu, Q.P. Yuan, Y. Zhu, Improved production of lycopene and β-carotene by Blakeslea trispora with oxygen-vectors, Process Biochem. 42 (2007) 289–293.
[23] T.L. Da Silva, A. Reis, J.C. Roseiro, C.J. Hewitt, Physiological effects of the addition of n-dodecane as an oxygen-vector during steady-state Bacillus licheniformis thermophillic fermentations perturbed by a starvation period or a glucose pulse, Biochem. Eng. J. 42 (2008) 202–216.
[24] M. Li, X. Meng, E. Diao, F. Du, X. Zhao, Productivity enhancement of S-adenosylmethionine in Saccharomyces cerevisiae using n-hexadecane as oxygen vector, J. Chem. Technol. Biotechnol. 87 (2012) 1379–1384.
[25] J. Vosvik, P. Hrncirik, J. Nahlik, J. Mares, Adaptive control of Saccharomyces cerevisiae yeasts fed batch cultivations, Chem. Biochem. Eng. Q. 27 (2013) 297–306.
[26] J.L. Rols, J.S. Condoret, C. Fonade, G. Goma, Mechanism of enhanced oxygen transfer in fermentation using emulsified oxygen-vectors, Biotechnol. Bioeng. 35 (1990) 427–435.
[27] E. Rosenfeld, B. Beauvoit, Role of the non-respiratory pathways in the utilization of molecular oxygen by Saccharomyces cerevisiae, Yeast 20 (2003) 1115–1144.
[28] T. Pfeiffer, A. Morley, An evolutionary perspective on the Crabtree effect, Front. Mol. Biosci. 1 (2014) 17.
[29] M. Shobayashi, S. Mitsueda, M. Ago, T. Fujii, K. Iwashita, H. Iefuji, Effect of culture conditions on ergosterol biosynthesis by Saccharomyces cerevisiae, Biosci. Biotechnol. Biochem. 69 (2005) 2381–2388.
[30] P. Bros, Some Aspects of Hydrocarbon Assimilation by Yeasts, Ph.D.-Thesis, Delft, 1975.

fermentation

MDPI

Article

Improved Production of α-Amylase by *Aspergillus terreus* in Presence of Oxygen-Vector

Alexandra Cristina Blaga [1], Dan Caşcaval [1,*] and Anca Irina Galaction [2]

[1] Department of Organic, Biochemical and Food Engineering, Cristofor Simionescu Faculty of Chemical Engineering and Environmental Protection, Gheorghe Asachi Technical University Iasi, 700050 Iasi, Romania; acblaga@tuiasi.ro

[2] Department of Biomedical Sciences, Faculty of Medical Bioengineering, Grigore T. Popa University of Medicine and Pharmacy, 700454 Iasi, Romania; anca.galaction@umfiasi.ro

* Correspondence: dan.cascaval@academic.tuiasi.ro; Tel.: +40-232278683

Abstract: *n*-Dodecane has been investigated as an oxygen-vector for improving α-amylase biosynthesis using the strain *Aspergillus terreus*. In aerobic microbial cultivation, continuous supply of oxygen is required especially due to its low solubility in the growth medium, in particular at high viscosity, but the limitations of oxygen mass transfer in these systems can be overcome by the addition of water-insoluble compounds which possess a strong affinity for oxygen, namely oxygen-vectors. The use of *n*-dodecane (as an oxygen-vector) in the fermentation medium of *A. terreus* can significantly improve the bioprocess performance and enhance α-amylase production. Using 5% *n*-dodecane at 35 °C, an increase of 1.8–2 times in the enzymatic activity was recorded. In the oxygen-vector's absence, the highest amount of biomass was obtained at 35 °C, while in the presence of 5% vol. *n*-dodecane, the amount of fungal biomass increased by approximately 70%, with a shift in optimum temperature to 40 °C, generating also an enzymatic activity increase of 2.30 times. Moreover, the oxygen-vector's addition in the fermentation broth influenced the fungal morphological development in the form of larger pellets with a more compact structure compared to the system without *n*-dodecane, with a positive effect on the fermentation performance (higher α-amylase activity production).

Keywords: *Aspergillus terreus*; α-amylase; enzymatic activity; oxygen-vector

Citation: Blaga, A.C.; Caşcaval, D.; Galaction, A.I. Improved Production of α-Amylase by *Aspergillus terreus* in Presence of Oxygen-Vector. *Fermentation* **2022**, *8*, 271. https://doi.org/10.3390/fermentation8060271

Academic Editor: Hiroshi Kitagaki

Received: 19 May 2022
Accepted: 7 June 2022
Published: 10 June 2022

1. Introduction

Amylases are one of the most important hydrolytic enzymes, in terms of their use at the domestic or industrial level, fungal amylase being the first enzyme produced at an industrial scale in 1894, using the strain *Rhizopus oryzae* [1].

α-Amylases catalyze the cleavage of α-1,4-glycosidic bonds from starch with the formation of lower molecular weight compounds, such as glucose, maltose, and oligosaccharides (maltotriose, dextrin) [2]. Although microbial, plant, or animal sources can be used to obtain α-amylases, the most utilized are microbial α-amylases (of bacterial, yeast, or filamentous fungal origin) due to the wider versatility in industrial applications (food, bakery, beverages, textiles, detergents, as well as pharmaceutical, clinical, or analytical uses) [2]. In fact, the chemical process for obtaining glucose by starch hydrolysis has been replaced almost completely, at the industrial level, by the enzymatic technology. In Asia, α-amylases, mainly fungal, are widely used to make traditional fermented foods, such as sake, sweet sake (koji amazake), soy sauce, and miso soup [3].

Due to its multiple applications, α-amylase is included in the category of "industrial enzymes", along with proteases and lipases, their market being in continuous growth, mainly due to biotechnology advances (in 2020, the market of industrial enzymes was estimated at over $6 billion, of which about 25% corresponded to amylases) [4].

In order to obtain α-amylases, microbial cultures are preferred because microorganisms can easily grow in large quantities and, implicitly, can ensure high enzyme productions.

The biosynthesis of α-amylases is performed in submerged or in solid state fermentations, the second case being specific to fungal cultures, as they are more naturally adapted to grow in a medium with low free water [5]. Enzymes produced by fungi have the advantage that they are extracellular products, which simplifies the fermentation broth downstream processing. In addition, fungi can grow in a variety of environments, even solids, and the biosynthesized α-amylases are preferred to those from other microbial cultures due to their GRAS (Generally Recognized as Safe) classification by the FDA (United States Food and Drug Administration) [6].

Thus, for α-amylase production, *Aspergillus* sp., *Penicillium* sp., *Rhizopus* sp., *Mucor* sp., *Thermomyces* sp., *Thermonospora* sp. [7,8] are used, which have the ability to grow on noncomplex culture media, generally by-products: wastewater from vegetable processing, banana peels, rice husks, molasses, wheat bran, straw, corn cobs and leaves, oilseed cakes, etc. [9].

Fermentation processes' optimization in order to obtain α-amylase must take into account many factors, including pH, temperature, carbon and nitrogen sources, the presence of metal ions in the environment (calcium, cobalt, magnesium, sodium, manganese), phosphate ions, etc. [8,10]. In addition, in submerged fermentations, mixing and aeration play important roles in achieving high productivity. Both aeration and agitation systems have a higher influence in fungal fermentations, mainly due to their determined role on the microorganisms' morphology and, implicitly, on the nutrients' consumption rates and enzyme biosynthesis [11].

Efficient aeration involves intense mixing or high air flow rates, both of which can generate mechanical forces that would destroy microbial cells. For this reason, a variety of oxygen-vectors (n-alkanes: *n*-dodecane, n-hexadecane; perfluorocarbons; vegetable oils) can be used to ensure in the fermentation broth an efficient oxygen supply in mild mechanical or pneumatic mixing conditions [12]. Oxygen-vectors are organic water-insoluble compounds, which have the ability significantly to increase the concentration of dissolved oxygen in the fermentation broth and its transfer rate from the gas phase to the microorganisms without the need to change the mixing or aeration conditions [13,14]. Obviously, oxygen-vectors should not be toxic to microorganisms, as they are often additional sources of nutrients. The addition of these compounds to the aerobic cultures of several microorganisms, through the effect induced on the oxygen mass transfer, can lead to an increase in target compound productivity [12,15]. Lai et al., 2002 investigated the use of *n*-dodecane in *A. terreus* cultivation for lovastatin production, registering an increase of 1.4 fold for 2.5% oxygen vector added in the media [16]. Zhang et al., 2018 reported an increase in fumarase activity to 124% for 2.5% *n*-dodecane used as the oxygen vector in the biosynthetic process using recombinant *E. coli* BL21-pET22b-fumR, without significant changes in the expression of the enzyme [17]. Xu et al., 2020 analyzed several oxygen vectors for the biosynthesis of L-amino acid oxidase and obtained an increase in enzyme activity of 8.6% for *Bacillus subtilis* HLZ-68 using 1.5% *n*-dodecane [18]. Amaral et al., 2008 studied the addition of 20% perfluorodecalin in a bioreactor with YPD (Yeast Extract–Peptone–Dextrose) medium, and 230% enhancement was registered [19]

In this context, previous studies on the positive effects of oxygen-vectors on aerobic fermentation processes are continued by analyzing the influence of *n*-dodecane on the biosynthesis of α-amylase using the fungus *A. terreus*. In this purpose, the effects of *n*-dodecane presence in the environment on the morphological characteristics of the fungi and, through morphology, on the enzyme production in the fermentation broth, were investigated. The information obtained is integrated into a broader framework with a number of other parameters, such as oxygen-vector concentration, biomass concentration, and fermentation broth viscosity.

2. Materials and Methods

2.1. Bioreactor and Operating Parameters

The fermentations were carried out in a batch system, using, in this purpose, the laboratory stirred bioreactor Fermac (1 L working-volume). The bioreactor was provided with one impeller of turbine type and three baffles. The bioreactor geometrical characteristics were previously given [12]. The fermentations were carried out at 35 °C (in the experiments studying the temperature influence, the fermentation temperature was 30, 35, or 40 °C). Depending on the experimental program, the pH-value was either allowed to vary freely, or maintained at 6 using a sterilized solution of 0.1 M NaOH. The air was distributed inside the broth through a perforated tube of 7 mm diameter, placed at 15 mm from the bioreactor bottom. The sparger was provided with 4 holes of 1 mm diameter. The air volumetric flow rate was 5 L/min, and the rotation speed of the impeller was maintained at 150 rpm.

2.2. Strain and Medium

The fungus *A. terreus* ATCC 32588 was used in the experiments. Before the fermentation process, the inoculum medium was prepared: sucrose 1.5 g, $NaNO_3$ 0.1 g, $MgSO_4$ 0.025 g, KCl 0.025 g, $FeSO_4$ 0.0005 g, K_2HPO_4 0.05 g for 50 mL [20]. The spores were germinated and the fungal cells grown at 35 °C in an incubator-shaker, at 150 rpm, for one day. The fungal biomass was transferred into the bioreactor, which contained a specific medium: soluble starch 6.7 g/L, 0.47 g KH_2PO_4, NH_4NO_3 3.3 g/L, KCl 0.16 g/L, $MgSO_4$ 0.03 g/L, $CaCl_2$ 0.13 g/L, $FeSO_4$ 0.003 g/L [20]. For controlling the foam formation and level, the silicone-based antifoam agent was selected (Antifoam 204, Merck, Darmstadt, Germany). The inoculum was added at 10% vol. after the sterilization of this medium at 121 °C for 20 min in a RAYPA AES-28 autoclave. Sterilized *n*-dodecane was used as the oxygen-vector, with specific characteristics related to its utilization for enhancing the oxygen transfer rate: density 750 g/L at 20 °C, oxygen solubility $54.9 \cdot 10^{-3}$ g/L at 35 °C, and atmospheric air pressure [12]. The hydrocarbon experimented concentrations into the broth varied between 2.5 and 10% vol.

2.3. Measurement and Analysis Methods

The biomass accumulation was analyzed by centrifugation of collected samples, drying at 80 °C until constant weight was achieved in order to calculate microbial biomass (d.w.) expressed in g/L. The supernatant, separated from the *n*-dodecane by centrifugation at 5000 rpm, was used for amylase analysis. The pellets' diameter was analyzed using an Optika Microscope B380 (Ponteranica, Italy) equipped with an Optika CB-10 video camera (Ponteranica, Italy) and Optika PROView software (Ponteranica, Italy). From each sample, 10 pellets were separated and evaluated for shape and diameter.

The activity of α-amylase was measured during the fermentation cycle using a commercial kit Amilase 405, kinetic unitest (Winer Lab., Rosario, Argentina). The analysis consists of measuring the absorbance at 405 nm of the colored 2-chloro-*p*-nitrophenol released from 2-chloro-*p*-nitrophenyl-α-D-maltotriose under enzyme action [21]. The enzymatic reaction occurred at 25 °C, in phosphate buffer medium, the optimum pH value being 6.00. The unit of enzyme activity was calculated as the amount of enzyme required to hydrolyze 1 μmole of substrate per minute [21]. The values of the oxygen transfer rate, quantified by means of k_La, were calculated using the dynamic method.

Each experiment was repeated three times, using identical conditions, the average value of measured parameters being used in calculations. The maximum error varied between 5.66 and 7.23%.

3. Results

3.1. The Oxygen-Vector Effect on the Fermentation Broth pH

Fungi are producers of carboxylic acids, either as the major product or as by-products (*Aspergillus* sp. Produces citric, gluconic, malic, and itaconic acids). Moreover, under stress conditions, such as limiting oxygen or nutrients, fungi can alter their metabolism, increasing

the production of carboxylic acids [22]. For these reasons, without strict control, the pH decreases during fermentation.

In this context, according to Figure 1, the pH evolution during the fermentation of *A. terreus* is different in the two systems, depending on oxygen-vector presence: in the first two days, the pH value is similar in both fermentation processes, with and without *n*-dodecane. The differences appear from the third day, the pH of the environment without the oxygen-vector decreasing faster. As fermentation progresses, these differences become more pronounced, especially as the pH value for the system containing the oxygen-vector varies very little from the fourth day. As previously mentioned, in the Introduction Section, in the absence of the oxygen-vector, the level of oxygen concentration is lower [13,14], and the destruction of pellets with formation of the filamentous mycelium further reduces the oxygen and nutrients transfer rate [22].

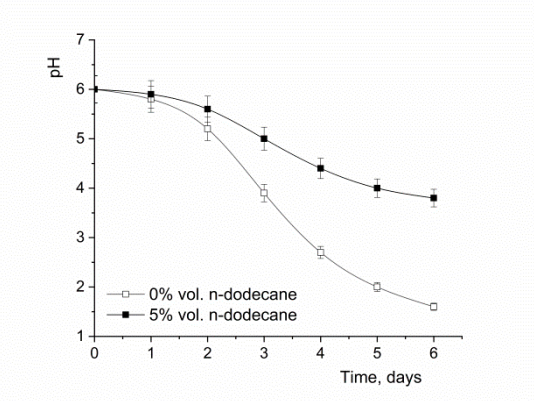

Figure 1. Comparison between the pH-values during the fermentation in absence and presence of *n*-dodecane.

Under these conditions, the metabolic response of *A. terreus* strains materializes mainly in the itaconic acid biosynthesis [23,24]. The acid accumulation as the main product of biosynthesis significantly reduces the pH value compared to the fermentation in the presence of *n*-dodecane.

3.2. The Effect of the Oxygen-Vector on A. terreus Morphology

It is known that fungi can develop in two morphological forms: dispersed mycelia and compact pellets. The fungal morphology is determined both by the genetic information and by the cultivation conditions in the bioreactor (dissolved oxygen level, pH value, mixing intensity, etc.). The strains of *A. terreus* used in these experiments grow under normal conditions in the form of pellets [25]. In the case of α-amylase biosynthesis, important differences in the morphological structure of the fungi were found in the absence or presence of *n*-dodecane. A first aspect observed is that by adding the oxygen-vector, the size of the formed pellets increases (Figure 2).

Moreover, *n*-dodecane supports the maintenance of the pellets' structural integrity throughout the fermentation process; only after the fifth day was destruction of pellets noted, as a consequence of nutrients' depletion in the environment. In the absence of the oxygen-vector, as the process progresses and, implicitly, as the biomass accumulates, branched forms of *A. terreus* appear, with the degradation of the spherical shape of the pellets from the second day of fermentation (Figure 3).

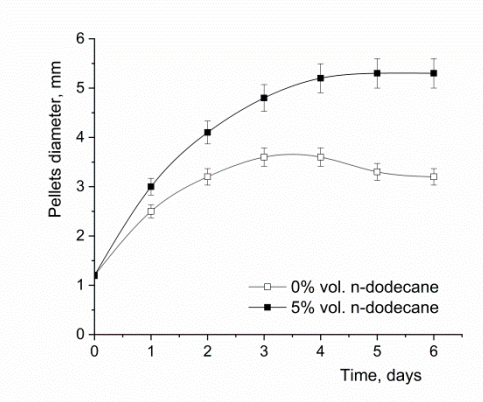

Figure 2. Comparison between the pellets' size in absence and presence of *n*-dodecane.

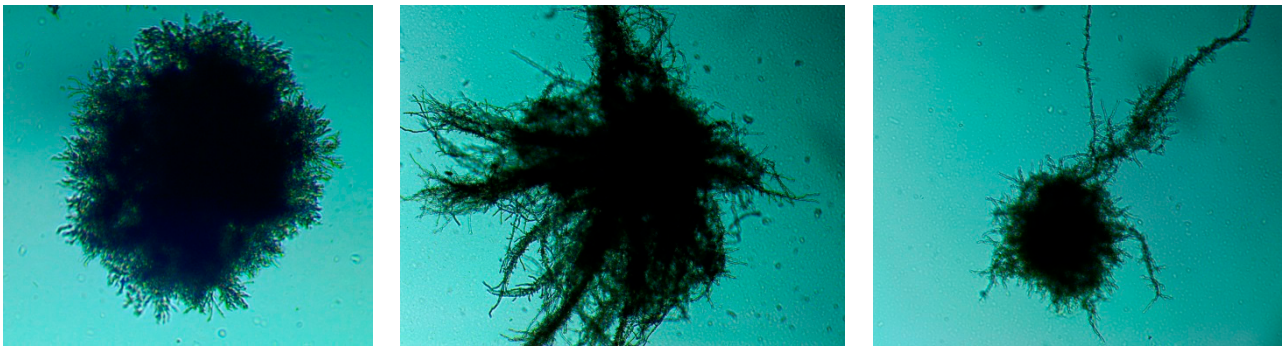

(**a**) (**b**) (**c**)

Figure 3. Pellets' shapes in presence of *n*-dodecane (**a**) and absence of *n*-dodecane (**b**,**c**) on the third day of fermentation.

3.3. The Effect of the Oxygen-Vector on the Biomass Accumulation and α-Amylase Activity

The oxygen-vector beneficial impact is potentiated by maintaining the pH value constant at 6 (Figure 4). From this figure, it can be noted that, regardless of the system used, with or without *n*-dodecane, maintaining the pH at 6 generates higher enzyme activities compared to the fermentation process in which no pH control is applied, the increase being about 1.20–1.40 times; the addition of *n*-dodecane could partially compensate the uncontrolled variation in pH during fermentation.

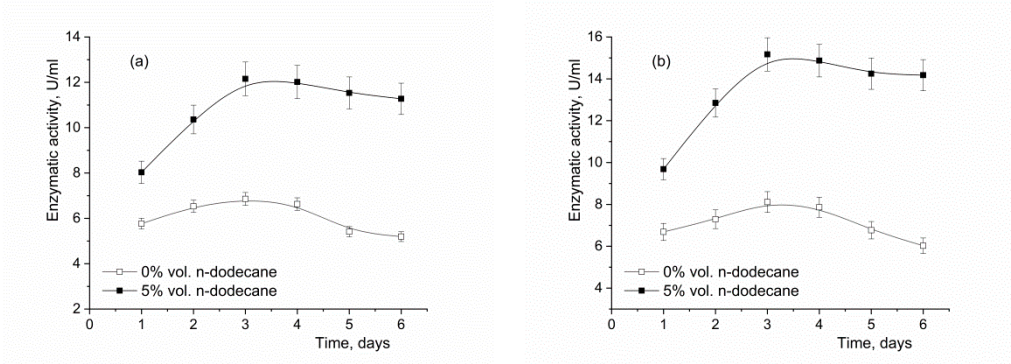

(**a**) (**b**)

Figure 4. Variation of α-amylase activity during the fermentation cycle for uncontrolled pH-value (**a**) and adjusted pH-value at 6 (**b**).

At the same time, for both used systems, with or without pH regulation, from Figure 4, it can be noted that the addition of *n*-dodecane generates a significant increase in enzyme

production, about 1.8–2.0 times. In both fermentation systems, the maximum activity of the enzyme is reached on the third day after the beginning of the process. However, according to Figure 5, increasing the volume fraction of the oxygen-vector may have a negative effect on α-amylase activity. Thus, as the oxygen-vector concentration increases, the enzymatic activity increases, reaches its maximum, after which it decreases. The variation is the result of two opposite effects that occur with increasing *n*-dodecane content in the fermentation broth: on one side—the increase in the amount of dissolved oxygen and its transfer rate, and on other side, as consequence of the former effect—the appearance of the oxygen inhibitory effect, known as oxidative stress [12,24]. Under these circumstances, Figure 5 suggests that the optimum concentration of *n*-dodecane is 5% vol.

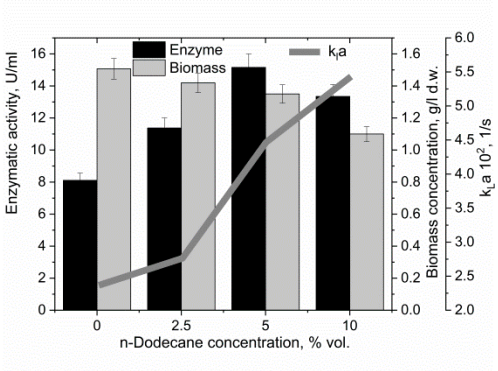

Figure 5. Variation in α-amylase activity and *A. terreus* biomass concentration with *n*-dodecane volumetric fraction on the third day of fermentation (pH = 6).

The effect of the oxygen-vector must also be analyzed in the conditions of fermentation temperature modification. In the absence of the oxygen-vector, the highest amount of biomass was obtained at a temperature of 35 °C, which decreased to half by increasing the temperature to 40 °C (Figure 6a). A similar variation was recorded for α-amylase activity, but the effect of increasing the temperature above 35 °C was less obvious. For this reason, the ratio between enzymatic activity and fungal biomass concentration increased significantly in the range of 30–40 °C, from 5.25 U/kg to 8.70 U/kg.

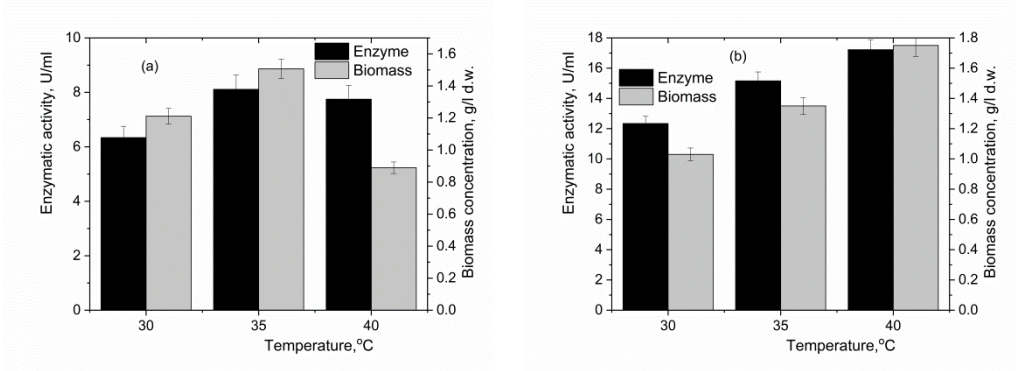

(**a**) (**b**)

Figure 6. Variation of α-amylase activity and *A. terreus* biomass concentration with temperature on the third day of fermentation without *n*-dodecane (**a**) and with 5% vol. *n*-dodecane (**b**) (pH = 6).

Contrarily, according to Figure 6b, in the presence of 5% vol. hydrocarbon, the increase in temperature showed a positive effect both on the amount of biomass accumulated and on the α-amylase production. The amount of fungal biomass increased with approximately 70% and the enzymatic activity by about 40% in the experimental temperature range. Under these conditions, the ratio between enzymatic activity and fungal biomass concentration was reduced in the range of 30–40 °C, from 12 U/kg to 9.80 U/kg.

Increasing the fermentation temperature determines the dissolved oxygen desorption, with negative effects on both the development of biomass and the production of α-amylase. The addition of *n*-dodecane compensates for the loss of oxygen from the fermentation broth and generates a positive evolution of the fermentation process at temperatures higher than 35 °C. For the suggestive rendering of the cumulative effects of the oxygen-vector and temperature on α-amylase production, the dependence of enzymatic activity on the two factors was plotted in Figure 7, which confirms that the optimal values of the two parameters are: 5% vol. for the hydrocarbon concentration and 40 °C for the fermentation temperature. By comparison with the fermentation system without *n*-dodecane, at 35 °C, the enzyme production increased 2.30 times.

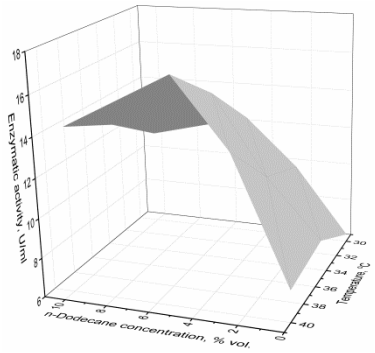

Figure 7. Variation of α-amylase activity with *n*-dodecane volumetric fraction and temperature in the third day of fermentation (pH = 6).

4. Discussion

The *A. terreus* growth under stress conditions, such as very low oxygen concentration or pH, can induce biomass morphological changes and reduce the amount of α-amylase [21]. As previously mentioned, these physiological changes can lead to the production of organic acids, mainly itaconic acid.

The different evolution of the morphology of *A. terreus* pellets in the two cultivation systems, with and without *n*-dodecane, represents the fungi physiological response to the modification of the cultivation conditions [22]. The higher level of dissolved oxygen in the medium, favored by the addition of the oxygen-vector, allows the development of larger spherical pellets, because, in this case, the resistance to internal diffusion of oxygen in the mycelial association is reduced. Under these conditions, the development of fungi continues even in the central regions of the pellets. Basically, due to the development of biomass and higher oxygen consumption, the pellets' growth stops after about four days from the beginning of fermentation, and after five days, the pellets' destruction is observed, due to fungal autolysis in the absence of oxygen and nutrients.

In contrast, in the absence of *n*-dodecane, the concentration of dissolved oxygen and its transfer rate are lower than in the system analyzed above [12,14], which has as the first effect the decrease in the oxygen diffusion rate inside the pellets and, respectively, the appearance of biologically inactive regions in the pellets' central zone, with direct consequences on their development. In response to these conditions, the fungal morphology changes after 2–3 days from the beginning of fermentation: filamentous branches appear, to which the access of oxygen and nutrients is direct, without involving internal diffusion and, therefore, faster. Degradation of the pellets' morphological structure also affects the viscosity of the fermentation broth, because for the same biomass concentration, the filamentous fungal cultures' viscosity is significantly higher than that of pellet fungi [11,23]. Implicitly, the viscosity increase reduces the efficiency of the mixing and transfer processes. As discussed below, morphological structural differences, cumulated with differences in cultivation conditions, generated directly or indirectly, will be reflected in different α-amylase productions.

The addition of *n*-dodecane has an obvious positive effect on α-amylase activity due to the increase in the amount of oxygen available in the environment. In addition, according to Figure 1, the presence of the oxygen-vector attenuates the strong pH reduction, with a beneficial influence on enzyme production. In general, the literature sustains the direct relationship between the amount of fungal biomass and the enzymatic activity [6,8,20]. At the same time, there are situations in which the biomass growth is not directly correlated with the accumulation of the enzyme due to environmental factors (concentration of: sugars, nitrogen sources, or dissolved oxygen, etc.) [1,22]. In this sense, from Figure 5, it can be observed the reduction in the amount of fungal biomass accumulated in the first three days of fermentation with the increase in the *n*-dodecane concentration and, implicitly, with the increase in the dissolved oxygen concentration in the fermentation broth. Basically, for 10% volumetric hydrocarbon fraction, the biomass amount decreased by about 40% compared to the fermentation system without the oxygen-vector.

This variation is the consequence of several phenomena that occur with the increase in the amount of *n*-dodecane in the fermentation broth. Firstly, higher amounts of hydrocarbons can induce fungal growth inhibition, as reported in the literature [26]. Secondly, as it can be observed from Figure 5, the oxygen mass transfer rate, described by oxygen transfer coefficient k_La, is continuously amplified by increasing the *n*-dodecane amount into the broth, a phenomenon that becomes more pronounced for a hydrocarbon volumetric fraction over 2.5%. For 10% vol. oxygen-vector, k_La is about 2.4 times higher than its value in absence of *n*-dodecane. This variation in k_La influences the above discussed aspects related to the biomass morphology or productivity, as it was previously reported for other fungal fermentation processes [12]. However, the acceleration of the oxygen transfer rate from the gaseous phase to the microorganisms, implicitly, the increase in oxygen concentration into the broth can generate, on the one hand, the oxidative stress, and, on the other hand, a more rapid consumption of the substrate, its faster depletion and, implicitly, the limitation in fungal growth [1]. This is also encountered in pressurized systems [27,28].

An interesting and apparent contradictory phenomenon with the literature data is the opposite variation of biomass concentration and α-amylase activity (Figure 5). Thus, if the ratio between enzymatic activity and biomass concentration is considered, it can be noted that it increases from 5.4 U/kg for the fermentation system without *n*-dodecane to 10.8 U/kg for 5% vol. *n*-dodecane, becoming 11.5 U/kg for the system containing 10% vol. hydrocarbon. The results are in agreement with the literature, which mentions the increase in enzymatic activity after fungal biomass development reduction or stopping [1]. Another important aspect, apart from the biomass concentration, is its morphology. The development of fungi in the form of larger pellets, in the presence of the oxygen-vector/higher oxygen concentration, hinders the access of the substrate inside the pellets, which creates conditions similar to the depletion of the substrate in the fermentation broth and promotes enzyme biosynthesis.

5. Conclusions

The biosynthesis of α-amylase by *A. terreus* can be greatly enhanced by the addition of an oxygen-vector into the fermentation broth. Using *n*-dodecane for this purpose, the enzymatic activity after three days from the beginning of fermentation was 1.8–2.0 times higher in the system with hydrocarbon compared to the system without the oxygen-vector, at 35 °C fermentation temperature. Moreover, the presence of the oxygen-vector may partially compensate for the lack of pH control during fermentation and the oxygen desorption from the environment at higher temperatures. At the same time, by adding *n*-dodecane, the fungal morphology can be controlled, the developed pellets having a more compact structure and a larger size.

Compared to the system without *n*-dodecane, in the presence of this hydrocarbon, no direct dependence on the amount of fungal biomass and α-amylase production is noticed, the ratio between enzymatic activity and biomass concentration ranging from 5.4 U/kg for the fermentation system without *n*-dodecane at 11.5 U/kg for 10% vol. hydrocarbon

added in the fermentation broth. The experimental data indicated that the optimal value of the oxygen-vector concentration is 5% vol.; above this level, the oxidative stress or the inhibition generated by a high hydrocarbon concentration is induced. The presence of *n*-dodecane shifted the optimum fermentation temperature to higher values, respectively, 40 °C, mainly as an effect of compensating for the depletion of dissolved oxygen by desorption. Under these conditions, the enzymatic activity was about 2.30 times higher than for the fermentation at 35 °C in the absence of the oxygen-vector.

Author Contributions: D.C. and A.C.B. conceived and designed research. A.C.B. conducted experiments. D.C. and A.I.G. analyzed data. D.C. wrote the manuscript. A.I.G. and A.C.B. reviewed and edited the manuscript. All authors have read and agreed to the published version of the manuscript.

Funding: This research received no external funding.

Institutional Review Board Statement: Not applicable.

Informed Consent Statement: Not applicable.

Data Availability Statement: The data presented in this study are available on reasonable request from the corresponding author.

Conflicts of Interest: The authors declare no conflict of interest.

References

1. Saranraj, P.; Stella, D. Fungal Amylase—A Review. *Int. J. Microbiol. Res.* **2013**, *4*, 203–211. [CrossRef]
2. Rajagopalan, G.; Krishnan, C. α-Amylase production from catabolite derepressed *Bacillus subtilis KCC103* utilizing sugarcane bagasse hydrolysate. *Bioresour. Technol.* **2008**, *99*, 3044–3050. [CrossRef] [PubMed]
3. Oguro, Y.; Nakamura, A.; Kurahashi, A. Effect of temperature on saccharification and oligosaccharide production efficiency in koji amazake. *J. Biosci. Bioeng.* **2019**, *127*, 570–574. [CrossRef] [PubMed]
4. Putri, A.Z.; Nakagawa, T. Microbial α-Amylases in the Industrial Extremozymes. *Rev. Agric. Sci.* **2020**, *8*, 158–169. [CrossRef]
5. Gopinath, S.C.B.; Anbu, P.; Arshad, M.K.M.; Lakshmipriya, T.; Voon, C.H.; Hashim, U.; Chinni, S.V. Biotechnological Processes in Microbial Amylase Production. *BioMed Res. Int.* **2017**, *2017*, 1272193. [CrossRef] [PubMed]
6. Gupta, R.; Gigras, P.; Mohapatra, H.; Goswami, V.K.; Chauhan, B. Microbial α-amylases: A biotechnological perspective. *Process Biochem.* **2003**, *38*, 1599–1616. [CrossRef]
7. Kunamneni, A.; Permaul, K.; Singh, S. Amylase production in solid state fermentation by the thermophilic fungus *Thermomyces lanuginosus*. *J. Biosci. Bioeng.* **2005**, *100*, 168–171. [CrossRef]
8. Sundarramand, A.; Murthy, T.P.K. α-Amylase production and applications: A review. *Appl. Environ. Microbiol.* **2014**, *2*, 166–175. [CrossRef]
9. Sethi, B.K.; Jana, A.; Nanda, P.K.; Das Mohapatra, P.K.; Sahoo, S.L.; Patra, J.K. Production of α-Amylase by *Aspergillus terreus NCFT 4269.10* using pearl millet and its structural characterization. *Front. Plant Sci.* **2016**, *7*, 639. [CrossRef]
10. Zaferanloo, B.; Bhattacharjee, S.; Ghorbani, M.M.; Mahon, P.J.; Palombo, E.A. Amylase production by *Preussia minima*, a fungus of endophytic origin: Optimization of fermentation conditions and analysis of fungal secretome. *BMC Microbiol.* **2014**, *14*, 55. [CrossRef]
11. Galaction, A.I.; Cascaval, D.; Oniscu, C.; Turnea, M. Evaluation and modelling of the aerobic stirred bioreactor performances for fungus broths. *Chem. Biochem. Eng. Q.* **2005**, *19*, 87–97.
12. Galaction, A.I.; Tucaliuc, A.; Ciobanu, C.; Caşcaval, D. Fumaric acid production by *Rhyzopus oryzae* in presence of n-dodecane as oxygen-vector. *Biochem. Eng. J.* **2020**, *164*, 107795. [CrossRef]
13. Dumont, E.; Andres, Y.; Le Cloirec, P. Effect of organic solvents on oxygen mass transfer in multiphase systems: Application to bioreactors in environmental protection. *Biochem. Eng. J.* **2006**, *30*, 245–252. [CrossRef]
14. Caşcaval, D.; Galaction, A.I.; Folescu, E.; Turnea, M. Comparative study on the effects of n-dodecane addition on oxygen transfer in stirred bioreactors for simulated, bacterial and yeasts broths. *Biochem. Eng. J.* **2006**, *31*, 56–66. [CrossRef]
15. Blaga, A.C.; Ciobanu, C.; Caşcaval, D.; Galaction, A.I. Enhancement of ergosterol production by *Saccharomyces cerevisiae* in batch and fed-batch fermentation processes using n-dodecane as oxygen-vector. *Biochem. Eng. J.* **2018**, *131*, 70–76. [CrossRef]
16. Lai, L.S.T.; Tsai, T.H.; Wang, T.C. Application of oxygen vectors to *Aspergillus terreus* cultivation. *J. Biosci. Bioeng.* **2002**, *94*, 453–459. [CrossRef]
17. Zhang, S.; Song, P.; Li, S. Application of n-dodecane as an oxygen vector to enhance the activity of fumarase in recombinant *Escherichia coli*: Role of intracellular microenvironment. *Braz. J. Microbiol.* **2018**, *49*, 662–667. [CrossRef]
18. Xu, P.; Pan, C.; Cui, G.; Wei, C.Y.; Wang, L.; Li, Y.; Li, X.; Huang, S. Enhancement of l-amino acid oxidase production by *Bacillus subtilis HLZ-68* with oxygen-vector and asymmetric degradation of dl-arginine to d-arginine. *Biotechnol. Biotechnol. Equip.* **2020**, *34*, 1273–1279. [CrossRef]

19. Amaral, P.F.; Freire, M.G.; Rocha-Leão, M.H.; Marrucho, I.M.; Coutinho, J.A.; Coelho, M.A. Optimization of oxygen mass transfer in a multiphase bioreactor with perfluorodecalin as a second liquid phase. *Biotechnol. Bioeng.* **2008**, *99*, 588–598. [CrossRef]
20. Keharom, S.; Mahachai, R.; Chanthai, S. The optimization study of α-amylase activity based on central composite design-response surface methodology by dinitrosalicylic acid method. *Int. Food Res. J.* **2016**, *23*, 10–17.
21. Porfiri, M.C.; Farruggia, B.M.; Romanini, D. Bioseparation of alpha-amylase by forming insoluble complexes with polyacrylate from a culture of *Aspergillus oryzae* grown in agricultural wastes. *Sep. Purif. Technol.* **2012**, *92*, 11–16. [CrossRef]
22. Songserm, P.; Karnchanatat, A.; Thitiprasert, S.; Tanasupawat, S.; Assabumrungrat, S.; Yang, S.T.; Thongchul, N. Metabolic responses of *Aspergillus terreus* under low dissolved oxygen and pH levels. *Ann. Microbiol.* **2018**, *68*, 195–205. [CrossRef]
23. Saha, B.C. Emerging biotechnologies for production of itaconic acid and its applications as a platform chemical. *J. Ind. Microbiol. Biotechnol.* **2017**, *44*, 303–315. [CrossRef] [PubMed]
24. Bai, Z.; Harvey, L.M.; McNeil, B. Oxidative stress in submerged cultures of fungi. *Crit. Rev. Biotechnol.* **2003**, *23*, 267–302. [CrossRef]
25. Dwiarti, L.; Otsuka, M.; Miura, S.; Yaguchi, M.; Okabe, M. Itaconic acid production using sago starch hydrolysate by *Aspergillus terreus* TN484-M1. *Bioresour. Technol.* **2007**, *98*, 3329–3337. [CrossRef]
26. Galitskaya, P.; Biktasheva, L.; Blagodatsky, S.; Selivanovskaya, S. Response of bacterial and fungal communities to high petroleum pollution in different soils. *Sci. Rep.* **2021**, *11*, 164. [CrossRef]
27. Coelho, M.A.Z.; Belo, I.; Pinheiro, R.; Amaral, A.L.; Mota, M.; Cutinho, J.A.P.; Ferreira, E.C. Effect of hyperbaric stress on yeast morphology: Study by automated image analysis. *Appl. Microbiol. Biotechnol.* **2004**, *66*, 318–324. [CrossRef]
28. Lopes, M.; Gomes, N.; Gonçalves, C.; Coelho, M.A.; Mota, M.; Belo, I. *Yarrowia lipolytica* lipase production enhanced by increased air pressure. *Lett. Appl. Microbiol.* **2008**, *46*, 255–260. [CrossRef]

Heliyon 10 (2024) e36113

Contents lists available at ScienceDirect

Heliyon

journal homepage: www.cell.com/heliyon

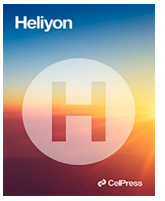

Research article

Reactive extraction of muconic acid by hydrophobic phosphonium ionic liquids - Experimental, modelling and optimisation with Artificial Neural Networks

Alexandra Cristina Blaga [a,*], Elena Niculina Dragoi [a], Alexandra Tucaliuc [a], Lenuta Kloetzer [a], Adrian-Catalin Puitel [a], Dan Cascaval [a,**], Anca Irina Galaction [b]

[a] "Gheorghe Asachi" Technical University of Iasi, "Cristofor Simionescu" Faculty of Chemical Engineering and Environmental Protection, Iasi, Romania

[b] "Grigore T. Popa" University of Medicine and Pharmacy, Faculty of Medical Bioengineering, Iasi, Romania

ARTICLE INFO

Keywords:
Reactive extraction
Mathematical modelling
Ionic liquid
Muconic acid
$[C_{14}C_6C_6C_6P][Dec]$

ABSTRACT

Muconic acid is a six-carbon dicarboxylic acid with conjugated double bonds that finds extensive use in the food (additive), chemical (production of adipic acid, monomer for functional resins and bio-plastics), and pharmaceutical sectors. The biosynthesis of muconic acid has been the subject of recent industrial and scientific attention. However, because of its low concentration in aqueous solutions and high purity requirement, downstream separation presents a significant problem. Artificial Neural Networks and Differential Evolution were used to optimize process parameters for the recovery of muconic acid from aqueous streams in a system with n-heptane as an organic diluent and ionic liquids as extractants. The system using 120 g/L tri-hexyl-tetra-decyl-phosphonium decanoate dissolved in n-heptane, pH of the aqueous phase 3, 20 min contact time, and 45 °C temperature assured a muconic acid extraction efficiency of 99,24 %. Low stripping efficiency compared to extraction efficiency was observed for the optimum conditions on the extraction step (120 g/L ionic liquids dissolved in heptane). However, re-extraction efficiencies obtained for the recycled organic phase in three consecutive stages were close to the first extraction stage. The mechanism analysis proved that the analysed phosphonium ionic liquids (PILSs) extracts only undissociated molecules of muconic acid through H-bonding.

1. Introduction

Muconic acid, MA, is a versatile building block with various applications: is an essential intermediate in the synthesis of adipic acid, a precursor for the production of bio-based polymers such as polyethylene terephthalate (PET) and polybutylene terephthalate (PBT), as the building block for the synthesis of various speciality chemicals: adipic dihydrazide, hexamethylene diamine, and cyclohexane-dicarboxylic acid, as a starting material for the production of bioplastics and biofuels [1–3]. It can be converted into renewable chemicals and materials through bio-based processes, contributing to a more sustainable and environmentally friendly approach.

* Corresponding author. "Gheorghe Asachi" Technical University of Iasi, "Cristofor Simionescu" Faculty of Chemical Engineering and Environmental Protection, D. Mangeron Av., no 67, Iasi, Romania.

** Corresponding author.

E-mail addresses: acblaga@tuiasi.ro (A.C. Blaga), dan.cascaval@academic.tuiasi.ro (D. Cascaval).

https://doi.org/10.1016/j.heliyon.2024.e36113
Received 8 May 2024; Received in revised form 17 July 2024; Accepted 9 August 2024
Available online 10 August 2024

Table 1
Production of muconic acid through biosynthesis.

Microorganism	Process	MA produced	Ref.
Engineered *Saccharomyces cerevisiae*	Fed-batch cultivation through the shikimate pathway 40 g/L glucose	1.2 g/l MA under prototrophic conditions 5.1 g/l MA when supplemented with amino acids	[6]
Engineered *Saccharomyces cerevisiae* ST10209	Fed-batch fermentation (50 L bioreactor) 10 g/L yeast extract	15.2 g/L (muconate)	[7]
Engineered *Escherichia coli*	Fed-batch fermentation 20 g/L glucose	3.153 ± 0.149 g/L	[8]
Engineered *Escherichia coli*	Batch fermentation 20 g/L glucose	4.45 g/L	[9]
Engineered *Corynebacterium glutamicum*	Fed-batch fermentation through 3-dehydroshikimate (DHS) pathway 55 g/L glucose	53.8 ± 5.5 g/L (muconate)	[10]
Engineered *Pseudomonas chlororaphis* HT66	Fed-batch fermentation 18 g/L glycerol	3.376 g/L	[11]
Engineered *Pseudomonas putida*	Fed-batch fermentation 10.6 g/L glucose	Strain LC224: 26.8 g/L (muconate) Strain QP478: 9.3 g/L (muconate)	[12]
Engineered *Klebsiella pneumoniae*	Flask cultivation 80 g/L of glucose	2.1 g/L	[13]
Engineered *Pichia occidentalis* LP635	Fed-batch fermentation 40 g/L glucose	38.8 g/L (muconate)	[14]

MA production is an active area in research and development, and new methods and technologies must be explored to improve the production process's efficiency, yield, and sustainability. MA can be produced through different processes, including both chemical and biological methods: chemical synthesis from benzene through a multi-step process or biological production from renewable feedstocks [4,5]. In chemical synthesis, benzene is first converted to catechol through a series of reactions. Then, catechol is oxidized to muconic acid, a process involving various chemical reagents and catalysts. Through microbial fermentation (Table 1), muconic acid can be produced using mainly glucose or glycerol as a carbon source.

MA separation from fermentation broth is realized through multiple steps, with high costs and important consumption of materials. Yoshikawa et al. suggested a multistep separation approach that involves filtering, adsorption/desorption, precipitation, ion exchange chromatography, and sedimentation to produce MA with a 95 % purity and 90 % yield [15]. Kohlstedt used catechol and p-coumaric acid as the substrates for the bioconversion of MA (cis-cis) in *Pseudomonas putida* fermentation. For the downstream part, the fermentation broth was treated with activated carbon to remove coloured compounds and proto-catechuic acid. MA was precipitated at pH 2 (32 % HCl) and 5 °C temperature, and spray drying (50 °C) was used as a recovery and purification step. Overall recovery yield was 74 %, and the resulting MA had a purity level higher than 97 % [16]. The traditional approaches have drawbacks such as waste production, excessive energy consumption, and material requirements that drive up expenses. Given that the downstream recovery process for most carboxylic acids accounts for 30–50 % of the total production cost [17], developing an efficient separation and recovery procedure for muconic acid is critical to minimizing costs.

Reactive extraction is utilized in various industries for purification and separation of chemicals: extraction of metals from ores, removal of impurities from solutions, recovery of valuable compounds, and transformation of chemical species into more desirable forms. For carboxylic acids, the reactive extraction process involves two immiscible phases: an aqueous phase that includes the acid and an organic phase that contains a complexing extractant. The critical step of the process is the reversible formation of a complex carboxylic acid-extractant, which is soluble in the organic phase. After the separation process is completed, the extractant is recovered from the complex by increasing the temperature or adding sodium hydroxide/sodium carbonate solutions [18]. The choice of solvents, extractants, and operating conditions depends on the specific application and the solute-solvent systems' properties. For muconic acid separation, several solvents were analysed, obtaining low extraction efficiency: 26.23 % for hexane, and 36.17 % for methyl isobutyl ketone [19]. Adding amines into the organic phase in a system with ethyl oleate, 1-dodecanol, and di-n-octylamine increased the extraction efficiency to 98.66 % [20]. Bahrami et al. (2018) analysed a supported hollow liquid membrane containing 1-octanol and 10 % w/v of Aliquat 336 for trans,trans-MA (benzene metabolite) extraction from human urine and stripping using a solution containing 3.0 mol/L sodium chloride, obtaining 87–95 % recovery [20]. Abbaszadeh et al. (2021) analysed an in-syringe ionic liquid-dispersive liquid-liquid microextraction process for preconcentration of trans,trans-MA in the human urine sample, using trihexyl(tetradecyl)phosphonium chloride as an easy and rapid analysis of low amounts of urinary t,t-MA with HPLC-UV [21]. A highly efficient and biocompatible approach of reactive extraction was developed by Tonjes et al. (2023) using 12.5 % (v/v) CYTOP 503 dissolved in canola oil in a direct extraction procedure from *Saccharomyces cerevisiae MDS130* fermentation broth, which laid the foundation for the environmentally friendly production of MA. The method was successfully realized in a fed-batch fermentation (10 L bioreactor volume), with a final MA titer of 4.33 g/L and the highest achieved productivity of 0.053 g/L [22,23].

The current methods of separating MA have several drawbacks, including low extraction efficiencies and increased prices for the finished product due to the high complexity of the separation procedures (such as chromatography), which also require extensive time and energy. Moreover, hazardous volatile chemical solvents are typically used. Due to these drawbacks, it is necessary to develop

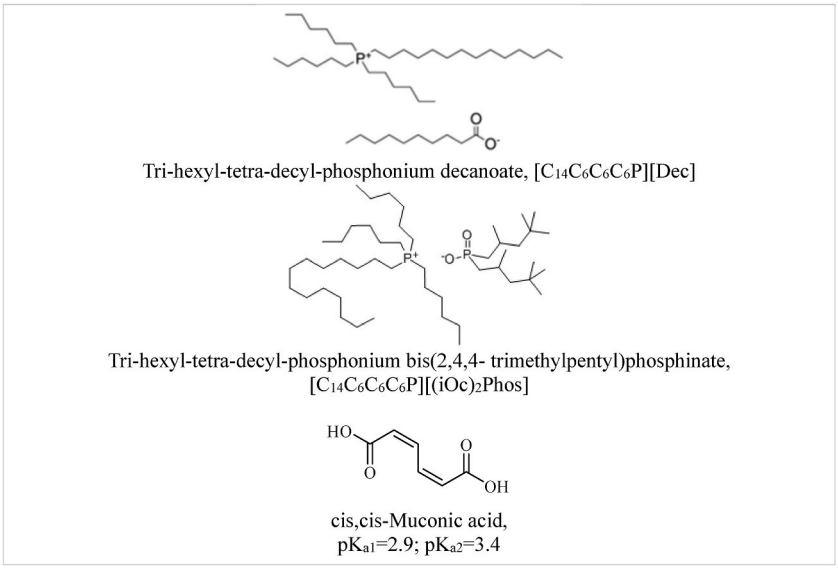

Fig. 1. Chemical structure of muconic acid and PILs used in this study.

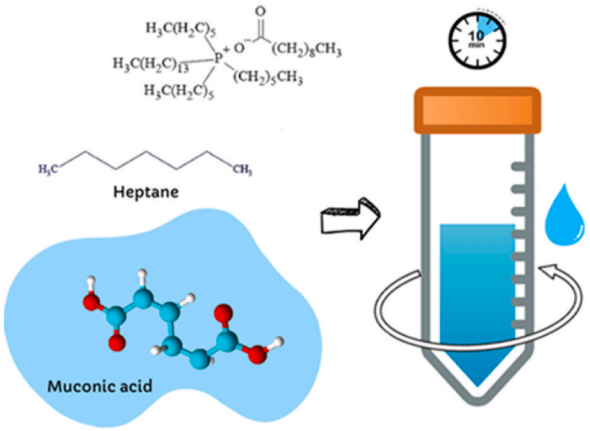

Fig. 2. Schematic representation of extraction step.

"greener" and more sustainable extraction and purification methods; one such method that has drawn interest is the use of ionic liquids (ILs), due to their excellent solvation ability. ILs have been proposed as promising extractants for carboxylic acids, such as lactic, butyric, and acetic [24–26].

Physical or mathematical modelling is vital in separation to correlate input and output design variables, and it may be used in the simulation and optimisation of the separation process to help find an efficient and economical method. Selecting a suitable technique for evaluating different process parameters and any interactions involved while minimizing the number of experimental runs is essential. In recent years, the rapid development of artificial intelligence (AI) techniques, especially of different types of neural networks (ANNs), coupled with advances in computing power, allowed the generation of robust systems that can be efficiently used for various tasks. Examples of ANN (simple or in combination with multiple algorithms) applied for modelling of processes focused on the extraction of various valuable products include: i) betalain pigment extraction from *Beta vulgaris*; a comparison between response surface methodology (RSM), classical one layer ANNs and a hybrid RSM - Genetic Algorithm (GA) approach was performed [27]; ii) bioactive compounds extraction from *Allium sativum* L. leaf powder; two strategies were used for process modelling and optimisation: RSM with a rotable central composite design and a hybrid ANN-GA approach [28]; iii) phycocyanin extraction from *Arthrospira platensis*; RSM with Box-Behnken design and one hidden layer ANN were used for process modelling and optimisation [29]; iv) ellagitannins extraction from black raspberry seeds; a one hidden layer with ten neurons ANN trained with Levenberg Marquardt and coupled with GA was used [30]; pseudomonic acids extraction; a shallow ANN model combined with DE, BackPropagation algorithm and a Local Search procedure was used to model and optimize the process [31]. While relatively easy to use, the AI-based systems must be prior trained and their optimal settings determined in order to provide good results. This is also applicable for ANNs, where their

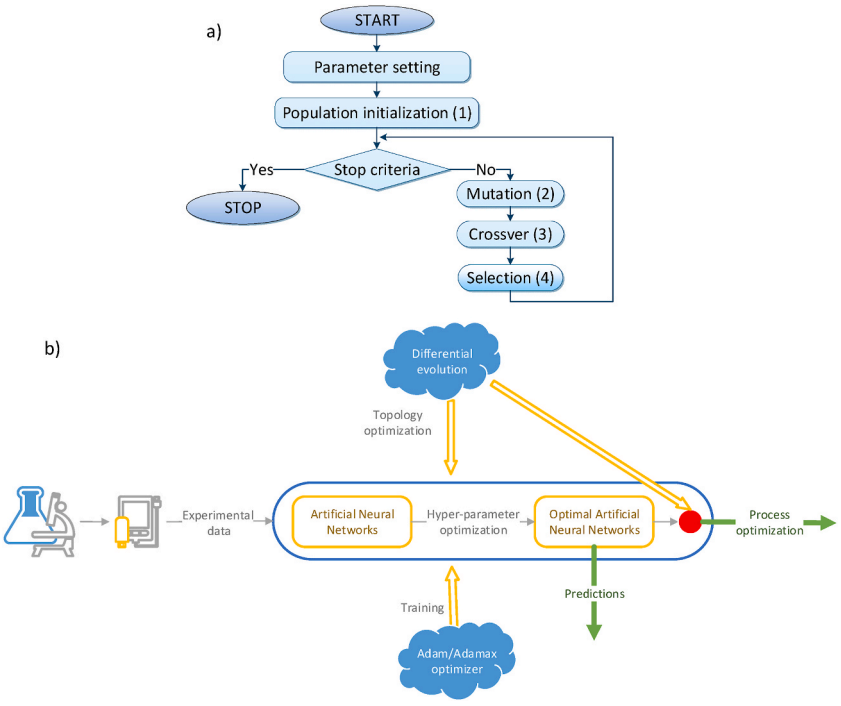

Fig. 3. Simplified schema of the a) DE algorithm; b) modeling and optimisation strategy.

topology and internal parameters are still challenging to determine, and the combination of ANN-DE used in this work aims to alleviate some of these challenges. The strategy describing the combination of the two approaches is presented in Section 2.2.

This study aims to search for a feasible downstream processing alternative for MA separation from aqueous media, resulting in an effective extraction system by analyzing two hydrophobic ionic liquids based on tetradecyl-(trihexyl) phosphonium – $[C_{14}C_6C_6C_6P]$: Cyphos IL104 – $[C_{14}C_6C_6C_6P][(iOc)_2Phos]$ and Cyphos IL103 - $[C_{14}C_6C_6C_6P][Dec]$ dissolved in n-heptane.

A thorough analysis was conducted of the variables influencing the extraction behaviour of MA, including temperature, aqueous phase pH, type and concentration of extractant, and contact time. The process was modelled and optimised using a deep neural network with an optimised structure obtained using the Differential Evolution (DE) algorithm.

2. Materials and methods

2.1. Chemical and methods

All chemicals, including muconic acid cis-cis (97.0 %), $[C_{14}C_6C_6C_6P][(iOc)_2Phos]$ (95 %), $[C_{14}C_6C_6C_6P][Dec]$ (95 %), heptane (99 %), sodium phosphate (99 %), sodium hydroxide (>97 %), sulfuric acid (95.0–98.0 %), and acetonitrile (99.99 %), were purchased from Sigma and used as received (see Fig. 1).

The experiments performed for MA extraction (Fig. 2.) were carried out using a vibration shaker that ensured a stirring speed of 1200 rpm (extraction time between 10 and 30 min and temperature 25–65 °C), using equal volumes (2 mL) of MA solution, and the organic phase using a glass cell. MA was extracted from aqueous solutions whose initial concentration was 0.8 g/L. The extraction was carried out either using Cyphos IL103 - Trihexyl-tetra-decyl-phosphonium decanoate and Cyphos IL104 - Tri-hexyl-tetra-decyl-phosphonium bis(2,4,4- trimethylpentyl)phosphinate, mixed with n-heptane, the ionic liquid concentration in the organic phase varied between 0 and 120 g/L. The pH of the initial aqueous phase was corrected to the predetermined value, using 4 % sulfuric acid and 4 % sodium hydroxide solutions, based on the indications of a Hanna Instruments pH 213 digital pH meter. The pH of MA solution 0.8 g/L was 3.05 before any adjustment, and its pH at equilibrium was 4.45. After extraction, the samples were separated by centrifugation at 4000 rpm for 5 min. The analysis of the process was carried out using the extraction efficiency, E (%), which was calculated by determining the MA concentration from the initial solution and the raffinate solution using a Dionex Ultimate HPLC system equipped with a Hypersil Gold column, the mobile phase being a mixture of 35 % acetonitrile and 65 % sodium phosphate solution with a flow rate of 0.75 mL/min, detection at 210 nm. The stripping experiments for MA separation were carried out using diluted sodium hydroxide solution (pH 12, modified using the indications of the digital pH meter (CONSORT C 836) in equal volumes with loaded organic phases organic phase (2 mL) using a vibratory shaker with 1200 rpm and 20 min contact time. After extraction, the aqueous exhausted phase was removed, and the organic extract was mixed with the stripping phase. The back extraction efficiency was calculated using the equation:

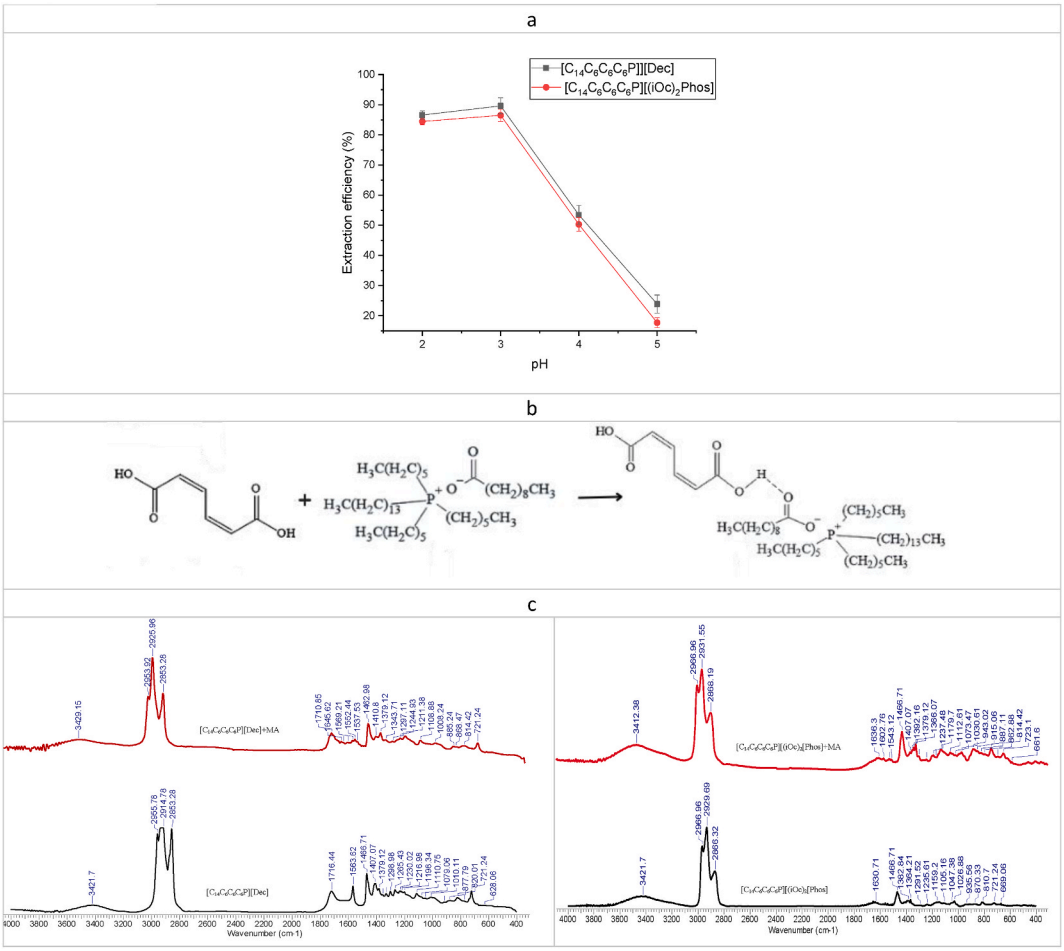

Fig. 4. pH influence on MA reactive extraction.

$$S = \left(\frac{C_s}{C_0\text{-}C}\right) \bullet 100, \%$$

where c_s, c_0, and c (g/L) are MA concentrations in the stripping solution, aqueous initial solutions, and the raffinate (exhausted initial solution after extraction). All experiments were performed in triplicate (n = 3, error between 1.5 and 4.5 %). An Agilent Cary 630 FTIR instrument (32 scans per sample at 4 cm^{-1} spectral resolution and 4000–400 cm^{-1} range) was used for FTIR analysis.

2.2. Modelling and optimisation

The process was modelled using a neuro-evolutionary approach in which a sequential multiple-layer ANN model's structure (the number of hidden layers and neurons in each hidden layer) is automatically determined using the DE algorithm. DE is a bio-inspired metaheuristic that has proved its efficiency in solving many problems. Considering the No Free Lunch theorem [32], many optimisers can provide good results for this problem. However, DE was chosen based on its simplicity, reduced number of parameters, and overall performance. As with every population-based algorithm, DE evolves (through a series of steps) a set of randomly generated potential solutions until a stop criterion is reached.

The initial solutions are generated using random number generators following different distribution functions (usually normal distribution) in the initialisation step (step 1). The other steps used by DE include mutation (step 2), crossover (step 3), and selection (step 3). The mutation introduces new information in the population through a specific DE operator called differentiation (in its simple form, to a base individual, a scaled differential term is added). In the crossover step, a new population is created by combining data from the individuals from the current and the mutated populations. The resulting individuals are compared with the existing population, and if their fitness (a measure that indicates their performance) is better, they are selected to form the new population. In this case, the stop criterion is represented by the number of iterations reaching a pre-determined value. The control parameters that direct the search are introduced into the individuals and are modified as the other parameters (the self-adaptation principle). The type of parameters and the mechanisms used in each algorithm step indicate its variant. Fig. 3a presents the simplified schema of the DE

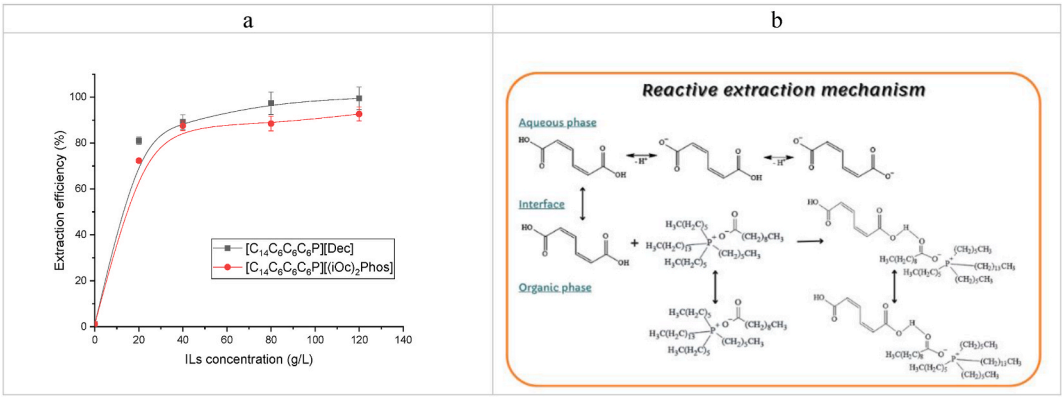

Fig. 5. PILs concentration influence on MA reactive extraction (0.8 g/L MA concentration, aqueous phase pH 3, 10 min contact time).

algorithm. The general principles of DE, the mathematical relations describing each step, and the concepts used to combine it with ANNs are described in Ref. [33]. The simplified schema of the modelling and optimisation strategy is presented in Fig. 3b.

The model's training was performed using the algorithms Adam (Adaptive Moment Estimation) and Adamax (Adam variant using infinite norm). Both algorithms are gradient-based variants and incorporate adaptive learning rates that improve efficiency and reduce training time. L1 regulation (also known as Lasso regulation) was applied to prevent overtraining. This involves adding a penalty to the loss function and has the effect of forming model parameters towards small values, thus introducing sparsity. The implementation was done in Python, using the TensorFlow and sklearn modules. The best-resulting models and the Python script for running it can be downloaded from https://elenadragoi.ro/CV/Documents/muconic_model.zip.

3. Results and discussion

3.1. Influence of various parameters on MA reactive extraction

Because of their hydrophilic nature and their dissociation in aqueous solutions, short-chain carboxylic acids, like MA, cannot be directly recovered in an organic solvent. Instead, if an extractant is added in the organic phase, it can form with MA a hydrophobic complex, soluble mainly in the organic phase. ILs are characterised by exceptional solvation ability, nonflammability, low volatility, and good chemical, thermal, and electrochemical stability. They can be used as extractants and diluents for hydrophilic carboxylic acid separation, which is much safer than conventional organic solvents. Due to their high viscosity, which makes them difficult to utilise alone, they are frequently combined with organic solvents (diluents) to improve extraction effectiveness. n-Heptane has been selected as the inactive diluent for this investigation due to its very low water solubility and good miscibility with PIls. The extraction of MA from aqueous solutions using a mixture of phosphonium ionic liquids - PILs and heptane-was examined using varying aqueous phase pH, time, temperature, and ionic liquid concentration.

The pH of the aqueous phase is a decisive factor in the efficiency of the reactive extraction process. Fig. 4a shows the influence of the aqueous phase pH on the extraction of MA by 40 g/L PIls diluted in n-heptane. The extraction efficiency increases in the pH range of 2–3, being reduced when the pH of the aqueous phase increases above pH 3. Carboxylic acids, in aqueous solutions, can be undissociated at pH lower than pKa (pKa_1 2.9 and pKa_2 3.4 for MA [34]) or dissociated at pH higher than pKa, with the degree of ionisation influencing its solubility and partitioning behaviour between the aqueous and organic phases. The highest extraction efficiency was observed in the experimental data at a pH lower than pKa; when pH increases above pKa_2, the acid equilibrium switches to dissociation of both carboxylic groups, and extraction efficiency decreases. Taking into account the characteristics of PILs and MA, the obtained results show that the formation of the complex MA-PIls is based on hydrogen bonds between the ionic liquid and the undissociated form of the MA, as to get optimal extraction efficiency, the pH of the aqueous phase needs to be lower than the pKa_2 (3.4). The cis-cis form of MA is in its protonated form at pH 3.4. However, the increase of pH until 6 and an increase in temperature could determine its irreversible conversion of CCM into cis, trans form, which is less available for reacting with PILs. This property can be exploited in the back-extraction step.

The extraction mechanism, presented in Fig. 4b, assumes H-bond formation between the protonated MA and the binding sites in the anion of the IL (for example, the oxygen of bis(2,4,4-trimethylpentyl) phosphinate, in the case of $[C_{14}C_6C_6C_6P][(iOc)_2Phos]$ or from decanoate - carboxylate for $[C_{14}C_6C_6C_6P][Dec]$). Due to extractant protonation, adding sulfuric acid for pH control (at pH 2) slowly decreases the extraction efficiency and PIL's extractant capacity to form H bonds with MA. Superior values of extraction yield were obtained in the case of $[C_{14}C_6C_6C_6P][Dec]$, probably due to less sterical hindrance (decanoate being smaller than bis(2,4,4- tri-methyl-pentyl)phosphinate).

The reaction between MA and PILs was further investigated by FTIR analysis (Fig. 4c) of the extract compared to the organic phase. It proves the formation of hydrogen bonds between MA and PILs for both extractants, similar to citric acid and tri-octylamine extraction systems [35]: the OH (hydrogen-bonded) stretch valence oscillation around 3400–3500 cm^{-1} domain can be detected,

Table 2
Loading factor values obtained for MA extraction.

$[C_{14}C_6C_6C_6P][Dec]$ concentration		Loading factor, Z	$[C_{14}C_6C_6C_6P][(iOc)_2Phos]$ concentration		Loading factor, Z
M	g/L	–	M	g/L	–
0.03	20	0.155	0.02	20	0.161
0.06	40	0.094	0.05	40	0.102
0.12	80	0.046	0.10	80	0.048
0.18	120	0.031	0.15	120	0.032

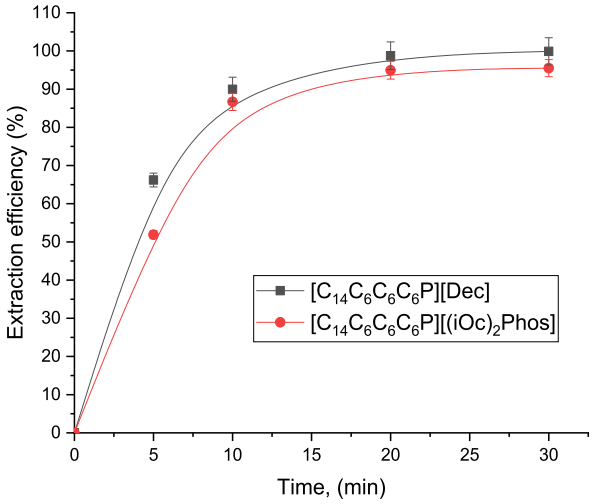

Fig. 6. Contact time influence on MA reactive extraction (0.8 g/L MA concentration, aqueous phase pH 3, 40 g/L PIls concentration).

and an increasing peak can be observed in the PILs extracts spectrum. The major peaks observed between 2800 and 3000 cm^{-1} corresponding to H–C–H stretch are representative for heptane, while for ionic liquid peaks are mainly visible in the 1800-600 cm^{-1} domain: at 1466 cm^{-1} corresponding to P–C stretching, at 1382 cm^{-1} to C - H in-plane bending, and the characteristic vibrations reflecting the presence of PIL anions: for $[C_{14}C_6C_6C_6P][(iOc)_2Phos]$: POO^- at ca. 1026 cm^{-1}, P–CH_2 at ca. 1467 cm^{-1} and COO- at ca. 1563 cm^{-1} and ca. 1406 cm^{-1}; and for $[C_{14}C_6C_6C_6P][Dec]$: stretching vibration of C=O at ca. 1716 cm^{-1}. FTIR spectroscopy of the MA extract spectrum showed the presence of novel bands at around 1634–1636 cm^{-1} (C=O stretching mode vibration) and at approximately 1559–1561 cm^{-1} (carboxylate peak) [36,37].

Fig. 5 shows the extraction yield as a function of PILs concentration in the organic phase: an improved yield can be observed with the increased extractant concentration in the inert diluent, and the maximum MA extraction is observed at approximately 0.12 mol/L (80 g/L) for both ionic liquids, corresponding to the optimal composition of the organic phase. Visual observations showed no third-phase formation for any of the analysed systems. Reaching the optimum conditions at equilibrium for different extraction systems and achieving reproducible results requires understanding emulsification. It is crucial to prevent this undesirable phenomenon while preserving the PILs-diluent system's capacity for easy regeneration. The dilution of PILs with n-heptane is likely the primary cause of the high stability of this extraction system (depending on the polarity of the diluent used, it is incorporated preferentially in the polar or non-polar domains of the IL) and the short time required to reach high extraction efficiencies in the investigated system (hydrophobic ionic liquids based on tetradecyl-(trihexyl) phosphonium diluted with heptane), as no emulsification was observed.

The analysis of different extraction systems points out that the extraction system behaviour is very different for specific ILs/carboxylic acid systems. Zhang et al. (2021) removed 55%–88 % perfluorooctanoic acid (its specific hydrophobic and oleophobic properties lead to low extraction efficiency and severe emulsification) in diluted wastewater using [methyltrioctylammonium][bis(trifluoromethylsulfonyl)imide], and observed that ILs addition could suppress the emulsification with high extraction efficiency [38]. Grabda et al. (2022) obtained an extraction efficiency of 80 %–91 % for perfluorooctanoic acid from water by using [trihexyltetradecylphosphonium][pivalic acid] as IL, without emulsification difficulties developed for a particular PFOA: IL ration of 1:1 and re-extraction using a 1 % NaOH solution [39]. Marták and Schlosser (2019) investigated the reactive extraction of monocarboxylic acids using hydrophobic ionic liquids diluted with dodecane in a setup where equilibrium requires more than 10 h in a rotating shaking water bath. They observed coextraction of acid and water, and competitive extraction of acid and water, probably due to extremely high time necessary for reaching equilibrium [40].

PILs with a hydrophobic anion form complexes with MA through H bond formation at the interface between the organic and aqueous phase, with different stoichiometry: 1:1 (when a molecule of MA and PILs are involved in the complex formation), n:1 (when more molecules of MA react with one molecule of PILs for the complex formation) or 1:n (when a molecule of MA and more molecules

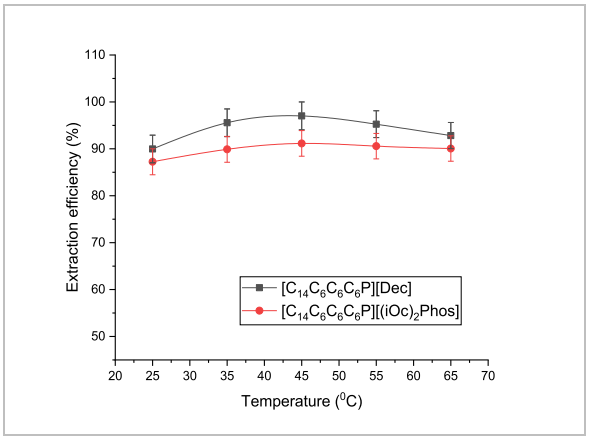

Fig. 7. Temperature influence on MA reactive extraction (0.8 g/L MA concentration, aqueous phase pH 3, 40 g/L PIls concentration).

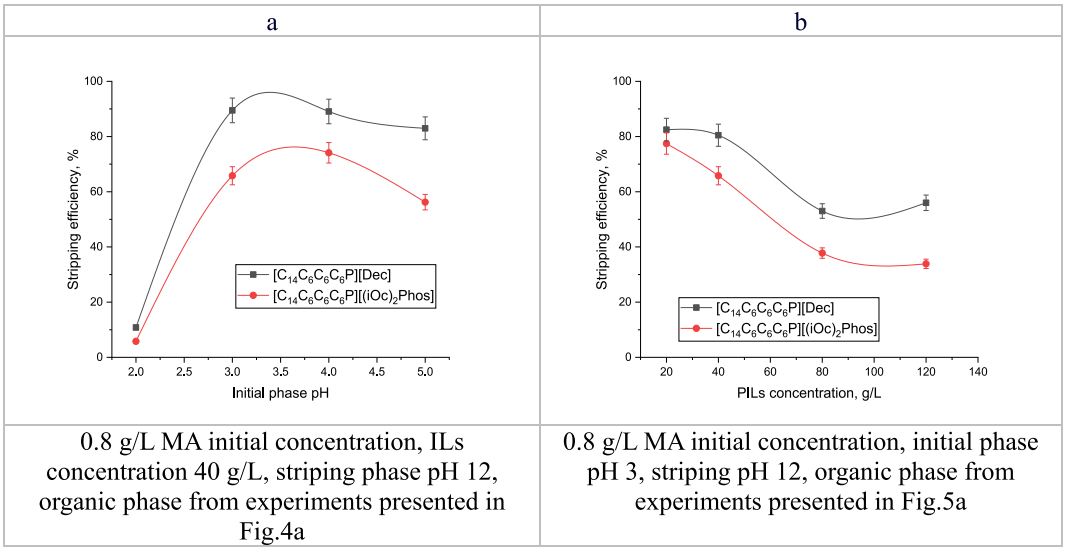

Fig. 8. Initial aqueous phase pH and PILs concentration on MA stripping (0.8 g/L MA initial concentration, final aqueous phase pH 12).

of PILs are involved in the complex formation).

To establish the number of molecules of MA and PILs involved in forming the hydrophobic complex, the loading ratio (Z, ($[MA]_{org}$/$[PIL]_{org}$) was calculated.

The results in Table 2 proved no overloading during the complex's formation, as evidenced by the loading ratio decreasing as PILs concentration increased and Z values below 1. This suggested the formation of an equimolecular complex including just one MA and one ionic liquid molecule.

Experiments were conducted for both PILs to examine the dependence of MA extraction efficiency on extraction time. The findings shown in Fig. 6 indicated that the maximum yield was reached for all systems after 10 min and stayed consistent during the whole investigation period. Good mixing conditions are necessary for reactive extraction as they help increase the contact between the solute and extractant, increasing the reaction rate. The optimum contact time (20 min) ensured intense mixing and intimate contact between the aqueous and organic phases, thus achieving equilibrium. These results are in accordance with findings obtained for muconic acid reactive extraction using amines [20].

Ionic liquids have a high viscosity by nature, and it has been observed that when temperature increases, the organic phase's viscosity decreases, improving mass transfer [41]. For MA, the extraction process was analysed at various temperatures between 25 and 65 °C using 40 g/L extractant at pH 3.0. Using PILs as extractants, MA extraction efficiency slowly decreased with the increase in temperature (Fig. 7). This phenomenon may be connected to MA back extraction in the aqueous phase, which appears at higher temperatures and reduces process efficiency overall. This parameter is of the lowest importance in the extraction process for the considered experimental domain.

Several studies have been conducted on the reactive extraction process of muconic acid. Demir et al. (2021) used tri-n-butyl

Table 3
Statistics for the determined models.

		Training					Testing				
		R^2 score	MAE	MSE	MAPE	r^2	R^2 score	MAE	MSE	MAPE	r^2
Case 1	M5 adam	**0.990**	**1.231**	**2.380**	**0.017**	**0.990**	**0.987**	**1.628**	**5.375**	**0.041**	**0.987**
	M5 adamax	0.973	1.577	6.430	0.020	0.973	0.960	2.423	16.754	0.052	0.960
	M6-adam	0.972	2.294	7.813	0.028	0.967	0.980	2.293	8.574	0.050	0.979
	M6-adamax	0.957	2.005	10.252	0.026	0.957	0.960	2.718	16.766	0.054	0.960
Case 2	M5 adam	**0.996**	**1.144**	**1.977**	**0.013**	**0.993**	**0.991**	**1.393**	**5.234**	**0.044**	**0.990**

phosphate (TBP) in concentrations between 10 and 50 % by volume and tri-n-octyl phosphine oxide (TOPO) in concentrations between 4 % and 16 % by volume dissolved in different solvents (1-butanol, isoamyl alcohol, methyl ethyl ketone, methyl isobutyl ketone, di-isobutyl ketone, iso-butanol, hexane, diethyl carbonate). They obtained extraction degrees between 70 and 93 % at an MA concentration of 0.007 mol/kg [19]. Gorden et al. (2015) analysed tri-n-octyl amine, or TOA, dissolved in ethyl oleate and obtained a 95 % efficiency rate for MA reactive extraction. However, in this system, a third phase situated at the interface but inside the organic phase was seen to form. Several phase modifiers, including ethanol, 1-butanol, 1-pentanol, 1-octanol, and 1-dodecanol, were examined in an attempt to address this issue; only ethanol was shown to be unable to stop the creation of the third phase, while butanol use yielded in a 95.66 % extraction degree [23]. The results obtained in this study allowed superior values for extraction efficiency: 99.24 %.

3.2. Stripping

Recovering MA from the loaded organic phase is crucial in the context of reusing the ionic liquid and protecting the environment. This investigation analysed a combined approach for muconic acid recovery: pH modification of the stripping phase pH at 12 (NaOH solutions) and an increased temperature at 50 °C. Regardless of the pH of the starting phase or the extractant concentration, the results from Fig. 8 demonstrated a more effective stripping of MA in the case of $[C_{14}C_6C_6C_6P][Dec]$ compared to $[C_{14}C_6C_6C_6P][(iOc)_2Phos]$.

Because MA dissociates in the aqueous phase in correlation to its pH, and the fact that for breaking the equimolecular complex formed with the extractant, MA has to be converted into its undissociated form, back-extraction efficiency of MA is higher when carried out using an aqueous solution with a high pH when MA is converted into its sodium salt. The maximum efficiency for MA stripping from the loaded organic phase is achieved at an initial aqueous phase pH equal to 3 because the organic phase is loaded with the highest complex amount corresponding to maximum extraction efficiency for 40 g/L PILs in the organic phase. Nearly 89 % MA was recovered in a single contact from the loaded organic phase for organic: aqueous volume ratio of 1:1. The MA dissociated form corresponding to high pH does not possess the ability to form a complex with the PILs and is re-extracted into the aqueous phase. Regarding PILSs concentration influence on the stripping efficiency, from Fig. 8, it can be observed that the stripping process is more effective at low extractant concentrations in the organic phase, probably correlated with an increased viscosity of the organic phase due to the increased proportion of PILs.

The FTIR analysis (Supplementary material) was carried out to check the form of the extractant after stripping. Comparing the spectra, all characteristic peaks appeared PILs spectra after the stripping, confirming their stability. The stability and recycling capacity of PILs were evaluated to assess its utility as an extractant for practical purposes. PILs characteristics have been investigated for MA separation in terms of stripping efficiencies change as percent. The re-extraction efficiencies obtained were 84.47 %, 82.04 %, and 81.11 %, for $[C_{14}C_6C_6C_6P][Dec]$ and 61.47 %, 58.47 %, and 56.86 % for $[C_{14}C_6C_6C_6P][(iOc)_2Phos]$ for the recycled organic phase in the next three stages, which were close to the first extraction stage. The gradual decrease in extraction yields observed while employing the regenerated PILs can be explained by a small pH increase during sodium hydroxide back-extraction, which lowers extraction efficiency [42]. Regeneration, recovery, and reuse of PILs remain a major issue. Ionic liquids are more environmentally friendly than organic solvents due to their high boiling point, making it more challenging to distil them to produce pure products. Recovering ionic liquids at a lower cost and with less impact on the environment is a difficult undertaking. Further improvements are required for MA back-extraction from the organic phase.

3.3. Modeling and optimisation

The modelling strategy was performed considering two cases: i) with contact time; and ii) without. In the first case, the following parameters were used to model the extraction process: pH, extractant concentration, contact time, temperature, and type of extractant ($[C_{14}C_6C_6C_6P][Dec]$ or $[C_{14}C_6C_6C_6P][(iOc)_2Phos]$). For this model to be applied, preliminary equilibrium studies are needed to verify the influence of the contact time between phases, as the contact time for reaching equilibrium is strictly related to the mixing conditions (hydrodynamic conditions) used. In the second case, the model was determined using the same parameters as in the first case (except contact time). Since the extractant type is a discrete parameter, a coding procedure of the One-Hot-Encoding type was used, where each type of extractant has its corresponding specific column, and the use of the type is identified by the value 1. The Min-Max approach [43] was used to normalise the data. Preliminary tests have indicated that the process is complex and that the experimental data obtained in the laboratory need to be revised to identify an optimal model. Thus, an interpolation procedure was applied, where each combination of parameters was modelled with a regression relationship of order 3, and intermediate points were extracted. Therefore, the database was expanded from 30 data to 340 points (for case 1) and from 22 to 240 (for case 2). If the first case also

Table 4
Characteristics of the best models.

	Layer (type)	Output Shape	Param #
Case 1	dense_122 (Dense)	(None, 11)	77
	dense_123 (Dense)	(None, 8)	96
	dense_124 (Dense)	(None, 1)	9
	Total params: 182		
	Trainable params: 182		
	Non-trainable params: 0		
Case 2	dense_626 (Dense)	(None, 17)	102
	dense_627 (Dense)	(None, 4)	72
	dense_628 (Dense)	(None, 8)	40
	dense_629 (Dense)	(None, 1)	9
	Total params: 671		
	Trainable params: 223		
	Non-trainable params: 0		

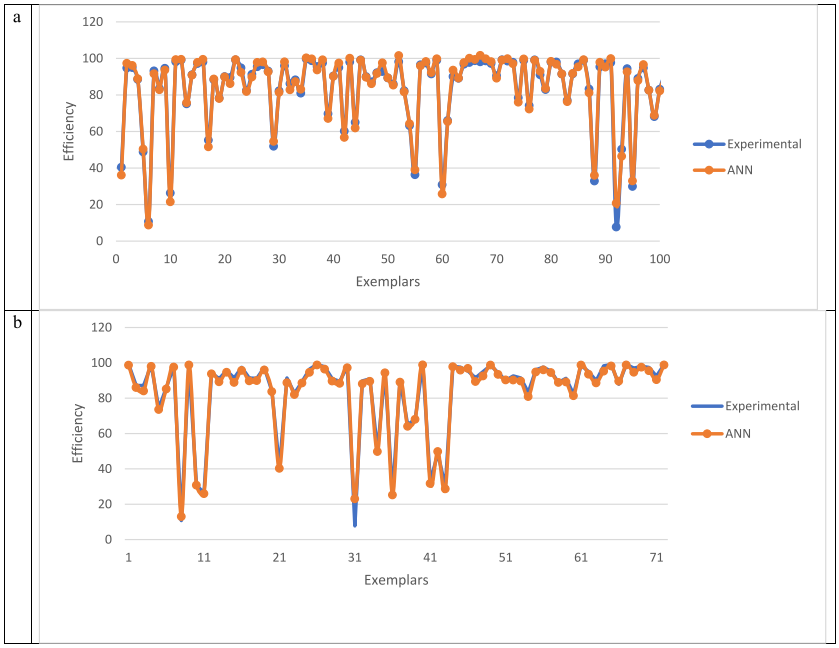

Fig. 9. Comparison of experimental and predicted data for a) case 1 and b) case 2.

considers a variation of contact time, the second case is determined only for a fixed contact time equal to 10 min. These were later used to determine the complete neural pattern. Statistical indicators for the best models obtained are presented in Table 3. After that, the best settings identified for case 1 were also applied in case 2.

In this table, M5 indicates a model with a limit of 5 hidden layers with limits of the maximum number of neurons set to Refs. [10,10,10,10,20], and M5 indicates a model with a maximum of 6 hidden layers with limits of [10,10,10,10,10,20]. R^2 score is the variation score, MAE is the mean absolute error, MSE is the mean square error, MAPE is the mean percentage absolute error, and r^2 is the coefficient of determination. The closer the R^2 score and r^2 are to 0, and the lower the MAE, MSE, and MAPE values, the higher the model's performance. As seen from Table 3, the Adam algorithm tends to give better results for the current process than Adamax. Regarding limits for the model structure, the variant with a maximum of 5 layers offers better results. This can be explained by the complexity of the search space, which increases with the number of layers, requiring a more significant number of iterations to identify an optimal pattern. Thus, the model identified as M5_Adam as the most suitable for the studied process was chosen.

The characteristics of the best models obtained in both cases are presented in Table 4. As can be seen, the best model for case 1 has two hidden layers, with 11 and 8 neurons respectively. On the other hand, the model for the second case is more complex and has 3 hidden layers with respectively 17, 4 and 8 neurons.

Fig. 9 compares experimental data with those predicted by the network. The differences are minimal in both cases, indicating that the neural model has learned the dynamics of the extraction process and can generate predictions.

An analysis of the importance of inputs to model outputs (identified by the Shap values [44]) is shown in Fig. 10. It is noted that the most important parameter is pH, for which small values tend to lead to an increase in output (small pH leads to a high yield). The next

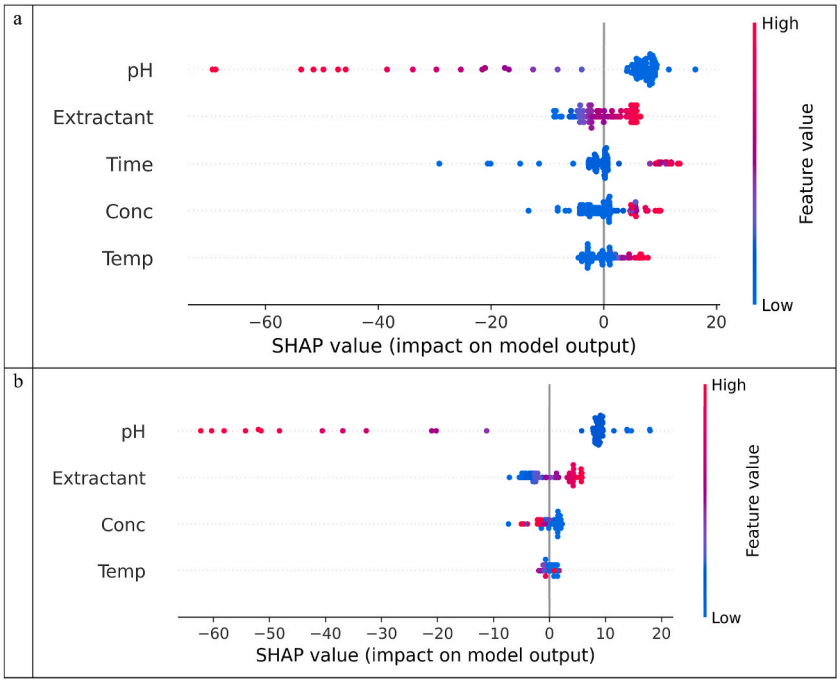

Fig. 10. Shap values a) case 1 and b) case 2.

Table 5
Optimisation results in case 1.

$[C_{14}C_6C_6C_6P]$ [Dec]	$[C_{14}C_6C_6C_6P]$ $[(iOc)_2Phos]$	pH	Extractant concentration (g/L)	Time (min)	Temperature (°C)	Extraction efficiency (%)
0	1	3.9	55.09	23.24	53.65	102.3
0	1	3.29	73.91	26.65	50.03	101.71
1	0	4.8	51.52	25.94	55.31	101.37
0	1	3.63	54.17	23.12	43.91	101.34
0	1	4.16	90.44	21.57	35.42	100.52
0	1	4.11	87.33	25.84	25.3	99.83
0	1	2.43	81.15	28.79	59.9	99.53
0	1	4.11	87.33	25.21	25.3	99.27
1	0	4.25	64.55	22.01	38.92	99.24
0	1	4.00	97.83	21.66	54.03	99.14
0	1	4.27	60.55	25.84	39.33	99.17
0	1	3.97	74.59	23.23	26.23	98.92
0	1	2.11	81.15	28.79	63.26	98.28
0	1	2.36	45.09	25.54	20.49	97.95
0	1	3.97	83.18	23.23	20.91	97.95
0	1	3.74	45.45	20.91	65.00	97.47
0	1	4.25	34.88	21.76	42.95	96.91
1	0	3.38	38.66	23.87	30.71	96.69
1	0	3.38	38.66	23.87	33.07	95.73
0	1	4.81	117.34	24.24	38.02	95.65
0	1	4.26	67.37	25.17	30.92	95.61
0	1	2.1	79.59	25.15	60.06	95.57
1	0	3.38	38.66	24.08	33.07	95.47
1	0	3.38	38.66	24.08	33.07	95.47
1	0	4.8	51.52	26.54	44.32	95.07

important parameter is the extractant, followed by Time (in case 1) and Concentration (in case 2). Temperature is the parameter with the least influence on the model. Overall, it can be observed that the elimination of contact time from the model does not change the impact of parameters on the output. Nevertheless, if for case 1 it can be observed clearly that increasing the temperature tends to result in a slight increase in efficiency, this is not applicable for case 2, where there is no clear distinction between the impact of low and high values for temperature.

In the final step, the best model obtained in combination with the same DE algorithm is used to optimize the process. Tables 5 and 6 present a set of process parameters that lead to high extraction efficiency.

Table 6
Optimisation results in case 2.

$[C_{14}C_6C_6C_6P]$ [Dec]	$[C_{14}C_6C_6C_6P]$ $[(iOc)_2Phos]$	pH	Extractant concentration (g/L)	Temperature (°C)	Extraction efficiency (%)
0	1	2.67	65.06	26.19	103.33
1	0	2.42	61.64	29.62	103.3
1	0	2.34	99.35	25.11	103.11
0	1	2.67	65.06	27.51	102.92
1	0	2.22	120	27.88	102.61
1	0	2.69	60.27	20.82	101.81
1	0	2.77	43.95	23.41	99.74
1	0	2.41	97.29	30	99.71
1	0	2.6	104.59	22.45	99.32

As observed, the extraction efficiency is higher than 100 % in some cases. The error introduced by the model can explain this, as no hard limits were set for the output during the optimisation phase. For the process parameters, the experimental limits are kept unchanged.

In case 1, the optimisation results show that both extractants can be highly efficient; the optimisation step does not favour a particular one. Moreover, the combinations of parameters are not focused on a particular set of values, indicating that the search space is complex and the DE algorithm was able to explore it efficiently.

In case 2, the solutions are somewhat closer, indicating that the process has a reduced pool of local optima.

4. Conclusions

A new extraction technique utilising hydrophobic ILs was investigated in this work to effectively extract muconic acid from aqueous solutions, such as fermentation broth. The findings demonstrated that the best extraction conditions for MA were pH = 3.0, 20 min contact time, 45 °C temperature, and above 40 g/L ionic liquid dissolved in heptane when using $[C_{14}C_6C_6C_6P][Dec]$ as the extractant. Additionally, an analysis of the extraction system's mechanism revealed an equimolecular hydrophobic complex between PILs and MA for both extractants examined. Low stripping efficiency compared to extraction efficiency was observed, so further investigation on the influence of stripping phase pH, contact time and temperature are required to improve stripping method efficiency. ANNs and DE algorithms were used to model and optimize the process, and the results obtained indicated that the selected approach could find a suitable model that can be further used to identify combinations of process parameters that lead to a high extraction efficiency.

Data availability

Data will be made available on request.

CRediT authorship contribution statement

Alexandra Cristina Blaga: Writing – review & editing, Writing – original draft, Supervision, Project administration, Funding acquisition, Conceptualization. **Elena Niculina Dragoi:** Writing – review & editing, Software, Formal analysis. **Alexandra Tucaliuc:** Writing – review & editing, Visualization, Methodology, Formal analysis. **Lenuta Kloetzer:** Visualization, Validation, Investigation. **Adrian-Catalin Puitel:** Formal analysis. **Dan Cascaval:** Writing – review & editing, Validation, Supervision, Resources, Data curation. **Anca Irina Galaction:** Writing – review & editing, Visualization, Validation, Funding acquisition.

Declaration of competing interest

The authors declare that they have no known competing financial interests or personal relationships that could have appeared to influence the work reported in this paper.

Acknowledgement

This work was supported by a grant from the Ministry of Research, Innovation and Digitization, CNCS - UEFISCDI, project number PN-III-P1-1.1-TE-2021-0153, within PNCDI III and CNFIS-FDI-2024-F-0099.

Appendix A. Supplementary data

Supplementary data to this article can be found online at https://doi.org/10.1016/j.heliyon.2024.e36113.

References

[1] Menglei Li, Jiayao Chen, Keqin He, Changsheng Su, Yilu Wu, Tianwei Tan, Corynebacterium glutamicum cell factory design for the efficient production of cis, cis-muconic acid, Metab. Eng. 82 (2024) 225–237, https://doi.org/10.1016/j.ymben.2024.02.005.

[2] Jingjing He, Yongjun Jiang, Bingjie Ding, Yajun Wang, Hewen Qiu, Sheng Dai, Xiuge Zhao, Zhenshan Hou, Zirconium phosphate supported copper catalyst for selective oxidation of phenol to cis, cis-muconic acid, Appl. Catal. Gen. 664 (2023) 119351, https://doi.org/10.1016/j.apcata.2023.119351.

[3] Sridevi Veluru, Ramakrishna Seeram, Biotechnological approaches: degradation and valorization of waste plastic to promote the circular economy, Circular Economy 3 (1) (2024) 100077, https://doi.org/10.1016/j.cec.2024.100077.

[4] C. Ling, G.L. Peabody, D. Salvachúa, et al., Muconic acid production from glucose and xylose in *Pseudomonas putida* via evolution and metabolic engineering, Nat. Commun. 13 (2022) 4925, https://doi.org/10.1038/s41467-022-32296-y.

[5] Robert S. Nelson, Eric P. Knoshaug, Ryan Spiller, Nick Nagle, Stefanie VanWychen, Matthew Wiatrowski, Ryan Davis, Philip T. Pienkos, Jacob S. Kruger, Muconic acid production from algae hydrolysate as a high-value co-product of an algae biorefinery, Algal Res. 75 (2023) 103300, https://doi.org/10.1016/j.algal.2023.103300.

[6] M.E. Pyne, L. Narcross, M. Melgar, K. Kevvai, S. Mookerjee, G.B. Leite, V.J.J. Martin, An engineered Aro1 protein degradation approach for increased cis,cis-muconic acid biosynthesis in Saccharomyces cerevisiae, Appl. Environ. Microbiol. 84 (17) (2018), https://doi.org/10.1128/AEM.01095-18.

[7] G. Wang, A. Tavares, S. Schmitz, L. França, H. Almeida, J. Cavalheiro, A. Carolas, S. Øzmerih, L.M. Blank, B.S. Ferreira, I. Borodina, An integrated yeast-based process for cis,cis-muconic acid production, Biotechnol. Bioeng. 119 (2) (2021) 376–387, https://doi.org/10.1002/bit.27992.

[8] B. Thompson, S. Pugh, M. Machas, D.R. Nielsen, Muconic acid production via alternative pathways and a synthetic "metabolic funnel", ACS Synth. Biol. 7 (2) (2017) 565–575, https://doi.org/10.1021/acssynbio.7b00331.

[9] R. Fujiwara, S. Noda, T. Tanaka, A. Kondo, Muconic acid production using gene-level fusion proteins in Escherichia coli, ACS Synth. Biol. 7 (11) (2018) 2698–2705, https://doi.org/10.1021/acssynbio.8b00380.

[10] H.-N. Lee, W.-S. Shin, S.-Y. Seo, S.-S. Choi, J. Song, J. Kim, J. Park, D. Lee, S.Y. Kim, S.J. Lee, G.-T. Chun, E.-S. Kim, Corynebacterium cell factory design and culture process optimization for muconic acid biosynthesis, Sci. Rep. 8 (2018) 18041, https://doi.org/10.1038/s41598-018-36320-4.

[11] S. Wang, M. Bilal, Y. Zong, H. Hu, W. Wang, X. Zhang, Development of a plasmid-free biosynthetic pathway for enhanced muconic acid production in Pseudomonas chlororaphis HT66, ACS Synth. Biol. 7 (5) (2018) 1131–1142, https://doi.org/10.1021/acssynbio.8b00047.

[12] C. Ling, G.L. Peabody, D. Salvachúa, Y.-M. Kim, C.M. Kneucker, C.H. Calvey, M.A. Monninger, N.M. Munoz, B.C. Poirier, K.J. Ramirez, P. C. St John, S. P. Woodworth, J.K. Magnuson, K.E. Burnum-Johnson, A.M. Guss, C.W. Johnson, G.T. Beckham, Muconic acid production from glucose and xylose in Pseudomonas putida via evolution and metabolic engineering, Nat. Commun. 13 (2022) 4925, https://doi.org/10.1038/s41467-022-32296-y.

[13] H.-M. Jung, M.-Y. Jung, M.-K. Oh, Metabolic engineering of Klebsiella pneumoniae for the production of cis,cis-muconic acid, Appl. Microbiol. Biotechnol. 99 (2015) 5217–5225, https://doi.org/10.1007/s00253-015-6442-3.

[14] M.E. Pyne, J.A. Bagley, L. Narcross, K. Kevvai, K. Exley, M. Davies, Q. Wang, M. Whiteway, V.J.J. Martin, Screening non-conventional yeasts for acid tolerance and engineering Pichia occidentalis for production of muconic acid, Nat. Commun. 14 (2023) 5294, https://doi.org/10.1038/s41467-023-41064-5.

[15] N. Yoshikawa, S. Mizuno, K. Ohta, M. Suzuki, Microbial production of cis, cis-muconic acid, J. Biotechnol. 14 (1990) 209–210, https://doi.org/10.1016/0168-1656(90)90009-Z.

[16] M. Kohlstedt, S. Starck, N. Barton, J. Stolzenberger, M. Selzer, K. Mehlmann, R. Schneider, D. Pleissner, J. Rinkel, J.S. Dickschat, et al., From lignin to nylon: cascaded chemical and biochemical conversion using metabolically engineered Pseudomonas putida, Metab. Eng. 47 (2018) 279–293, https://doi.org/10.1016/j.ymben.2018.03.003.

[17] V. Inyang, D. Lokhat, Reactive extraction of malic acid using trioctylamine in 1–decanol: equilibrium studies by response surface methodology using Box behnken optimization technique, Sci. Rep. 10 (2020) 2400, https://doi.org/10.1038/s41598-020-59273-z.

[18] D. Małgorzata, H. Marek, Reactive extraction of carboxylic acids using organic solvents and supercritical fluids: a review, Separ. Purif. Technol. 201 (2018) 106–119, https://doi.org/10.1016/j.seppur.2018.02.010.

[19] Ö. Demir, A. Gök, H. Uslu, Ş.İ. Kırbaşlar, Reactive extraction of cis,cis-muconic acid from aqueous solution using phosphorus-bonded extractants, tri-n-octylphosphineoxide and tri-n-butyl phosphate: equilibrium and thermodynamic study, Sep. Purif. Technol. 272 (2021) 118899, https://doi.org/10.1016/j.seppur.2021.118899.

[20] A. Bahrami, F. Ghamari, Y. Yamini, F.G. Shahna, A. Koolivand, Ion-pair-based hollow-fiber liquid-phase microextraction combined with high-performance liquid chromatography for the simultaneous determination of urinary benzene, toluene, and styrene metabolites, J. Separ. Sci. 41 (2018) 501, https://doi.org/10.1002/jssc.201700685.

[21] S. Abbaszadeh, S. Yousefinejad, S. Jafari, E. Soleimani, In-syringe ionic liquid-dispersive liquid-liquid microextraction coupled with HPLC for the determination of trans,trans-muconic acid in human urine sample, J. Separ. Sci. 44 (2021) 3126, https://doi.org/10.1002/jssc.202100044.

[22] S. Tönjes, E. Uitterhaegen, P. De Brabander, E. Verhoeven, T. Delmulle, K. De Winter, W. Soetaert, In situ product recovery as a powerful tool to improve the fermentative production of muconic acid in *Saccharomyces cerevisiae*, Biochem. Eng. J. 190 (2023) 108746, https://doi.org/10.1016/j.bej.2022.108746.

[23] J. Gorden, T. Zeiner, C. Brandenbusch, Reactive extraction of cis,cis-muconic acid, Fluid Phase Equil. 393 (2015) 78–84, https://doi.org/10.1016/j.fluid.2015.02.030.

[24] M. Blahusiak, S. Schlosser, J. Martak, Extraction of butyric acid with a solvent containing ammonium ionic liquid, Sep. Purif. Technol. 19 (2013) 102–111, https://doi.org/10.1016/j.seppur.2013.09.005.

[25] J. Marták, Š. Schlosser, Phosphonium ionic liquids as new, reactive extractants of lactic acid, Chem. Pap. 60 (5) (2006) 395–398, https://doi.org/10.2478/s11696-006-0072-2.

[26] J. Marták, Š. Schlosser, New mechanism and model of butyric acid extraction by phosphonium ionic liquid, J. Chem. Eng. Data 61 (9) (2016) 2979–2996, https://doi.org/10.1021/acs.jced.5b01082.

[27] S.V. Prabhu, V. Varadharajan, S. Mohanasundaram, S. Manivannan, J.M. Khaled, M. Goel, K. Srihari, A comparative study on process optimization of betalain pigment extraction from Beta vulgaris subsp. vulgaris : RSM, ANN, and hybrid RSM-GA methods, Biomass Conversion and Biorefinery (2023), https://doi.org/10.1007/s13399-023-04581-3.

[28] S. Shekhar, P. Prakash, P. Singha, K. Prasad, S.K. Singh, Modeling and optimization of ultrasound-assisted extraction of bioactive compounds from Allium sativum leaves using response surface methodology and artificial neural network coupled with genetic algorithm, Foods 12 (2023), https://doi.org/10.3390/foods12091925.

[29] S. Hilali, L. Wils, A. Chevalley, B. Clément-Larosière, L. Boudesocque-Delaye, Glycerol-based NaDES as green solvents for ultrasound-assisted extraction of phycocyanin from Arthrospira platensis—RSM optimization and ANN modelling, Biomass Conversion and Biorefinery 12 (2022) 157–170, https://doi.org/10.1007/s13399-021-02263-6.

[30] G.E. Lee, R.H. Kim, T. Lim, J. Kim, S. Kim, H.G. Kim, K.T. Hwang, Optimization of accelerated solvent extraction of ellagitannins in black raspberry seeds using artificial neural network coupled with genetic algorithm, Food Chem. 396 (2022) 133712, https://doi.org/10.1016/j.foodchem.2022.133712.

[31] R.G. Lazar, A.C. Blaga, E.N. Dragoi, A.I. Galaction, D. Cascaval, Application of reactive extraction for the separation of pseudomonic acids: influencing factors, interfacial mechanism, and process modelling, Can. J. Chem. Eng. 100 (2021), https://doi.org/10.1002/cjce.24124.

[32] D.H. Wolpert, W.G. Macready, No free lunch theorems for optimization, IEEE T Evol Comput 1 (1997) 67–82, https://doi.org/10.1109/4235.585893.

[33] E.N. Dragoi, S. Curteanu, A.I. Galaction, D. Cascaval, Optimization methodology based on neural networks and self-adaptive differential evolution algorithm applied to an aerobic fermentation process, Appl. Soft Comput. 13 (1) (2013) 222–238, https://doi.org/10.1016/j.asoc.2012.08.004.

[34] I. Khalil, G. Quintens, T. Junker, M. Dusselier, Muconic acid isomers as platform chemicals and monomers in the biobased economy, Green Chem. 22 (2020) 1517–1541, https://doi.org/10.1039/C9GC04161C.

[35] L. Nolte, M. Nowaczyk, C. Brandenbusch, Monitoring and investigating reactive extraction of (di)carboxylic acids using online FTIR – Part I: Characterization of the complex formed between itaconic acid and tri-n-octylamine, J. Mol. Liq. 352 (2022) 118721, https://doi.org/10.1016/j.molliq.2022.118721.

[36] H. Beneš, J. Kredatusová, J. Peter, S. Livi, S. Bujok, E. Pavlova, J. Hodan, S. Abbrent, M. Konefał, P. Ecorchard, Ionic liquids as delaminating agents of layered double hydroxide during in-situ synthesis of poly (butylene adipate-co-terephthalate) nanocomposites, Nanomaterials 9 (4) (2019) 618, https://doi.org/10.3390/nano9040618.
[37] V.R. Dhongde, B.S. De, K.L. Wasewar, Experimental study on reactive extraction of malonic acid with validation by Fourier Transform Infrared Spectroscopy, J. Chem. Eng. Data 64 (3) (2019) 1072–1084, https://doi.org/10.1021/acs.jced.8b00972.
[38] K. Zhang, D. Kujawski, C. Spurrell, D. Wang, J. Yan, J.C. Crittenden, Extraction of PFOA from dilute wastewater using ionic liquids that are dissolved in n-octanol, J. Hazard Mater. (2021) 124091, https://doi.org/10.1016/j.jhazmat.2020.124091.
[39] M. Grabda, M. Zawadzki, S. Oleszek, M. Matsumoto, M. Królikowski, Y. Tahara, Removal of perfluorooctanoic acid from water using a hydrophobic ionic liquid selected using the conductor-like screening model for realistic solvents, Environ. Sci. Technol. 56 (10) (2022) 6445–6454, https://doi.org/10.1021/acs.est.1c08537.
[40] J. Marták, Š. Schlosser, Influence of anion and cation structure of ionic liquids on carboxylic acids extraction, Front. Chem. 7 (2019) 117, https://doi.org/10.3389/fchem.2019.00117.
[41] B.B. Mishra, N. Devi, K. Sarangi, Solvent extraction and separation of samarium from transition and rare-earth metals using phosphonium ionic liquid Cyphos IL 104, Monatsh. Chem. 152 (2021) 767–775, https://doi.org/10.1007/s00706-021-02792-w.
[42] A.F.M. Cláudio, A.M. Ferreira, C.S.R. Freire, A.J.D. Silvestre, M.G. Freire, J.A.P. Coutinho, Sep. Purif. Technol. 97 (2012) 142, https://doi.org/10.1021/jp204865a.
[43] D. Fryer, I. Strümke, H. Nguyen, Shapley values for feature selection: the good, the bad, and the axioms, IEEE Access 9 (2021) 144352–144360, https://doi.org/10.1109/ACCESS.2021.3119110.
[44] K. Priddy, P. Keller, Artificial Neural Networks:An Introduction, SPIE Press, Washington, 2005.